

ABSTRACT

Title of Thesis: ENVIRONMENTAL PERFORMANCE AND
SUSTAINABILITY OF BIORETENTION CELLS

Philip Sumner Jones, Master of Science, 2009

Thesis directed by: Professor Allen P. Davis
Department of Civil and Environmental Engineering

Bioretention cells use vegetation and soil media for source control of urban stormwater runoff, alleviating waterway impairment. Environmental performance of two cells was investigated. First, a cell capturing road runoff was monitored for one year. At a second cell, media were sampled to measure lifetime metal accumulation and evaluate the environmental, health, and maintenance implications of metal sequestration.

Monitoring found high metal and suspended solids removal, generally poor nutrient performance, and chloride export. Runoff volume and peak flow rate reduction occurred for small storm events. For larger events, outflow volume consistently exceeded inflow because of unique site conditions.

Lead, copper, and zinc media concentrations in the second cell were elevated but well below cleanup thresholds. Metals were strongly bound to bioretention media and largely immobile; lead bioavailability was comparable to generic soil estimates. Most metal accumulation was near the inflow point in the top 3 to 12 cm of media.

ENVIRONMENTAL PERFORMANCE AND SUSTAINABILITY OF
BIORETENTION CELLS

by

Philip Sumner Jones

Thesis submitted to the Faculty of the Graduate School of the
University of Maryland, College Park in partial fulfillment
of the requirements for the degree of
Master of Science
2009

Advisory Committee:

Professor Allen P. Davis, Chair
Professor Richard H. McCuen
Associate Professor Eric A. Seagren

© Copyright by
Philip Sumner Jones
2009

Dedicated to Dr. William Claron Sumner, Sr.
of Roanoke, Virginia
1914 – 2008

ACKNOWLEDGMENTS

Sincere thanks are due to Dr. Mow-Soung Cheng and the staff of the Prince George's County Department of Environmental Resources for their continued leadership in advancing bioretention technology and for funding this research effort.

The author is greatly indebted to Dr. Allen Davis for the invaluable mentoring, judgment, and vision that he provided throughout this project.

Dr. Richard McCuen, Dr. Eric Seagren, Dr. Glenn Moglen, Matt Hafner, HOUNG Li, Lan Zhang, Eliea Jamil, and Hunho Kim have provided much-appreciated advice and a spirit of collaboration over the course of several years.

Kristen W. Jones has been a steadfast source of support and encouragement.

TABLE OF CONTENTS

DEDICATION..... ii

ACKNOWLEDGEMENTS..... iii

LIST OF TABLES..... vi

LIST OF FIGURES vii

CHAPTER 1. INTRODUCTION 1

 1.1 Background..... 1

 1.2 Research goals 3

CHAPTER 2. MATERIALS AND METHODS 6

 2.1 Kenilworth Avenue monitoring 6

 2.1.1 Site description..... 6

 2.1.2 Monitoring chronology 12

 2.1.3 Instrumentation and sampling protocol 12

 2.1.4 Water quality analysis..... 16

 2.1.4.1 Quality verification 17

 2.2 Metal accumulation..... 19

 2.2.1 Site description..... 19

 2.2.2 Flow patterns..... 22

 2.2.3 Zone delineation..... 25

 2.2.4 Media sampling and analysis 27

 2.2.4.1 Surface samples and total metal..... 27

 2.2.4.2 Core samples and sequential extraction..... 29

 2.2.4.3 Bioavailability sampling and analysis 34

 2.2.4.4 Media pH and organic matter 36

 2.2.4.5 Measurement of metal concentrations 37

 2.2.5 Quality control and verification 38

 2.2.5.1 AAS protocol 38

 2.2.5.2 Controls without media..... 38

 2.2.5.3 Comparison of results between methods 39

 2.2.5.4 Reproducibility 40

CHAPTER 3. RESULTS AND DISCUSSION –
BIORETENTION MONITORING.. 43

 3.1 Hydrology 43

 3.1.1 Storm event characterization..... 43

 3.1.2 Hydrologic performance 45

 3.1.2.1 Example event..... 48

 3.1.2.2 Volume..... 49

3.1.2.3	Peak flow rate	51
3.1.2.4	Hydrograph timing.....	53
3.1.2.5	Cumulative exposure to flow	53
3.2	Water quality.....	56
3.2.1	Sampling approach and event characterization.....	56
3.2.2	Data handling.....	58
3.2.2.1	Pollutant concentration	58
3.2.2.2	Pollutant mass	60
3.2.3	Water quality performance	61
3.2.3.1	Overview of changes in concentration.....	62
3.2.3.2	Chloride.....	63
3.2.3.3	Nutrients.....	65
3.2.3.4	Metals and TSS	68
3.2.3.5	Biochemical oxygen demand.....	71
3.2.3.6	Changes in pollutant mass	72
CHAPTER 4.	RESULTS AND DISCUSSION – MEDIA ANALYSIS.....	76
4.1	Media composition.....	76
4.1.1	Organic matter content.....	78
4.1.2	Cation exchange capacity	82
4.1.3	Media pH	82
4.2	Total metal at cell surface	86
4.2.1	Regulatory implications.....	88
4.2.2	Variation with distance on cell surface.....	89
4.2.2.1	Cumulative infiltration concept	91
4.2.2.2	Other flow-related variation.....	96
4.2.2.3	Role of OM content within zones	97
4.2.2.4	Surface metal ratios.....	100
4.3	Variation with depth	102
4.3.1	Sorption and particle capture	103
4.3.2	Micro-trends with depth.....	107
4.3.3	Maintenance implications	108
4.4	Environmental availability and bioavailability	111
4.4.1	Sequential extraction.....	112
4.4.1.1	Fractionation trends in organic media.....	113
4.4.1.2	Zinc in F1 and F2.....	117
4.4.1.3	BSM fractionation.....	118
4.4.1.4	Spatial variation of fractionation in organic media.....	118
4.4.2	Bioavailability.....	121
4.5	Mass balance and environmental pathways.....	123
4.5.1	Inflow and outflow calculations.....	124
4.5.2	Metal masses in media	126
4.5.3	Results of mass balance	127
CHAPTER 5.	CONCLUSIONS AND RECOMMENDATIONS.....	130
5.1	Hydrologic and water quality performance	130

5.1.1 Future research.....	132
5.2 Media evolution and metal accumulation.....	134
5.2.1 Maintenance implications.....	136
5.2.2 Future research.....	137
5.3 General design recommendations.....	138
APPENDIX A. KENILWORTH AVENUE MONITORING DATA.....	141
APPENDIX B. MEDIA ANALYSIS DATA.....	175
APPENDIX C. MATLAB SCRIPTS.....	181
REFERENCES.....	188

LIST OF TABLES

Table 2-1	Minimum detection limit and analytical method for each pollutant	17
Table 2-2	Number and concentration range of blanks for each pollutant analyzed at the Kenilworth cell	18
Table 2-3	Sequential extraction procedure for Pb, Cu, and Zn	33
Table 2-4	Specifications of sequential extraction reagents	33
Table 2-5	Calibration ranges and quantitation limits for AAS analysis.....	37
Table 2-6	Number and concentration range of controls above the smallest standard	39
Table 2-7	Comparison of total metal results between sequential extraction and 3050B methods.....	40
Table 2-8	Reproducibility of media analyses	42
Table 3-1	Rainfall depth and duration for all 65 events at the Kenilworth cell	44

Table 3-2	Frequency distribution of storm events at the Beltsville Agricultural Research Center and at the Kenilworth cell	45
Table 3-3	Frequency distribution of sampled events	57
Table 3-4	Comparison of median inflow EMCs at Kenilworth Avenue to results from recent monitoring studies in suburban Maryland	62
Table 3-5	Median, mean, and standard deviation (SD) of inflow and outflow pollutant concentrations at the Kenilworth bioretention cell	63
Table 3-6	Annual unit-area mass loadings of monitored pollutants	75
Table 4-1	Organic matter content in media samples	78
Table 4-2	Media pH of organic and BSM segments	82
Table 4-3	Mean and standard deviation of total Pb, Cu, and Zn surface concentrations in Zones 2 and 3 after four years of operation	86
Table 4-4	Total and bioavailable Pb and absolute bioavailability of nine organic and BSM media samples	122
Table 4-5	Concentration and mass data used to estimate net metal mass retained in the Lot 11 cell	125

LIST OF FIGURES

Figure 1-1	Typical bioretention cell cross-section	2
Figure 2-1	Location of the Kenilworth Avenue cell in Greenbelt, Maryland and the Lot 11 cell at the University of Maryland, College Park, Maryland	6
Figure 2-2	Plan view of Kenilworth Avenue study site	7

Figure 2-3	Manhole and flow splitter upstream of the Kenilworth cell.....	9
Figure 2-4	Inflow area for the Kenilworth Avenue cell.....	9
Figure 2-5	Plan view of Kenilworth Avenue cell with spot elevations	10
Figure 2-6	Outflow weir at Kenilworth cell.....	11
Figure 2-7	June 2003 photograph of Lot 11 east cell.....	20
Figure 2-8	Vegetative cover in August 2006 and February 2008	21
Figure 2-9	August 2006 flow test.....	23
Figure 2-10	Development of flow patterns during the flow test	25
Figure 2-11	Location of each zone as shown on a February 2007 photograph	26
Figure 2-12	Typical media profile in the Lot 11 cell	27
Figure 3-1	Depth-duration plots for all 65 monitored events at the Kenilworth cell....	46
Figure 3-2	Hyetograph and inflow and outflow hydrographs from April 20, 2008	49
Figure 3-3	Dependence of Kenilworth cell inflow and outflow volume on rainfall depth.....	51
Figure 3-4	Probability distribution of peak inflow and outflow rates.....	52
Figure 3-5	Cumulative exposure time to average inflow and outflow rates	55
Figure 3-6	Chloride EMC box-and-whisker plot	64
Figure 3-7	Nitrate EMC box-and-whisker plot.....	67
Figure 3-8	TKN EMC box-and-whisker plot.....	67
Figure 3-9	TP EMC box-and-whisker plot	68
Figure 3-10	Lead EMC box-and-whisker plot	69
Figure 3-11	Zinc EMC box-and-whisker plot.....	70
Figure 3-12	TSS EMC box-and-whisker plot	70

Figure 3-13	Inflow and outflow bottles from the July 28, 2007 event	71
Figure 3-14	BOD EMC box-and-whisker plot.....	72
Figure 3-15	Probability plot of mass ratios for all events with outflow	74
Figure 4-1	Organic matter content on cell surface.....	79
Figure 4-2	Variation in pH with depth in each zone.....	83
Figure 4-3	Pb, Cu, and Zn surface concentrations vs. distance	90
Figure 4-4	Illustration of water spreading and infiltration concept	93
Figure 4-5	Storm hydrograph and cell surface divided into ten sections.....	94
Figure 4-6	Four-year cumulative depth of infiltrated water and total surface metals...95	
Figure 4-7	Metal concentration vs. OM content	99
Figure 4-8	Paired metal concentrations for all 28 surface samples	101
Figure 4-9	Mean lead concentration as a function of media depth	104
Figure 4-10	Mean copper concentration as a function of media	105
Figure 4-11	Mean zinc concentration as a function of media depth	106
Figure 4-12	Media fractionation shown as the mean and standard deviation of normalized sequential extraction results for organic and BSM samples...114	
Figure 4-13	Normalized mean metal fractionation of organic media as a function of media depth in Zone 2	120
Figure 4-14	Cell footprint with regions used for metal mass balances.....	127

Chapter 1

INTRODUCTION

1.1 Background

Within the last decade, urban stormwater runoff has achieved widespread recognition as one of the most important and intractable causes of environmental degradation in urban waterways. Altered hydrology and increased pollutant loads are the two main types of impairment associated with urban stormwater runoff. Common hydrologic impacts include higher runoff volumes and peak flow rates, shorter delays to runoff generation, and decreased groundwater recharge (Cheng et al. 2003). These impacts can be seen in urban streams in the form of habitat degradation, unstable morphology, decreased baseflow, and increased water temperatures, among other responses (Walsh et al. 2005). Urban hydrology can indirectly harm water quality by triggering combined sewer overflows in response to modest rainfall (DCWASA 2004).

The propagation of non-point source pollution by urban runoff is a leading cause of water quality impairment in many urban watersheds (Novotny 1995). Diffuse pollutant loadings arise from sources such as atmospheric deposition, building components, and vehicles (Davis et al. 2001b). Efficient drainage from impervious surfaces and limited opportunities for infiltration cause pollutants such as particulates, oil and grease, heavy metals, and nutrients to be transported to receiving waters with little attenuation (MDE 2000).

Recent advances in stormwater management and land development practices have the potential to improve environmental outcomes in urban watersheds. Bioretention is

the exemplar of this new approach to urban stormwater management. Pioneered by Prince George's County, Maryland in the 1990s, bioretention cells, also known as rain gardens, are small-scale, shallow vegetated depressions underlain by engineered soil media (Figure 1-1). Bioretention cells replicate elements of the natural hydrologic cycle such as surface storage, evapotranspiration, and infiltration. These processes result in hydrologic benefits such as volume and peak flow rate reduction, increased peak delay, and groundwater recharge. Temporary ponding and infiltration through the media layers facilitate pollutant removal through physical, biological, and chemical processes, including settling, straining, depth filtration, plant uptake, microbial degradation, sorption, and precipitation.

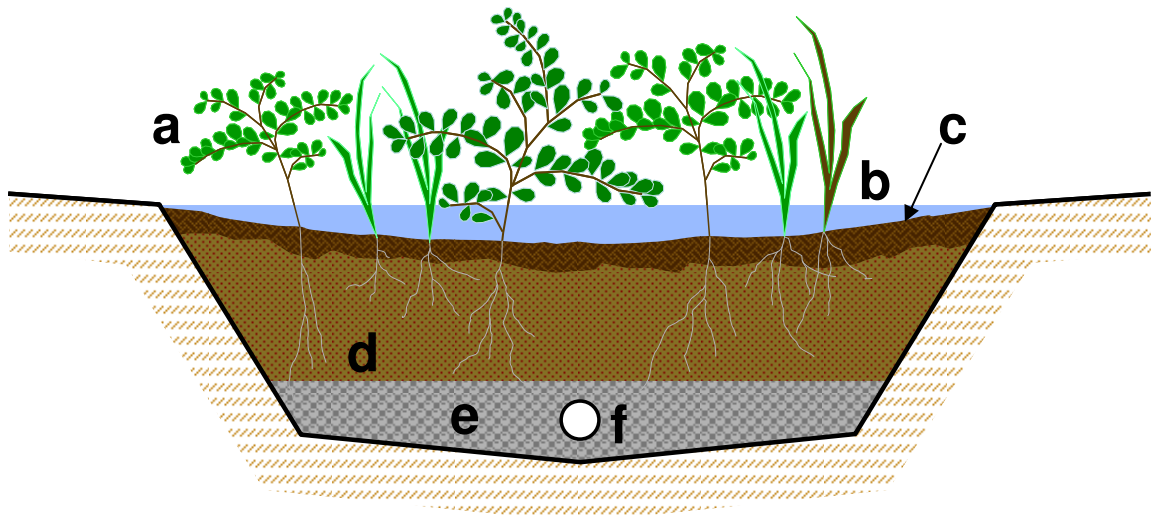


Figure 1-1. Typical bioretention cell cross-section. Components include (a) vegetation, (b) ponding area, (c) mulch, (d) engineered sandy loam soil media, (e) stone bedding, and (f) perforated underdrain.

Bioretention cells capture and treat runoff at or near the source, in contrast to traditional end-of-pipe approaches that are typically located near the watershed outlet. Drainage areas to bioretention cells are by definition small, ranging in size from a single

residential rooftop to approximately 0.4 ha. As a result, cells are distributed throughout the upland areas of a watershed, providing decentralized control of runoff.

1.2 Research goals

Since its introduction in the 1990s, bioretention has become an increasingly popular tool for treating runoff in developed areas. Studies of bioretention at the field scale have generally found very good hydrologic and water quality performance, with the exception of nutrient removal (Davis 2007, Hatt et al. 2008b, Hunt et al. 2008, Li and Davis 2009). There is an ongoing need for additional field assessments in order to keep pace with developments in laboratory research into bioretention processes, and with the establishment of new pollutants of interest (PDGER 2004). Additionally, monitoring efforts should be oriented toward assessing the suitability of bioretention in new watershed, infrastructure, and environmental contexts. Performance data may inform improvements in design, construction, and maintenance practices.

In the present study, two different field investigations were carried out in parallel. The first consisted of a monitoring effort designed to assess the water quality and hydrologic performance of a roadside bioretention cell. In the second investigation, bioretention media in another cell was sampled to quantify lifetime metal accumulation in the media and to address several long-term management concerns.

The first investigation reflects the increasing interest in bioretention as a means to treat road runoff. Roads are a repository for a wide range of pollutants from a variety of sources (Young et al. 1996). Roadway storm drain networks are ubiquitous and older roads commonly lack facilities to capture and treat runoff. Instead, road runoff is

delivered directly to surface waters without first mitigating hydrologic and water quality impacts. Therefore, one specific application with potential for widespread future use is retrofitting an existing roadway storm drain network with bioretention.

Bioretention can potentially lessen the environmental impacts of road runoff. Regularly-spaced inlets and drainage divides created by road crests can effectively divide road segments into relatively small drainage areas. In addition, open space suitable for bioretention cells may be found in medians and near interchanges. Diverting a portion of piped stormwater flow into a bioretention cell adjacent to the road offers opportunities for distributed runoff treatment as well as habitat enhancement and aesthetic improvements.

A bioretention cell in Greenbelt, Maryland was monitored to evaluate its ability to alleviate the hydrologic and water quality impacts of road runoff. Constructed in 2006 along a heavily-used secondary road, the cell intercepts runoff from a storm drain network with a 0.29 ha asphalt drainage area. Inflow, outflow, and rainfall data were collected for 65 storm events from April 2007 to May 2008 to characterize hydrologic performance. Automated inflow and outflow sampling of 11 storm events during this period and analysis for nine common pollutants, including heavy metals, nutrients, suspended solids, and chloride, were carried out to determine the effect of the cell on downstream water quality.

The impetus for the second investigation stems from the fact that bioretention creates a new treatment paradigm by acting as a sink for captured pollutants. Pollutants are retained within the cell, where they are either transformed into other substances or sequestered in media and vegetation. In the latter case, pollutant sequestration creates *de facto* ownership. Heavy metals are a unique concern because they cannot be broken

down and may pose ecological and human health risks in the upland environment as well as downstream (Li and Davis 2008a). Long-term management concerns include accumulated metals' environmental availability, oral bioavailability, relationship to regulatory cleanup thresholds, and spatial distribution within the cell.

The present study engaged with these questions by investigating lead, copper, and zinc accumulation in the media of a four-year-old bioretention cell at the University of Maryland, College Park. Bioretention media was sampled across the cell surface and to a depth of 90 cm to assess the spatial distribution of accumulated metals in the media. Total metal, environmentally-available metal, bioavailable lead, and media pH and organic matter content were analyzed to determine cumulative metal accumulation over four years, long-term environmental fate, human health risks, and factors that influence metal concentrations in media. The findings will help to refine bioretention design and maintenance considerations and will help to address the long-term sustainability of bioretention as a stormwater management practice.

MATERIALS AND METHODS

2.1 Kenilworth Avenue monitoring**2.1.1 Site description**

The study site consists of a bioretention cell and associated drainage network located in Greenbelt, Maryland, at the Kenilworth Avenue interchange with the Capital Beltway (I-495/I-95) (Figure 2-1). The cell sits immediately west of the southbound lanes of Kenilworth Avenue, between the entrance ramp to the outer loop of the Beltway and the Kenilworth Avenue overpass at the Beltway (Figure 2-2). The cell is located in the watershed of Indian Creek, a tributary of the Anacostia River.

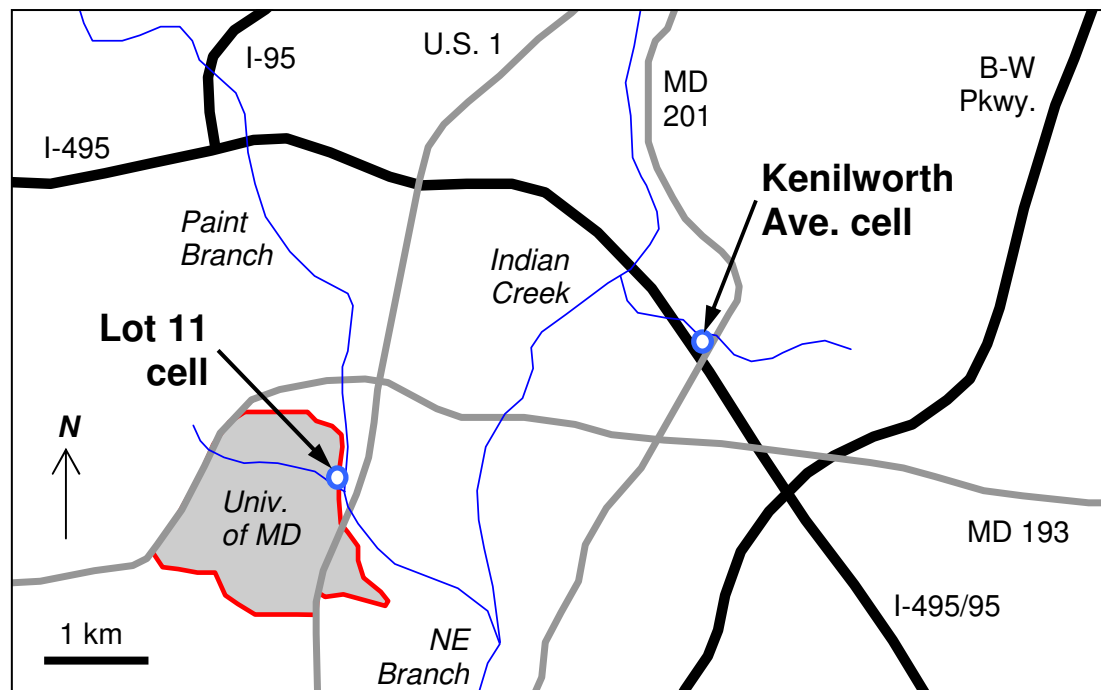


Figure 2-1. Location of the Kenilworth Avenue cell in Greenbelt, Maryland and the Lot 11 cell at the University of Maryland, College Park, Maryland.

The cell was constructed as part of a larger effort by Prince George’s County and the City of Greenbelt to improve landscape amenities and stormwater management on an approximately 0.8 km section of Kenilworth Avenue extending south from the intersection with Crescent Road. Three additional cells were constructed along with median improvements. The cell in this study is the largest and is the only site with provisions for monitoring.

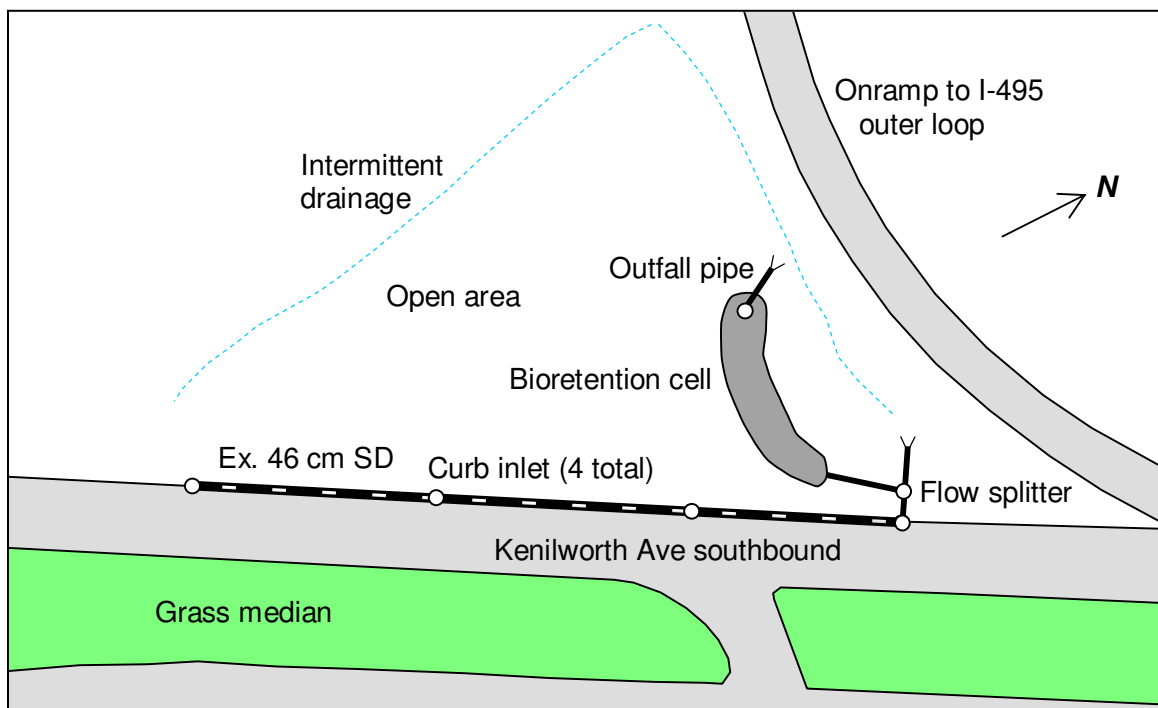


Figure 2-2. Plan view of Kenilworth Avenue study site, including the existing storm drain system draining to the bioretention cell.

The cell has a surface area of 260 m² and sits on the northeast corner of a triangular, 0.53 ha area of rubble fill (Aist 2007). The fill is believed to consist of broken pieces of asphalt and concrete up to 0.3 m across, mixed with local clayey soil. This heterogeneous fill likely contains gaps and fissures to easily convey subsurface flow.

The cell receives runoff from Kenilworth Avenue, a heavily-used, secondary state-maintained road. The drainage regime for this cell is novel because it receives concentrated flow from an existing storm drain rather than sheet flow from the pavement. The drainage area consists of approximately 0.29 ha of asphalt, comprising the full width of the southbound lanes of Kenilworth Avenue from the cell south to the Kenilworth overpass over the Beltway. This section of roadway is curbed and drains to the west side, where four curb inlets feed a 130 m long, 46 cm diameter concrete storm drain. The storm drain and inlets were thoroughly cleaned by vacuum truck in April 2007.

The existing 46 cm storm drain is intended to be the source of all surface water to the cell. At the northern-most inlet, adjacent to the cell, flow turns 90 degrees west into another 46 cm pipe. A new manhole was added to this pipe with a flow splitter device (Figure 2-3). The flow splitter directs runoff to the cell via a 20 cm PVC pipe. This pipe empties into a 4.4 m long concrete channel with a rectangular cross-section (38 cm wide, 29 cm high). A 91 x 20 cm cutthroat flume (Tracom) was installed in the channel to serve as the inflow level measurement point (Figure 2-4).

The established flow path follows the south perimeter of the cell before turning north near the first pair of cleanouts (Figure 2-5). The sharp change in direction is caused by elevation differences in the cell surface. As shown in Figure 2-5, the front 76 m² of the cell surface are generally much lower relative to the inflow channel than the rear of the cell. The change in elevation coincides closely with the location of the first pair of cleanouts and may have resulted from construction errors. Spot elevations in the rear of the cell confirm visual observations that with the exception of a sliver of cell surface



Figure 2-3. Manhole and flow splitter upstream of the Kenilworth cell. Flow enters from the 46 cm storm drain (top) and is directed to a 20 cm PVC pipe (right) that leads to the cell. During periods of extreme discharge, flow may bypass to the existing 46 cm pipe (bottom of image), which daylights to an existing ditch.



Figure 2-4. Inflow area for the Kenilworth Avenue cell, with sampler and housing, channel, and cutthroat flume. Samples are taken at the upstream end of the channel. Inflow level is measured at a prescribed point in the flume.

along the north side, the rear of the cell is higher than the inflow channel. As a result, the effective surface area of the cell is less than half of the total surface area.

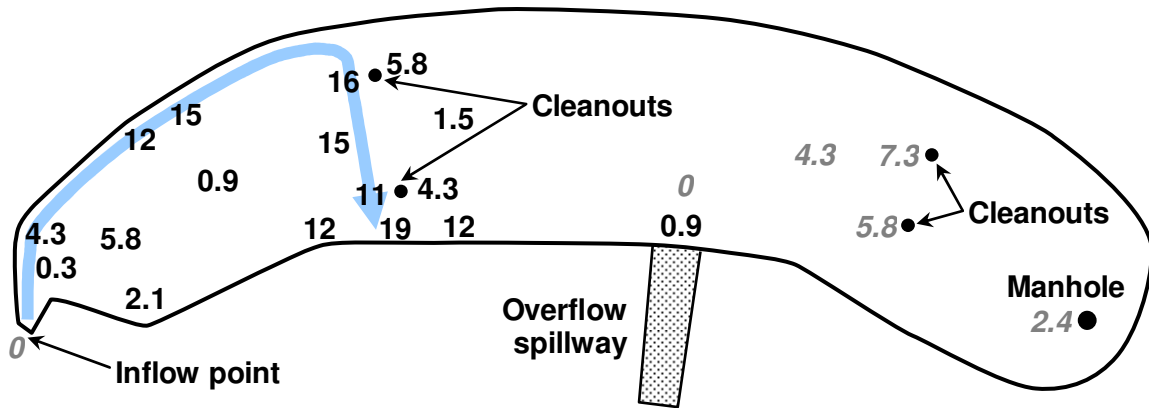


Figure 2-5. Plan view of Kenilworth Avenue cell with spot elevations (cm) measured on June 2, 2008. Surface elevations are relative to the front of the inflow channel. Black text denotes points that are lower than the front of the inflow channel; gray italics indicates points that are higher. The flow path follows the blue arrow.

Stormwater infiltrates into the media layers and enters two parallel 20 cm perforated underdrains. The underdrains merge and discharge into an observation manhole. This manhole is not an overflow device; the lid is solid. Accordingly, outflow measurements only reflect flows that have entered the underdrain and exclude overflow events. (A stone-lined spillway was constructed to provide overflow conveyance into the existing ditch.) A non-perforated outfall pipe conveys the flow to a manmade earthen channel with a stone apron. Outflow level measurements are taken at a 20 cm volumetric weir (Thel-Mar) inserted at the end of the outfall pipe (Figure 2-6), which is the only point where cell outflow is discharged to the surface. The manufacturer-supplied rating table is valid to the top of the rectangular section of the weir, above which the level-to-flow relationship cannot reliably be quantified.



Figure 2-6. Outflow weir at Kenilworth cell (20 cm diameter). Outflow levels higher than the horizontal bar exceed the measurable range of the weir. Above this point, the level-to-flow rate conversion is undefined. Photo taken April 15, 2007.

From top to bottom, cell components include shredded hardwood mulch (8 cm depth), bioretention soil media (BSM) (46 cm), pea gravel (8 cm), #57 stone (5 cm), and a slotted PVC underdrain pipe (20 cm diameter). Specifications for bioretention media at this site stipulate a composition of 60% ASTM C-33 sand, 35% topsoil, and 5% leaf compost, by volume (PGDER 2004). The BSM is required to have a clay content no greater than 8%. The top 30 cm of BSM was mixed with Soil Moist, a water absorbent polymer (JRM Chemical) or equivalent substance prior to placement (PGDER 2004).

Four vertical cleanout pipes provide surface access to the underdrains. The cell is planted with a variety of grasses, perennials, and shrubs. An impermeable plastic liner surrounds the sides of the cell, from the mulch layer down to the level of the underdrain. However, the bottom of the cell is unlined (Aist 2007), creating the potential for water to infiltrate into the subsurface, or conversely, for subsurface flows to enter the cell.

2.1.2 Monitoring chronology

Excavation at the site began in June 2006. Installation of the flow splitter and media occurred in early September. Remaining minor construction, such as installation of concrete sampler pads, was complete in December. Sampler enclosures were installed by University of Maryland personnel in January 2007 and all sampling equipment was in place by early February. Freezing temperatures and little rain in February effectively delayed the start of sampling to early March.

Sampling efforts were suspended in late March 2007 after discovering that outflow volumes were far in excess of inflow volumes for large storms (Section 3.1). Flow monitoring and sampling attempts resumed in late April after confirming the existence of the problem. Until late July, water quality sampling was unsuccessful because all but one monitored storm had either too little inflow to produce outflow, or rainfall greater than approximately 1.3 cm, causing excess outflow to occur. The first successful sampling event, with a small amount of outflow, occurred on July 28, 2007. Also in July, a decision was made to include in the sampling effort storms that generated no outflow because of the scarcity of suitable sampling events with outflow. Flow and rainfall data were continuously logged and processed from April 25, 2007 to May 10, 2008, with the exception of approximately ten storms because of equipment malfunction or complete battery discharge.

2.1.3 Instrumentation and sampling protocol

The cell was designed with one inflow point and one outflow point so that all inputs and outputs to the system could be accounted for. One Avalanche portable

refrigerated sampler (Teledyne Isco) was placed adjacent to the inflow channel (Figure 2-4). Another Avalanche sampler was placed between the observation manhole and the cell outfall. A Teledyne Isco 730 Bubbler Flow Module was installed in each sampler to measure flow level. The samplers were installed on concrete pads and secured in locked fiberglass housings (Tracom). A Teledyne Isco 674 tipping bucket rain gauge (0.254 mm sensitivity) was installed on top of the outflow sampler housing. The rain gauge was located sufficiently far from trees to avoid error in rainfall measurement. Level and rainfall data were logged at one-minute intervals, the smallest time increment available.

Bubble meters were checked for drift every time clean bottles were installed in the samplers in preparation for the next event, and also immediately after each storm. Any discrepancy was noted in order to correct level readings from the previous event. Drift was minor to nonexistent and bubblers were promptly calibrated when necessary.

Inflow and outflow level data were subsequently converted to flow rates. Inflow data were converted using a general cutthroat flume equation with appropriate coefficients. Results were verified by plotting against the rating curve supplied by the manufacturer, with excellent agreement. Outflow data were converted by linearly interpolating between points in a rating table supplied by the manufacturer.

Suction tubes for retrieving samples were located at the head of the inflow channel and in the observation manhole. The tubes were oriented vertically, with the end of each tube approximately 6 mm from the bottom of the channel. The vertical orientation was chosen to minimize the potential for clogging. The tubes were held in place with PVC pipes securely anchored to the ground and to the observation manhole at the inflow and outflow points, respectively.

Threshold flow levels to enable sampling were chosen as a tradeoff between the ability to sample at the minimum flow level possible and the need to ensure a submerged sampling tube. Inflow threshold levels were 7 and 12 mm in the first two sampled events, but the threshold was subsequently increased to 15 mm. The outflow threshold level was 20 to 26 mm, gradually increasing over the course of the sampling period.

Four 5-L polyethylene sample bottles (Teledyne Isco) were used in each sampler. For the final sampling event (April 26, 2008) as well as numerous unsuccessful sampling attempts in 2008, these bottles were replaced with four 2-L glass jars to allow automatic collection of samples for total petroleum hydrocarbon (TPH) analysis. The same glass jars were used to collect grab samples for TPH analysis during the April 3, 2008 event. Teflon suction lines were used for all sampling efforts to avoid interference with TPH analysis. Glass jars could not be used for all events because the minimum sample volume required for all analyses (2900 mL), including TPH, exceeded the total jar volume. Glass jars with a larger volume did not fit into the sampler.

Up to four inflow bottles and three outflow bottles were filled for each event, depending on the duration of inflow and outflow. The fourth bottle in the outflow sampler remained empty to serve as a field blank. Several liters of deionized water (DI) were added to the empty bottle and agitated to create the blank solution.

Taking flow-weighted composites across multiple bottles was the original sampling intent. Each bottle would be associated with a fixed time interval and have a fixed number of subsamples, but the volume of each subsample would be proportional to the flow volume calculated within each subsample time interval. However, the inherent variability of storm events in terms of both intensity and duration, combined with the

need to meet minimum sample volumes for each bottle while avoiding overflow, caused the flow-weighted composite approach to be abandoned.

It was instead decided that each bottle would receive a simple composite, with a fixed number of subsamples and a fixed subsample volume. This approach made sample collection far more reliable. As a result, however, intervals of low flow volume have a greater influence on the final concentration in a given bottle than intervals with a high flow volume. The fact that a bottle may not reflect the true flow-weighted concentration is an inherent limitation of this sampling approach. Interpretation of these results assumes that the concentration in each bottle is a reasonable approximation.

The inflow sampler used a two-part program to allow two different sampling intervals. Inflow sampling was focused on the start of each event. For most events, 30 to 40% of the total inflow sampling duration was assigned to the first three bottles (approximately 30 minutes), with the fourth bottle assigned to the remaining duration (approximately one hour), if applicable. The relatively short sampling interval for the first three bottles was chosen in response to the short times to peak and short inflow durations observed for many storms. The outflow sampler also used a two-part program, with the entire sampling duration assigned to the first three bottles (typically 2 – 2.5 hours) and the fourth used as a field blank.

The two sampling efforts in April were designed to target larger storms. As a result, the sampling durations increased proportionally. The first three inflow bottles were associated with the first 45 – 72 minutes of inflow and the fourth inflow bottle collected samples for another 2 – 2.5 hours. The outflow sampling duration in these storms was approximately four hours.

2.1.4 Water quality analysis

The pollutants of interest for the water quality analysis were chloride, nitrate, total Kjeldahl nitrogen (TKN), total phosphorus (TP), lead, zinc, biochemical oxygen demand (BOD), total suspended solids (TSS), and total petroleum hydrocarbon (TPH).

Samples were kept cold ($1 - 3\text{ }^{\circ}\text{C}$, ± 1) by the refrigerated samplers until retrieval, after which they were transported to the University of Maryland, College Park Environmental Engineering Laboratory, dispensed into individual bottles, and delivered to the refrigerator at the contract laboratory.

All water quality analyses were performed by the Washington Suburban Sanitary Commission (WSSC) Laboratory Services Group (Silver Spring, Maryland). Chain-of-custody procedures were strictly followed. Table 2-1 lists the analytical method and minimum detection limit (MDL) for each pollutant.

TPH samples were limited to the final two events because practical constraints on bottle type (Section 2.1.3) led to the decision to focus on the other nine pollutants and use larger-capacity plastic bottles, which are not compatible with TPH analysis. Reaching the site in time to take TPH grab samples in glass jars proved to be difficult.

Fecal coliform was another pollutant of interest, but no analysis was performed. The six-hour hold time, combined with the inherent unpredictability of storm events, made delivery of samples during laboratory business hours and within the required time frame extremely difficult.

All plastic and glass bottles and caps were acid-washed for a minimum of 12 hours in 0.2 to 0.5 N HNO_3 and triple-rinsed with DI. During sampling standby periods, bottle caps remained wrapped in fresh aluminum foil to prevent contamination.

Table 2-1. Minimum detection limit (MDL) and analytical method for each pollutant. A range of MDLs is listed for several pollutants because MDLs varied by batch. MDL was not specified for TSS and TPH; instead, the reporting detection limit (RDL) is listed.

Pollutant	MDL (mg/L)	Method
Chloride	0.19	Lachat 10-117-07-1-B
Nitrate*	0.026 – 0.028	Lachat 10-107-04-1-A
TKN*	0.055 – 0.07	Lachat 10-107-06-2-D
TP*	0.042	Lachat 10-115-01-1-E
Lead	0.0001 – 0.0007	EPA 200.8, revision 5.4
Zinc	0.0007 – 0.0019	EPA 200.8, revision 5.4
BOD	0.95	Standard Methods 5210B
TSS	1 (RDL)	Standard Methods 2540D
TPH	5 (RDL)	EPA 1664

* Nitrate and total Kjeldahl nitrogen (TKN) are expressed as N; TP is expressed as P.

2.1.4.1 Quality verification

With the exception of a few BOD outflow results with a concentration of zero mg/L, and all but one total petroleum hydrocarbon (TPH) result, all concentrations in individual bottles and all EMCs were above the MDL.

Analysis of blanks from each event indicates that bottle cleaning and sample handling procedures were effective in preventing sample contamination. Generally, blank concentrations were either below the MDL (Table 2-1) or negligible compared to inflow and outflow EMCs. Some blank concentrations were close to several inflow or outflow EMCs. Overall conclusions regarding water quality performance remain unchanged, however. Table 2-2 summarizes blank results.

Table 2-2. Number and concentration range of blanks for each pollutant analyzed at the Kenilworth cell.

Pollutant	# blanks ≥ MDL	Conc. of blanks ≥ MDL (mg/L)	Comment
Chloride	4 of 9	0.19 – 0.51	Negligible compared to inflow and outflow
Nitrate*	0 of 10	n/a	
TKN*	7 of 10	0.073 – 0.41	Same order of magnitude as several EMCs, but lower than all EMCs
TP*	0 of 10	n/a	
Lead	4 of 10	0.0001 – 0.0019	MDLs varied; each blank was compared to its respective MDL. 0.0019 mg/L close to several outflow EMCs.
Zinc	10 of 10	0.0021 – 0.012	0.012 mg/L same order of magnitude as most outflow EMCs. Other blanks are negligible compared to inflow and outflow.
BOD	3 of 8	1.3 – 3.1	Close to several inflow and outflow EMCs but generally negligible
TSS	4 of 10**	1 – 14	14 mg/L (7/28/07) is half the event outflow EMC. Others are negligible.
TPH	0 of 2**	n/a	

* Nitrate and total Kjeldahl nitrogen (TKN) are expressed as N; TP is expressed as P.

** Based on reporting detection limit (RDL) because MDL was not specified.

2.2 Metal accumulation

The investigation of metal accumulation in bioretention media consisted of efforts to observe flow patterns and delineate sampling locations, collection of surface and core media samples, three metal extraction procedures, and measurement of media pH and organic content.

2.2.1 Site description

The site consists of a pair of bioretention cells treating a total of 0.25 ha of a commuter student parking lot (Lot 11) at the University of Maryland, College Park, Maryland (Figure 2-1). The site is located in the watershed of Paint Branch, a major tributary of the Anacostia River. The drainage area is entirely asphalt pavement, with no buildings or vegetation. Paired cells were constructed to accommodate an existing subsurface utility line that bisects the site. The cells were completed in May 2003 and have been operational to the present. All research for this project was conducted at the east cell (Figure 2-7). The east cell was selected because its vegetation was less dense, allowing greater access to the cell surface; and because of its closer proximity to a nearby stream to assist in an initial flow pattern investigation (Section 2.2.2).

Sheet flow from Lot 11 enters a wide, shallow channel at the southeast corner of the parking lot. The channel immediately splits, dividing the flow evenly between two concrete channels that each lead to one cell (Figure 2-7). The surface area of the east cell is 25 m², with a length-to-width ratio of approximately 5.0. (The other cell is similarly sized.) The east cell has a media depth of approximately 0.9 m and is lined with impermeable plastic to precisely quantify the inflow and outflow.



Figure 2-7. June 2003 photograph of Lot 11 east cell. A second cell is located below bottom of image. Inflow from Lot 11 is evenly split between two concrete channels. Outflow enters Campus Creek, to the right of the cell. Note sediment deposition at the end of the inflow channel.

The primary flow path is percolation downward through the media layers, with a total depth of approximately 0.9 m. After the media becomes saturated, water enters a 15 cm perforated PVC underdrain, which is located along the centerline of the cell. The underdrain empties into an overflow manhole. During a storm, surface water storage may accumulate approximately 27 cm, above which overflow into the manhole occurs. The manhole drains to Campus Creek, a tributary of Paint Branch.

The cell has not been maintained in most respects. Notably, the mulch layer has not been replenished from the end of construction to the present. This neglect is beneficial from a research standpoint because the media and accumulated metals have not

been significantly disturbed by human activity over the lifetime of the cell. Trash has been allowed to accumulate, especially near the end of the inflow channel. It is unknown whether periodic trash removal occurs.

Prior to January 2008, cell vegetation had little or no maintenance and had been thriving from a biomass standpoint (Figure 2-8). With the surviving original stock augmented by colonization, including invasives, the cell was densely vegetated during the growing season. In late January 2008, all vegetation except the largest trees was removed by University maintenance staff (Figure 2-8). The activity appears not to have disturbed the media. A robust vegetative cover was naturally reestablished during the 2008 growing season.



Figure 2-8. *Left:* Vegetative cover in August 2006, with a density typical of the growing season. *Right:* Photograph taken from approximately the same location in February 2008 after vegetation removal by University maintenance staff spared only the largest trees.

To facilitate previous research/demonstration on runoff denitrification, the east cell was constructed with a 0.3 m thick anaerobic sump layer containing a sand and

shredded newspaper mixture. The sump is located below the bioretention soil media (BSM) and the invert of the underdrain (Davis 2007). The sump is the only major design feature differentiating the two cells and was not a factor in this investigation.

2.2.2 Flow patterns

Observing flow patterns across the surface of the cell was a critical first step in the analysis. This process provided a means to justify the selection of media sampling locations. In addition, it was hypothesized that knowledge of flow patterns would help to explain the spatial distribution of metal accumulation on the cell surface. The underlying assumption is that major flow patterns are consistent from storm to storm and changes to the preferential flow path occur only gradually.

A portable pump was used in August 2006 to simulate stormwater flow into the cell by pumping water from the adjacent Paint Branch to the concrete channel leading to the cell (Figure 2-9). Approximately three-quarters of the accumulated trash in the cell was removed prior to the start of the test to minimize any potential influence on the resulting flow patterns. Tracer dye (Bright Dyes Fluorescent Yellow/Green tablets, Kingscote Chemicals) allowed clear observation of the flow patterns throughout the test. Dye tablets were suspended in a mesh tea strainer in the inflow channel and were periodically replaced upon dissolving.



Figure 2-9. August 2006 flow test. *Left:* Pumping water from Paint Branch. *Right:* Water enters the east cell via the right-facing inflow channel to simulate a rainfall event.

The total inflow time was 90 minutes. The flow rate was kept relatively constant except for an increase of approximately 25% at 17 minutes to speed the progress of the test. As much inflow as possible was directed into the east cell (Figure 2-9). A level reading in the Parshall flume in the inflow channel at 45 minutes indicated an inflow rate of approximately 4.2 L/s. Using the Rational Formula with $C = 0.95$ and $A = 0.13$ ha (half the drainage area), the equivalent rainfall intensity is 1.3 cm/hr.

In first minute of inflow, all water infiltrated in a small area (approx. 0.1 m^2) in front of the inflow channel. Subsequently, a flow path began to form on the east (right) side of the cell (Figure 2-10). A second flow path formed at three minutes, ultimately wrapping around the top of the cell and paralleling the west side. A third, smaller trickle appeared at about 10 minutes, roughly following the centerline of the cell. Throughout the flow test, the flow path on the east side of the cell remained dominant.

Inflow stopped advancing forward from the 15 to 20 minute mark, instead pooling at a location approximately 2.7 m from the inflow point. Subsequent inspection found a subtle ridge across the width of the cell at that location. The flow rate was increased at

17 minutes, as noted above. At 20 minutes, water resumed advancing toward the back of the cell. Forward movement paused again for several minutes at the 28 minute mark. The cell was now wet across its entire width up to 5.0 m from the inflow point, but was dry in front of that point except for a small trickle on the right side.

The entire cell surface was wet at 40 minutes and steady flow from the underdrain into the manhole was observed. Underdrain flow may have begun earlier. Tracer dye indicated that the main flow path continued to follow the east side, with a secondary path on the west side. Dye diffused from both sides toward the center of the cell.

At 70 minutes, the water had risen to a point almost level with the bottom of the inflow channel, up to approximately 27 cm above the cell surface. Tracer dye indicated that the water was no longer following the previous flow paths. Instead, inflow leaving the channel continued straight into the cell without changing direction. Pondered water overflowed into the manhole around the 70 minute mark.

Pondered water drained within approximately 2.5 hours after halting inflow, indicating good hydraulic performance despite the lack of maintenance over the four-year operating life of the cell. Given a ponding depth of approximately 27 cm, the estimated infiltration velocity is 11 cm/hr under saturated or nearly-saturated conditions. Using a double-ring infiltrometer, Dietz and Clausen (2005) measured infiltration velocities of 12.6 and 10.3 cm/hr in BSM of similar textural classification to this cell's. Subsequent observations during actual rain events found flow patterns similar to this test.

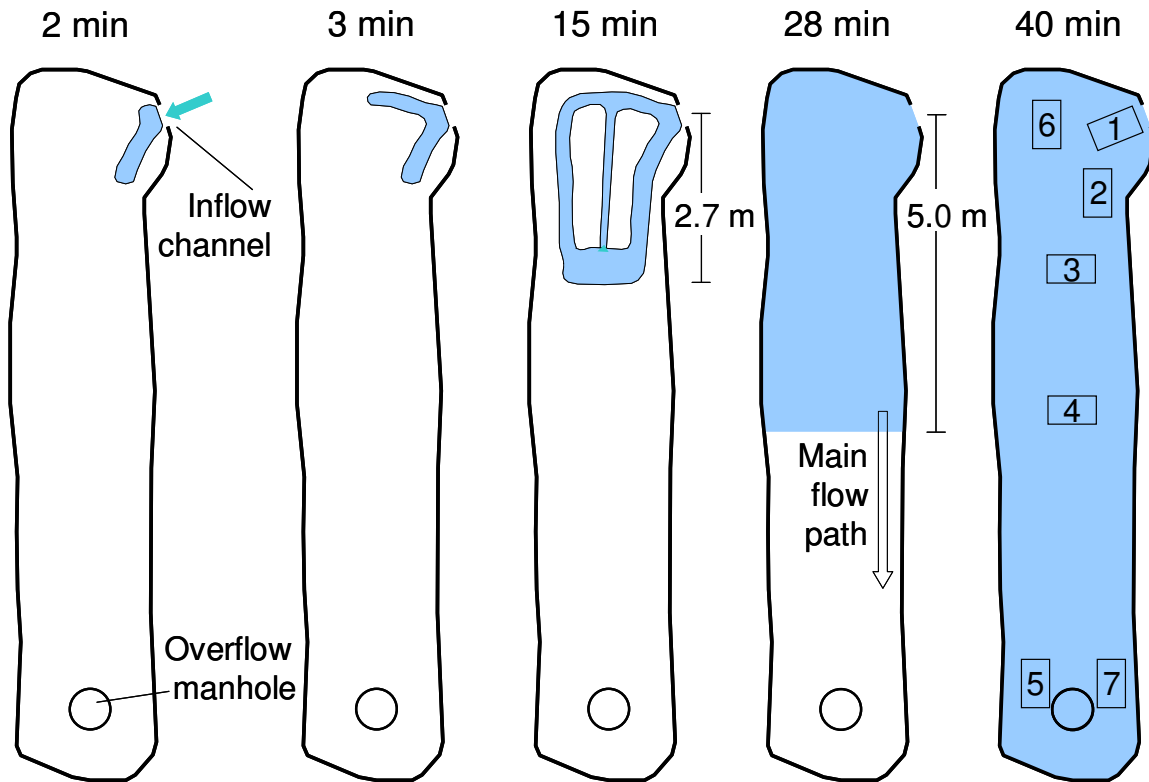


Figure 2-10. Development of flow patterns during the flow test. Forward movement of water paused for several minutes at the 15 and 28 minute marks at the locations shown. Zones delineated for the purposes of media sampling are shown to scale (Section 2.2.3).

2.2.3 Zone delineation

Seven 45 x 75 cm zones were delineated for collecting media samples. The locations of each zone are shown in Figures 2-10 and 2-11. A measuring tape was permanently extended between the center of the overflow manhole and a cleanout pipe near the inflow channel. This served as the “axis” of the cell and as the reference point for the delineation of zones. The location of each sampling point was recorded in terms of its position along the tape and its perpendicular distance to the tape.

Zones 1, 2, 3, 4, and 7 are located along the main flow path, as identified in the flow test. Zone 1 covers most of the area first contacted by inflow; Zone 2 is just

downstream. Portions of Zone 1 have been subject to scouring and sediment deposition (Figure 2-7). No other zone shows evidence of similar activity. Zones 3 and 4 are located at the two points at which the forward movement of water paused for several minutes during the flow test (Figure 2-10). Zones 7 and 5 are located on opposite sides of the overflow manhole. Based on its location at the back of the cell and away from the main flow path, Zone 5 is believed to be the “driest” area of the cell, or the area least frequently wetted. Zone 6 is located outside of the main flow path, but adjacent to the inflow area. Samples were taken from Zone 6 to gauge the effect of proximity to the flow path on metal accumulation.

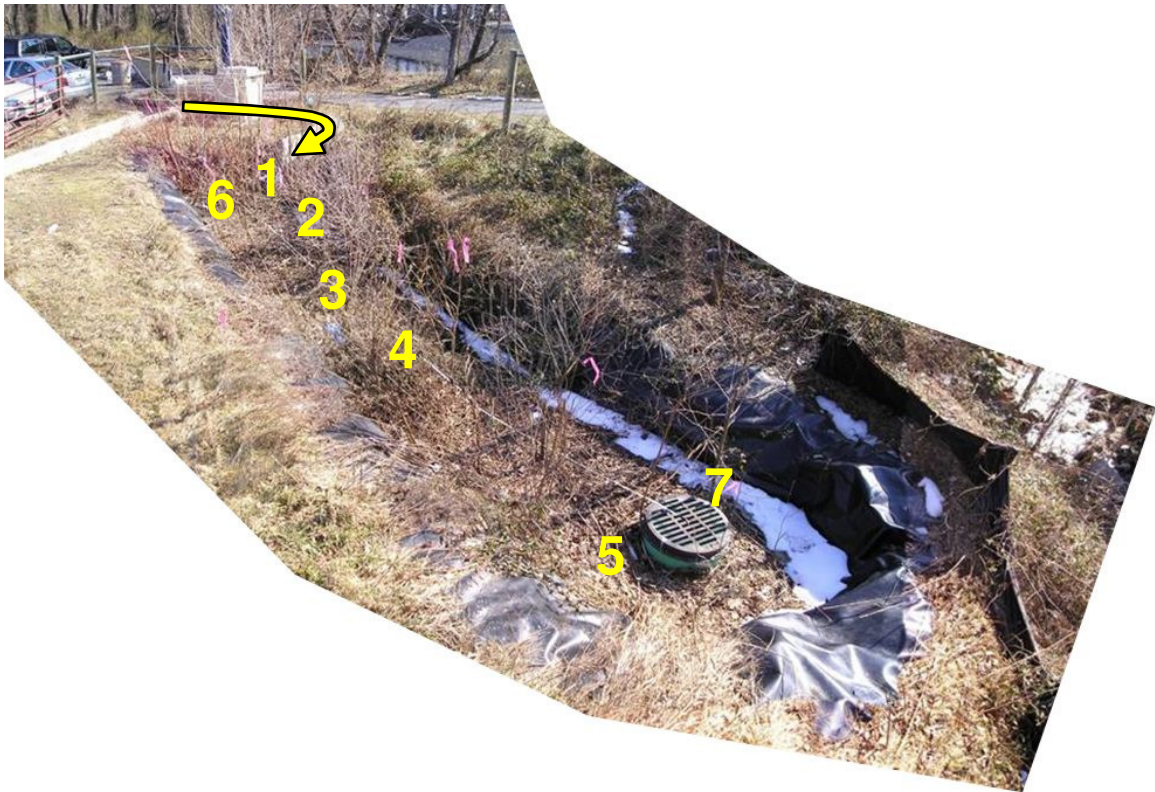


Figure 2-11. Location of each zone as shown on a February 2007 photograph. The inflow channel is indicated by an arrow. (The curvature was created by photo stitching.)

2.2.4 Media sampling and analysis

In all zones, the top several cm of the media profile consists of a dark-colored layer that will be referred to as the “organic layer” (Figure 2-12). This layer is distinct from the underlying bioretention soil media (BSM), which is a mixture of sand, topsoil and mulch, and occupies the remainder of the media profile (Section 4.1).



Figure 2-12. Typical media profile in the Lot 11 cell, as shown in a Zone 7 core sample. The darker organic media (left) occupies the top 5 cm in this core, followed by a sharp transition to the BSM layer (right).

2.2.4.1 Surface samples and total metal

Surface sampling occurred in September 2006. Loose debris was first cleared away from the top of the media profile at the sampling locations. Three surface samples were taken at different points in each zone, using a fresh plastic spoon for each sample. Each sample covered an approximately 7 cm² area and extended approximately 2.5 cm deep. A total of 21 surface samples were collected and their locations were recorded.

Samples were air-dried for several days. Each sample was then crushed by hand within an individual bag for one minute and sieved with a 2 mm mesh. Passing material was oven-dried at 103-105 °C for at least three days. Organic matter (OM) content was subsequently analyzed by loss on ignition (Section 2.2.4.4).

Surface samples were analyzed for total metal with the U.S. Environmental Protection Agency (EPA) 3050B method (EPA 1996). Two replicates of each sample

were extracted independently. One control without media (blank) was carried through the process for each of five batches of surface samples (Section 2.2.4.6).

The 3050B method calls for 1.0 g of 103 °C-dried media to be extracted using 1:1 HNO₃ (Fisher Scientific), followed by concentrated HNO₃ (Fisher Scientific), 30% H₂O₂ (Fisher Scientific) and concentrated HCl (J.T. Baker). A conical flask covered by a watch glass was used as the extraction vessel for each sample. A glass shard was securely taped to the side of each flask to prop the watch glass and allow venting. Samples were refluxed on an electric skillet at 95 °C ± 5 °C without boiling throughout the extraction, with cooling between each step. Finally, extracts were filtered through Whatman No. 41 filter paper, diluted to 50 mL in volumetric flasks with deionized (DI) water, and transferred to 50 mL plastic centrifuge tubes for storage.

The HNO₃ step was modified from the published procedure, which calls for periodic additions of 5 mL concentrated HNO₃ until brown fumes cease to be generated, indicating complete reaction of organic matter with the acid. The high organic content in some samples caused this step to become laborious because of the large volume of acid to be evaporated. To standardize the process for all samples, HNO₃ addition proceeded in three stages, with volumes of 15, 10 and finally 5 mL. Each addition was followed by a two-hour reflux period and at least ten minutes of cooling before the next HNO₃ addition.

Metal concentrations in the extracts were analyzed by atomic adsorption spectrophotometry (AAS; Section 2.2.4.5). Copper, zinc, and initially lead were analyzed in the flame module. It was later determined that extract lead concentrations were close to the flame quantitation limit, causing erroneously high results. Lead was re-analyzed in the furnace module after manually diluting extracts by a factor of 5 to 10.

In all laboratory analysis, plastic- and glassware were thoroughly cleaned with detergent and tap water, submerged for a minimum of 12 hours in 0.2 to 0.5 N HNO₃ acid wash, and triple-rinsed with deionized water (DI). Extractions involving hazardous reagents were carried out under a fume hood, with appropriate personal safety equipment. To avoid sample contamination, nitrile gloves were worn when handling media samples directly and when handling acid-washed items.

2.2.4.2 Core samples and sequential extraction

Core samples were collected in December 2006 after the surface samples were analyzed. The 2.5 cm-diameter, 90 cm-long Hoffer Soil Sampler (JBK Manufacturing) was initially cleaned by soaking overnight in an approximately 9% disodium EDTA solution and rinsing with DI water. Loose debris was cleared away from the top of the media profile at each sampling location. One core sample was taken near the center of each zone and its location was recorded. The sampling depth was 90 cm, retrieved in three to four passes to minimize media compression. After each pass, the sampler was wiped with an EDTA-soaked cloth, rinsed thoroughly with DI water, and dried with paper towels. Sampling in Zone 4 ended at 63 cm when the sampler hit the underdrain.

Cores were carefully divided into segments with a clean plastic knife immediately after sampling. Upper cores had a sharp transition between the organic and BSM layers, which provided a convenient point at which to divide the cores and segregate media types (Figure 2-12). BSM appearance was uniform with depth, although the deepest cores were saturated with water. The organic layer was subdivided into 2.0 or 2.5 cm long segments if the total organic layer depth was at least 4 cm. The BSM layer was

subdivided into segments ranging from 3 to 30 cm long. Table B-2 lists the segment lengths in each core.

Compression of the media during sampling was taken into account when dividing the cores into segments. The upper portion of each core, including the organic layer, typically did not compress. At greater depths, resistance to the sampler caused the samples to begin to compress, as indicated by the top of the core sinking below the media surface. The current insertion depth was noted at the onset of compression. Portions of the core sample below that depth were assumed to experience the same compression ratio, and portions above that depth were considered to be uncompressed. The compression ratio, used to correct for segment lengths when segmenting compressed portions of the core, is the ratio of the length of the compressed portion to the length of the corresponding depth interval in the media profile. Deeper cores could not be monitored for compression. Segment lengths in these cores were corrected by applying the ratio of total core length to total insertion depth.

Core sampling attempts in Zone 1 were unsuccessful. Pebbles and roots in the BSM layer obstructed the sampler and caused significant compression. Instead, a sample pit was dug to retrieve the top 27 cm of media. This approach has less precision with respect to depth, and a greater potential for cross-contamination, but was determined to be the best alternative to the sampler. Samples were excavated from the wall of the pit, at increments noted in Table B-2, using a clean plastic knife each time. For the upper intervals, a clean sample bag was inserted below each excavation point. For two deeper intervals, material was caught in an aluminum dish that was taped to a dowel and

replaced for each sample. The sampler successfully retrieved cores between 33 and 90 cm. Samples were not taken from the 27 – 33 cm interval.

Each core segment was air-dried for several days. While still in the bag, the segments were crushed by hand for one minute. Segments were then sieved with a 2 mm mesh. For further homogenization, passing particles were crushed between clean paper towels with a rolling cylinder. To minimize changes in chemical affiliation between the metals and media constituents, the samples were not oven-dried. To correct for the difference between the air-dried and oven-dried mass, two samples of each segment from the organic layer and selected segments from the BSM layer were precisely weighed and oven-dried at 103-105 °C for at least three days. The water content of each sample was then determined from the oven-dried mass and a correction factor was calculated.

A sequential extraction procedure was applied to all organic segments and one-third of BSM segments to find total metal and metal strength of affiliation with media. Initial findings for BSM segments indicated low metal concentrations and consistent fractionation. The remaining BSM segments, from the deepest portions of the media profile, were analyzed only for total metal with the EPA 3050B method (two replicates; Section 2.2.4.1). Tables B-3 – B-5 each list the extraction method used on each segment.

The five-step sequential extraction used the method of Li and Davis (2008a), adapted from Ahnstrom and Parker (1999). Two 0.5 g replicates of each sample were extracted independently. One control without media was carried through the process with each batch, resulting in one control per fraction per batch (Section 2.2.4.6). Tables 2-3 and 2-4 list the sequential extraction procedure and reagent specifications. Acids for

extractions and pH adjustment are trace metal grade (TMG). Unless otherwise noted, other chemicals are ACS reagent-grade or better.

All extractions occurred in 15 mL plastic centrifuge tubes. Each media sample remained in its respective tube throughout the entire process. Fractions F3 – F5 were extracted with the tubes submerged in a water bath at the specified temperature. Samples were centrifuged at 3000 RPM for 10 minutes at the end of each extraction step. The separated extract was poured into a 60 mL syringe and filtered through a 0.2 µm pore size, 25 mm diameter membrane disk filter (Millipore Express PLUS or Pall Supor-200). Filtered extracts were diluted to 50 mL with DI water in volumetric flasks and transferred to 50 mL plastic centrifuge tubes for storage. One to two drops of TMG HNO₃ were added to each extract, although F2 – F4 are well-buffered and F5 is highly acidic. After each extraction step, 1.5 mL of 0.1 M NaCl was added to the solid residue in each tube.

Tubes were refrigerated between extraction steps. The lag time between extraction and analysis caused mold to grow in some extracts. These were re-centrifuged and re-filtered as above; no substances were added. Metal concentrations in the extracts were analyzed by AAS (Section 2.2.4.5). Zinc was analyzed in the flame module; copper and lead were analyzed in the furnace module.

Table 2-3. Sequential extraction procedure for Pb, Cu, and Zn follows the method of Li and Davis (2008a), which is adapted from Ahnstrom and Parker (1999).

Step	Fraction	Extraction procedure	Solid:liquid ratio (g:mL)
F1	“Soluble-exchangeable”	0.1 M Sr(NO ₃) ₂ (4 hr). Rotate at 24 RPM at room temperature.	1:16
F2	“Sorbed-carbonate”	1 M Na-acetate (pH 5, 5 hr). Adjust pH with TMG glacial acetic acid. Rotate at 24 RPM at room temperature. Open cap occasionally to expel CO ₂ .	1:16
F3	“Oxidizable”	5% NaOCl (pH 8.5, 1.5 hr, 90-95 °C, in water bath). Adjust pH with TMG HCl. Vortex three times during extraction. Open and close cap before vortexing to vent gases.	1:8
F4	“Reducible”	0.2 M oxalic acid + 0.2 M NH ₄ oxalate + 0.1 M ascorbic acid (pH 3, 1.5 hr, 90-95 °C, in water bath). Adjust pH with TMG NH ₄ OH. Vortex three times as in F3. Add a drop of toluene to extracts.	1:25
F5	“Residual”	Aqua regia (3 parts HNO ₃ + 1 part HCl, 1.5 hr, 70 °C, in water bath). Dispense each acid into the tubes individually. Vortex three times as in F3.	1:16

Table 2-4. Specifications of sequential extraction reagents, listed in order of Table 2-3.

Reagent	Formula	Manufacturer	Trace impurities (mg/L)
Strontium nitrate	Sr(NO ₃) ₂	J.T. Baker	Heavy metals as Pb: <3
Sodium acetate	CH ₃ COONa	J.T. Baker	Heavy metals as Pb: <5
Acetic acid, glacial	CH ₃ COOH	Fisher Scientific	TMG
Sodium hypochlorite	NaOCl	Fisher Scientific	Not specified
Hydrochloric acid	HCl	Fisher Scientific	TMG
Oxalic acid	(COOH) ₂ • 2H ₂ O	Fisher Scientific	Heavy metals as Pb: 3
Ammonium oxalate	C ₂ H ₈ N ₂ O ₄ • H ₂ O	Acros	Not specified
Ascorbic acid	C ₆ H ₈ O ₆	J.T. Baker	Not specified
Ammonium hydroxide	NH ₃ [aq]	Fisher Scientific	TMG
Toluene	C ₆ H ₅ CH ₃	J.T. Baker	Pb <0.2, Cu 0.003
Nitric acid	HNO ₃	Fisher Scientific	TMG

2.2.4.3 Bioavailability sampling and analysis

Additional samples were collected in August 2008 to estimate the bioavailability of lead in bioretention media. Zones 1, 2, 3, and 6 were targeted because of their proximity to the inlet. Loose debris was first cleared away from the top of the media profile at the sampling locations. A fresh plastic spoon was used for each sample. A total of nine samples were taken at the surface and up to 12 cm deep, including organic media and BSM. Their locations and depths were recorded. Particles from the inflow channel were also collected. Table B-6 lists the depth and media type for each sample.

Samples were air-dried for one day and then gently crushed by hand before oven-drying for three days at 37 °C. Each oven-dried media sample was passed through a 250 µm sieve. The passing material was used for all analyses. A correction factor for each sample's equivalent 103 °C-dried mass was calculated by drying a separate portion of each sample at that temperature. Total lead was analyzed for two replicates per sample with the EPA 3050B method (Section 2.2.4.1). Extracts were manually diluted by a factor of 10 to 40 and analyzed by furnace AAS (Section 2.2.4.5). Media pH and OM content were determined with the methods described in Section 2.2.4.4.

Lead bioavailability was measured with the EPA *in vitro* method, a simple model for human stomach conditions (EPA 2008a). The extraction fluid is a buffered solution of 0.4 M glycine (Fisher Scientific), brought to pH 1.5 with TMG concentrated HCl. The method calls for 1.0 g media to be extracted in 100 mL of solution for one hour at 37 °C. Additional detail is provided in EPA (2007) and Drexler and Brattin (2007). In lieu of the rotating water bath apparatus specified by the method, samples were rotated end-over-end (30 RPM) inside an incubator at 37 °C. Two replicates of each sample

were extracted and a control was carried through the process. The extraction fluid pH was checked for all samples at the end of the procedure. All values remained within 0.5 units of pH 1.5, indicating that media was not significantly buffering the fluid.

After a brief settling period, extraction fluid was poured into a 60 mL syringe and filtered through a 0.2 µm pore size, 25 mm diameter membrane disk filter (Millipore Express PLUS or Pall Supor-200). Extracts were stored in 50 mL plastic centrifuge tubes, then manually diluted by a factor of 5 to 10 and analyzed by furnace AAS (Section 2.2.45). *In vitro* lead bioaccessibility (IVBA) of each sample was calculated using Equation 2-1.

$$\text{IVBA} = \text{IV extractable lead (mg/kg)} / \text{Total lead (mg/kg)} \quad (\text{Eq. 2-1})$$

IVBA results were converted to relative bioavailability (RBA) using Equation 2-2. The equation is a linear regression between IVBA and *in vivo* RBA in swine for 19 soil samples impacted by mining and milling activity ($R^2 = 0.924$; EPA 2007).

$$\text{RBA} = 0.878 * \text{IVBA} - 0.028 \quad (\text{Eq. 2-2})$$

Finally, RBA values were converted to absolute bioaccessibility (ABA) estimates based on the assumption that the typical ABA of lead in food and water is 50% in children (Equation 2-3; EPA 2007).

$$\text{ABA} = \text{RBA} * 0.50 \quad (\text{Eq. 2-3})$$

2.2.4.4 Media pH and organic matter

Media pH was measured using the method of Hendershot et al. (1993), and was not measured in surface samples. One replicate of each sample was suspended in 0.01 M CaCl₂ (J.T. Baker). Samples were typically analyzed using 0.5 g media in 5 mL solution. A few samples had less than 0.5 g available, but in all cases the pH electrode tip was submerged without contacting settled material. Media and solution were dispensed into 14 mL culture tubes and the tops were sealed with Parafilm. The tubes were agitated every five minutes for 30 minutes before standing for an additional hour. Measurements were performed with a Thermo Orion 720A+ meter and Thermo Orion ROSS Ultra Combination pH electrode. Buffer solutions at pH 4, 7, and 10 were used for calibration.

OM content was estimated by loss on ignition (APHA et al. 1995) after media was dried at 103 °C for at least three days. Two replicates of each sample were used, with a typical replicate mass of 0.4 – 1.0 g. Some core segments had less media available and as little as 0.1 g per replicate was used. For each sample, the masses of a clean aluminum dish and oven-dried media were recorded before igniting at 550 °C for a total of one hour. The combined mass of the dish and media was measured after each ignition and a cooling period. Two 30-minute ignitions were used for organic media samples. In all cases, the additional mass lost in the second ignition was small or negligible compared to the total mass lost, confirming that the 60-minute ignition time was sufficient. Some BSM samples were ignited for a continuous 60-minute period as a result. OM content was calculated as the percentage of 103 °C-dried mass lost on ignition.

2.2.4.5 Measurement of metal concentrations

A Perkin-Elmer 5100PC atomic absorption spectrophotometer was used for all AAS analysis. Flame analysis employed an air-acetylene mixture. For furnace analysis, a 5100ZL furnace module was used, with transversely heated graphite atomizer (THGA) tubes and argon as an inert gas. The furnace rinsing solution was 2% TMG HNO₃. Standard furnace maintenance was performed when replacing the graphite tube every 200 to 300 firings. Element-specific hollow cathode lamps (HCL) were the energy source.

All calibrations used a minimum of four standards, not including a DI blank. Only calibrations with $R \geq 0.999$ were accepted. Table 2-5 lists all calibration ranges that were used. Extract concentrations were adjusted to fall within the calibration range by first manually diluting with DI. Additional auto-dilution was performed by the furnace module using DI, up to a dilution factor of 5.0.

Table 2-5. Calibration ranges and quantitation limits for AAS analysis. Quantitation limits are taken to be the lowest standard in each calibration and are listed in terms of the equivalent media concentration (mg/kg).

	Pb	Cu	Zn
Flame range (mg/L)	n/a	0.1 – 1.0	0.05 – 1.0
Flame limit (mg/kg)	n/a	5.0	2.5 and 5.0*
Furnace range (µg/L)	2 – 100	2 – 60	n/a
Furnace limit (mg/kg)	0.2	0.2	n/a

* Zinc quantitation limits are 2.5, including and 5.0 mg/kg for 3050B and sequential extractions, respectively, because the methods used different media masses.

Subsequent data processing was straightforward. Media metal concentrations were calculated from extract concentrations by accounting for sample mass, final extract volume, manual- and auto-dilution ratios, and the ratio of oven-dried to air-dried mass.

Any sample replicate with a media concentration below the appropriate quantitation limit (Table 2-5) was assigned a value of half the quantitation limit. This value was used in all subsequent analysis of results.

2.2.5 Quality control and verification

Several previously-discussed practices helped to maintain data integrity, including conducting all extractions and OM analysis in duplicate, practicing proper sample handling and equipment cleaning, and performing regular instrument maintenance. Practices discussed below were used to control, verify, and quantify data quality.

2.2.5.1 AAS protocol

Each extract was analyzed in duplicate, with two flame readings or two furnace ignitions. The calibration was checked for drift by analyzing a standard after every 10 samples. The instrument was re-calibrated if the result varied by more than $\pm 10\%$ from the concentration of the standard, and in many cases if more than a $\pm 5\%$ difference was found. Reliability of the furnace auto-dilution feature was periodically verified by comparing the result for an auto-diluted extract against a different auto-dilution ratio or a manual dilution.

2.2.5.2 Controls without media

Controls without media (blanks) were carried through each batch of extractions. Most control concentrations are below the smallest standard (Table 2-5) for the given metal and analysis method. Table 2-6 summarizes the results of the control analysis.

Table 2-6. Number and concentration range of controls above the smallest standard (SS) for sequential extraction and 3050B methods.

Value	Pb	Cu	Zn
Sequential extraction SS	2 µg/L	2 µg/L	n/a
# Sequential controls above SS	5 of 18	15 of 18	3 of 18
Conc. of seq. controls above SS	2.8 – 13 µg/L	2.0 – 13 µg/L	0.05 – 0.09 mg/L
3050B SS	n/a	0.1 mg/L	0.05 mg/L
# 3050B controls above SS	4 of 13	0 of 13	4 of 12
Conc. of 3050B controls above SS	2.6 – 15 µg/L	n/a	0.06 – 0.07 mg/L

All control concentrations exceeding the smallest standard are inconsequential when expressed in terms of the corresponding media concentration. All four lead F3 controls are above the smallest standard, possibly as a result of minor contamination from the NaOCl reagent. The *in vitro* extraction control is below the smallest standard. The maximum value of copper sequential extraction controls is 13 µg/L, but the other 14 control concentrations are smaller, not exceeding 6.1 µg/L. Such copper control results occur in all five fractions, suggesting a consistent but minor background source of copper contamination throughout the sequential extractions. The three zinc sequential extraction controls above the smallest standard are all from the same batch (F3 – F5 controls).

2.2.5.3 Comparison of results between methods

The sequential extraction (SE) and 3050B procedures use different reagents and methodologies. Total metal was measured directly with the 3050B method and was calculated as the sum of the five fractions from the sequential method. Three core segments and the original BSM were analyzed using to both methods to compare the methods' recoveries. Segments were selected that had high metal concentrations and

enough remaining media for at least one 3050B analysis. Segments 2A and 6A had only approximately one gram remaining, enough for one replicate. Segment 1A and the original BSM were analyzed in duplicate.

The sample size is too small to definitively characterize differences in recovery between the two methods, but the results suggest that agreement is generally good (Table 2-7). A major exception is the pair of segment 6A copper results, which may be caused by one or more incomplete SE steps, contamination during sample handling or 3050B extraction, or media heterogeneity. Zinc generally has excellent agreement, possibly because total zinc is an order of magnitude higher than total copper and lead. Lead has a somewhat lower recovery from 3050B extractions as compared to sequential results.

Table 2-7. Comparison of total metal results between sequential extraction and 3050B methods for three core segments and original BSM.

	Pb (mg/kg)	Cu (mg/kg)	Zn (mg/kg)
1A - Sequential	35 – 36	31 – 36	177 – 184
1A - 3050B	27 – 36	40 – 41	178 – 180
2A - Sequential	60 – 65	45 – 51	239 – 255
2A - 3050B	53	49	252
6A - Sequential	30 – 31	16 – 17	122 – 123
6A - 3050B	26	58	122
Orig. BSM - Sequential	6.3 – 6.7	11 – 13	29 – 31
Orig. BSM - 3050B	2.6 – 2.7	10 – 13	16 – 20

2.2.5.4 Reproducibility

All metal and OM content analysis was carried out in duplicate. (Media pH was measured for one replicate per sample.) Reproducibility of the analysis for each sample

can be quantified using the relative standard deviation (RSD). RSD is a percentage calculated for each sample using the standard deviation (SD) and mean of the two replicates, as shown in Equation 2-4.

$$\text{RSD} = 100 * \text{SD} / \text{Mean} \quad (\text{Eq. 2-4})$$

Aggregated for each dataset (metal and analytical method), individual RSD values cover a wide range, from zero to nearly 80% in some datasets. An RSD of 10% was designated as a metric for good reproducibility. As shown in Table 2-8, 60 to 90% of samples in all datasets have $\text{RSD} \leq 10\%$, indicating generally good reproducibility. Zinc datasets have a higher proportion of analyses with $\text{RSD} \leq 10\%$ than lead or copper, possibly because higher zinc concentrations lead to more consistent results.

For total metal, lead and zinc have greater reproducibility in sequential extractions than in 3050B extractions; copper reproducibility is nearly the same. With all five fractions aggregated, sequential extraction fractions have lower reproducibility than sequential extraction totals. This finding may indicate that summing five fractions to obtain total metal may cancel out positive and negative differences between replicates in individual fractions.

Table 2-8. Reproducibility of media analyses, as expressed by relative standard deviation (RSD). All samples were analyzed in duplicate. The analysis excludes samples with one lost replicate and those with both replicates below the quantitation limit (Table 2-5). Sequential fractions include F1 – F5 (Section 2.2.4.2). Surface and some core samples were analyzed by the 3050B method (Section 2.2.4.1). Bioavailability samples were analyzed for total lead using the 3050B method.

Dataset	Number of samples	Percent of samples with RSD \leq 10%
Pb sequential fractions	100	63
Cu sequential fractions	115	63
Zn sequential fractions	100	76
Pb sequential totals	25	76
Cu sequential totals	25	72
Zn sequential totals	25	84
Pb 3050B totals	48	60
Cu 3050B totals	37	73
Zn 3050B totals	39	74
Pb - <i>in vitro</i> extractable	10	90
Organic matter content	65	71

In vitro-extractable lead has the highest reproducibility of any dataset. Of the 10 *in vitro* results, nine have RSD \leq 10%. This may be caused by the relatively simple *in vitro* extraction methodology or by the fact that media for this analysis was sieved through a much smaller mesh size than for the other analyses.

The 10% RSD metric does not capture scenarios in which replicates have a high RSD but an insignificant absolute difference (e.g., when metal concentrations or OM contents are low). From a practical standpoint, reproducibility is therefore likely higher than stated in Table 2-8. For all datasets except for OM content and bioavailability, samples with the highest values generally had the lowest RSD.

RESULTS AND DISCUSSION – BIORETENTION MONITORING

3.1 Hydrology

3.1.1 Storm event characterization

Inflow, outflow, and rainfall data were collected for 65 events from April 25, 2007 to May 10, 2008 to characterize the performance of the Kenilworth bioretention cell. Periods of rain separated by at least six hours without rain were considered to be separate events. Table 3-1 lists the total rainfall depth and duration for all events.

Owing to the fact that the monitored events are the basis for all analysis, an important consideration is the extent to which they are representative of the long-term distribution of all events at the site. Frequency distributions were developed for the 65 monitored events and for 4 years of continuous local rainfall data, collected 5.0 km from the Kenilworth site at Station 6 of the Beltsville Agricultural Research Center.

As shown in Table 3-2, the frequency distributions of the two data sets agree reasonably well. The Kenilworth data set is skewed toward events with a smaller depth and duration, with the largest deficits in events within the 12 – 24 hour duration range and events between 25 and 60 mm of rainfall. A possible explanation is that approximately five Kenilworth events were not analyzed because of 1) winter precipitation or 2) excessive sediment deposition in the inflow channel that was believed to have invalidated the inflow level measurement. The Kenilworth data set excludes snow/ice events, while Beltsville data include all precipitation types.

Table 3-1. Rainfall depth and duration for all 65 events at the Kenilworth bioretention cell. Stormwater quality samples were collected for events listed in bold italics. Sampling for the Sep. 10, 2007 event was limited to the first burst. Events with complete capture are shaded gray. Asterisk and double asterisk denote events with truncated outflow hydrographs and with no inflow, respectively.

Date	Depth (mm)	Duration (hr)	Date	Depth (mm)	Duration (hr)
4/25/07	1.5	0.5	11/26/07	1.3	0.3
4/26/07	6.9	10	<i>12/2/07</i>	<i>6.4</i>	<i>4.1</i>
5/12/07*	11	1.0	12/6/07**	3.3	4.1
5/13/07	1.3	0.4	12/7/07	4.6	10
5/16/07	1.5	0.1	12/16/07*	22	13
5/27/07	1.8	0.6	<i>12/23/07</i>	<i>3.8</i>	<i>1.1</i>
6/3/07	15	8.4	12/26/07	8.6	6.6
6/20/07	3.6	2.3	12/28/07*	10	4.7
6/21/07	2.0	0.08	12/30/07	6.9	10
6/28/07	2.0	2.8	1/6/08	1.5	2.2
7/5/07	1.5	0.4	<i>1/10/08</i>	<i>2.3</i>	<i>3.4</i>
7/10/07	2.3	0.4	<i>1/11/08</i>	<i>2.5</i>	<i>1.4</i>
7/11/07	4.3	0.8	1/30/08	0.8	1.3
<i>7/28/07 am</i>	<i>8.1</i>	<i>1.5</i>	2/6/08	2.0	0.1
7/28/07 pm	0.8	0.05	2/18/08 am	0.5	0.07
7/29/07	2.5	2.4	<i>2/18/08 pm</i>	<i>3.6</i>	<i>1.8</i>
7/30/07	5.8	0.3	3/1/08	0.8	0.2
8/9/07	1.3	0.08	3/4/08*	12	8.8
8/20/07 am*	24	6.3	3/7/08*	12	7.1
8/20/07 pm	2.5	2.0	3/8/08	3.0	6.2
8/21/07*	21	7.8	3/16/08	7.1	7.2
8/25/07	13	4.4	3/19/08*	10	3.7
<i>9/10/07*</i>	<i>19</i>	<i>2.6</i>	3/20/08	2.3	0.7
9/11/07	1.5	0.7	<i>4/3/08*</i>	<i>15</i>	<i>11</i>
9/14/07**	2.0	3.3	4/6/08	7.1	9.3
<i>10/19/07</i>	<i>9.4</i>	<i>1.6</i>	4/11/08	2.0	0.2
10/24/07*	36	26	4/20/08*	43	12
11/5/07**	1.8	1.9	4/21/08*	25	20
11/6/07**	1.0	0.7	<i>4/26/08*</i>	<i>12</i>	<i>5.4</i>
11/9/07**	1.5	4.4	4/28/08*	21	11
<i>11/12/07</i>	<i>5.6</i>	<i>7.0</i>	5/8/08*	63	15
<i>11/13/07</i>	<i>2.5</i>	<i>1.8</i>	5/10/08	5.8	4.5
11/15/07*	18	5.9			

Table 3-2. Frequency distribution (%) of storm events with a given rainfall depth and duration range. *Top:* Beltsville Agricultural Research Center, Station 6, Dec. 1, 2002 – Nov. 20, 2006. *Bottom:* Kenilworth Ave. bioretention cell, Apr. 25, 2007 – May 10, 2008.

Beltsville							
	0 < 3 mm	3 < 10 mm	10 < 25 mm	25 < 40 mm	40 < 60 mm	> 60 mm	Sum (%)
0 < 0.3 hr	6.5	0.6	0	0	0	0	7.1
0.3 < 1 hr	8.0	1.9	0	0.4	0	0	10
1 < 4 hr	15	12	2.8	0.4	0	0	30
4 < 12 hr	6.9	11	9.7	2.4	0.9	0.6	31
12 < 24 hr	0.2	3.7	6.9	4.1	2.8	0.4	18
> 24 hr	0	0.2	1.3	0.4	0.6	0.9	3.4
Sum (%)	36	29	21	7.8	4.3	1.9	100

Kenilworth site							
	0 < 3 mm	3 < 10 mm	10 < 25 mm	25 < 40 mm	40 < 60 mm	> 60 mm	Sum (%)
0 < 0.3 hr	14	1.5	0	0	0	0	15
0.3 < 1 hr	12	1.5	1.5	0	0	0	15
1 < 4 hr	15	7.7	3.1	0	0	0	26
4 < 12 hr	1.5	17	17	0	0	0	35
12 < 24 hr	0	0	3.1	0	1.5	1.5	6.2
> 24 hr	0	0	0	1.5	0	0	1.5
Sum (%)	43	28	25	1.5	1.5	1.5	100

3.1.2 Hydrologic performance

Monitored events can be classified as those with 1) no inflow, 2) no outflow, or 3) outflow. Table A-1 lists the complete hydrologic data set for all events. Five no-inflow events were included as examples of events with a sufficiently low average rainfall intensity such that no measurable runoff reached the inflow channel at the cell. Additional no-inflow events were logged but were not further analyzed because they are not relevant to the performance of the bioretention cell itself.

Inflow was completely captured in 23 events; no outflow was generated. As shown in Figure 3-1, all but one no-outflow event had a rainfall depth of less than 5 mm. Several events with less than 5 mm rainfall did generate outflow, however. The dashed

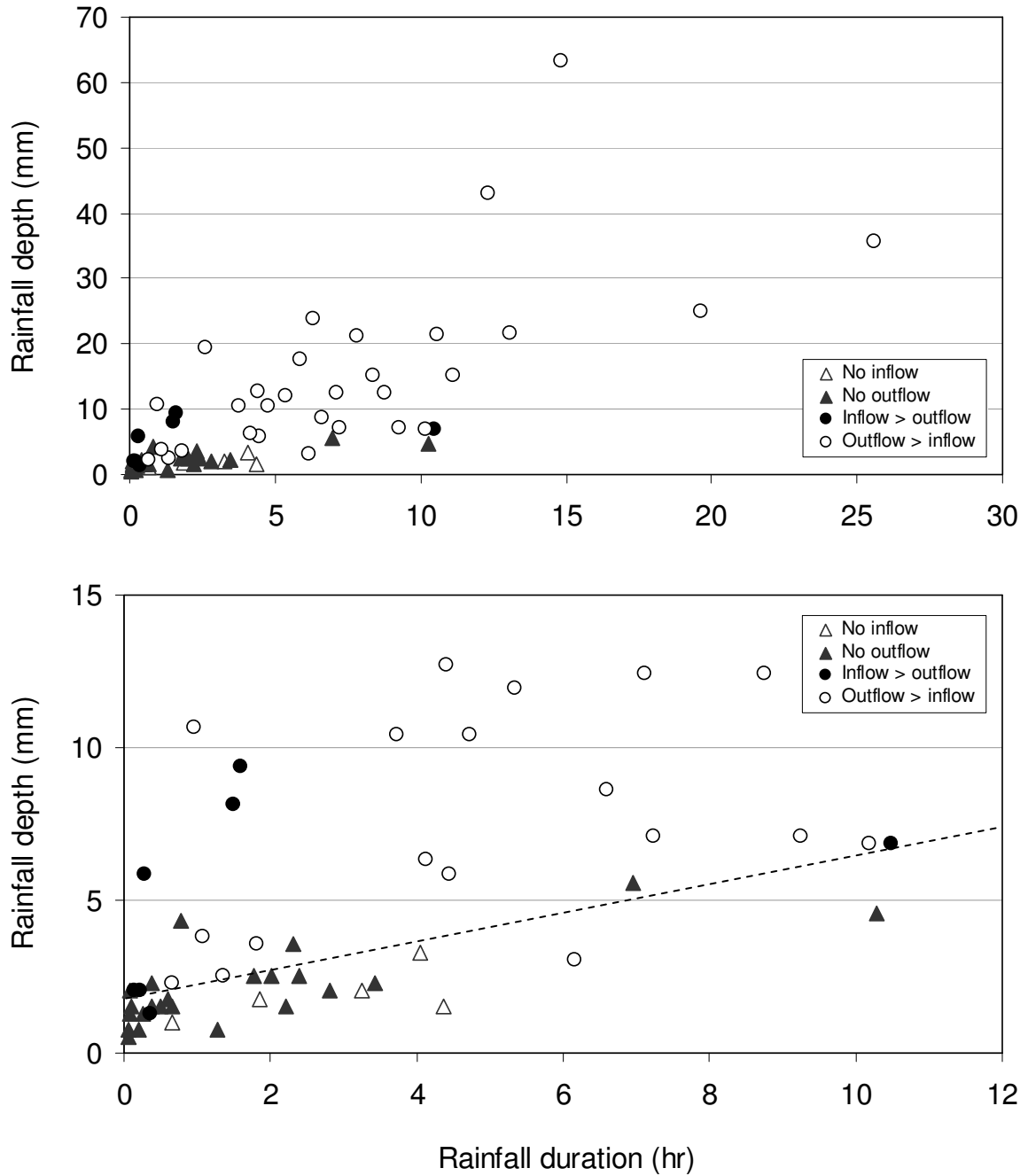


Figure 3-1. *Top:* Depth-duration plots for all 65 monitored events at the Kenilworth cell. *Bottom:* Detail view showing events with smaller rainfall depth and duration. The slope of the dashed line corresponds to the average rainfall intensity, approximately 0.5 mm/hr, above which outflow is generated.

line drawn manually in Figure 3-1 illustrates the approximate threshold rainfall intensity, 0.5 mm/hr, separating events that generate outflow from those that are completely captured. While rainfall intensity is likely the primary factor influencing the generation of outflow, the antecedent moisture condition (AMC) may play a secondary role. At a given site, AMC is influenced by inherent variation in rainfall patterns and by seasonal changes in evapotranspiration rates.

The 37 events that generated outflow can be further classified in several ways. Volume reduction occurred in only seven events, all of which had less than 10 mm of rainfall. Volume export occurred in the other 30 events, with an outflow volume in excess of the inflow volume. The outflow volume and peak flow rate could not be quantified with complete accuracy in 17 out of the 30 events with volume export because of high flow rates that exceeded the depth measurement limit of the outflow weir. The outflow hydrograph is truncated at 327 L/min in such events (Figure 3-2) and the outflow volume is underestimated to varying extents.

Several possible explanations for volume export can be ruled out. The pervious area on which the cell is located is a local high point and no underdrain flow was observed during dry periods, indicating that the cell has not intercepted a water table. Only minor sheet flow was observed onto the cell from the surrounding grass area during large events. An old storm drain not shown on the construction drawing passes near the cell, but a dye test did not indicate any hydraulic connection between the cell and the storm drain. Finally, the volume of rain falling on the cell itself is not sufficient to account for the excess outflow.

The most likely explanation is that the underdrain serves as an outlet for rainfall-generated subsurface flow in the surrounding rubble fill. As noted in Section 2.1.1, the bottom of the cell is unlined, hydraulically connecting it to the adjacent pervious area, which is also slightly higher in elevation than the cell itself. Under this explanation, volume export results from both site characteristics and cell design. Either a fully lined cell or low permeability in the adjacent soil would likely prevent most export events from occurring. The prevalence of volume export indicates that hydrologic and water quality performance findings for this site reflect not only bioretention processes, but also the influence of subsurface flow of varying and unknown quality and quantity.

3.1.2.1 Example event

Figure 3-2 illustrates the response of the cell to rainfall on April 20, 2008. Hydrographs and hyetographs for all events are provided in Appendix A. Inflow behavior was typical of most events: the delay between rainfall and inflow was minor, the inflow hydrograph mirrored the rainfall hyetograph, and the inflow rate dropped rapidly after cessation of rainfall. The first 3.3 mm of rainfall generated 5.3 m³ inflow and 2.1 m³ outflow, with a substantial peak reduction and delay. A second burst with 2.8 mm rainfall produced 7.3 m³ inflow and 10.8 m³ outflow, not including the previous volumes. Although the inflow peak was higher in the second burst, the volume export suggests that the surrounding pervious area had accumulated a sufficient amount of moisture prior to, or during, the second burst to cause subsurface flow to enter the underdrain.

The majority of the rainfall for the event, 36 mm, occurred in the third burst and resulted in a truncated outflow hydrograph. The inflow volume for this burst was 116

m³; the quantifiable outflow volume was 105 m³, but the actual amount is expected to be higher. The outflow hydrograph has a long receding limb associated with the dewatering period, typical for large events at this site.

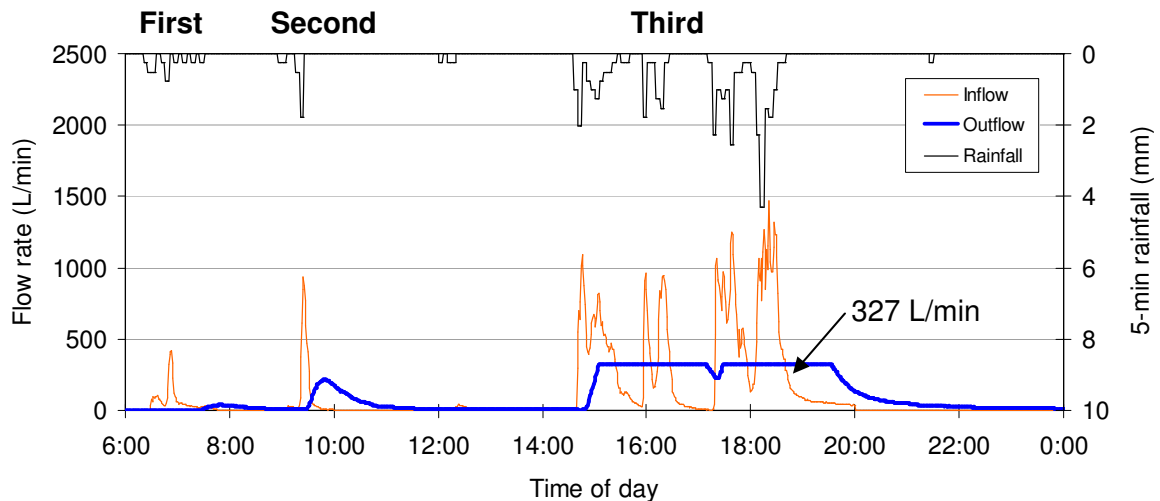


Figure 3-2. Hyetograph and inflow and outflow hydrographs from April 20, 2008. Hyetograph is displayed as the sum of rainfall in discrete five-minute intervals.

3.1.2.2 Volume

Complete inflow capture occurred in 23 out of the 60 events with inflow; all but one event had a rainfall depth less than 5 mm. Of the 37 events with outflow, 7 had a reduction in volume, with outflow/inflow volume ratios of 0.02 to 0.92 and a median of 0.25. Rainfall depths for these events ranged from 1.3 to 9.4 mm.

These findings suggest that good to excellent volume performance can potentially be achieved for events with approximately 10 mm or less of rainfall. As indicated in Table 3-2, this range of rainfall occurred for 65% of all events in Beltsville. Analysis of the Beltsville rainfall data indicates that such events contributed 19% of the total rainfall depth over a five year period (2002-2006). These percentages likely represent an upper

limit for their respective performance metrics, however. As shown in Figure 3-1, numerous events in this range had volume export. It is expected that other factors, such as short-term rainfall intensity or AMC, influence hydrologic outcomes in any given event and reduce the occurrence of good to excellent volume performance. It is possible that if the entire cell surface were able to accept inflow, rather than only the front 29% of the surface (Section 2.1.1), volume reductions would be greater because of increased media storage.

As discussed above, volume export was considerably more common than volume reduction among events that generated outflow. Volume performance was sensitive to rainfall depth. All events with more than 10 mm rainfall had volume export. Among all volume export events, the lowest outflow/inflow ratio (1.12) as well as the four highest (3.2, 3.3, 3.7, 7.5) were all associated with events without a truncated outflow hydrograph. In other words, these ratios represent actual values and not minimum estimates. Given that frequent volume export is atypical for bioretention (Hunt et al. 2006, Davis 2008), is likely caused by unique circumstances at the site, and cannot be completely quantified, a more detailed analysis of volume ratios was not performed.

Figure 3-3 illustrates the dependence of both inflow and outflow volume on rainfall depth. Outflow volume would generally be expected to increase with rainfall depth in any bioretention cell. At this site, however, the outflow volume has a greater dependence on rainfall depth than does the measured inflow volume, providing additional evidence that inputs to the system are not limited to flow from the inflow channel.

The slope of the inflow best fit line in Figure 3-3, $2.26 \text{ m}^3/\text{mm}$, can be used as a rough check on the contributing drainage area. Assuming that 90% of rainfall within the

paved drainage area is converted to runoff that reaches the inflow channel, the estimated drainage area is 0.25 ha. This value is approximately 10% smaller than the design drainage area of 0.29 ha. Agreement between these values is reasonable given the approximate nature of the slope calculation.

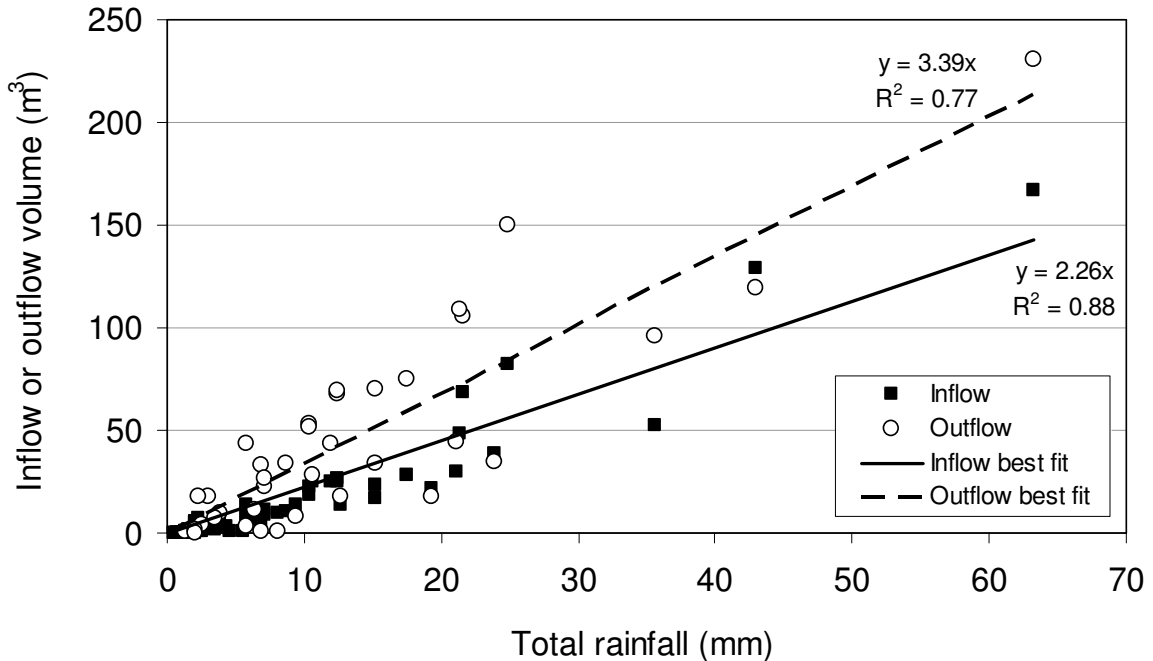


Figure 3-3. Dependence of Kenilworth cell inflow and outflow volume on rainfall depth.

3.1.2.3 Peak flow rate

Bioretention cells can alter the timing and the flow peak(s) of runoff hydrographs by providing temporary surface storage and promoting flow through porous media. Their ability to achieve such modifications are additional measures of hydrologic performance. Figure 3-4 shows the distribution of peak inflow and outflow rates. The distribution of peak inflow rates is roughly linear, spanning two orders of magnitude from 9 to 2008 L/min. The median peak inflow rate is 295 L/min.

As with the volume results (Section 3.1.2.2), the outflow peak distribution reflects the bifurcated nature of hydrologic performance at this site. Many events were completely captured and had 100% peak reduction. Among the events with outflow, a truncated outflow hydrograph was the most common outcome. The actual peak flow rates for the truncated events are larger than indicated in Figure 3-4. Beyond noting the minimum possible peak value of 327 L/min for truncated events, peak outflow rates cannot be characterized with certainty. Peak ratios were not analyzed for this reason.

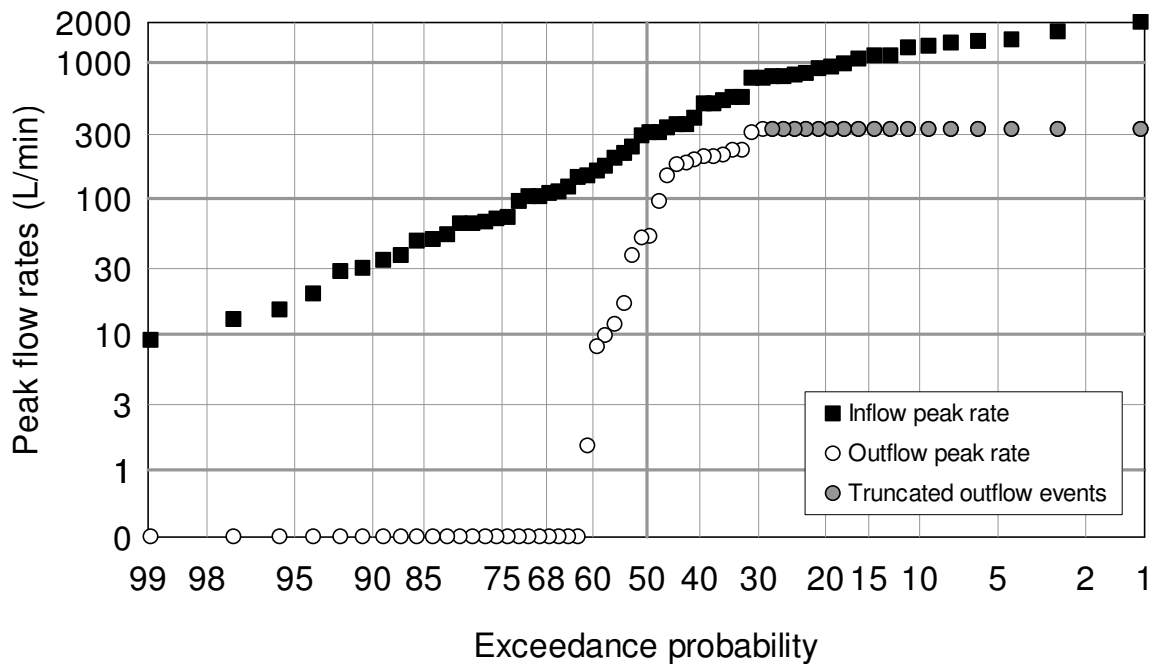


Figure 3-4. Probability distribution of peak inflow and outflow rates. The plot was constructed as described in Davis (2007). The x axis indicates the probability that an event will exceed a given flow rate. Outflow data points in gray represent minimum estimates (327 L/min) of the peak flow rate for events with truncated outflow.

A truncated outflow hydrograph does not necessarily signify pipe-full flow. Of the 17 events with truncated hydrographs, 5 events had outflow depths that indicated pipe-full flow for a period of time. Several cm of head likely accumulated above the

underdrain during these events. Outflow depths for the other 12 truncated events indicate that the pipe was flowing less than full.

3.1.2.4 Hydrograph timing

Quantifying the delay time between the start of measureable inflow and the start of outflow is another way to characterize hydrograph modifications. Inflow at this site is typically “flashy,” with a minimal delay from the start of rainfall to the start of inflow. A short runoff time of concentration is a common characteristic of highly impervious drainage areas with directly connected, hardened conveyance systems.

Among the 37 events with outflow, the delay times were distributed relatively linearly from 9 to 162 minutes, with a median delay of 57 minutes. Events that began with low-intensity or intermittent rainfall had the longest delay, as well as those with a completely captured initial burst. In some cases, the delay likely results from percolation through the media. The median delay time might have been greater if the entire cell surface were able to accept inflow (Section 2.1.1). For events with high rainfall depth or high rainfall intensity, however, the delay was likely controlled by the movement of water below the surface of the adjacent pervious area, rather than percolation downward through the cell media. The events with volume reduction had delays ranging from 30 to 162 minutes and were not uniquely associated with longer delay times.

3.1.2.5 Cumulative exposure to flow

Volume, peak flow rate, and hydrograph timing analyses each contribute to an understanding of how the Kenilworth cell alters the hydrology of its subwatershed.

Aggregating hydrologic data from across all monitored events allows the overall impact of the cell to be characterized, integrating the individual performance metrics of volume, peak flow rate, and timing.

A complete set of inflow and outflow rates from all events was compiled. Inflow and outflow rates were each averaged every four minutes for the entire inflow and outflow duration of each event. The averages from all events were assembled into one inflow list and one outflow list and were sorted in descending order. The resulting lists indicate the cumulative duration of exposure of the subwatershed to flow rates greater than, or less than, a given target value.

One rationale for this approach is that stream channel impacts of stormwater runoff are strongly influenced by the duration over which a threshold flow rate occurs in the channel (McCuen and Moglen 1988). The longer the channel-forming flow rate is met or exceeded, the greater the impacts on channel morphology.

Figure 3-5 indicates that the Kenilworth cell has increased the downstream exposure time to all flow rates compared to the direct highway discharge, represented by the inflow curve. This observation is valid for all flow rates except possibly the very highest values, for which the true outflow rate cannot be determined. A channel-forming flow rate was not determined for this site; 100 L/min can be used as an arbitrary value. Figure 3-5 shows that the cell experiences 41 hours of inflow at 100 L/min or higher. By comparison, 89 hours of outflow are associated with the same range of flow rates.

Outflow duration itself is not a concern. It must be considered in conjunction with the magnitude of the flow rates occurring over that duration. For instance, a long cumulative outflow duration dominated by low flow rates would represent a hydrologic

benefit because it would approximate baseflow conditions and correspond to a smaller volume than the cumulative inflow volume.

The longer cumulative duration of outflow at elevated rates reflects the fact that volume export occurs in many events. Regardless of the source, a large outflow volume requires a longer dewatering time. Figure 3-5 also indicates that the cumulative duration of outflow above the weir detection limit amounts to less than 5% of the total outflow duration. The inability to accurately quantify high flows through the weir does not alter the main conclusion about the hydrologic impact of the Kenilworth cell.

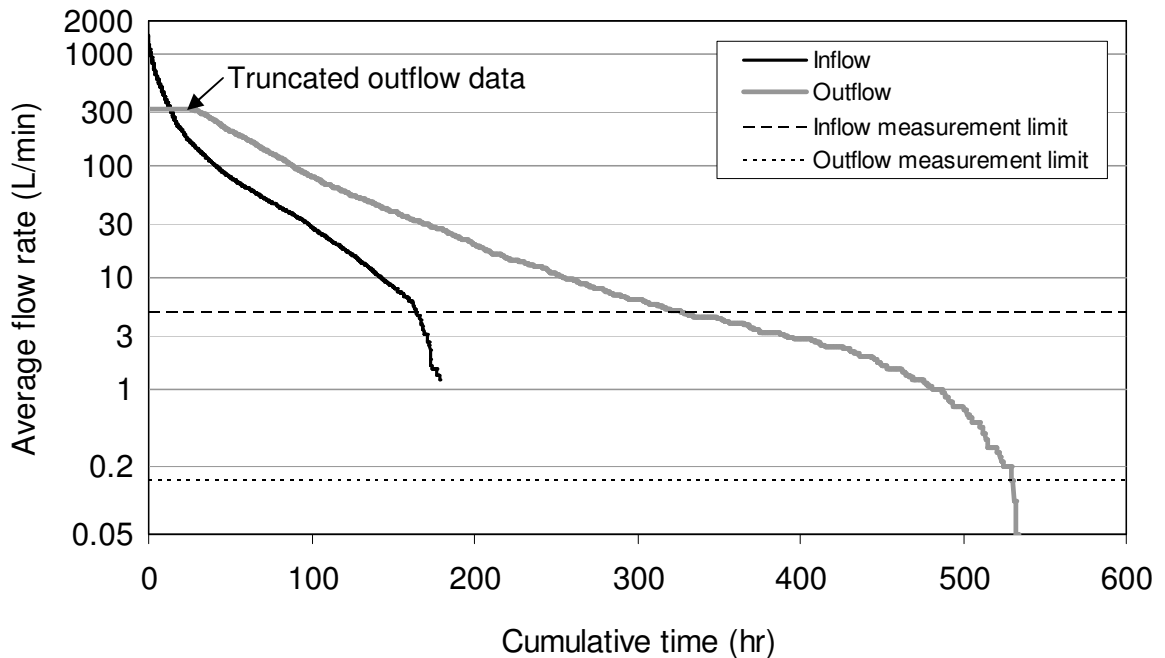


Figure 3-5. Cumulative exposure time to average (4-min) inflow and outflow rates. Measurement limits are shown because averages may be smaller than the minimum flow rates that can be measured by the inflow flume (4.9 L/min) or outflow weir (0.15 L/min).

By providing an outlet for subsurface flow in the immediate vicinity of the cell, the underdrain has increased the duration over which downstream channels are exposed

to any given flow rate. This condition unfortunately outweighs the hydrologic benefits provided by the cell for small events. It is conceivable that prior to cell construction, subsurface flow had no comparable surface outlet, and by remaining belowground, caused a smaller hydrologic impact on receiving waters than under the current design.

3.2 Water quality

3.2.1 Sampling approach and event characterization

Water quality samples were collected for 11 events from July 28, 2007 to April 26, 2008. Of the 11 events, 3 had complete capture, 2 had volume reduction, and 6 had volume export. Sampling the complete capture events allowed inflow concentrations to be more thoroughly characterized. Throughout most of the monitoring period, samples were analyzed only if outflow rates remained within the measurement limit of the weir. This criterion allowed outflow pollutant masses to be accurately quantified but also biased sampling toward events with a smaller rainfall depth or lower average intensity.

To better understand cell performance over the population of all events, samples from the two April 2008 events were analyzed despite violating the truncated flow screening criterion for outflow. Calculation of outflow concentrations and masses for these two events are therefore not exact, but this limitation is not expected to substantially alter conclusions about cell performance.

The Sep. 10, 2007 event was considered to be complete capture for the purposes of water quality analysis. The first burst of rainfall generated only inflow, which was successfully sampled. A second rainfall burst an hour later generated inflow, followed by outflow after 20 minutes (Appendix A). The inflow sampling program was too short to

capture most of the second inflow burst. As a result, only the initial burst was analyzed for water quality. By contrast, the Oct. 19, 2007 event had a longer inflow sampling duration, allowing both bursts to be fully sampled and analyzed, along with outflow.

The opposite scenario occurred for the Jan. 10, 2008 event, in which two rainfall bursts occurred approximately 15 hours apart. With a dry period exceeding 6 hours, the bursts are counted as two separate events from a hydrologic standpoint. The second inflow bottle captured portions of both bursts, dictating that they be considered a single event for the water quality analysis. As compared to the Sep. 10 and Jan. 10 events, the other 9 events had a more straightforward relationship between inflow and outflow.

Table 3-3 shows the frequency distribution of rainfall depth and duration among the sampled events, confirming the bias away from events of longer duration and greater depth. One-third of the sampled events had a rainfall depth between 3 and 10 mm and a duration between 1 and 4 hours. Despite the preponderance of these events, and considering the relatively small data set, the frequency distribution of the sampled events approximates that of the full set of 65 monitored events.

Table 3-3. Frequency distribution (%) of sampled events with a given rainfall depth and duration range at the Kenilworth bioretention cell, July 28, 2007 – April 26, 2008. For the Sep. 10, 2007 event, only rainfall associated with the first inflow burst was counted.

	0 < 3 mm	3 < 10 mm	10 < 25 mm	25 < 40 mm	40 < 60 mm	> 60 mm	Sum (%)
0 < 0.3 hr	0	8.3	0	0	0	0	8
0.3 < 1 hr	0	0	0	0	0	0	0
1 < 4 hr	25	33	0	0	0	0	58
4 < 12 hr	0	17	17	0	0	0	33
12 < 24 hr	0	0	0	0	0	0	0
> 24 hr	0	0	0	0	0	0	0
Sum (%)	25	58	17	0	0	0	100

3.2.2 Data handling

3.2.2.1 Pollutant concentration

Change in pollutant concentration, brought about by chemical, biological, and physical processes within the bioretention cell, is a common way to understand water quality performance. The event mean concentration (EMC) is the flow-weighted average concentration of the inflow or outflow for a given event, as shown in Equation 3-1.

$$\text{EMC} = \text{Total pollutant mass} / \text{Total volume} \quad (\text{Eq. 3-1})$$

As discussed in Section 2.1.3, the sampling protocol at the Kenilworth site called for samples to be collected in up to four inflow and three outflow bottles per event. Subsamples within each bottle were not flow-weighted because of the difficulty of coordinating sampling programs with inherently unpredictable behavior of storm events. As a result of using fixed volumes, subsamples associated with intervals of low flow volume had a disproportionate influence on the final concentration in a given bottle. Concentrations within individual bottles are therefore not strictly representative of the actual values, but are expected to be reasonably close. Flow weighting was used to calculate the inflow and outflow EMCs from bottle concentrations, however.

$$\text{EMC}_{\text{in}} = \frac{(C_{\text{in},1}V_{\text{in},1} + C_{\text{in},2}V_{\text{in},2} + C_{\text{in},3}V_{\text{in},3} + C_{\text{in},4}V_{\text{in},4})}{(V_{\text{in},1} + V_{\text{in},2} + V_{\text{in},3} + V_{\text{in},4})} \quad (\text{Eq. 3-2})$$

In Equation 3-2, $V_{\text{in},n}$ equals the volume of inflow that entered the cell over the sampling duration associated with bottle n . $C_{\text{in},n}$ equals the concentration of bottle n . Outflow EMCs are calculated in the same manner.

The ratio of EMC_{out} to EMC_{in} has been commonly used to describe pollutant removal performance. Given the variability in inflow concentrations, the EMC ratio can potentially cause incorrect interpretations of performance (Davis 2007). A preferred approach is to examine water quality performance in the context of threshold concentrations for environmental or human health (Strecker et al. 2001).

Probability plots and box-and-whisker plots are two methods for graphically displaying the relationship between EMC data and pollutant thresholds. Given the relatively small sample size, a probability-based interpretation of water quality data may be of limited value. Box plot features, including whisker lengths and interquartile ranges, do not necessarily represent the population of all events because of the small sample size.

The box-and-whisker plots shown in Figures 3-6 to 3-14 were created by calculating the 75th and 25th percentiles for each set of inflow and outflow EMC data. These values correspond to the top and bottom of the box. The median is represented by a thick line through the box. Whiskers extend to the maximum and minimum values. The width of each box is proportional to the sample size (Ayyub and McCuen 2003), which differs between inflow and outflow EMCs because of complete capture events.

The Wilcoxon signed-rank test with $\alpha = 5\%$ was used to determine the statistical significance of changes in concentration for events with both inflow and outflow (Ott and Longnecker 2001). A two-tailed test was employed so as to equally favor pollutants whose concentrations are expected to decrease or to increase after bioretention treatment.

3.2.2.2 Pollutant mass

Pollutant removal performance with respect to mass is affected by changes in volume as well as changes in concentration. Equation 3-3 shows the calculation of inflow mass from concentrations and volumes associated with individual bottles; the approach is the same for outflow.

$$\text{Mass}_{\text{in}} = C_{\text{in},1}V_{\text{in},1} + C_{\text{in},2}V_{\text{in},2} + C_{\text{in},3}V_{\text{in},3} + C_{\text{in},4}V_{\text{in},4} \quad (\text{Eq. 3-3})$$

The annual unit-area mass load normalizes mass results to the drainage area, allowing for a more physical interpretation of mass results. This metric also permits a consistent comparison of mass-based performance between different sites and between various types of BMPs. For inflow, the Simple Method calculates this metric as shown in Equation 3-4 (Davis and McCuen 2005).

$$L_{\text{in}} = P * C_{\text{F}} * R_{\text{V}} * C / 100 \quad (\text{Eq. 3-4})$$

In Equation 3-4, P equals 1077 mm, the average annual rainfall at Station 6 of the Beltsville Agricultural Research Center during the five year period of 2002 – 2006. As discussed in Section 3.1.2, not all precipitation events produce runoff, requiring a C_{F} coefficient of 0.9. A runoff coefficient R_{V} , also equal to 0.9, is needed to account for rainfall abstraction among events that produce runoff. Finally, C represents a composite inflow EMC and is calculated by dividing the total inflow mass of each pollutant by the total inflow volume associated with those sampled events (Li and Davis 2009). Some pollutants, such as chloride, were not analyzed for every sampled event because of low sample volumes; therefore, total inflow volume for the composite EMC calculation varies

by pollutant. The annual unit-area mass load for outflow, L_{out} , is calculated by multiplying L_{in} for each pollutant by its ratio of outflow mass to inflow mass. As discussed in Section 3.2.1, the outflow mass ratio is an approximate value because the outflow rate exceeded the measurement limit of the weir for portions of some events.

3.2.3 Water quality performance

Before assessing water quality performance of the Kenilworth cell, median inflow EMCs from Kenilworth Avenue can be compared with other EMCs from suburban Maryland to determine the extent to which they are mutually consistent. Water quality was analyzed at five sites within a ten-mile radius of the Kenilworth cell from 2002 to 2007. All drainage areas consist entirely of asphalt pavement and include parking lots, streets, and divided highways. As shown in Table 3-4, median inflow EMCs at Kenilworth Avenue are bracketed by values from other sites for all pollutants except for chloride, suggesting that Kenilworth inflow EMCs are generally representative of local conditions. (BOD was not analyzed at the other five sites.)

Chloride inflow EMCs may be higher at Kenilworth Avenue because the other efforts collected inflow samples immediately after sheet flow was concentrated in a channel or inlet. Inflow at the Kenilworth site is delivered to the sampling point via a 130 m long storm drain with four curb inlets (Section 2.1.1). It is possible that residual chloride deposits in the storm drain system may contribute to the inflow loading.

Table 3-4. Comparison of median inflow EMCs at Kenilworth Avenue to results from recent monitoring studies in suburban Maryland.

(a): Lot 11, Univ. of Maryland, College Park; *n* = 9 to 12 and 3 for nitrate (Davis 2007)

(b): Maryland Route 32, Columbia, MD; *n* = 10 to 18 (Stagge 2006).

(c): Rhode Island Avenue, Mount Rainier, MD; *n* = 24 to 32 (Flint and Davis 2007)

(d): Unnamed road, Univ. of Maryland, College Park; *n* = 15 (Li and Davis 2009)

(e): Dennis Ave Health Center parking lot, Silver Spring, MD; *n* = 15 (Li and Davis 2009)

Pollutant	Median inflow EMC (mg/L)					
	Kenilworth	Parking ^a	Road ^b	Road ^c	Road ^d	Parking ^e
Chloride	79		10		6	3
Nitrate*	0.67	0.13	2.2	0.66	0.36	0.34
TKN*	2.2		3.2	2.5	1.2	0.5
TP*	0.14	0.61	0.38	0.46	0.1	<0.1
Lead	0.019	0.058	0.024	0.1	0.006	<0.002
Zinc	0.50	0.11	0.35	0.88	0.071	0.015
TSS	85	34	93	400	66	17

* Nitrate and total Kjeldahl nitrogen (TKN) are expressed as N; TP is expressed as P.

3.2.3.1 Overview of changes in concentration

Table 3-5 shows the treatment performance trends in median EMCs for the pollutants of interest. Median EMCs increased from input to output for chloride, nitrate, and TP. Total Kjeldahl nitrogen (TKN), lead, zinc, BOD, and total suspended solids (TSS) demonstrated a decrease in median EMC. Total petroleum hydrocarbon (TPH) data was not analyzed because all samples except one were below the reporting detection limit of 5 mg/L (Table 2-1).

Table 3-5. Median, mean, and standard deviation (SD) of inflow and outflow pollutant concentrations at the Kenilworth bioretention cell.

Pollutant	Inflow EMC (mg/L)				Outflow EMC (mg/L)			
	<i>n</i>	Median	Mean	SD	<i>n</i>	Median	Mean	SD
Chloride	9	79	94	95	7	184	257	237
Nitrate*	11	0.67	0.83	0.68	8	0.72	0.73	0.31
TKN*	11	2.2	2.5	2.0	8	1.3	1.7	1.2
TP*	11	0.14	0.18	0.096	8	0.22	0.22	0.05
Lead	11	0.019	0.023	0.016	8	0.0042	0.0044	0.0025
Zinc	11	0.50	0.51	0.26	8	0.044	0.047	0.021
BOD	9	11	14	9.0	6	8.2	8.3	8.2
TSS	10	85	114	93	8	26	26	16

* Nitrate and TKN are expressed as N; TP is expressed as P.

3.2.3.2 Chloride

As shown in Figure 3-6, the Kenilworth cell increases both the magnitude and range of chloride EMCs. The threshold concentration of 250 mg/L for drinking water quality (CFR 2008) and chronic impacts to freshwater life (Kaushal et al. 2005) is exceeded for both inflow (1 out of 9) and outflow (2 out of 7) events. Outflow EMCs show a greater tendency to approach or exceed the threshold.

Construction was largely complete by November 2006, allowing chloride inputs from winter road salting to occur before the start of sampling. The sample size and time span is insufficient to draw conclusions about long-term trends in outflow EMCs, but a general increasing trend can be observed over the sampling period (Table A-13).

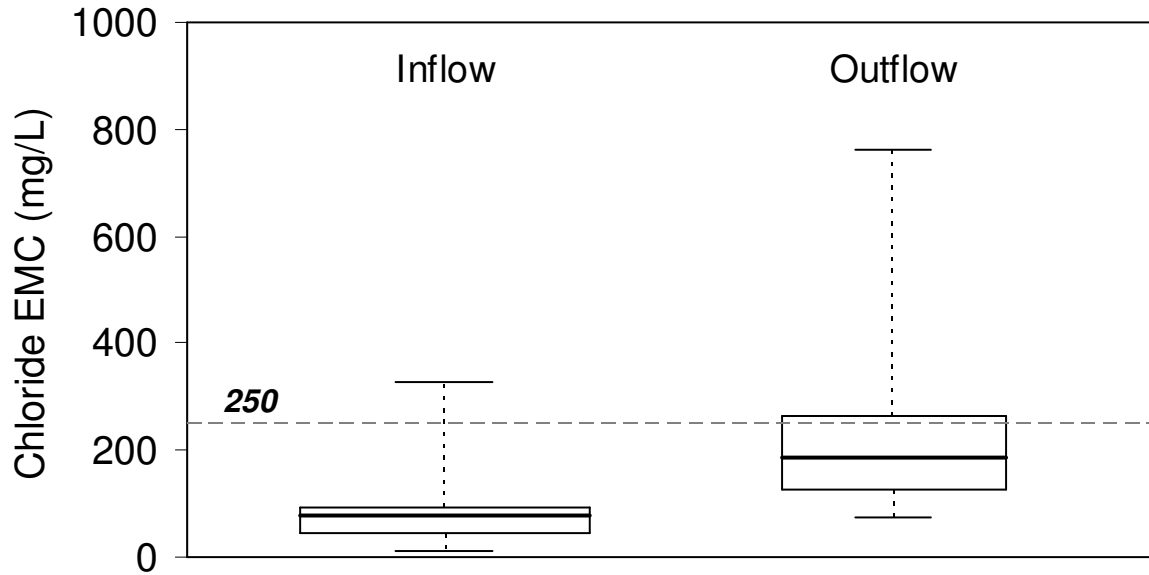


Figure 3-6. Chloride EMC box-and-whisker plot showing chloride concentrations for 9 inflow and 7 outflow events at the Kenilworth cell. Plot features correspond to the max/min, 25/75 percentile, and median. Also shown is the threshold concentration for both drinking water quality and freshwater life (CFR 2008, Kaushal et al. 2005)

The export of chloride agrees with recent studies of two grass swales (Stagge 2006) and a bioretention cell (Li and Davis 2009), which also noted increases in chloride EMC. Median outflow EMCs from the swales were 31 and 125 mg/L. The Li and Davis cell had a median outflow EMC of 29 mg/L. The maximum EMCs from one of the swales and from the Li and Davis cell were 1540 and 3320 mg/L, respectively, considerably higher than the maximum outflow EMC at the Kenilworth site. It should be noted that a second bioretention cell in the Li and Davis study experienced a reduction in median chloride EMC. The drainage area to this cell is a parking lot and may have received a lower dosing of road salt in the winter. Despite this finding, past work in combination with the present study suggests that soil-based BMPs can accumulate chloride, presumably over the winter, and export it year-round.

3.2.3.3 Nutrients

Nitrate and TP data show a consistent trend of an increase in EMC, with the exception of one decrease in EMC per pollutant (Table A-13). As a result of these exceptions and the small sample size, changes in nitrate and TP concentrations are not statistically significant. The trend for TKN is less clear, with small increases in EMC occurring for four events and slightly larger decreases occurring for the other four (Table A-13). The Wilcoxon test found the change in TKN concentration to be non-significant.

As shown in Figure 3-7, the Kenilworth cell slightly increased the median nitrate EMC, but the interquartile ranges of the inflow and outflow datasets were very similar, suggesting that the net effect on water quality outcomes is minimal. Both inflow and outflow EMCs consistently exceeded 0.2 mg/L, the nitrate concentration associated with excellent water quality in the Potomac River basin (Davis and McCuen 2005).

This result generally agrees with other recent studies (Hunt et al. 2008, Hatt et al. 2008b). Hatt et al. (2008a) observed that nitrate is a conservative substance and will not be retained in media unless denitrification occurs. Hsieh et al. (2007) noted that anoxic pockets may temporarily form in media and create favorable conditions for denitrification, even if aerobic conditions are generally prevailing. By monitoring nitrate concentrations over the course of a simulated runoff event in a media column, the authors found evidence of denitrification in a saturated, low-permeability layer. It is possible that anoxic zones were present in poorly-draining regions of the Kenilworth media, but overall conditions were not favorable to denitrification, and accordingly, nitrate concentrations were relatively unchanged.

Although effects on TKN were non-significant, Figure 3-8 shows a narrowing of the interquartile range and a decrease in median concentration. The trend agrees with Hunt et al. (2008), who found a decrease in TKN concentrations in a field study. The authors suggested that ammonification and nitrification could explain the drop in TKN and increase in nitrate concentrations. Box prototype studies also found a decrease in TKN (Davis et al. 2001a). The variability in TKN performance may be caused in part by the influence of external flows, which may be a source of organic nitrogen.

Figure 3-9 shows that all outflow TP concentrations exceeded a threshold concentration of 0.1 mg/L, specified for flowing waters that do not directly enter a lake or reservoir (EPA 1986). Past bioretention monitoring efforts and column studies have found decreases in TP concentration (Davis 2007, Bratieres et al. 2008, Hunt et al. 2008) as well as increases (Hunt et al. 2006, Hatt et al. 2008). TP performance appears to depend on vegetation type and media organic matter content (Bratieres et al. 2008), as well as background media phosphorus content (Hunt et al. 2006). Monitoring of a bioretention cell with a low media phosphorus content found a moderate but non-significant reduction in TP concentration (Hunt et al. 2008).

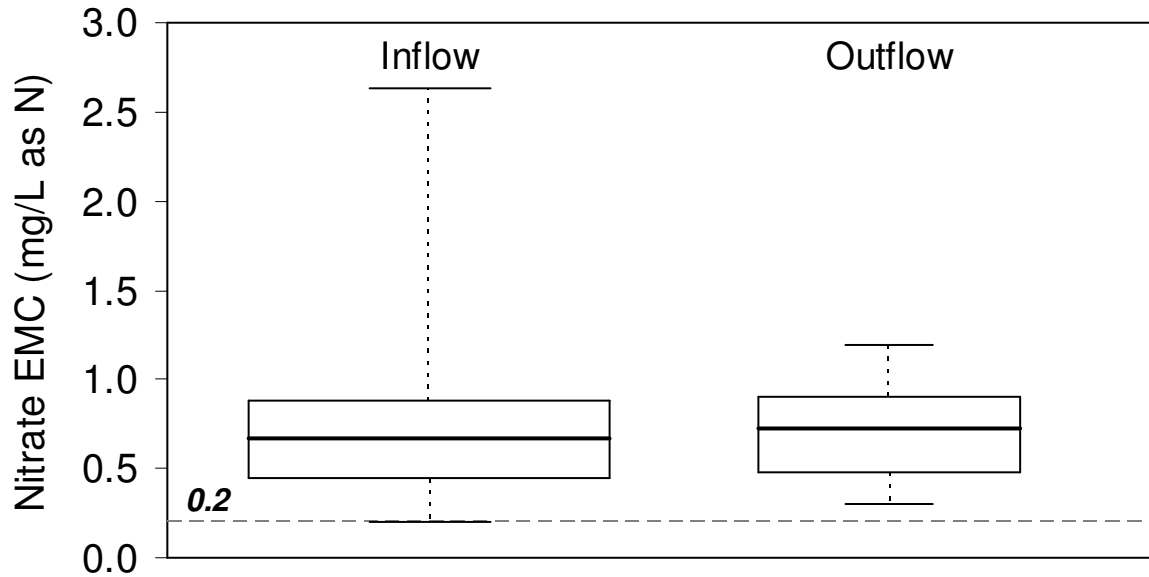


Figure 3-7. Nitrate EMC box-and-whisker plot showing nitrate concentrations for 11 inflow and 8 outflow events at the Kenilworth cell. Plot features correspond to the max/min, 25/75 percentile, and median. Also shown is the target concentration, 0.2 mg/L, associated with excellent water quality in the Potomac River basin (Davis and McCuen 2005).

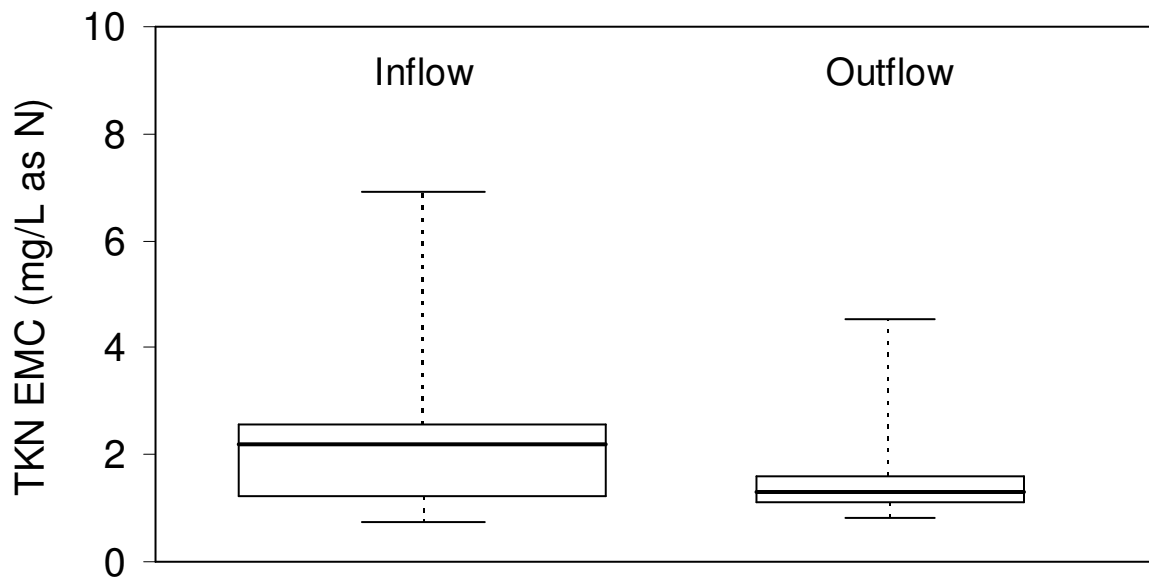


Figure 3-8. TKN EMC box-and-whisker plot showing TKN concentrations for 11 inflow and 8 outflow events at the Kenilworth cell. Plot features correspond to the max/min, 25/75 percentile, and median.

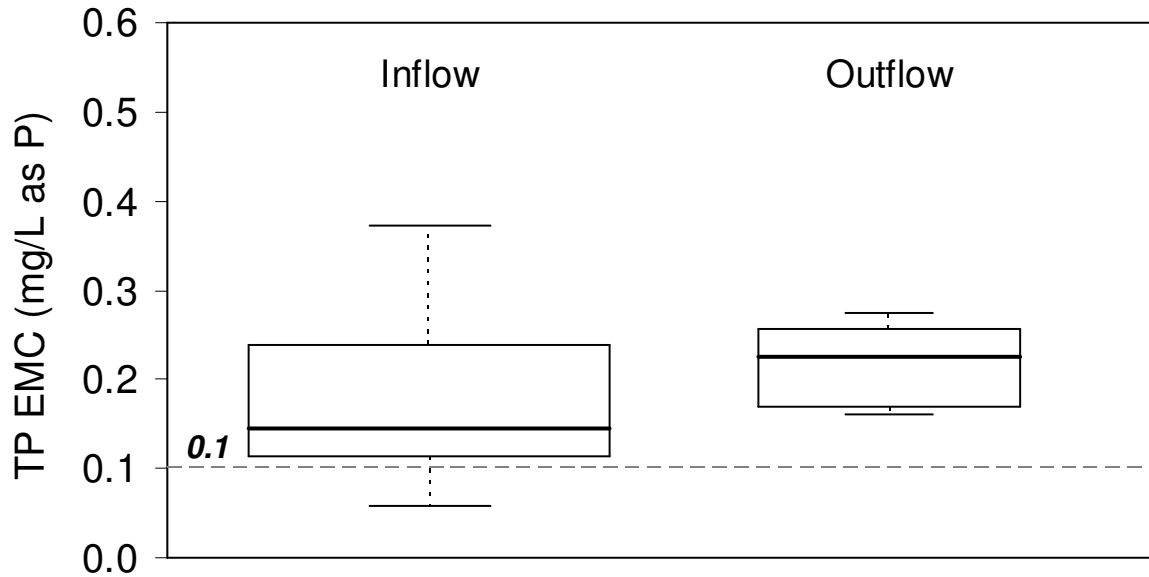


Figure 3-9. TP EMC box-and-whisker plot showing TP concentrations for 11 inflow and 8 outflow events at the Kenilworth cell. Plot features correspond to the max/min, 25/75 percentile, and median. Also shown is the target concentration, 0.1 mg/L, for flowing waters that do not directly enter a lake or reservoir (EPA 1986).

3.2.3.4 Metals and TSS

Consistent with previous bioretention monitoring efforts, large reductions were observed in lead, zinc, and TSS EMCs (Davis 2007, Hatt et al. 2008b, Hunt et al. 2008, Li and Davis 2009). In the present study, EMCs decreased in terms of both magnitude and range (Figures 3-10 to 3-12). Lead outflow EMCs fell below the EPA action level for drinking water treatment (0.015 mg/L, EPA 2003) but largely remained above the State of Maryland threshold for chronic freshwater toxicity (0.0025 mg/L, COMAR 2006). Zinc outflow EMCs were consistently below 0.12 mg/L, the Maryland threshold for acute and chronic freshwater toxicity, while all EMCs exceeded that value (COMAR 2006). Half of the TSS outflow EMCs were below the target concentration associated with excellent water quality in the Potomac River basin (25 mg/L, Davis and McCuen 2005). All TSS inflow EMCs exceeded that threshold.

The results are not surprising, given the unit processes in bioretention that are suited to removal of these pollutants. Both mulch and bioretention media have been shown to readily sorb dissolved metals (Davis et al. 2001a, Jang et al. 2005, Hatt et al. 2008a). Chapter 4 discusses metal accumulation in detail. Physical capture of runoff particles is also important for lead removal, as particulate-bound lead is prevalent in urban runoff (Sansalone and Buchberger 1997). Physical removal of runoff particles occurs through settling, surface straining, and depth filtration (Li and Davis 2008b).

Figure 3-13 illustrates the change in TSS concentration. The first inflow bottle concentration was 226 mg/L, an order of magnitude higher than outflow concentration of 28 mg/L. The orange-brown tint of the outflow may be caused by dissolved organic matter. Outflow TSS concentrations may decrease over time as fine particles wash out of the media (Davis 2007), although a trend was not apparent over the sampling period.

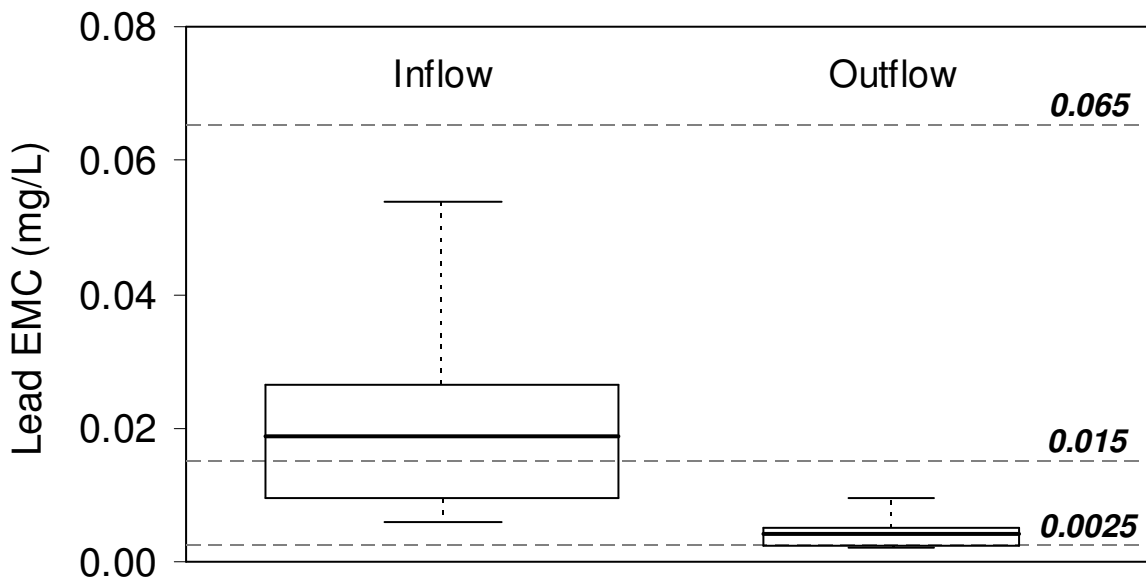


Figure 3-10. Lead EMC box-and-whisker plot showing lead concentrations for 11 inflow and 8 outflow events at the Kenilworth cell. Plot features correspond to the max/min, 25/75 percentile, and median. Also shown is the EPA action level for drinking water treatment (0.015 mg/L, EPA 2003) and State of Maryland threshold for acute and chronic freshwater toxicity (0.065 and 0.0025 mg/L, respectively; COMAR 2006).

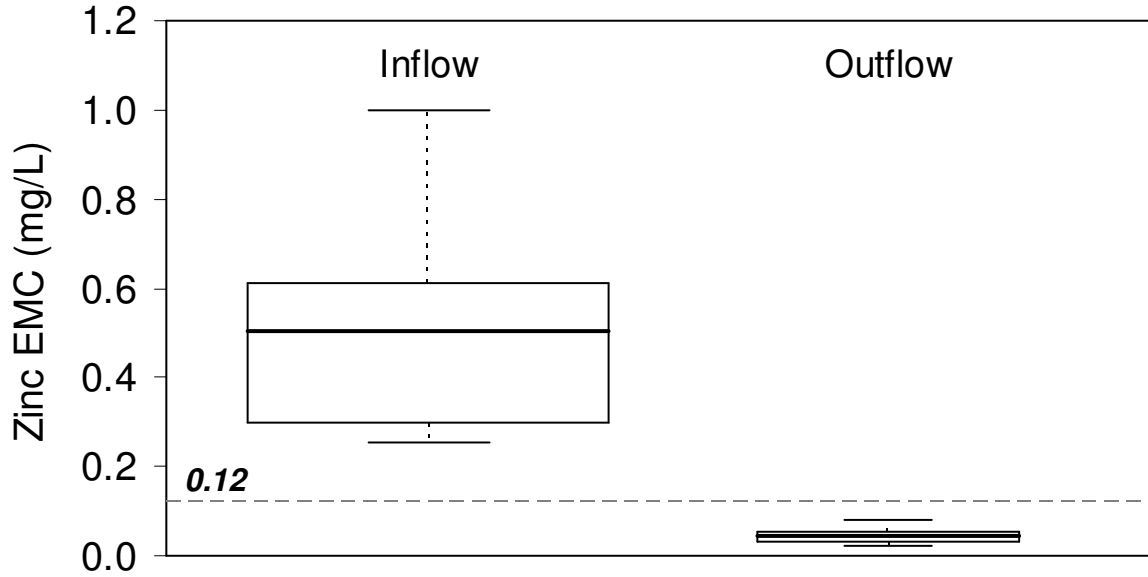


Figure 3-11. Zinc EMC box-and-whisker plot showing zinc concentrations for 11 inflow and 8 outflow events at the Kenilworth cell. Plot features correspond to the max/min, 25/75 percentile, and median. Also shown is the State of Maryland threshold for acute and chronic freshwater toxicity (0.12 mg/L, COMAR 2006).

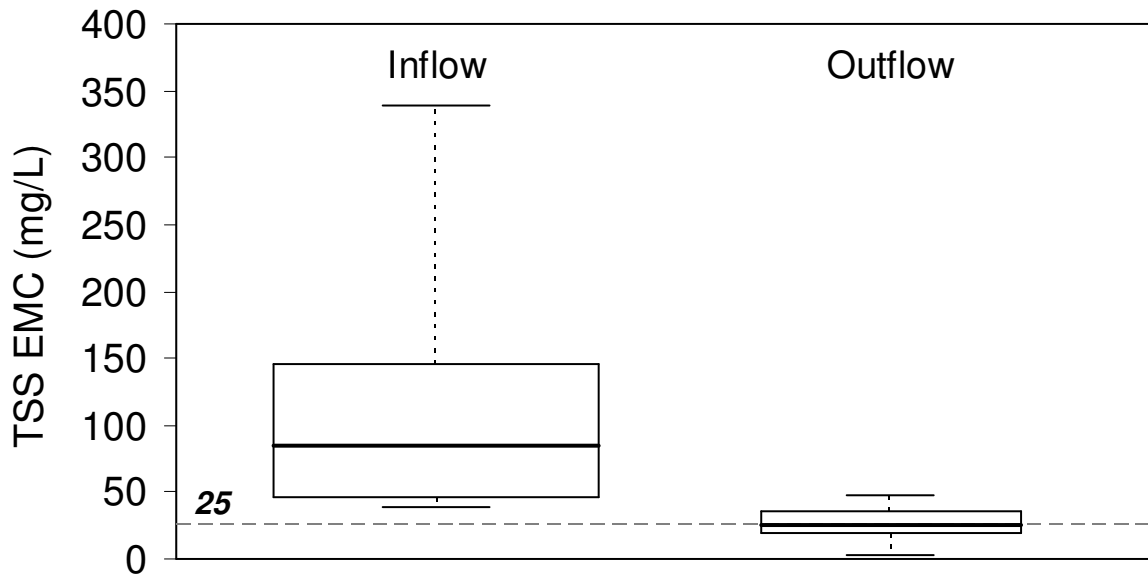


Figure 3-12. TSS EMC box-and-whisker plot showing TSS concentrations for 10 inflow and 8 outflow events at the Kenilworth cell. Plot features correspond to the max/min, 25/75 percentile, and median. Also shown is the target concentration, 25 mg/L, associated with excellent water quality in the Potomac River basin (Davis and McCuen 2005).



Figure 3-13. Inflow and outflow bottles from the July 28, 2007 event. The group of four inflow bottles are shown with the first bottle (earliest sample) on the left and the last bottle on the right. Only one outflow bottle was filled for this event (far right). The orange-brown tint of the outflow sample is typical for outflow at this site.

3.2.3.5 Biochemical oxygen demand

Bioretention performance with respect to biochemical oxygen demand (BOD) has not been well studied to date. However, bioretention unit processes are expected to facilitate BOD removal. Figure 3-14 shows that the Kenilworth cell achieved an overall reduction in outflow BOD concentrations. The change in BOD concentration was found to be statistically significant. The extent of BOD removal was variable, ranging from two events with outflow that had complete removal to one event that had no change in EMC (Table A-13). At this site, the role of external flows in augmenting or diluting BOD is not clear.

Hua et al. (2003) found large reductions in chemical oxygen demand (COD) of raw sewage after trickling through the top 25-50 cm of sand columns. Sand filters reduce

BOD by physically removing larger particles and through sorption and precipitation of soluble material (Sansalone and Hird 2003). Microbial populations in the media may also contribute to BOD removal, as occurs after land application of secondary wastewater effluent (Dunne and Leopold 1998).

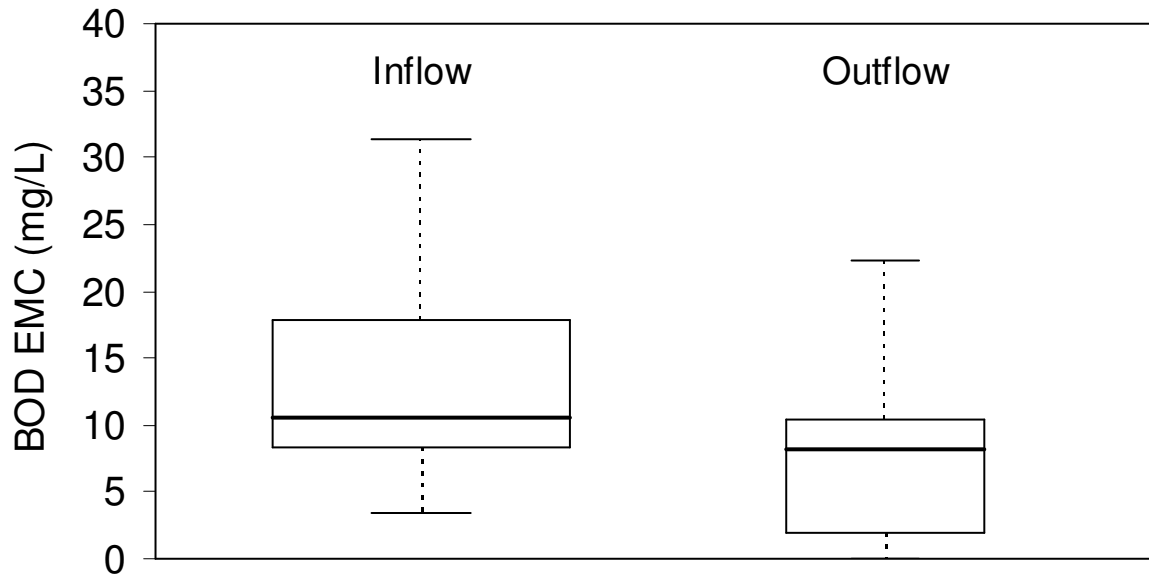


Figure 3-14. BOD EMC box-and-whisker plot showing BOD concentrations for 9 inflow and 6 outflow events at the Kenilworth cell. Plot features correspond to the max/min, 25/75 percentile, and median. Two events with outflow had outflow EMCs of 0 mg/L.

3.2.3.6 Changes in pollutant mass

Bioretention allows for storage and evapotranspiration of captured runoff, potentially achieving volume reductions that increase the extent of pollutant mass removal. Volume export, as measured at the underdrain outlet, may occur if external flows enter the cell (Section 3.1). As stored runoff evaporates or is taken up by vegetation between storm events, pollutant mass may be transformed and attenuated within the media, accumulated by cell flora and fauna, or permanently sequestered in the

media. Any of these pathways results in a net reduction in pollutant mass leaving the cell, provided that the cell components do not act as a pollutant source.

Water quality performance can be analyzed in terms of the change in pollutant mass from inflow to outflow. This approach incorporates changes in both concentration and volume. Figure 3-15 shows the ratio of outflow to inflow mass for each storm. The log-linearity of the mass ratios as plotted in Figure 3-15 suggests a lognormal distribution. With the exception of one event, metal and TSS mass decreased in every event by up to two orders of magnitude. Masses of the other pollutants generally increased, but mass reductions occurred for every pollutant in at least one event.

Broadly speaking, mass ratios follow the same trends as the concentration results. Numerically, however, the changes in nutrient, chloride and BOD mass indicate poorer performance than implied by the change in median EMC. This finding suggests that 1) the pervious area is a source for these pollutants, which are propagated by external flows; or 2) that the additional subsurface volume mobilizes pollutants from the bioretention media, as suggested by Hatt et al. (2008b) for phosphorus. Both explanations may be valid. The latter scenario seems most probable for chloride. Given the presence of curbs along the roadway, it is unlikely that the pervious area adjacent to the cell has received chloride-laden road runoff over the years.

By contrast, the changes in median EMCs and mass loadings for lead, zinc, and TSS are similar, implying that additional export of these pollutants is not occurring as a result of external flows. It is not known whether 1) external flows are relatively “clean” with respect to metals and TSS and are diluting the outflow without affecting mass, or 2) these pollutants are propagated by external flows but are subsequently removed by

physical and chemical processes in the bioretention media. The first explanation may be more likely because the pervious area has apparently been stable for many years and is isolated from the roadway, as discussed above.

Generalizing cell performance beyond the 11 sampled events, the frequency of volume export is expected to reduce the occurrence of events with mass reduction, exacerbating downstream nutrient and chloride impacts. Smaller events with volume reduction or complete capture would still result in nutrient mass reductions (Table A-14), and to a lesser extent chloride mass reductions. Owing to excellent concentration performance for metals and TSS, mass reductions should still occur for those pollutants in most events despite the tendency for volume export.

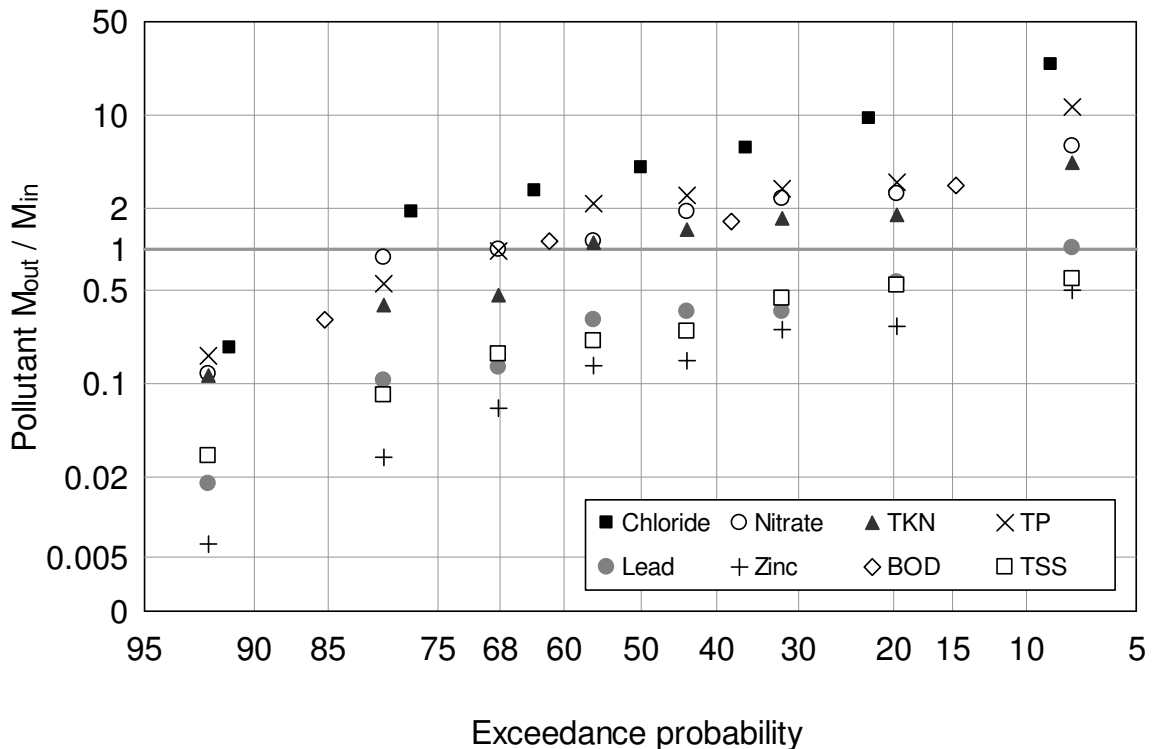


Figure 3-15. Probability distribution of mass ratios for all events with outflow at the Kenilworth cell. Ratios are plotted on a normal probability scale (Davis 2007). The x axis indicates the probability that an event will exceed a given mass ratio.

A mass-based interpretation of water quality lends greater importance to complete capture events, which have 100% mass removal. Given the tendency for volume export to occur, the fraction of annual pollutant mass represented by complete capture events is likely to be modest, however.

Annual unit-area mass loadings aggregate the mass performance for all events. The results shown in Table 3-6 reflect the trends in Figure 3-15. In contrast to this study, mass loadings decreased for all pollutants except total organic carbon in the two cells monitored by Li and Davis (2009). In the present study, chloride has the highest change in mass loading, at nearly 400%, followed by TP at 123%. The increase in the nitrate mass loading is smaller, at 32%. TKN and BOD mass loadings indicate that the cell has had only a marginal effect on these pollutants. Lead, zinc, and TSS mass loadings have been reduced considerably despite the unique hydrologic behavior of this site.

Table 3-6. Annual unit-area mass loadings of monitored pollutants at the Kenilworth site. Change in loading is calculated as a percent of the inflow value.

Pollutant	L_{in} (kg/ha-yr)	L_{out} (kg/ha-yr)	% change
Chloride	571	2832	396
Nitrate*	5.8	7.7	32
TKN*	21	19	-8.4
TP*	1.3	3.0	123
Lead	0.14	0.037	-74
Zinc	3.8	0.58	-84
BOD	116	121	4
TSS	767	209	-73

* Nitrate and total Kjeldahl nitrogen (TKN) are expressed as N; TP is expressed as P.

RESULTS AND DISCUSSION – MEDIA ANALYSIS

4.1 Media composition

As discussed in Chapter 2, the Lot 11 cell contains two basic types of media: the top organic layer and the bioretention soil media (BSM) beneath. Both are expected to have considerable sorption capacity for dissolved metals (Davis et al. 2001a, Jang et al. 2005). Additionally, bioretention soil media has been shown to effectively strain and filter particles over a wide range of sizes (Li and Davis 2008b).

The organic layer found in the Lot 11 cell is characterized by a dark, loamy appearance and texture and a high but variable organic matter (OM) content. BSM is light brown with a mixture of silt-sized particles, mulch pieces, and small stones up to approximately 4 mm across their shortest axis, and generally resembles a mineral agricultural soil. OM content is the key quantitative distinction between the two media types for the purposes of this study. General appearance and texture, and the location in the media profile, are the two main qualitative differences.

Originally, the cell was constructed with approximately 8 cm of rough shredded hardwood mulch placed over the BSM (Davis 2007). Although mulch replenishment is recommended every six months (PGDER 2002), no maintenance was performed between completion of construction and time of sampling. The lack of disturbance conveniently allows for straightforward and accurate measurements of lifetime metal accumulation.

In the absence of replenishment or other disturbance, the mulch layer has evolved into what will be termed the organic layer. It is thought to consist primarily of the

degraded remnants of the original mulch, augmented by plant litter at various stages of decay, stormwater constituents, and earthworm castings. Humic substances in the organic layer are likely responsible for much of its sorption capacity (Jang et al. 2005).

The organic layer covers the top 3 to 12 cm and extends across the entire surface. The transition between the organic and BSM layers is very abrupt, on the order of 0.5 cm, which allows each core segment to be definitively classified (Figure 2-12). It is notable that such clear stratification was evident 3.5 years after construction, which suggests minimal physical disturbance by inflow, soil animals, and plant activity. Portions of Zone 1 have a less distinct transition or little organic layer coverage, however, because of scouring and particle deposition that has occurred from completion of construction to the present (Weinstein 2008), as shown in Figure 2-7. The area of Zone 1 from which segments were taken did display a clear stratification between the two layers, however.

Considering the entire cell, the organic layer is dwarfed in terms of mass and volume by the BSM, which fills a depth of approximately 90 cm. BSM for this cell was specified as a mixture of 50% construction sand, 30% topsoil, and 20% twice-shredded hardwood mulch, by volume (Davis 2007). A 2008 particle size analysis of the original BSM indicated a composition of 89% sand, 7% silt, and 4% clay, resulting in a textural classification of “sand.” A high sand content in the topsoil component, combined with the construction sand, explains the high percentage of sand-sized particles in the BSM. Regardless of origin, the high sand and low clay content is consistent with rapid drainage that is desirable in bioretention systems and that has been observed at this site.

4.1.1 Organic matter content

Organic matter (OM) content shows a high degree of variability throughout the cell. The most obvious variability is between the organic and BSM samples, which reflects their different composition. Mean OM content in organic samples is nearly an order of magnitude higher than in BSM samples (Table 4-1). OM content is believed to be chiefly responsible for the retention of dissolved metal species at the top of the media profile (Sections 4.2.2.3 and 4.3.1).

Table 4-1. Organic matter (OM) content (%) in media samples. Organic samples include core segments and surface samples; BSM samples are core segments only. RSD is relative standard deviation.

Media	Min	Max	Mean	Median	SD	% RSD	<i>n</i>
Organic	1.9	43	18	17	10	55	35
BSM	0.7	4.7	2.0	2.0	0.8	41	30

Considerable variation in OM content exists within the organic layer, as indicated in Table 4-1. Tables B-1, B-2, and B-6 provide complete OM data. Among surface samples, all of which are from the organic layer, a clear spatial trend is evident despite variation among individual samples in a zone. Figure 4-1 shows that OM content is low in areas closest to the inflow point (Zones 1, 2, and 6) and steadily increases with distance from that point. Zones 3, 4, 5 and 7 have a relatively constant mean OM content of approximately 25%, indicating no discernable dependence on distance. There is reasonably good agreement among the four samples in Zones 1, 2, and 4. Other zones show a surprisingly wide variation in OM content, especially Zone 7.

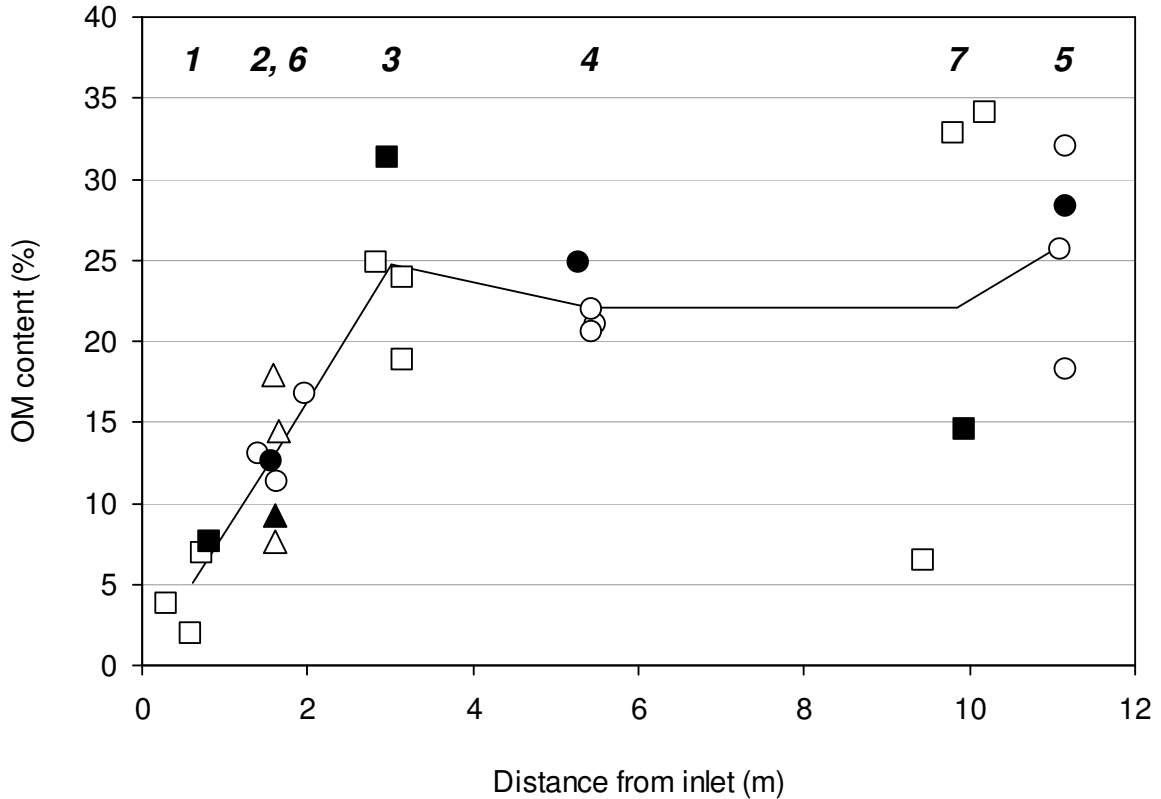


Figure 4-1. Organic matter (OM) content on cell surface. Each point on the curve is the mean OM content and distance along the main flow path of the four samples in each zone. Filled points indicate uppermost core segments (top 2 – 3 cm). Hollow points are surface samples (top 2.5 – 3.2 cm). Triangles denote Zone 6; other zones alternate between squares and circles. Zones are labeled at top of figure.

With respect to depth, OM content within each zone’s organic segments is relatively consistent. Exceptions are the 6-9 cm segment in Zone 2 (2C) and the Zone 5 segments. (Zones 1 and 4 each have only one organic segment). Three of the four organic segments in Zone 2 have approximately the same OM content (8.5 – 13%), but segment 2C has an unexpectedly high value of 43%, the highest of any segment measured (Table B-2). OM content decreases sharply in Zone 5 from the top segment, with 28% OM content, to the subsequent segment (13%). It is unclear why the organic layer in Zone 2 is deeper (12 cm) than elsewhere in the cell, where the thickness is relatively constant at 3 to 5 cm. The cell surface elevation in Zone 2 is not substantially

different than elsewhere. Variation in mulch depth during construction is a possible explanation. Another possibility is that high-velocity inflow events could have carried mulch away from Zone 1 and along the main flow path into Zone 2.

Variation in OM content with distance, with depth (Zones 2 and 5), and within several zones is surprising in light of the assumed homogeneity and uniform application of the original mulch. Bioretention cells are highly engineered systems, and media composition is intended to be consistent between cross-sections. These results, after four years of operation, suggest that natural processes may play an important role in altering media characteristics over time compared to the original engineered design. Possible factors affecting OM content include “dilution” by particle penetration; scouring and gross transport of particles or media/mulch by high-energy flows; spatial differences in plant type, location, biological activity, and decay rates; microbial and soil animal activity (e.g., earthworms); flow patterns; overall OM decomposition rates; and possibly even trash deposition and degradation. Bohn et al. (2001) noted that the mass of soil OM in temperate soils decreases 50-80% one year after being added to the soil. Complete mineralization of OM in mulch should take far longer than for colloidal OM. In the absence of mulch replacement at the Lot 11 cell, however, decaying plant matter from cell vegetation as well as plant material and paper-based trash carried by inflow may contribute to the maintenance of high OM content at the top of the media profile.

The relatively low OM content in the Zone 1 samples is likely caused by a combination of particle deposition and removal of mulch and organic media by scouring. Both phenomena should generally have the greatest influence near the inflow point. Scouring appears to be limited to Zone 1 but its influence on OM content throughout

Zone 1 may not be uniform. Two organic media samples taken in 2008 for the bioavailability analysis (Section 4.4.2) have OM contents of 25% (Table B-6), as compared to the mean of 5.1% found in four surface samples from 2006. This indicates that media composition within Zone 1 is highly heterogeneous and that the influence of particle deposition and scouring varies even within a relative small area.

The influence of particle deposition likely affects the portion of the cell closest to the inflow point, including Zones 1, 2, and 6. The low OM content in these zones may partly be caused by particles settling near the inflow point and penetrating into the media profile. Particles sampled from the inflow channel were found to have an OM content of 5.6% (Table B-6). If scouring is minimal, as expected outside of Zone 1, particle deposition would reduce the mass proportion of OM content in the media without decreasing the mass of organic matter. Total sorption capacity would be relatively unchanged, but metal capture would be augmented by settling and filtering of particles. The steady increase in mean % OM content with distance could be explained by a decrease in particle deposition with distance from the inflow point.

The unusually high OM content in segment 2C may be related to its deeper position in the media profile. At a depth of 6 to 9 cm, particle settling would not apply and the segments above would largely shield it from particle penetration (Li and Davis 2008b). Heterogeneity in the original mulch could also contribute to local high or low values, both in segment 2C and in Zones 5 and 7.

4.1.2 Cation exchange capacity

Cation exchange capacity is one component of total sorption capacity for metals. As CEC generally reflects OM content, BSM samples should have lower CEC than the organic media. CEC corresponds only to outer-sphere complexation and may be far lower than the total sorption capacity, however (Alloway 1995). CEC was measured in the original Lot 11 BSM and original Kenilworth mulch (used as a surrogate for the original Lot 11 mulch). Measurements were made at pH 7.0, higher than the pH of all organic and BSM samples (Section 4.1.3). This discrepancy may inflate the mulch CEC, but the value should still be a reasonable estimate because many functional groups dissociated at pH 7.0 would also be dissociated at the *in situ* pH (Bohn et al. 2001).

CEC values for BSM and unground mulch are 3.48 and 26.2 meq/100g, respectively. By comparison, the geometric mean of 57 agricultural mineral soil samples in Maryland is 3.2 meq/100g (Holmgren et al. 1993). The mulch was also ground to pass a #20 sieve (0.85 mm opening), resulting in a CEC of 44.9 meq/100g. The increase in CEC after grinding is likely related to an increase in surface area.

4.1.3 Media pH

Media pH of both organic and BSM segments falls within the 5 to 6 range (Table 4-2). The full data set is given in Table B-2.

Table 4-2. Media pH of organic and BSM segments, measured in 0.01 M CaCl₂. RSD is relative standard deviation.

Media	Min	Max	Mean	Median	SD	% RSD	<i>n</i>
Organic	5.1	6.2	5.6	5.7	0.3	4.9	13
BSM	5.0	6.3	5.4	5.4	0.3	5.3	30

Figure 4-2 shows a clear trend of decreasing pH with depth. The only exceptions are Segment 2C and three segments at the bottom of the media profile. The trend is most apparent for Zones 1 and 2, which have measurements for every segment in the cores. No pH discontinuity occurs between the organic and BSM layers despite their different composition. As shown in Figure 4-2, pH values have generally increased over the original BSM pH of 5.2. The pH of the uppermost BSM segment in each zone ranges from 5.3 to 5.9, and the pH of most BSM segments is greater than 5.2. Original mulch pH is unknown because no material is available.

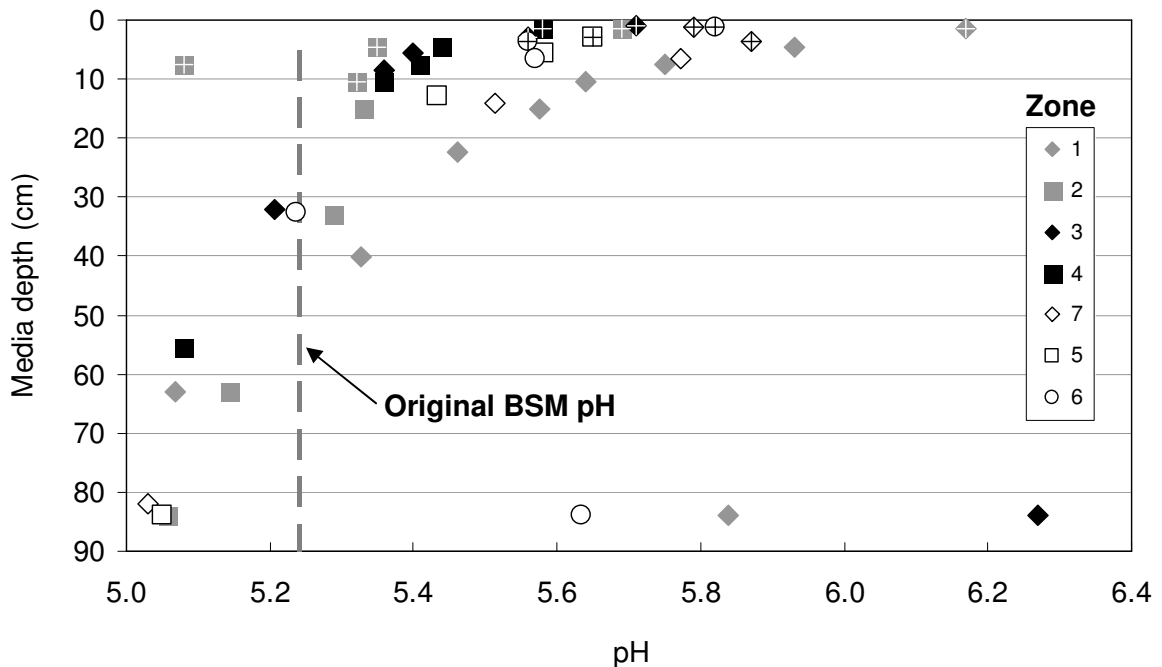


Figure 4-2. Variation in pH with depth in each zone. Crosses denote an organic segment. Dashed line indicates original BSM pH.

Li and Davis (2008a) also found a decrease in pH with depth in a bioretention cell of approximately the same age. Media pH (measured in deionized water) was 6.8-6.9 in the surface street particle layer, 5.8-6.0 in the 10-60 cm layer, and 4.9-5.3 in the 60-90 cm

layer. The Zone 1 profile shows a pH decrease of similar magnitude from the surface to 40 cm, as it has the highest surface pH of any zone. The magnitude of pH decrease through the top 40 cm in other zones is more gradual because surface pH values are lower. The additional pH decrease observed by Li and Davis in the 60-90 cm layer is of a greater magnitude than observed in any zone in the Lot 11 cell.

Buffering by particulate or dissolved constituents of infiltrating runoff is a likely explanation for the higher pH at the surface and decrease with depth. Particles sampled from the inflow channel have a pH of 7.0, the highest value among all samples measured in this study (Table B-6). Smolders and Degryse (2002) observed an increase in pH of approximately 0.5 – 1.5 units in soil amended with fine car and truck tire particles after 11 months of weathering. They posited that accumulation of tire particles, as well as concrete particles and fill materials, could be linked to commonly-noted presence of elevated soil pH adjacent to roads compared to soils sampled at a greater distance.

Road runoff has a near-neutral pH because of contact with pavement materials. Sansalone and Buchberger (1997) reported pH values for the initial and final 10 L of runoff from an asphalt pavement highway surface in five storms. From a rainfall pH of 4.1, the initial and final runoff pH was 6.0 and 6.7, respectively, indicating that the road surface contributed a moderate amount of alkalinity. Dean et al. (2005) found that the pH of runoff from a concrete highway surface generally ranged from 7.0 to 7.5. Runoff pH slightly increased over the duration of most events, presumably because of buffering through contact with the cement. Less buffering may occur in more extreme events because the runoff volume is larger while the contact time with pavement is smaller.

These phenomena are expected to apply in the Lot 11 drainage area, which has an asphalt pavement surface and a concrete channel to convey inflow. Over four years of operation as of the time of sampling, infiltrating runoff is likely to have partially overcome the buffer capacity of the organic and BSM segments. Upper portions of the media profile will consume alkalinity first, making the runoff less effective in raising the pH of lower layers. As a result, the decrease in pH with depth is expected. Additionally, particle penetration is likely limited to the top several cm of media (Section 4.3.1). Leaching of organic acids from the mulch/organic media layer may also contribute to the decrease in pH with depth.

Most BSM segments below approximately 30 cm have pH values less than that of the original media. Given the relatively small difference (0.2 units or less) in pH values compared to the original media, however, it is difficult to assign a definite cause for the continued drop in pH. Also, the original BSM was stored in a closed plastic bucket for 5.5 years before pH measurement. Possible microbial activity during that time introduces some uncertainty into the accuracy of the pH value of this material.

The deepest segments in Zones 1, 3, and 6 have relatively high pH values, between 5.6 and 6.3. Three other segments at similar depths have pH values between 5.0 and 5.1 that agree with the overall pH trend. It is likely that reducing conditions occur in deeper portions of the cell because of periodic saturation in the anaerobic sump (Section 2.2.1). Consumption of protons by reduction processes would account for the higher pH.

Segment 2C, with a pH of 5.1, is another notable outlier. A likely explanation is the production of organic acids during the degradation of mulch and other organic

substances (Sposito 2008). Segment 2C has the highest OM content of any segment, at 43%, possibly leading to greater production of organic acids relative to other segments.

4.2 Total metal at cell surface

To determine total metal accumulation at the cell surface, three samples were taken from each zone to depths of 2.5 – 3.2 cm and digested using the EPA 3050B method (EPA 1996). Combined with the top segment (2 – 3 cm depth) from each core, measured by sequential extraction (Section 2.2.4.2), the samples show that considerable surface accumulation of metals has occurred during the first four years of operation.

Zone 2 contains the highest mean metal concentrations of the seven zones (Table 4-3), followed closely by Zone 3. Table B-1 gives complete surface sampling results.

Table 4-3. Mean and standard deviation ($n = 4$) of total Pb, Cu, and Zn surface concentrations in Zones 2 and 3 after four years of operation. Results are compared with local background levels and two residential cleanup standards (MDE 2008, EPA 2008b). Also shown are total surface metal concentrations after 3.5 and 4.5 years of operation, respectively, in a Washington, DC bioretention cell (Li and Davis 2008a).

Source	Pb (mg/kg)	Cu (mg/kg)	Zn (mg/kg)
Zone 2 – Lot 11 cell	64 ± 7	49 ± 5	257 ± 25
Zone 3 – Lot 11 cell	59 ± 13	43 ± 5	230 ± 32
Eastern MD background	45	12	63
MD residential cleanup	400	310	2300
EPA residential cleanup	400	3100	23000
Street particles (Li and Davis)	399, 660	29, 75	111, 532
0 – 10 cm layer (Li and Davis)	580, 50	50, 30	180, 120

Raw mulch samples were not preserved during construction, which precludes a baseline for comparison with current surface concentrations. Raw BSM samples can

provide one point of reference; however, all surface samples consist of organic media rather than BSM. Total Pb, Cu, and Zn concentrations in the raw BSM are 2.6, 12, and 18 mg/kg, respectively, using values from the 3050B method (EPA 1996).

Another reference material is raw mulch from the Kenilworth cell, collected within several days of application. Both cells used shredded hardwood bark mulch from Prince George's County, but given the four-year age difference between the cells, the source stockpiles are presumably different. Total Pb, Cu, and Zn concentrations in the raw Kenilworth mulch are 3.8, 11, and 28 mg/kg, respectively. Compared to either reference material, Pb and Zn concentrations in Zones 2 and 3 have increased by about one order of magnitude, and Cu has increased by half an order of magnitude.

Bioretention metal accumulation data are currently limited. Li and Davis (2008a) investigated a cell with approximately the same age, geographic location, drainage area:cell area ratio, and drainage area type (parking lot). Street particles and a media core were sampled after approximately 3.5 and 4.5 years of operation. Media results agree with Lot 11 findings within an order of magnitude, with the exception of one lead result (Table 4-3). Zinc concentrations are approximately 25-50% lower in the Li and Davis cell, but this may reflect the average over a 10 cm sampling interval. Street particles had far higher concentrations for lead (both years) and zinc (one year) than any value measured in the Lot 11 cell, where similar particle deposits were not observed. Variation between each year's results may be spatial in origin rather than solely temporal.

Dietz and Clausen (2006) measured metal uptake in mulch in a bioretention cell receiving asphalt shingle roof runoff. The original and two-year copper concentrations in mulch were 4 and 52 mg/kg, respectively. The result is similar to the Lot 11 cell but lead

accumulation rates apparently vary, given the cells' age differences. Two-year Pb and Zn concentrations were lower than in the Lot 11 cell, at 12 and 42 mg/kg, respectively, likely reflecting the fact that the cell received runoff from a roof instead of a parking lot.

4.2.1 Regulatory implications

After four years of operation, metal concentrations are well below cleanup levels stipulated by the Maryland Department of the Environment (MDE) and the United States Environmental Protection Agency (EPA) (Table 4-3). Mean total copper and zinc in Zones 2 and 3 exceed Eastern Maryland soil background levels by approximately half an order of magnitude. Total lead in these zones is slightly above the background level, indicating that the media is relatively “clean” with respect to lead. In comparison, soil adjacent to roadways and in common open areas can have considerably higher lead levels (Turer et al. 2001, Petersen et al. 2006). Such areas present potential health risks that are both more widespread and of a greater magnitude compared to bioretention. Assuming constant accumulation rates, lead, copper, and zinc levels will reach the more restrictive MDE cleanup standard after 20, 20 and 30 additional years of operation, respectively. Application of fresh mulch would dilute metal concentrations at or near the surface.

Another common metric for evaluating potentially hazardous substances is the Toxicity Characteristic Leaching Procedure (TCLP), which subjects material to leaching under standardized conditions (EPA 1992). Lead is the only metal of the three considered a toxic contaminant under EPA-promulgated regulations stemming from the federal Resource Conservation and Recovery Act (RCRA). Material producing a lead concentration of 5.0 mg/L or higher in the TCLP extract is considered to possess the

characteristic of toxicity (CFR 2007). The highest lead concentration found in any media sample is 76 mg/kg, from the 2.5-5 cm organic segment in the Zone 6 core (Section 4.3.1). The corresponding maximum TCLP extract concentration would be 3.8 mg/L, assuming complete extraction of lead. As a result, the bioretention media has not attained hazardous lead levels. The actual extract concentration would likely be far lower than 3.8 mg/L. A mean of only 15% of total lead in the organic media was extracted using similarly strong reagents in the sequential extraction (Section 2.2.4.2, 4.4.1).

4.2.2 Variation with distance on cell surface

In addition to measuring metal concentrations to quantify lifetime accumulation, a key motivation for this study was to determine the spatial variation in concentrations throughout the cell. Surface samples provide a snapshot in time of metal accumulation in two dimensions. The cell's linear geometry, single inflow point, and observed linear flow regime (Section 2.2.2), suggest that metal accumulation may be influenced by distance from the inflow point. The surface analysis tests the hypothesis that metal concentrations are greatest near the inflow point and decrease with distance.

Figure 4-3 largely confirms the first hypothesis. Despite the scatter evident in the figure, deposition of metal mass is clearly weighted toward the front of the cell, with the exception of Zone 1. Total surface metal concentrations decrease with distance beginning at Zone 2. Mean Pb, Cu, and Zn concentrations in Zone 2 are 3.5, 2.1, and 2.9 times higher, respectively, than those at the end of the flow path in Zone 5.

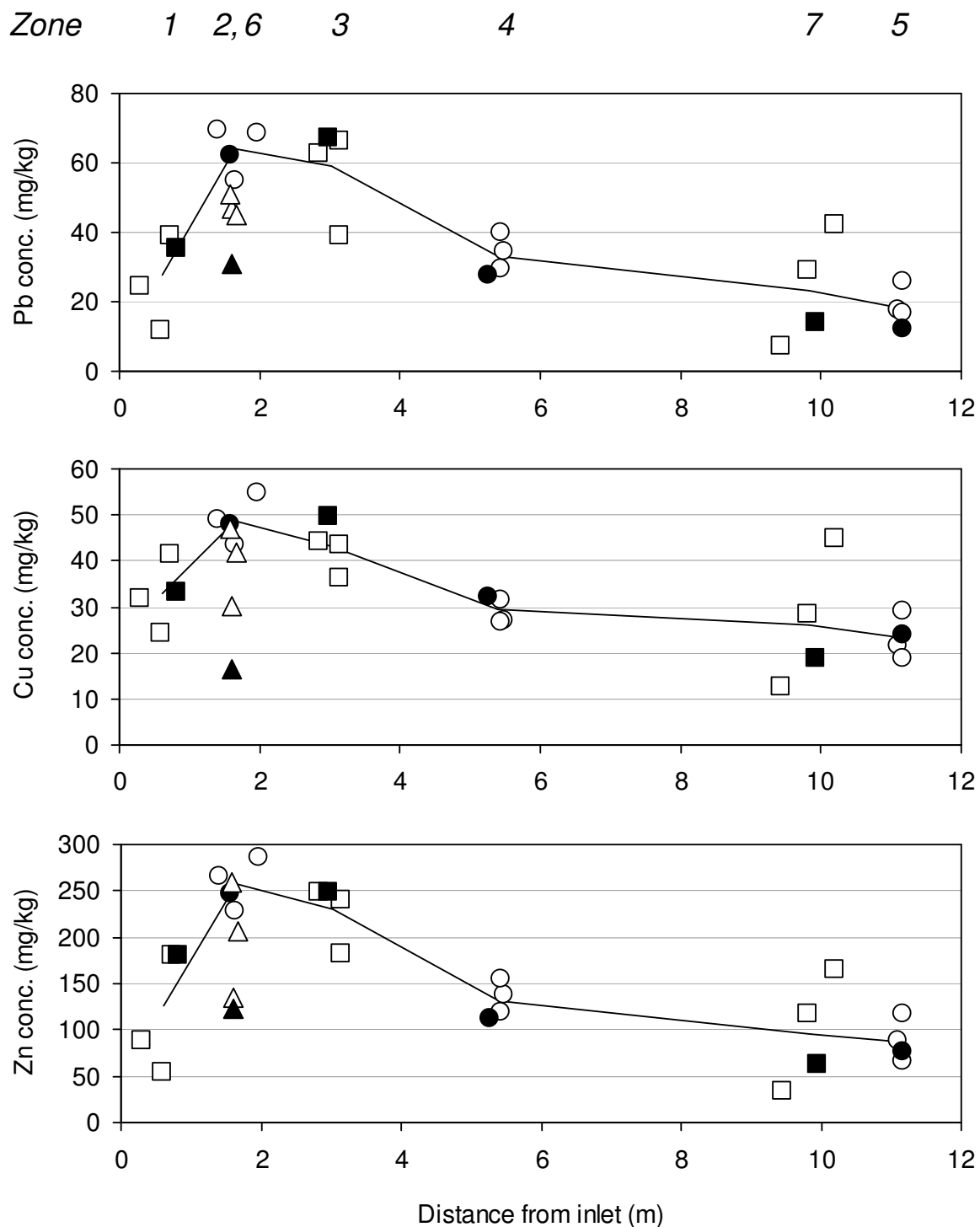


Figure 4-3. Pb, Cu, and Zn surface concentrations vs. distance from the inflow point. Each point on the curve is the mean distance and concentration of the four samples in each zone in the main flow path. Filled points indicate top core segments (top 2 – 3 cm) digested by sequential extraction. Hollow points are surface samples (top 2.5 – 3.2 cm) digested by 3050B method (EPA 1996). Triangles denote Zone 6; other zones alternate between squares and circles.

Similar trends have been observed in studies of soil adjacent to highways, in which metal concentrations were shown to decrease with distance from the roadway (Turer et al. 2001). In highway settings, however, spatial variation in metal accumulation cannot be attributed solely to runoff, but also likely results from deposition of exhaust and other airborne particles. A more fitting analogy is the trend in zinc levels observed in soil surrounding a galvanized electrical transmission tower (Jones and Burgess 1984). Extremely high zinc concentrations in soil adjacent to the tower were said to result solely from tower runoff (and to a lesser extent from windblown spray). Zinc concentrations returned to near-background levels with increasing distance from the tower.

4.2.2.1 Cumulative infiltration concept

It is hypothesized that the distance trend reflects the cumulative effect of unequal exposure of four years of runoff inflow and infiltration at various distances along the cell. Long-term mass accumulation is hypothesized to be proportional to the total depth of water infiltration at any point, which should be greatest at the front of the cell. This hypothesis also implies that variations in mass flushing from individual events will average out over time.

A simple model was developed to simulate flow behavior in the cell and to estimate the total depth of runoff that has infiltrated through each point during the first four years of operation. Precipitation events were developed from four years of rainfall data between Dec. 1, 2002 and Nov. 30, 2006, close to the date of first inflow and dates of media sampling, respectively. The data were collected 2.75 km from the cell at Station 6 of the Beltsville Agricultural Research Center. Continuous 5-minute data were grouped

into 467 storm events using a six-hour minimum inter-event dry period to define events. Rainfall in 85 events was only 0.254 mm (0.01 inch, a single rain gauge tip). Such events are unlikely to generate runoff and were excluded from further analysis. The remaining 382 events had rainfall depths ranging from 0.508 to 171 mm, with a four-year total of 4569 mm. The rainfall processor script is provided in Appendix C.

A symmetrical triangular hydrograph was assumed for each event (Kreeb and McCuen 2003). The runoff duration was set to equal the rainfall duration, which is reasonable for a small impervious watershed. The area under the hydrograph equals the storm runoff volume, which is the rainfall depth multiplied by a runoff coefficient of 0.9 and half the drainage area (assuming an even split between the two Lot 11 cells).

The model is driven by inflow rate, as measured along the triangular hydrograph. A key assumption is that water spreads across the cell surface only until the flow rate downward through the media (infiltration velocity * wetted area) equals the inflow rate (Figure 4-4). The mean media infiltration velocity is fixed at 11 cm/hr, based on an estimate derived from the initial flow test (Section 2.2.2).

The model assumes that there are no other constraints on the movement of water between the cell surface and the cell outfall, and that the infiltration velocity is constant in space and time. Wetting is assumed to cover the entire width of the cell at all distances, and to instantaneously advance or recede linearly along the cell axis in response to changes in flow rate. Ponding occurs whenever the inflow rate exceeds the infiltration rate through the entire cell surface.

Both the wetted area and the wetted distance along the cell axis are directly proportional to the inflow rate. Each point along the length of the cell is associated with

a flow rate that causes the wetted area to reach that point. The model divides the cell into n sections, each as wide as the cell and with a length of $1/n$ the total cell length. Distances to the front and back of each section correspond to flow rates that cause the wetted area to reach each point. During a storm, the volume that infiltrates into each section can be calculated from the portion of the inflow hydrograph bracketed by these flow rates.

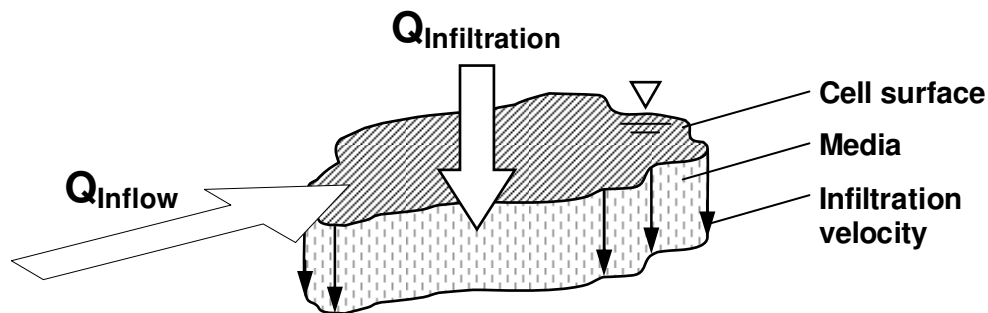


Figure 4-4. Illustration of water spreading and infiltration concept. Wetted area expands or contracts so that flow rate through media equals the inflow rate, given a fixed infiltration velocity. No ponding occurs until entire bioretention cell surface is wet.

Figure 4-5 illustrates the concept. The volume in each hydrograph section equals the volume infiltrating into the corresponding section of the cell surface. Infiltration at a given point continues throughout the entire storm as long as the inflow rate meets or exceeds the flow rate required reach that point. If ponding occurs, any volume greater than the available surface storage is assumed to pass through the overflow riser and is disregarded. The remainder is evenly distributed among all cell sections. The cumulative volume infiltrating through a section equals the sum of volumes at that section from all 382 events. As illustrated in Figure 4-5, the cumulative infiltration volume decreases with distance from the inflow point. Dividing a section's cumulative volume by its area gives the cumulative depth infiltrated at that section. Decreasing the

section size approximates a continuous distribution of infiltrated depths. The script used to calculate cumulative infiltration is provided in Appendix C.

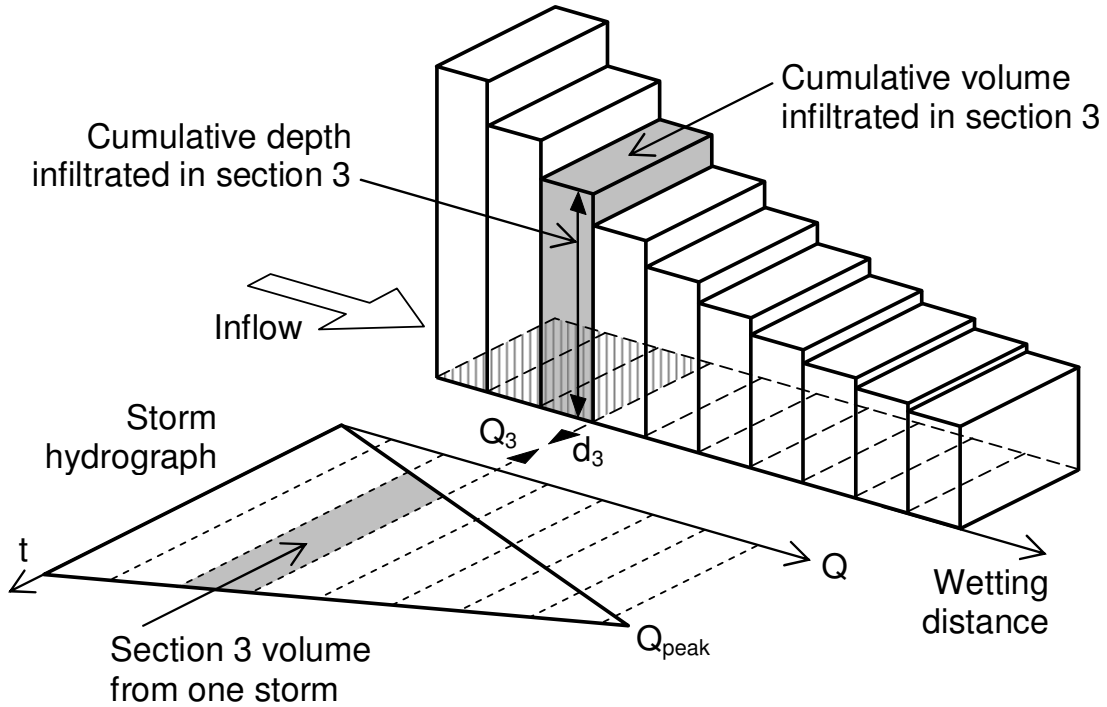


Figure 4-5. Storm hydrograph and cell surface divided into ten sections. The distance to the front of each section (e.g. d_3) corresponds to the minimum flow rate (e.g., Q_3) required to extend the total wetted area (hatched) to that point, given a fixed media infiltration velocity. The volume infiltrating through section n is calculated from the portion of the hydrograph between flow rates Q_n and Q_{n-1} . The infiltrated volume at each section is summed across all storms. Cumulative depth of infiltrated water in a section is found by dividing its total infiltrated volume by section area.

Figure 4-6 shows mean concentrations of all three metals normalized to their respective Zone 2 means in order to achieve a uniform scale. Also shown is a line representing the cumulative depth of infiltrated water, as calculated above. Five zones have very good agreement between normalized mean metal concentrations and depth of cumulative infiltrated runoff, with both data sets plotted relative to distance along the axis of the cell (the vertical component in Figure 2-10). The model indicates that cumulative

infiltration decreases relatively quickly with distance at the front of the cell, with a smaller decrease at the back. Zones 4, 7, and 5 infiltrate 60 to 40% of the total depth infiltrated at Zone 2, which agrees with the normalized metal means at those locations.

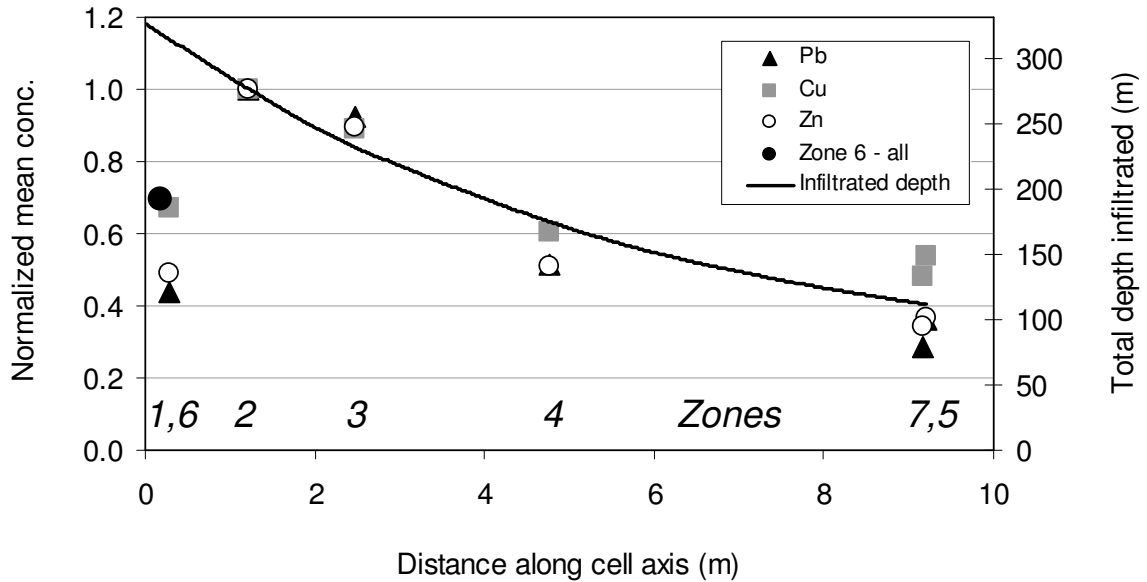


Figure 4-6. Four-year cumulative depth of infiltrated water along the length of the cell. Normalized mean total surface metal concentrations are also shown for all seven zones. Metal data are normalized to the Zone 2 means. Total distance is shorter than in Figure 4-3 because it is measured along the cell axis. Normalized mean metal concentrations in Zone 6 are very similar and are shown as one point for clarity.

The agreement between the model results and metal data suggests that hydrologic behavior explains much of the trend in mean surface metal concentrations, with the exception of Zones 1 and 6 (Section 4.2.2.2). Assumptions regarding hydrograph shape, infiltration behavior, and mass flushing allow the model to remain relatively simple and suggest that additional model complexity is not warranted at this level of analysis.

4.2.2.2 Other flow-related variation

Zones 1 and 6 do not fit the model, even though their position along the cell axis indicates that they should experience the highest cumulative infiltration of all the zones. Other impacts of flow behavior appear to be responsible for the lower metal accumulation in those zones.

Proximity to the inflow point exposes Zone 1 not only to a high cumulative depth of runoff but also to scouring by high-energy flows, which was observed beginning in the earliest weeks of operation (Figure 2-7). Zone 1 serves as the de facto means of energy dissipation, as it is the first point of contact for stormwater entering the cell and there are no energy dissipation devices upstream. Evidence of scouring was localized to Zone 1. Scouring may disturb the mulch/organic media layer sufficiently to lower the sorption capacity at the surface, resulting in decreased metal concentrations. Metal accumulation would still be expected to result from particle deposition, but scouring may resuspend both sorbed and particulate metals and carry them out of Zone 1.

The impact of scouring varies within Zone 1, however. Two surface organic media samples collected from Zone 1 in 2008 for the bioavailability analysis (Section 4.4.2) have lead concentrations of 78 and 83 mg/kg (Table B-6). These results are likely caused by the fact that the samples were taken from relatively undisturbed areas within Zone 1, as suggested by their high OM content (Section 4.1.1). Other differences between the 2006 and 2008 samples, such as age and sieved particle size, are not expected to explain the 2008 findings. Mulch was not replenished between 2006 and 2008.

Zone 6 has low mean metal concentrations despite its proximity to the inflow point. During the initial flow test, most inflow was observed to bypass Zone 6, based on

the path taken by the tracer dye (Section 2.2.2). The flow path is well-defined at the front of the cell, following the east edge, and becomes broader with distance from the inflow point. Metal accumulation in areas at the front of the cell appears to be more sensitive to the flow path than to proximity to the inflow point, counter to the assumption of the cumulative infiltration model.

4.2.2.3 Role of OM content within zones

Sampling zones were sized and located so that exposure to inflow would be expected to be uniform within a zone. Therefore, variation in metal concentrations among the four surface samples within each zone is not likely to be caused by differences in cumulative infiltrated depth but instead by smaller-scale factors. One such factor is OM content, which varies among the four samples in each zone, as shown in Figure 4-1.

Humic substances in soil organic matter have a strong affinity for metals, largely as a result of their carboxylic and phenolic functional groups (Alloway 1995, Chang Chien et al. 2006, Sposito 2008). Chemical extractions of OM from whole soils produced a substantial reduction in sorption capacity for Cu and Zn, as indicated by changes in the distribution coefficient K_d (Covelo et al. 2004b, Vega et al. 2007). Given the affinity of OM for metals and its importance for sorption within the whole soil, differences in OM content may be largely responsible for the variation in metal content found within each zone.

To test this hypothesis, metal concentration was plotted against OM content for each sample, as shown in Figure 4-7. Regression lines are plotted through the four samples in each zone. The plots suggest that a positive relationship exists between OM

content and metal concentration in many cases, supporting the hypothesis that differences in OM content may at least partly explain local variations in metal concentration between samples. Section 4.1.1 discusses possible reasons for spatial variation in OM content.

A correlation coefficient (R) was calculated for each line. Zones with the strongest positive relationships ($R \geq 0.9$) are 1 and 7 for lead; 2, 3, and 5 for copper; and 1, 2, 6, and 7 for zinc. Correlation coefficients in these cases ranged between 0.93 and 0.99. Given the small size of each data set ($n = 4$), however, R values do not definitively reflect the actual relationship between OM content and metal concentration that would be found if more samples had been analyzed (Ayyub and McCuen 2003). A larger sample size in each zone would be needed to more rigorously describe any such relationship.

No zone had $R \geq 0.9$ for all three metals. Zone 7 comes close, with $R = 0.89$ for Cu. Zones 1, 2, and 7 each had $R \geq 0.9$ for two metals. The exact reason for the strong correlation in these zones, but not in the others, is unclear. It is possible that the high cumulative infiltrated depth in Zones 1 and 2 has provided the greatest opportunity for the relationship between OM content and metal accumulation to be developed. Surface media in Zone 7 was unexpectedly heterogeneous, with the widest range of OM content of any zone and among the highest range in metal concentrations.

Zone 4 had a weak negative correlation with OM content for lead and zinc and a moderately high positive correlation for copper ($R = 0.80$). OM and metal values are tightly clustered in Zone 4 compared to the other zones, however. Given the limited range of values and small sample size, means are likely the best predictors of OM and metal content in Zone 4. No other zones had negative correlations for any metal.

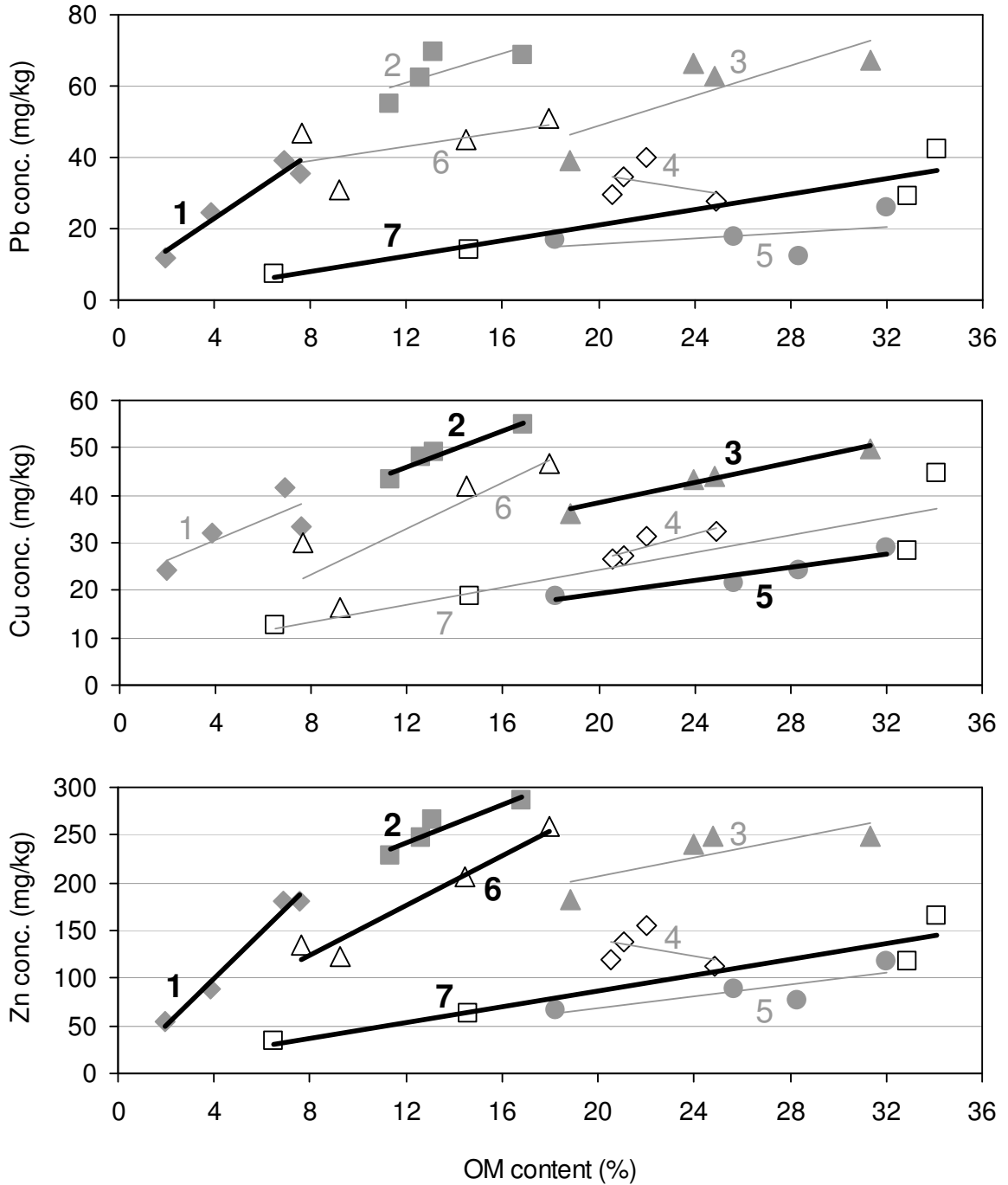


Figure 4-7. Metal concentration vs. OM content for each set of four surface samples within each zone. Linear regression lines are shown for each zone. Thick lines indicate zones with the strongest positive correlations ($R \geq 0.9$). Each data point is the mean of two replicates for OM content and metal concentration.

4.2.2.4 Surface metal ratios

Past work has established differences in partitioning among the three metals in stormwater runoff (Sansalone and Buchberger 1997), as well as differences in their affinity for mulch and organic substances (Jang et al. 2005, Chang Chien et al. 2006). Given these findings, it should not be assumed that spatial distributions of these metals will be consistent within the cell. However, the close resemblance of the curves in Figure 4-3 and the results of the cumulative infiltration model (Section 4.2.2.1) suggest that metal accumulation patterns on the surface are driven primarily by distance from the inflow point rather than intrinsic geochemical properties of the metals. Local variation in OM content is also likely to be an important small-scale factor influencing metal accumulation, as discussed in the previous section. For instance, the four samples in Zone 7 follow the same order, from lowest to highest concentration, for each metal.

Figure 4-8 shows paired metal concentrations from all 28 surface samples. The ratio between metal concentrations throughout the cell can be expressed as the slope of the regression line. The data show an aggregate Zn:Cu media concentration ratio of 6.0 ($R = 0.86$), a Pb:Cu ratio of 1.5 ($R = 0.93$) and a Zn:Pb ratio of 3.7 ($R = 0.96$). The high R values are consistent with the similarity between curves in Figure 4-3 and imply that a relatively constant ratio exists, on average, between concentrations of any two metals throughout the cell. Scatter in the plots indicates that ratios will vary locally.

The ratios likely reflect a lifetime “average” of the metal input concentrations as well as the long-term fate of retained metals, including strength of affiliation, which relates to mobility; and plant uptake. In turn, input concentrations reflect the contribution of vehicular and atmospheric metal inputs to the watershed. The physical meaning of the

intercepts in Figure 4-8 is unclear. Further study of the factors that contribute to the metal ratios, and the basis for zero or non-zero intercepts, is beyond the project scope.

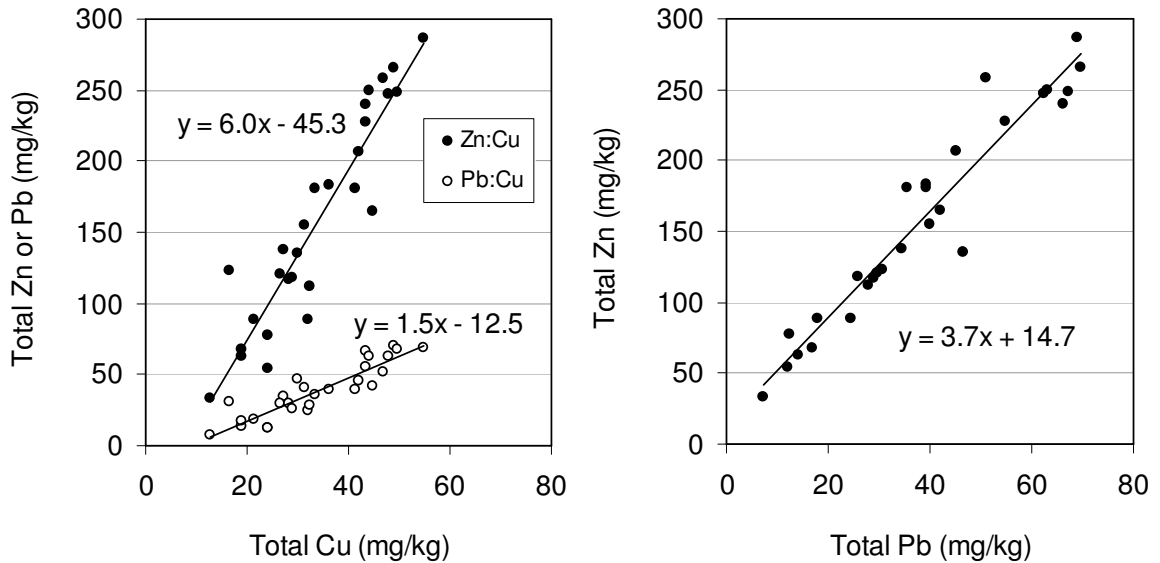


Figure 4-8. Paired metal concentrations for all 28 surface samples (Zn and Cu, Pb and Cu, and Zn and Pb). The slopes of the regression lines indicate relatively constant ratios between metal concentrations across the cell surface and over the full range of values.

Water quality monitoring at the cell in 2003 and 2004 over 9 storm events (12 events for zinc) provided total mass estimates for inflow and outflow over these events (Davis 2007). Total metal input for these events was 7.0, 0.97, and 15.2 g for Pb, Cu, and Zn, respectively. Output masses were 0.87, 0.17, and 7 g. Taking the difference to be the mass retained in the cell and ignoring plant uptake, the resulting ratios are 10.3, 7.7, and 1.3 for Zn:Cu, Pb:Cu, and Zn:Pb. The Zn:Cu ratios are reasonably in agreement, given the very different methodologies, time scales, and sample types. The two ratios involving lead do not agree well with their counterparts shown in Figure 4-8. Ratios from water sampling indicate that a higher mass of lead was retained in the media relative to the other metals than suggested by the metal extraction ratios. It is possible that plant uptake

could partly resolve the disagreement between the two sets of ratios, but it is more likely that the differences stem from the limited sample size in the water quality monitoring.

4.3 Variation with depth

One 90-cm media core sample was taken at each zone (63 cm in Zone 4). Combined with the surface sampling results (Section 4.2.2), these seven core samples complete a three-dimensional snapshot of metal accumulation in cell media after four years of operation. Past research has found a top-heavy metal profile in infiltration basins (Nightingale 1987, Dechesne et al. 2005) and in lab- and full-scale bioretention cells (Davis et al. 2001a, Li and Davis 2008a). The general trend observed in these studies was enrichment in the top 5 to 10 cm followed by a rapid drop to background concentrations with increasing depth. Given these findings, it was hypothesized that total metal concentrations would follow a top-heavy profile.

Figures 4-9 through 4-11 show a distinctly top-heavy profile and a decrease in total metal concentrations with depth, confirming the hypothesis. Tables B-3 – B-5 give the range of total metal concentrations in each segment ($n = 2$). The vast majority of metal accumulation occurs in the top 5 cm, with the exception of Zone 2, which has a thicker organic layer. This depth of accumulation is quite small compared to a total media depth of 90 – 100 cm throughout the cell. These results indicate that metal breakthrough within the full media profile is not at all close to occurring.

Hatt et al. (2008a) observed a link between effluent quality and media metal concentration profiles. Effluent sampling ports in columns of sandy loam, with no mulch layer, revealed that Pb, Cu, and Zn concentrations in simulated stormwater decreased 80-

90% in the top 10 cm and approached zero through the remainder of the 100 cm columns. Subsequent media analysis was consistent with effluent results: metal accumulation was confined to the top 10 cm, with a sharp drop in media concentrations within the top 2.5 cm. Li and Davis (2008a) found a similar media profile in a bioretention field study. The highest lead and zinc concentrations occurred in the surface layer (mulch and accumulated particles) and in the top 10 cm of BSM. Copper had a somewhat different trend, with one core showing a high concentration in the 70-80 cm segment and the other showing a top-heavy profile, but with relatively high concentrations deeper in the profile.

4.3.1 Sorption and particle capture

Top-heavy metal concentrations in bioretention media are expected to occur as a result of 1) efficient capture of dissolved metals through various sorption mechanisms and 2) settling, surface straining, and depth filtration of particulate-bound metals. A simple mathematical model by Li and Davis (2008a) describing total metal accumulation with depth predicted that all accumulation would occur in the top 10 cm, based on mechanistic equations describing particle capture and sorption phenomena.

The surface organic layer may exacerbate the top-heavy profile by enhancing media affinity for dissolved metals. Metal concentrations in BSM segments, by comparison, approach that of the original material, indicating that little metal accumulation has occurred in this layer despite the demonstrated affinity of sandy loam soil for dissolved metals (Hatt et al. 2008a). Box studies by Davis et al. (2001a) had a similar result, with all measureable metal accumulation occurring in the 2.5 cm top mulch layer, leaving the sorption capacity of the underlying sandy loam soil untapped. Sorption

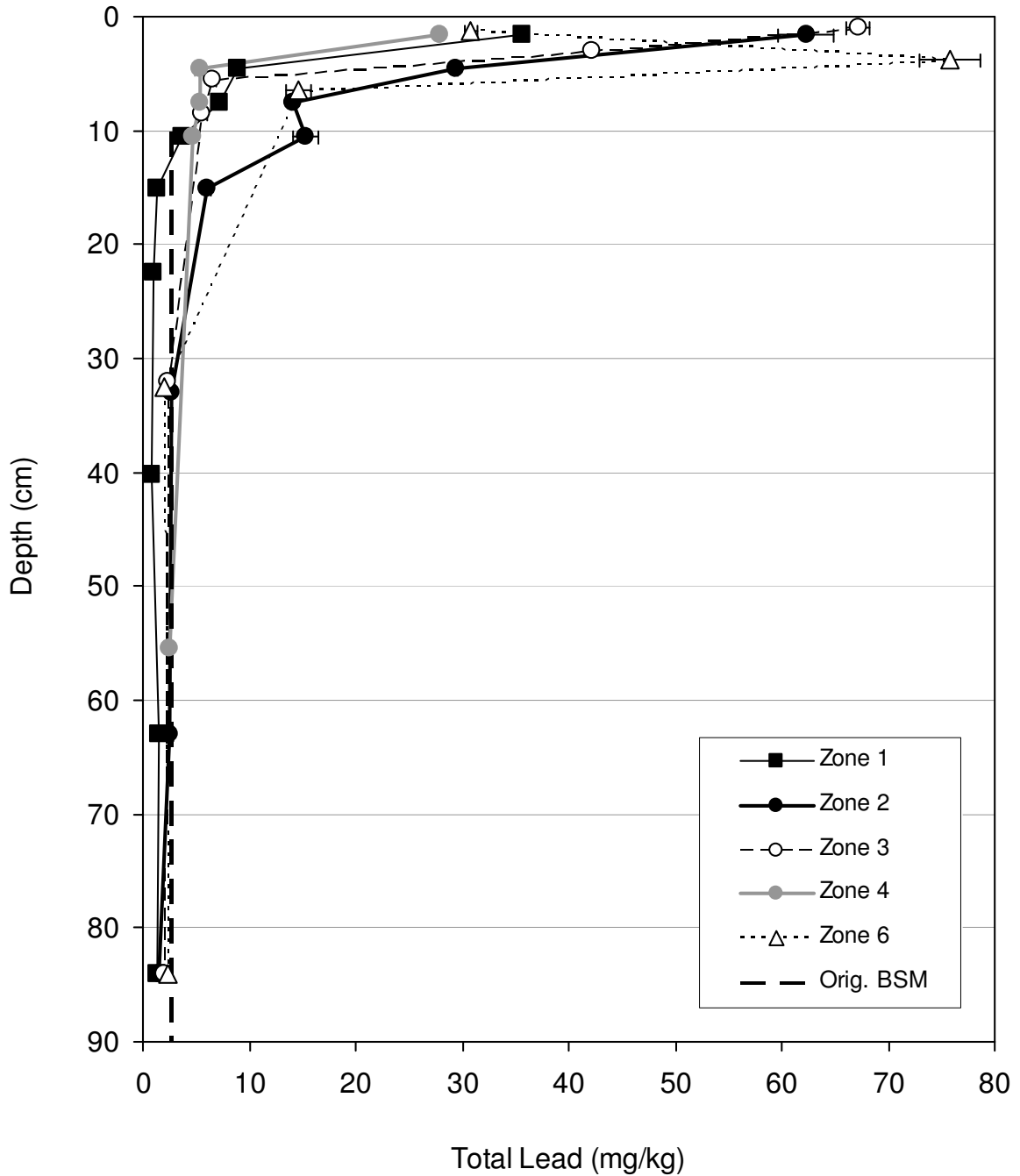


Figure 4-9. Mean lead concentration ($n = 2$) as a function of media depth in core samples from selected zones. Zones 5 and 7 are omitted for clarity. Error bars indicate the range of two replicates. Totals are the sum of sequential extraction results for upper segments and 3050B results (EPA 1996) for lower segments, as indicated in Table B-3. For original BSM, the 3050B result is shown because most BSM segments were digested using that procedure.

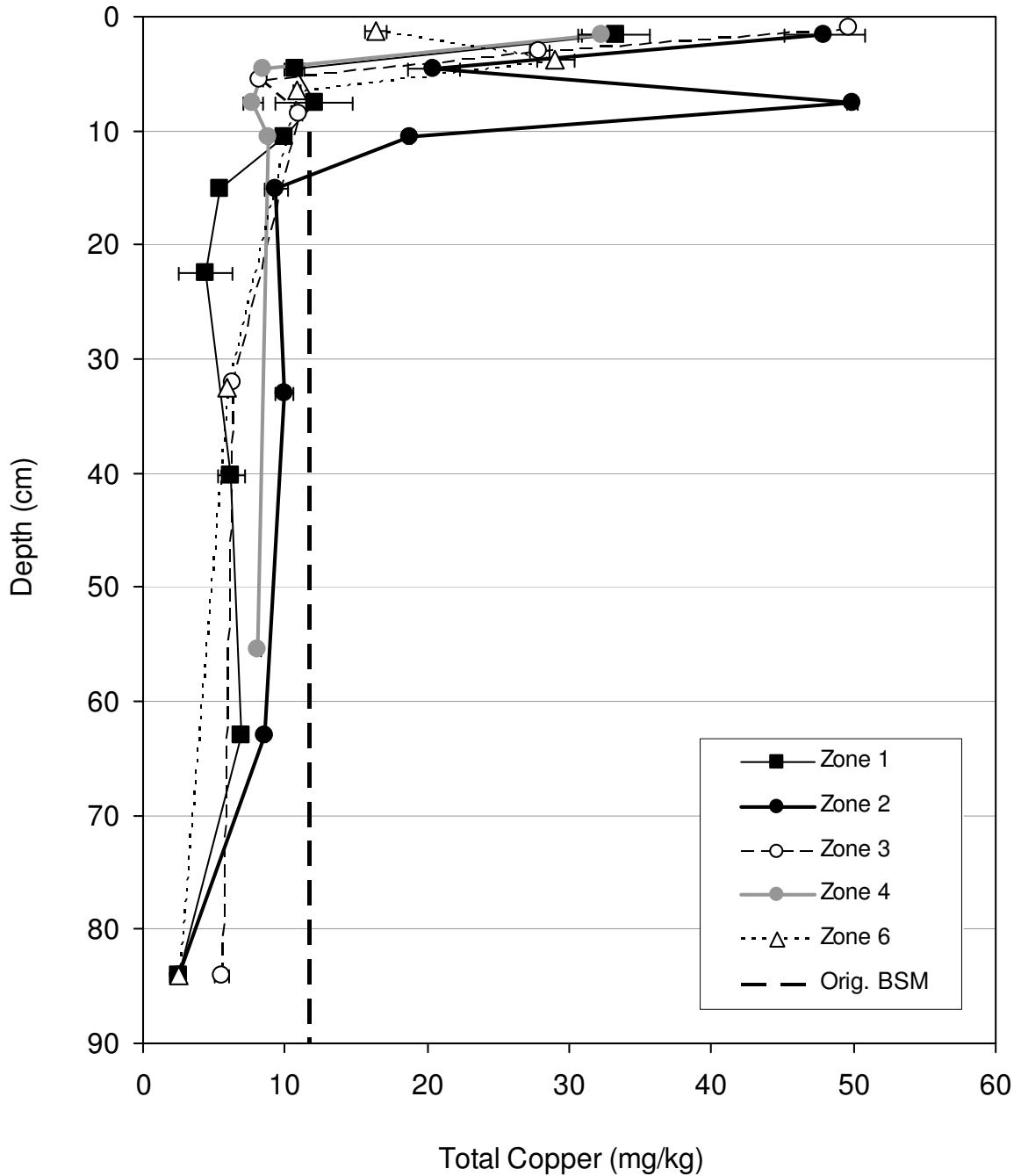


Figure 4-10. Mean copper concentration ($n = 2$) as a function of media depth in core samples from selected zones. Zones 5 and 7 are omitted for clarity. Error bars indicate the range of two replicates. Totals are the sum of sequential extraction results for upper segments and 3050B results (EPA 1996) for lower segments, as indicated in Table B-4. For original BSM, the 3050B result is shown because most BSM segments were digested using that procedure.

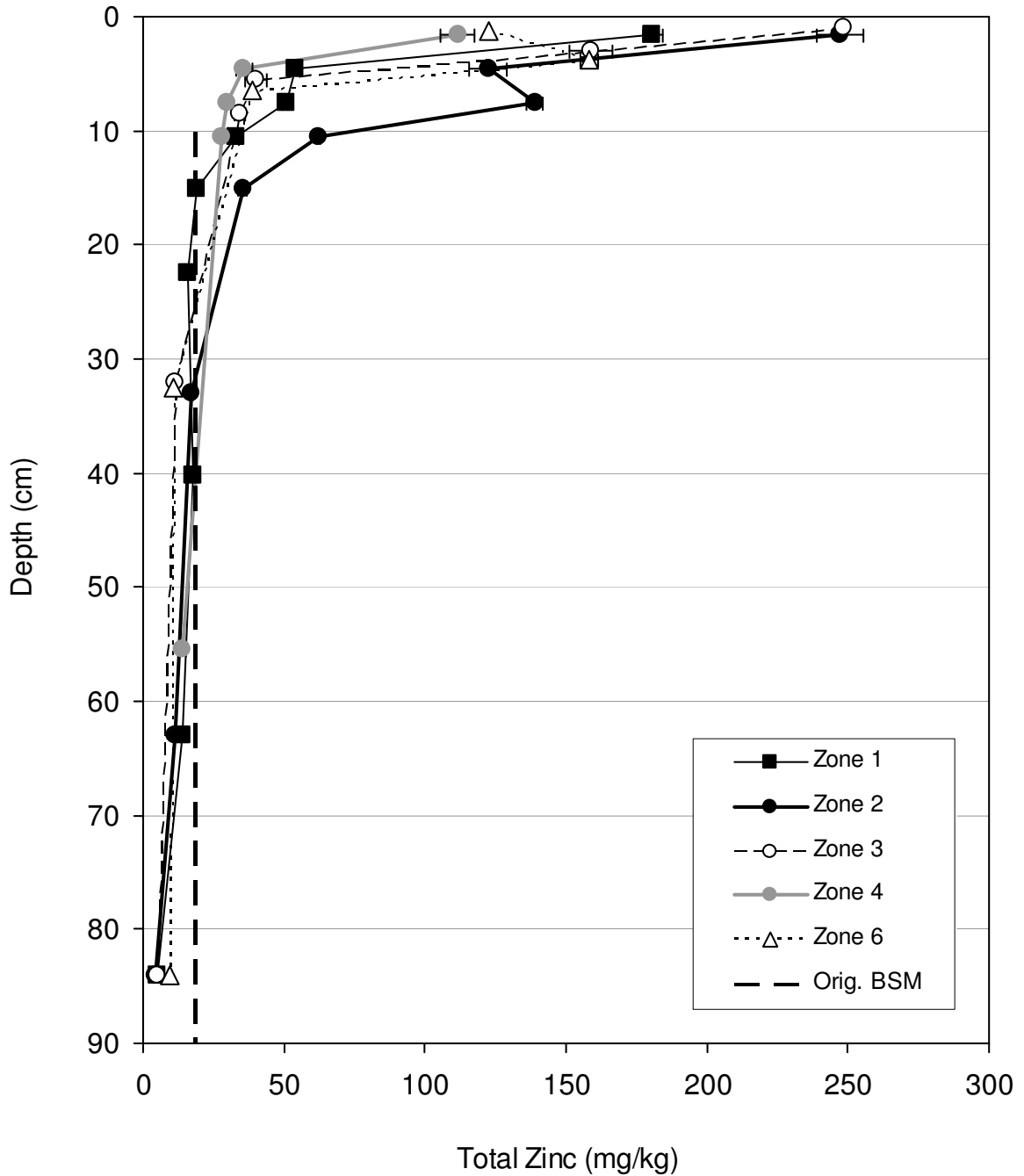


Figure 4-11. Mean zinc concentration ($n = 2$) as a function of media depth in core samples from selected zones. Zones 5 and 7 are omitted for clarity. Error bars indicate the range of two replicates. Totals are the sum of sequential extraction results for upper segments and 3050B results (EPA 1996) for lower segments, as indicated in Table B-5. For original BSM, the 3050B result is shown because most BSM segments were digested using that procedure.

as well as filtration may be operative in the uppermost BSM segments in the Zone 1 and Zone 4 cores because the adjacent organic segments are only 3 cm thick.

Particulate-bound metals are also trapped within the top several cm of media. Dechesne et al. (2005) found particle size (d_{10}) to increase with depth in the media profile of several infiltration basins, indicating surface trapping of fines. Similarly, Nightingale (1975) found the proportion of clay-sized particles in a sand recharge pit to decrease sharply in the top 15 cm. Column studies by Li and Davis (2008b) showed that small particles could only penetrate the top 5-10 cm of bioretention media. The authors noted that larger particles will settle or be strained at the media surface, but their larger size makes them of less concern for both metal accumulation and clogging potential.

4.3.2 Micro-trends with depth

As a result of the sorption and particle capture that occurs at the top of the media profile, most discernable trends from segment to segment occur within the surface organic layer. The Zone 2 core offers the clearest illustration of variation in total metal with depth because it has the thickest organic layer (12 cm). Lead, copper, and zinc concentrations drop sharply from segment 2A (0-3 cm) to 2B (3-6 cm). From segment 2B to 2C (6-9 cm), copper and zinc concentrations increase (Figures 4-10 and 4-11). This condition is likely caused by the unusually high OM content in segment 2C, as discussed in Section 4.1.1. Chang Chien et al. (2006) found that among three humic substances, binding strength increased with total acidity and percentage of carboxylic C, both of which should be higher in segment 2C than in surrounding segments with lower OM content. Lead concentrations, however, do not follow this trend. Although lead has

a high affinity for OM, as noted elsewhere in this report, it is also more particulate-bound in runoff than copper or zinc (Sansalone and Buchberger 1997). Variation in media OM content should have less impact on lead capture because less lead is in dissolved form.

Metal concentrations decrease with depth in the two organic segments in Zones 3, 5, and 7. In Zones 3 and 7, this occurs despite a nearly identical OM content within each pair of segments, suggesting that the higher position of the top segment favors sorption and filtration there. In Zone 6, concentrations of all three metals sharply increase from segment 6A (0-2.5 cm) to 6B (2.5-5 cm), even though OM contents and pH values are relatively constant. No explanation for the Zone 6 results is easily discernable from the data. Cores taken in Zones 1 and 4 each have a single 3 cm long organic segment.

Concentrations in the top several segments of each core vary strongly by depth, but the change from one BSM segment to the next is small. Metal concentrations in the BSM layer continue to decrease with depth, with a few minor variations, and generally fall slightly below that of the original BSM (3050B result). The deepest segments in Zones 1, 2, 3, 6, and 7 extend to 90 cm and have especially low metal concentrations, with several copper results below the detection limit (5 mg/kg for flame). For these segments, the corer may have sampled the sand-and-newspaper anaerobic sump at the bottom of the cell (Davis 2007), which likely has a lower native metal concentration than BSM. The underdrain blocked sampling past 63 cm in Zone 4.

4.3.3 Maintenance implications

The depth results complete the three-dimensional analysis of total metal accumulation in the media. The operating lifetime of bioretention media with respect to

metals may be clogging-limited, breakthrough-limited, or limited by regulatory cleanup levels (Section 4.2.1). Given the flow patterns and metal accumulation trends in the cell, any of these scenarios is likely to first occur locally, near the inflow point, rather than throughout the entire cell at once. The metal spatial distribution in the Lot 11 cell can be conceived as an approximately 5 cm thick “hotspot” at the cell surface in the vicinity of Zones 1, 2, 3, and 6, with metal concentrations decreasing with distance and depth from that portion of the media. This represents a relatively small amount of media to potentially be replaced when its capacity is exhausted or regulatory limits are reached.

Clogging does not appear to be a concern to date at the Lot 11 cell. A clogging layer has not been observed and the cell continues to function well hydraulically (Section 2.2.2). Creation and renewal of macropores can partly counteract the tendency for clogging caused by the continual influx of runoff particles. Hatt et al. (2008a) and Li and Davis (2008b) noted that macropores at the media surface are continually renewed by shrinkage and cracking during dry periods, by root growth and decay, and by earthworm and other soil fauna activity. Surface and depth filtration of particulate-bound metal is expected to continue near the surface, reinforcing a top-heavy metal profile. The location may shift away from the current hotspot over time if the infiltration rate decreases locally. Cake layers would likely be easily detectable and could be removed; none have been observed to date. Turbulence from inflow may also help to break up cake layers.

The operating lifetime of the organic layer may also be breakthrough-limited. In this scenario, effective sorption capacity would be exhausted before triggering cleanup action. Bioretention cells are not likely to be breakthrough-limited because of the potential for renewal of the organic media. Bioretention is a dynamic system and the

deposition and decay of plant material and paper-based trash will continuously add fresh OM. Periodic mulch replenishment would also renew sorption capacity at the media surface, preserving a top-heavy profile. The rate of OM replenishment compared to the rate of consumption of binding sites is unknown, however. If breakthrough does occur in the organic layer, dissolved metal capture would shift to the underlying BSM layer, where currently the sorption capacity is nearly unused after four years of operation. Assuming that clogging is not a limiting factor, the cell likely has several decades' worth of metal sorption capacity (or longer if mulch is replenished), given the fact that the metal hotspot is limited to a relatively small mass of media after four years.

The relationship between sorption capacity and cleanup levels is unclear because the sorption capacity of the organic layer is not known. Characteristics of the organic layer change over time with the continual influx of runoff particles and the decay and replenishment of plant matter. Even if the effects of media evolution could be quantified, media sorption capacity would not be a fixed value because sorption of dissolved metals occurs in equilibrium with dissolved metals that remain in solution. If regulatory limits are reached before exhausting the effective organic media sorption capacity, media removal should focus on the top 5-10 cm near the inflow point. Capture of particulate-bound metals will accelerate the timeframe in which cleanup levels are reached.

Given the good hydraulic performance observed to date and the ample supply of relatively clean media in the profile, attainment of one or more regulatory cleanup levels at a localized hotspot may be the most probable trigger for maintenance action at this cell. This scenario may be able to be delayed through simple maintenance actions such as

periodic mulch replenishment, removal of any deposits of parking lot particles, and efforts to keep the inflow as evenly distributed as possible across the cell surface.

4.4 Environmental availability and bioavailability

The inherently decentralized nature of bioretention cells causes metals to be collected and retained throughout the landscape. From an ecological standpoint, their position in upland areas raises the concern of subsequent metal remobilization into the watershed. Similarly, the placement of bioretention cells in yards, parking lots, and other developed areas increases the chance for human contact with accumulated pollutants, including metals. The long-term environmental fate of captured metals, including environmental and physiological pathways, is therefore of concern (Li and Davis 2008a).

As discussed in Section 4.2.1, total metal concentrations are low relative to cleanup levels established by the State of Maryland and the U.S. EPA. Total metal is a commonly-used and relatively straightforward metric for quantifying the extent of metal pollution in soils and related media. Its use as the basis for determining environmental fate or human health risks may be overly conservative, however, if only a fraction of total metal is bio- or environmentally available.

Questions of environmental or physiological fate can be addressed through extractions designed to assess the strength of metal affiliation with the media under various chemical, physical, and biological conditions. The fraction of total metal released in a given extraction has the potential to be mobile under analogous environmental or physiological conditions, while the remainder will remain immobile or

inaccessible. Two different extraction methods are used in this study to estimate the environmental availability of lead, copper, and zinc; and the bioavailability of lead.

4.4.1 Sequential extraction

Metals exist in a variety of forms in bioretention media, reflecting the diversity of metal sources in urban watersheds as well as the complex surface chemistry of bioretention media particles. As a result, metal strengths of affiliation range from water-soluble to highly refractory. Strength of affiliation between metals and the solid phases, whether bioretention media or runoff particles trapped in the media, is an important measure of the mobility of accumulated metals. Weakly-held, easily mobilized metals are of primary concern because of their expected high bioavailability (Dean et al. 2005).

Metal mobilized in each sequential extraction step is operationally defined by parameters such as reagents used, pH, temperature, and mixing. Results can indicate metals' relative strength of affiliation with the media and offer qualitative insights into their long-term fate, but do not correspond to specific types of binding (Bäckström et al. 2004). Results represent a snapshot in time of metal fractionation, which may change over time with the ongoing influx of runoff and biological and chemical activity.

A five-step sequential extraction procedure was carried out on 14 organic and 10 BSM segments. The steps generally progress from relatively gentle to very harsh in the following order: F1, "soluble-exchangeable"; F2, "sorbed-carbonate"; F3, "oxidizable"; F4, "reducible"; F5, "residual" (Section 2.2.4.2). Fractions were named by Ahnstrom and Parker (1999), whose method was modified by Li and Davis (2008a).

4.4.1.1 Fractionation trends in organic media

Figure 4-12 shows the normalized mean affiliated metal fractionation of all organic and BSM samples. Tables B-3 – B-5 list each segment's fractionation. Among the organic segments, metal fractions in F1 (“soluble-exchangeable”) are generally low, with mean lead, copper, and zinc F1 fractions of 3.9, 3.9, and 13%, respectively. With the majority occurring in environmentally inaccessible fractions (F2 through F5), metals captured in bioretention media are expected to remain largely immobile. Following the same method as this study, Li and Davis (2008a) reported low F1 fractions in bioretention media for all three metals. Using two different methods, Nörrstrom and Jacks (1998) and Turer et al. (2001) also found “exchangeable” lead, copper, and zinc to be low in soils adjacent to highways.

On average, nearly 50% of lead in organic media occurs in F4 (“reducible”), with F3 (“oxidizable”) of secondary importance, at 22%. At first glance, the dominance of F4 for lead is somewhat surprising, given that lead has been shown to have a similar or slightly greater affinity than copper for humic substances (Jin et al. 1996, Chang Chien et al. 2006), mulch (Jang et al. 2005, Ray et al. 2006), and whole soils (Elliott et al. 1986, Covelo et al. 2004a). The F4 results for lead can likely be explained by lead partitioning in runoff. Lead in urban runoff exists mainly in the particulate-bound fraction, while copper is mainly dissolved or intermediate between the two phases (Sansalone and Buchberger 1997, Dean et al. 2005, Prestes et al. 2006). Runoff particles are expected to be captured within the top several cm of media, coinciding with the location of the organic layer (Section 4.3.1). The dominance of F4 in lead fractionation therefore likely reflects the presence of captured runoff particles at the top of the media profile.

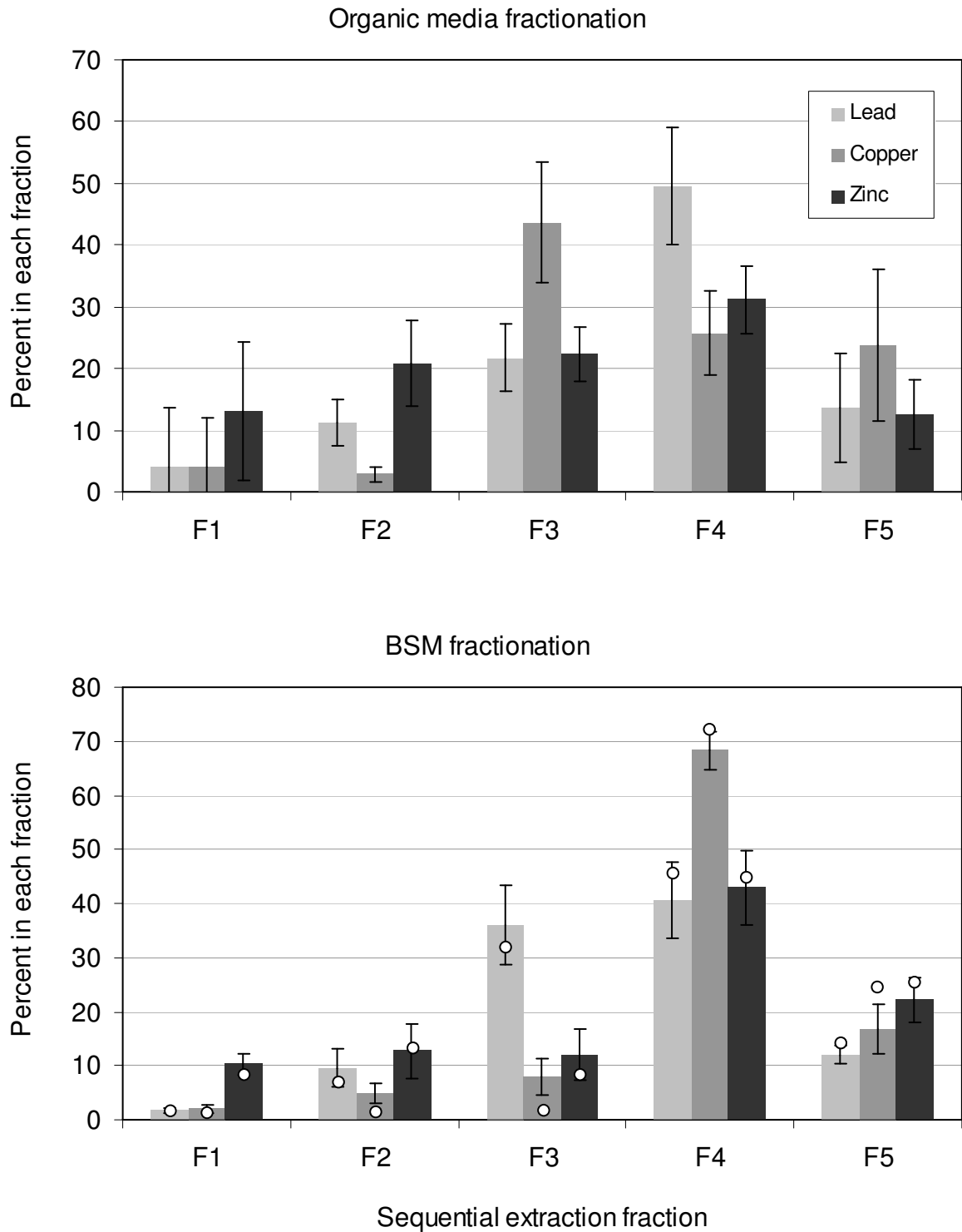


Figure 4-12. Media fractionation shown as the mean and standard deviation of normalized sequential extraction results for organic ($n = 14$) and BSM ($n = 10$) samples. Fractionation of original BSM for each metal is shown as open circles.

Lead fractionation varies in other studies, however. In the 2004 bioretention media core analyzed by Li and Davis (2008a), F2 and F5 almost exclusively dominate the fractionation of lead. The 2005 core in that study was also dominated by F2 and F5 but had a greater proportion of F4. Turer et al. (2001) found the greatest proportion of lead in roadside soils in the “residual” fraction, with nearly as much present in the “carbonate bound” fraction. “Reducible” and “oxidizable” fractions were equally predominant in a study of roadside soils by Bäckström et al. (2004). Nörrstrom and Jacks (1998) found the “oxide-bound” fraction to be dominant in roadside and infiltration pond soils, followed by the “carbonate-bound” fraction. Roadside soils may have legacy lead contamination, which could affect fractionation. This source of lead should be absent from bioretention unless particles of roadway soil are washed in.

F4 should not be interpreted as a more tightly-held fraction than F3 based on sequence. Ahnstrom and Parker (1999) placed the “oxidizable” extraction before the “reducible” extraction, counter to the typical order, to improve reagent selectivity and specificity. Organic and oxide soil phases can be highly interrelated, with complimentary influences on metal sorption (Adediran and Kramer 1987, Alloway 1995, Petrović et al. 1999). F3 and F4 findings should not necessarily be interpreted as 1) representing increasing strengths of affiliation or 2) being strictly selective for specific phases.

Copper is dominated by F3, with F4 and F5 of secondary importance. F2 is negligible for copper. Li and Davis (2008a) found F2, F3, F4, and F5 to be roughly equal in the top two segments of the 2005 core. The 2004 core was dominated by F2, F4, and F5 at the top of the profile. In a study by Nörrstrom and Jacks (1998), copper was mainly “organically-bound” in infiltration pond soil, but “organically-bound” and “residual”

fractions were roughly equal in roadside soil. Bäckström et al. (2004) found the “oxidizable” fraction to be dominant in roadside soil, with the “residual” fraction of secondary importance. Turer et al. (2001) observed the reverse.

Among organic media samples, copper F3 and F4 concentrations have correlation coefficients of 0.47 and 0.75 with %OM, respectively. In comparison, Nörrstrom and Jacks (1998) reported a strong correlation between “organically bound” Cu and %OM ($R = 0.86$). The moderately strong correlation between F4 and %OM suggests that organic and oxide media components may be interrelated, as discussed above. No other Cu fractions and no fractions of lead or zinc have positive correlations with %OM.

Zinc has the most relatively even distribution across all five fractions. The greatest proportion of zinc occurs in F4, followed closely by F3 and F2. F1 and F5 are of tertiary importance, each with approximately the same average proportion of zinc. Li and Davis (2008a) also found a relatively even distribution of zinc, but with less present in F3. The top two segments in their 2004 core were dominated by F2, F4, and F5; the corresponding segments in the 2005 core had a higher proportion of F3 but were also dominated by F2, F4, and F5. Bäckström et al. (2004) found the three most tightly-held fractions, “reducible,” “oxidizable,” and “residual,” to have roughly the same importance. Other researchers found zinc dominated by a single fraction. In infiltration pond and roadside soil samples, Nörrstrom and Jacks (1998) found the “oxide” fraction to dominate, although some roadside samples also had a substantial “residual” fraction. The “residual” fraction was highly dominant in roadside soil in a study by Turer et al. (2001).

4.4.1.2 Zinc in F1 and F2

The relatively high proportion of zinc in F1 and F2 is consistent with other studies showing higher zinc mobility and lower media binding strength compared to copper and lead. Li and Davis (2008a) found zinc to have a higher mean F1 proportion (18%) than lead (1%) or copper (3%), consistent with the findings of this study. In batch studies by Ray et al. (2006), zinc removal from solution by sorption to hardwood mulch was lower (58%) than that of lead or copper (92 and 86%, respectively), after one hour of contact time. More zinc (9.6%) than lead or copper (2.9 and 1.9%, respectively) was desorbed after washing with deionized water for one hour. Chang Chien et al. (2006) found that for three different humic substances under various initial metal concentrations and pH values, a greater proportion of zinc consistently remained in solution compared to lead and copper. Zinc and copper adsorption was studied under the same experimental conditions employing a variety of soils (Covelo et al. 2004b, Vega et al. 2007). Distribution coefficients for copper were one to two orders of magnitude greater than those for zinc, indicating that more zinc remained in solution after the sorption procedure.

The high proportion of zinc in F1 and possibly in F2 may therefore be related to the partitioning of zinc between the solid phase and soil solution. Li and Davis (2008a) found a good correlation between F1 percentages and results of a mechanistic model calculating the dissolved metal component. Dissolved zinc species may temporarily form weak bonds with media particles during the drying process or co-precipitate with other soil solution constituents to maintain electroneutrality of the dry media.

The contribution of tire wear to zinc release in the environment has been well-documented (Davis et al. 2001b, Adachi and Tainosho 2004, Councell et al. 2004). Tire

particle weathering may contribute to loosely-held Zn fractions. Smolders and Degryse (2002) found that after 11 months of weathering outdoors, 10-40% of total Zn added to soils in the form of fine car and truck tire particles shifted to the labile pool. Labile Zn is defined as being isotopically exchangeable with Zn^{2+} . They also noted that an increase in labile Zn species did not proportionately increase Zn leaching, most likely because of an increase in soil pH brought about by the presence of the tire tread particles. Labile zinc remained largely immobilized, albeit likely in a loosely-held fraction.

4.4.1.3 BSM fractionation

Top-heavy metal accumulation combined with low metal concentrations in BSM segments (Section 4.3) imply that BSM fractionation mainly reflects that of the native metals in the media. This hypothesis is also supported by the fact that the original BSM fractionation closely matches the mean fractionation for all BSM samples (Figure 4-12). F4 dominates among copper and zinc, which may be related to Fe and Mn oxides in topsoil and sand components. The F3 and F4 fractions for lead are of similar magnitude.

4.4.1.4 Spatial variation of fractionation in organic media

Fractionation results are relatively consistent between zones. The major exception is Zone 5, where the top organic segment (5A) has far higher F1 percentages than the mean for all three metals (Tables B-3 – B-5). Enrichment of F1 is at the expense of F4 and F5 for lead, F3 and F5 for copper, and F2 and F4 for zinc. The second Zone 5 organic segment (5B) also has high F1 concentrations, though not as high as the top segment. For both Zone 5 organic segments, absolute concentrations in fractions F2 – F5

are roughly on par with those in Zone 7, which is located at the same distance from the inflow point as Zone 5. This suggests that the Zone 5 results could be caused by error or contamination during extraction or analysis. No obvious physical explanation exists for the high proportion of loosely-held metals in Zone 5 organic media.

Zone 2 provides the best opportunity to examine fractionation trends with depth because it has four organic segments. Figure 4-13 shows normalized fractionation with depth in Zone 2 organic media for each metal. F1 is essentially constant for all three metals. A few sharp inflection points exist, such as segment 2B (4.5 cm) for copper (F3, F4) and 2C (7.5 cm) for lead and zinc (F4, F5). Segment 2B has a lower proportion of copper in F3 than the other segments. As shown in Table B-4, copper concentrations in all segments except F3 are roughly similar in segments 2A, 2B, and 2C. Segment 2B has a much lower F3 concentration, resulting in a lower total copper concentration than in its adjacent segments. It is unclear whether this condition is caused by media characteristics or experimental error.

The inflection point in F4 and F5 for lead and zinc in segment 2C (7.5 cm) may be related to its unexpectedly high OM content (Section 4.1.1). Both lead and zinc show an increase in the proportion of F5, which may reflect a greater proportion of refractory metal-OM complex. No fraction has an inflection point in segment 2C for copper. Turer et al. (2001) found that a large proportion of OM in roadside soils existed in a refractory form, retaining metals (especially Pb and Zn) that were not released until the final, “residual” extraction step. The authors attributed the refractory OM to vehicle exhaust and asphalt particles, however, rather than plant-based material.

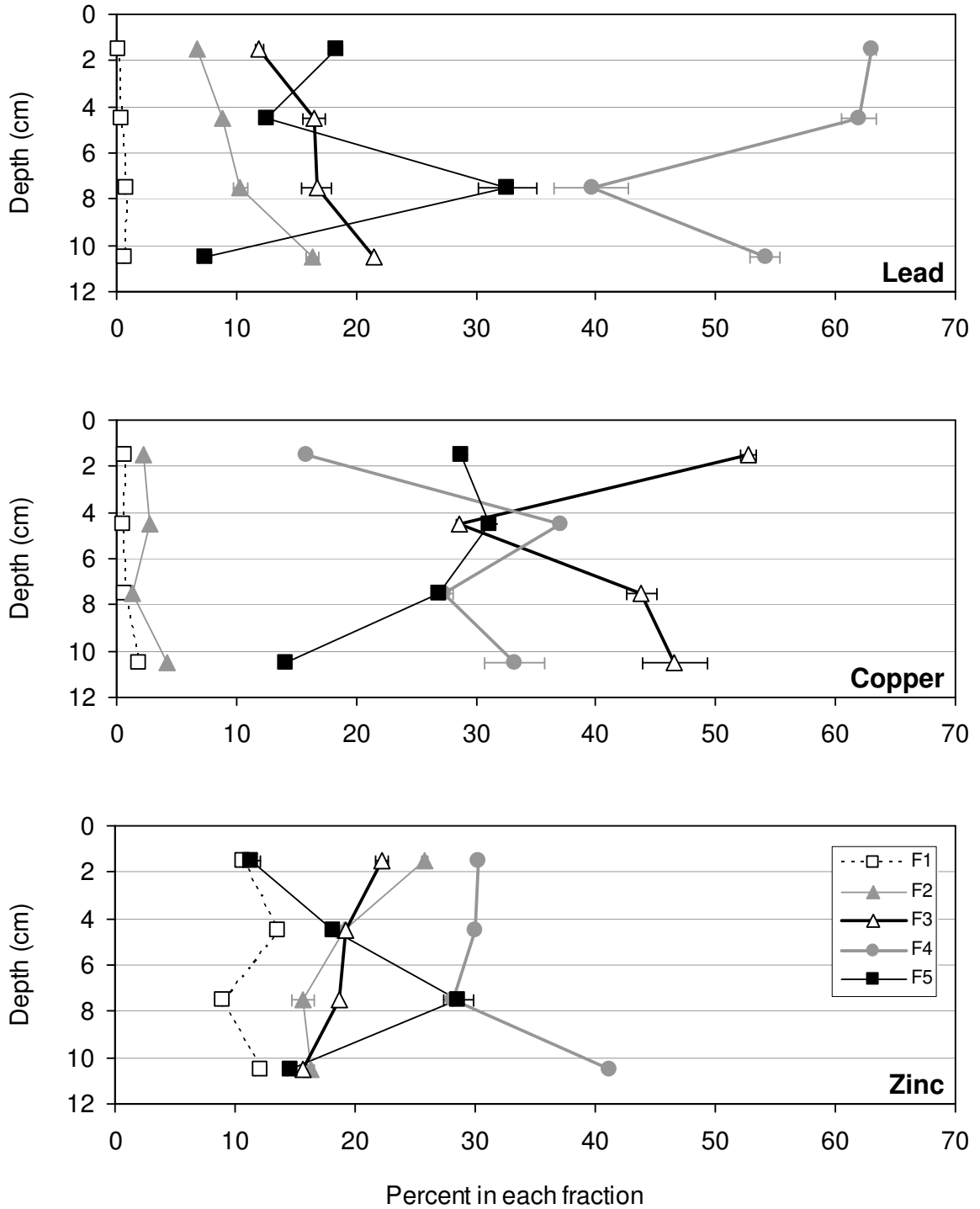


Figure 4-13. Normalized mean metal fractionation ($n = 2$) of organic media as a function of media depth in Zone 2. Error bars indicate the range of two replicates.

In general, metal type and metal partitioning in runoff appear to dominate fractionation behavior in the media, rather than media characteristics or spatial influences. Localized variations in media characteristics, such as in segment 2C, may be a secondary factor. The influence of spatial differences within the cell is inconclusive but likely of minor importance.

4.4.2 Bioavailability

Little correlation is expected to exist between environmental availability and oral bioavailability (Kelley et al. 2002). Conditions in the human gastrointestinal tract are far different than those in an environmental setting in terms of pH, solution chemistry, mixing, residence time, and usually temperature. A different methodology is therefore required to investigate the physiological fate of media-captured lead, which is of interest because of its high toxicity to humans and other mammals (Davies 1995).

Fresh samples of bioretention media and inflow channel particles were extracted using the EPA *in vitro* method (EPA 2007). *In-vitro* bioaccessibility (IVBA) values were converted to relative bioavailability (RBA) and finally to absolute bioavailability (ABA) (Section 2.2.4.3). Table 4-4 summarizes the results; Table B-6 provides the complete data set. The mean ABA in media samples is $25\% \pm 1.6\%$ ($n = 9$), including both organic media and BSM. ABA values range from 23% to 29%. Mean total lead and ABA in inflow channel particles is 49 mg/kg and 26%, respectively. The ABA results are quite consistent despite differences in media type (organic, BSM, particles) and OM content. No correlation was found between ABA and either pH or %OM.

Table 4-4. Total and bioavailable Pb and absolute bioavailability (ABA) of nine organic and BSM media samples. Total Pb was measured using the 3050B method (EPA 1996). Bioavailable lead is estimated using mean ABA.

	Total Pb (mg/kg)	ABA (%)	Bioavail. Pb (mg/kg)
Mean	58 ± 19	25 ± 1.6	14
Minimum	21	23	5.2
Maximum	83	29	21

ABA is the best estimate of the fraction of total lead that would be absorbed into the body if ingested. The generic estimate of lead ABA in soil and dust is 30% (EPA 2007). Bioretention media and inflow channel particles have approximately the same bioavailable fraction of lead as generic soil, implying that the potential health risk from ingestion of cell media is similar to the risk associated with “typical” contaminated soil. As with the sequential extraction findings, bioavailability results represent a snapshot in time. Weathering, evolution of the organic layer, and biological activity could each cause long-term shifts in lead speciation and potentially in bioavailability (Ruby et al. 1999).

In the broader context of contaminated soils, researchers have found lead bioavailability to vary greatly depending on media type, with ABA results that are both higher and lower than in the Lot 11 cell media. Results are typically presented as IVBA (%) but are expressed here as ABA using the same conversions performed on the Lot 11 media. During development of the EPA *in vitro* method, the ABA of 19 soil samples primarily related to mining and milling activity was found to range from 0.6% to 37%, with a mean of approximately 23% (EPA 2007). Using the same method, Oomen et al. (2002) found the ABA of three historically contaminated soils to range from 23% to

39%. Navarro et al. (2006) analyzed 18 samples of various soils and wastes from an old mine site. The resulting ABA values ranged from 0% to 36%, with a mean of 9.6%.

Several assumptions introduce a degree of uncertainty into the ABA results. The *in vitro* method was developed using soils from mining and milling sites, with total concentrations far in excess of those measured in the Lot 11 cell (Drexler and Brattin 2007). The best-fit line described by Equation 2-2 offers the best estimate of relative bioavailability (RBA), and in turn ABA, based on the IVBA-RBA correlation that was found during development of the *in vitro* method (EPA 2007). Actual RBA and ABA values may be higher or lower. The 95% confidence interval is quite wide for a mean ABA of 25%, with lower and upper bounds of 5.2% and 37%. Finally, ABA results assume that the typical ABA of lead in food and water is 50% in children (EPA 2007).

4.5 Mass balance and environmental pathways

The net metal mass retained in bioretention systems is caused by changes in both concentration and volume from inflow to outflow. In turn, retained metals have several potential short- and long-term environmental fate pathways. Two related pathways are sequestration in media as 1) surface-strained or depth-filtered particles and 2) sorbed dissolved metals. Additional environmental pathways include uptake by plants, desorption and flushing of dissolved metals, and washout of media or trapped particles. Human-induced pathways include media replacement and accidental ingestion.

Extensive plant uptake, as well as long-term washout of dissolved or particulate-bound metal, appears unlikely. Sun and Davis (2007) found uptake by plants to account for only 0.5-3.3% of input metal mass in a laboratory pot study. Muthanna et al. (2007)

measured metal uptake in a pilot-scale bioretention system to be 2, 3, and 7% of total input mass for lead, copper, and zinc, respectively. Sequential extraction analysis has shown lead, copper, and to a slightly lesser extent zinc, to be predominantly immobile, based on the F1 fraction (Section 4.4.1.1).

In addition, breakthrough of particulate-bound metals is not expected. Li and Davis (2008b) found bioretention columns to be clogging-limited instead of breakthrough-limited. Media depth profiles in the Lot 11 cell are top-heavy, indicating efficient particle capture in the top several cm of media (Section 4.3.1). Water quality monitoring at the site (Davis 2007) showed moderate (59%) mass removal of TSS. A greater TSS removal was likely hindered by initial TSS washout from the bottom of the media profile. Assuming the pathways discussed above are of minor to negligible importance, sequestration in bioretention media is expected to be the dominant pathway for metals that do not immediately overflow or flow through.

The combination of water quality monitoring data (Davis 2007) and media sampling in this study allows a mass balance to be attempted between the two data sets. This calculation determines the extent to which the results from each study are mutually consistent, given simplifying assumptions about metal fate. Metal sequestration in media should largely account for the difference between lifetime inflow and outflow mass.

4.5.1 Inflow and outflow calculations

The mass balance requires an estimate of the net metal retention, expressed as the difference between the cumulative inflow and outflow metal mass over four years. The rainfall data set used in Section 4.2.2.1 indicates that 4569 mm of rain fell between Dec.

1, 2002 and Nov. 30, 2006, excluding isolated events with a single rain gauge tip (0.254 mm). Inflow volume was calculated by multiplying rainfall depth by a runoff coefficient of 0.9, the drainage area of 0.25 ha, and a factor of 0.5 because runoff is evenly split between two cells. The resulting value, 5158 m³, is an estimate of the total inflow volume into the cell from completion of construction to the time of sampling.

Table 4-5 lists the mean inflow EMC values for each metal from a 14-month monitoring period (Davis 2007). Pb, Cu, and Zn EMCs were measured for 9, 9, and 12 inflow events, respectively. Mean EMCs were used instead of medians because means reflect the physical significance of outlier values. Estimates of cumulative inflow mass were taken as the product of each mean EMC and the total inflow volume, 5158 m³. Cumulative outflow mass for each metal was calculated by multiplying its respective inflow mass by the ratio of total outflow mass to total inflow mass measured over all events in the monitoring period (Davis 2007). The difference between the cumulative inflow and outflow mass for each metal equals the total metal mass retained in the cell up to the time of sampling (Table 4-5).

Table 4-5. Concentration and mass data used to estimate net metal mass retained in the Lot 11 cell, based on results from Davis (2007), rainfall, and drainage area. Also shown are estimates of total metal mass in organic media, based on media sampling results.

	Pb	Cu	Zn
Mean inflow EMC (mg/L)	0.087	0.014	0.117
Cumulative inflow mass (g)	451	70	604
Cumulative outflow mass (g)	56	12	278
Net mass retained in cell (g)	395	58	326
Total mass in organic media (g)	13	11	49

4.5.2 Metal masses in media

To attempt to complete the mass balance, cumulative metal mass retained in the cell was extrapolated from the results of the media analysis. The cell footprint was divided into seven regions based on the sampling locations for each zone (Figure 4-14). Region boundaries are equidistant between each cluster of samples. Each region was treated as a column of media divided into slices at the same depth intervals as their respective core segments. Each slice was assigned the total metal concentrations of the corresponding segment. This approach assumes that total metal measured in a core segment is representative of the mean concentration throughout the corresponding slice. Another key assumption is that metal concentrations in the original mulch are negligible compared to those measured after four years of bioretention operation. Means of the four surface samples within each zone were used for the uppermost slices. Only organic segments were used in the mass balance calculation; metal accumulation was assumed to be negligible in BSM segments, as discussed previously.

Organic media bulk density was estimated from the volume and equivalent oven-dry mass (passing 2 mm sieve) of six samples taken for the bioavailability analysis in 2008 (Section 4.4.2). The mean organic media bulk density is $0.38 \pm 0.08 \text{ g/cm}^3$. This value was assumed not to have changed substantially over time, and the mean value was assumed to be representative of organic media throughout the cell.

The volume of each slice was calculated as the product of its corresponding segment thickness and the surface area of each region. Slice volumes were converted to organic media mass by multiplying by the mean organic media bulk density. Mass of a given metal in each slice was determined by multiplying the mass of the slice by the

metal concentration in the corresponding segment. Metal masses in each slice were summed to arrive at an estimate of the total mass accumulated in the organic media throughout the cell during the first four years of operation (Table 4-5).

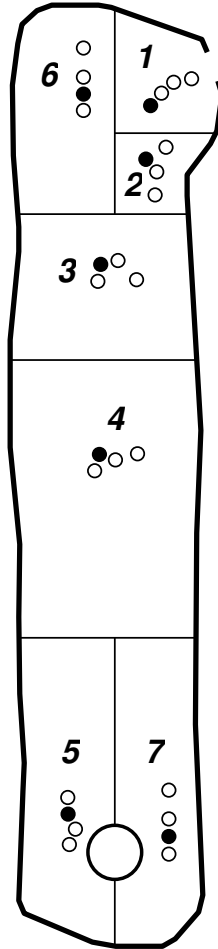


Figure 4-14. Cell footprint with regions used for metal mass balances. Filled and hollow circles denote core and surface samples, respectively. Circle diameter is not to scale.

4.5.3 Results of mass balance

Extrapolating the results of the media and water quality data sets under the stated assumptions cannot close the metal mass balance (Table 4-5). The differences between the estimated total inflow and outflow masses far exceed the estimates of accumulated

metals from the media analysis. Copper estimates are in closest agreement, differing between the two methods by approximately half an order of magnitude, while lead and zinc estimates differ by about one order of magnitude.

Several factors in the extrapolation of both data sets could have potentially contributed to the discrepancy in results. The greatest discrepancy is between the lead results. The difference between the total inflow and total outflow mass is 395 g, while the extrapolated media results indicate that only 13 g have accumulated in the organic media. The mean inflow EMC for lead appears to be somewhat high, in comparison to mean EMCs found at two roadway sites. Mean inflow EMCs in both the Kenilworth Avenue study (Table 3-5) and in Stagge (2006) were 0.023 ± 0.016 mg/L ($n = 11$ in both studies). It is possible that a larger sample size would have resulted in a lower mean inflow Pb EMC from Lot 11 runoff, although the two roadway studies cited above also had small sample sizes ($n = 9$ and 11 , respectively). Mean copper and zinc EMCs reported by Davis (2007) were relatively low compared to those in the two roadway studies cited above.

Other variables in the water quality calculations could also have contributed to the discrepancy in the mass balance. The drainage area may be smaller or larger than stated. Nearly flat surfaces such as the Lot 11 drainage area are difficult to delineate with a high degree of confidence. If the drainage area is smaller than the given value, metal masses calculated from water quality results would be overestimated. Mass removal ratios may also have been influenced by the small sample size, although lead, copper, and zinc ratios reported by Davis (2007) are reasonable for bioretention, at 88, 83%, and 54%, respectively. By comparison, pilot-scale studies found mass removals of close to 100%

for all metals (Davis et al. 2003); and 82, 72, and 90% for lead, copper, and zinc, respectively (Muthanna et al. 2007). Twelve-month lead, copper, and zinc mass removals in field-scale study by Hunt et al. (2006) were 81, 99, and 98%, respectively.

It is possible that sampling efforts missed denser pockets of organic media or hotspots of accumulated metal with concentrations exceeding those reported in Section 4.2. A more exhaustive sampling effort, combined with a rigorous accounting of plant uptake and metal capture in BSM, may result in a higher estimate of cumulative metal mass sequestered in the cell. Combining this approach with revised estimates of long-term mean inflow EMCs, it may be possible to reconcile the extrapolated results of the two data sets and complete the mass balance.

Chapter 5

CONCLUSIONS AND RECOMMENDATIONS

5.1 Hydrologic and water quality performance

Good to excellent hydrologic performance at the Kenilworth Avenue bioretention cell, including complete inflow capture, is possible for events with 10 mm rainfall or less. Such events are characterized by a reduction in runoff volume and peak flow rate, as well as a substantial delay in the generation of outflow. In addition to rainfall depth, rainfall intensity also differentiates hydrologic outcomes. At this site, an average rainfall intensity of 0.5 mm/hr is the approximate threshold between events with complete capture and those that generate outflow (Figure 3-1).

Volume export occurred for several events with less than 10 mm rainfall, which may be ascribed to secondary factors such as short-term high rainfall intensity and the antecedent moisture condition (AMC). In total, volume export occurred in 30 of the 37 events with outflow, including all events with more than 10 mm rainfall. The outflow rate and volume could not be fully quantified in 17 out of the 30 events with volume export because the outflow rate exceeded the measureable limit of the weir. The inability to fully quantify outflow rates in these events has little bearing on the overall assessment of hydrologic performance, however. Analysis of the aggregated flow data from all events indicates that the Kenilworth cell has substantially increased the duration over which receiving waters are subjected to any given flow rate, as compared to direct runoff from the roadway storm drain network. Increasing the exposure of downstream channels to elevated flow rates is the opposite of the desired hydrologic outcome for bioretention.

The most likely explanation for the prevalence of volume export is the movement of external subsurface flows, originating from the adjacent pervious area, into the cell media and ultimately the underdrain. This explanation dovetails with the known site conditions (local topographic low point, pervious fill material) and cell characteristics (open, unlined system with underdrain). The increase in flow rate exposure time is related to the longer dewatering time required by large outflow volumes.

Despite the unexpected hydrologic behavior at the site, water quality results are generally consistent with those from previous bioretention monitoring studies (Davis 2007, Hatt et al. 2008b, Hunt et al. 2008, Li and Davis 2009). Chloride concentrations and mass loadings substantially increased, while the opposite occurred for metals and TSS. Moderate nitrate and TP export occurred, but the cell had no clear effect on TKN and BOD loadings. The results suggest that pollutant export and capture processes common in bioretention systems are also operative at the Kenilworth cell, although the mechanics of the external flows are unknown.

Samples from the two April 2008 events were analyzed to determine whether outflow water quality from these larger events (> 10 mm rainfall) was substantially different from the other sampled events, which have smaller rainfall depths (< 10 mm) and presumably generate less external subsurface flow. Outflow EMCs from the April 2008 events are generally in keeping with findings from the other six events with outflow, suggesting that overall water quality trends from inflow to outflow at the Kenilworth site are the same regardless of event size.

Trends in median EMC for each pollutant mirror that of the mass loading, but the latter is believed to more closely reflect the environmental impact of the cell because the

mass loading calculation incorporates hydrologic performance while the EMC does not. Li and Davis (2009) noted that mass removals typically exceeded EMC removals because of the reduction in runoff volume at the study sites. At the Kenilworth site, by contrast, changes in median EMCs of nutrients, chloride, and BOD indicate better performance than do the mass loading data. This finding suggests that additional masses of these pollutants are being mobilized by external flows. Metals and TSS appear not to be mobilized in this manner because the changes in median EMCs are similar to changes in the mass loadings.

The water quality results underscore the relationship between pollutant removal and hydrologic performance, and emphasize the need to maximize volume reduction in bioretention facilities. While metal and TSS removal is very good even in the presence of external flows, environmental impacts with respect to the other pollutants are strongly dependent on volume reduction or export. As shown in Table A-14, the best chloride and nutrient mass reductions occurred in the July 28, 2007 and Oct. 19, 2007 events, which had volume reduction; and in the Jan. 10, 2008 event, which had little change in volume.

5.1.1 Future research

The combination of site conditions and cell characteristics that are expected to have caused volume export at the Kenilworth site will likely recur elsewhere, given the increasing popularity of bioretention. The Kenilworth site therefore offers an opportunity to study possible means of mitigating the effects of a “leaky” cell. One simple alteration to the design would be to cap the underdrain, preventing a surface outlet except for overflow in extreme events. This scenario would be analogous to pre-construction

conditions and could greatly lessen the cumulative downstream exposure to high surface flow rates. Subsurface flows external to the cell, as well as flows exfiltrating from the cell, would ultimately merge with groundwater or seek a surface outlet, possibly in the ditches at the base of the fill area. The surface of the media profile at the back of the cell could also be lowered to maximize surface storage and lessen the tendency for overflows to occur.

Additional hydrologic and water quality monitoring would help to provide proof-of-concept for this approach. From a hydrologic standpoint, the most salient question is whether a capped underdrain causes a substantial increase in the occurrence of overflow. A secondary hydrologic concern is whether the lack of a surface outlet causes persistent surface ponding or media storage. Drawdown times could be calculated from water level measurements in new observation wells or in the existing cleanouts. Observation wells could also be used to collect samples for nitrate analysis, which would indicate whether temporary denitrification zones were forming under saturated conditions.

The position of the Kenilworth cell at the downstream end of a roadway storm drain network creates challenging conditions, including high solids loadings and concentrated flows, that could increase the level of effort required to maintain long-term performance and appearance. An additional research opportunity would be to study the effects of a pretreatment area located between the storm drain and the cell. The pretreatment area may lessen the potential for media clogging by trapping fines, which could periodically be removed without disturbing the cell media profile or vegetation. Capture and subsequent removal of fine particles in the pretreatment area would also

potentially lower the metal accumulation rates in the cell. A second benefit of the pretreatment area would be to reduce media scouring by encouraging dispersed flows.

Such a pretreatment area could consist of a stone-filled level spreader followed by a filter strip planted with stiff-stemmed grasses. By measuring flow rates and taking water quality samples on the upstream and downstream ends of the pretreatment area, the reduction in pollutant delivery to the cell could be quantified. Pollutants of greatest interest would likely include TSS and metals. Street particle samples retrieved from the stone level spreader and grass filter strip after 1 – 2 years could be compared to surface cell media samples taken downstream of the pretreatment area to determine the extent to which metal accumulation was lessened in the cell. A variation on this research design would be to conduct a paired study of two cells, one with a pretreatment area and one without. Similarly to the Lot 11 site, inflow would be split evenly between the cells.

5.2 Media evolution and metal accumulation

Analysis of media samples from the Lot 11 cell indicates that chemical and physical characteristics of the media have been altered by inflow constituents and hydrologic behavior over the life of the cell. Trends in organic matter (OM) content with distance along the cell surface, as well as localized variability, may be caused by scouring, particle and debris deposition, and biological activity, among other factors. Trends in media pH with depth suggest that inflow alkalinity is consumed as flow percolates downward, partly overcoming the buffer capacity of the media and slightly raising the media pH.

Metal concentrations in the media have increased substantially over the original values, indicating that the Lot 11 cell acts as a sink for metals. This observation is consistent with the high TSS and metal removal found in many bioretention monitoring studies (Davis et al. 2001a, Hatt et al. 2008a, Li and Davis 2009). Metal accumulation is largely confined to the top several cm of media, coinciding with the organic layer, while little change has occurred in the underlying bioretention soil media (BSM) layer (Figures 4-9 to 4-11). This top-heavy profile agrees with a previous bioretention study (Li and Davis 2008a) and studies of infiltration basins (Nightingale 1987, Dechesne et al. 2005). Sorption and particle capture are the mechanisms responsible for surface accumulation.

A second spatial trend is the relationship between surface concentrations and distance from the inflow point. Metal concentrations at the cell surface are highest in Zone 2 (near the inlet) and decrease with distance from the inflow point (Figure 4-3). In addition, metal concentrations appear to be highest in areas along the main flow path. The lower metal concentrations in the Zone 1 samples likely result from disturbance of the organic layer by scouring. A simple mechanistic model for inflow behavior over four years of Lot 11 cell operation suggests that the trend in metal concentrations with distance can be explained by cumulative exposure to inflow volume, which is highest near the inflow point and decreases with distance. Localized variations in surface metal concentrations are at least partly explained by differences in OM content.

Lead, copper, and zinc concentrations generally exceeded soil background estimates for eastern Maryland, but were far below EPA and Maryland residential cleanup standards (Table 4-3). Lead concentrations did not attain the Federally-specified threshold for toxicity (CFR 2007). An *in vitro* bioavailability assay indicated that

approximately 25% of lead in surface media would be absorbed into the body if ingested, which is comparable to generic estimates for soil (EPA 2007). This result implies that the potential health risk from ingestion of Lot 11 cell media is similar to the risk associated with “typical” contaminated soil containing the same total lead concentration.

A five-step sequential extraction procedure found all three metals to be tightly bound to the media. The mean fractions of lead, copper, and zinc in the most environmentally available fraction (“soluble-exchangeable”) were 3.9, 3.9, and 13%, respectively. The greater mobility for zinc is consistent with past metal sorption studies (Ray et al. 2006, Chang Chien et al. 2006). While metal fractionation in any sequential extraction procedure is operationally defined and not necessarily representative of natural phenomena, the results strongly suggest that captured metals should remain immobile and be sequestered indefinitely in bioretention media. This finding agrees with previous sequential extraction studies of bioretention media (Li and Davis 2008a) and roadway soils (Nörrstrom and Jacks 1998, Turer et al. 2001).

5.2.1 Maintenance implications

The Lot 11 cell has functioned as a resilient, self-contained system despite a lack of basic maintenance. Hydrologic performance remains good, with a drawdown time of approximately 2.5 hours from the maximum ponding depth. Vegetation had evolved into a dense mix of original plantings and volunteers (Figure 2-8) and naturally reestablished itself in the first growing season following extensive clearing in early 2008.

Long-term sequestration of metals within bioretention media raises the question of appropriate maintenance practices. The operating life of the Lot 11 cell is unlikely to

be either clogging- or breakthrough limited, given the absence of any clogging layer and the abundance of clean BSM below the surface. Plant and animal activity within the cell and energetic inflow may discourage the formation of a clogging layer.

The most likely constraint on continued operation is the formation of metal hotspots that reach regulatory thresholds. Assuming constant accumulation rates, metal concentrations will reach the more restrictive cleanup standard (MDE 2008) after 20 additional years of operation for lead and copper and 30 years for zinc. The greatest metal accumulation has occurred along the first 30% (3.3 m) of the flow path, in the organic layer (0-12 cm depth). This hotspot represents a relatively small area for any future remedial action such as media replacement. The need for cleanup actions could be forestalled through simple maintenance practices such as replacing mulch every 1 – 2 years, removing any large deposits of runoff particles, and keeping flows as evenly distributed across the cell surface as possible. Mulch replacement would also ensure a continued high affinity for metals at the top of the media profile.

5.2.2 Future research

This effort focused on sampling representative areas across the entire cell surface. The findings revealed clear spatial trends, but the incomplete mass balance (Section 4.5.3) and variation in the Zone 1 results (Sections 4.1.1 and 4.2.2.2) suggest that the inflow point of any cell may require a denser sampling effort to fully capture local variability. The apparent media diversity near the inflow point, caused by scouring, particle deposition, and other factors, may complicate general claims about bioretention media composition, total and environmentally available metal, and lead bioavailability.

Densely sampling near the inflow point of the Lot 11 cell, or any cell receiving concentrated flow, would help to bolster or refine conclusions about metal environmental fate and lead bioavailability, and may reveal metal hotspots. Surface media samples could be analyzed for OM content, pH, cation exchange capacity, particle size distribution, lead bioavailability, the “soluble-exchangeable” (F1) fraction, and total lead, copper, and zinc. As demonstrated in Section 4.2.2.3, local variations in media characteristics may help to explain differences in total metal, the F1 fraction, or lead bioavailability. Generalizations about environmentally available metal, overall fractionation, and lead bioavailability would be further enhanced by applying the methods used in Chapter 2 to media samples from other bioretention cells.

5.3 General design recommendations

The Kenilworth results indicate that subsurface conditions should be considered carefully during the planning and design of bioretention cells. The investigation should include adjacent areas that could be a source of surface or subsurface flow into the cell. Site history, including earthwork activity, may be as important a consideration as infiltration tests, which provide spot checks but may not represent the entire site. A cell may be designed as a closed system with a liner and underdrain, or as an open system with no underdrain, if significant subsurface flow is suspected to occur. Alternately, an open system with an underdrain could be installed, with the option of plugging the underdrain if it proved to be an outlet for external subsurface flows.

Chloride and phosphorus export may be controlled most effectively through designs that maximize volume reduction, thereby limiting the amount of leaching that can

occur. Selecting media with low phosphorus content (Hunt et al. 2008) is also critical for that pollutant. Although nitrification may generate temporary spikes in nitrate concentrations (Hsieh et al. 2007), bioretention is not expected to substantially alter nitrate concentrations (Figure 3-7) in the absence of widespread denitrification zones in the media. The leading strategy for reducing nitrate delivery to surface waters, then, is volume reduction through media storage, exfiltration, and evapotranspiration.

The Lot 11 results suggest that the location, number, and type of inflow points will influence the development of flow paths, and accordingly, metal accumulation patterns. Inflow configurations that maintain dispersed flows should result in a more even accumulation of metals across the cell surface. A cell in a roadway setting may only have a single inflow point, however, especially if the cell is associated with a storm drain system. Regardless of inflow configuration, metal accumulation should be more uniform in cells with a lower ratio of cell surface area to drainage area because ponding across the entire surface will occur more readily. Overflow may also occur more frequently, however. If mulch is periodically replaced (every 1 – 2 years; Section 5.2.1), metal accumulation patterns may be less important because media concentrations will be unlikely to reach regulatory thresholds before the next mulch replacement.

If metals are the primary pollutant of interest, bioretention cells could be constructed with a shallow media layer, on the order of 50 cm, because metal removal occurs largely within the first several cm of media. As noted by Li and Davis (2008a), this approach could reduce design costs and the potential for utility conflicts. Other water quality and hydrologic goals, such as volume reduction and denitrification, may require a deeper media layer. A possible compromise in sites that are constrained

vertically would be to reduce the depth of the media layer and increase the ponding depth. By converting media storage to an equivalent ponding depth, excavation and media costs could be reduced without affecting metal removal.

The Kenilworth and Lot 11 studies both demonstrate that bioretention cells are dynamic and still somewhat unpredictable systems, subject to outside influences that may modify their performance or composition. As systems that rely on natural processes, bioretention cells cannot be expected to be static, nor free of influence from their surrounding environments. An ongoing need exists to develop a deeper understanding of the design elements that mediate the interactions between bioretention cells and their drainage areas and receiving waters. These efforts will lead to improvements in bioretention design that in turn will foster greater environmental performance and long-term sustainability.

Appendix A

KENILWORTH AVENUE MONITORING DATA

Table A-1. Hydrologic data for all 65 events at the Kenilworth bioretention cell. Stormwater quality samples were collected for events listed in bold italics. Sampling for the Sep. 10, 2007 event was limited to the first burst. Inflow and outflow duration is calculated for flow above the minimum limit for depth measurement. Delay to outflow is calculated from start of inflow to start of outflow.

Date	Rainfall		Inflow			Outflow			Delay to outflow (hr)
	Depth (mm)	Duration (hr)	Volume (m ³)	Duration (hr)	Peak (L/min)	Volume (m ³)	Duration (hr)	Peak (L/min)	
4/25/07	1.5	0.50	1.9	0.70	286				
4/26/07	6.9	10	3.2	2.0	303	0.64	5.4	8.0	2.7
5/12/07	11	0.97	25	1.5	1114	28	6.4	>327	0.50
5/13/07	1.3	0.35	1.2	0.78	70	1.1	7.7	9.7	0.55
5/16/07	1.5	0.10	2.0	0.48	303				
5/27/07	1.8	0.60	1.0	0.78	54				
6/3/07	15	8.4	17	6.0	798	34	16	326	0.78
6/20/07	3.6	2.3	1.7	1.4	161				
6/21/07	2.0	0.083	1.1	0.23	354				
6/28/07	2.0	2.8	0.44	0.22	104				
7/5/07	1.5	0.38	0.65	0.40	94				
7/10/07	2.3	0.38	0.78	0.38	66				
7/11/07	4.3	0.78	2.9	0.47	762				
7/28/07 am	8.1	1.5	9.4	2.1	926	0.80	3.3	12	0.92
7/28/07 pm	0.76	0.050	0.36	0.45	38				
7/29/07	2.5	2.4	1.2	1.7	29				
7/30/07	5.8	0.28	8.3	1.1	1133	2.9	5.9	53	0.50
8/9/07	1.3	0.083	0.81	0.60	122				
8/20/07 am	24	6.3	39	2.5	1708	35	3.5	>327	0.35
8/20/07 pm	2.5	2.0	1.0	0.37	198				
8/21/07	21	7.8	30	5.6	1322	44	13	>327	1.7
8/25/07	13	4.4	14	1.4	1409	18	13	202	0.58
9/10/07	19	2.6	22	2.2	1441	18	5.6	>327	1.7
9/11/07	1.5	0.67	0.30	0.22	72				
9/14/07	2.0	3.3							
10/19/07	9.4	1.6	14	0.70	842	7.7	4.3	191	1.7
10/24/07	36	26	52	7.7	790	96	13	>327	1.9
11/5/07	1.8	1.9							

(Table A-1 continued)

Date	Rainfall		Inflow			Outflow			Delay to outflow (hr)
	Depth (mm)	Duration (hr)	Volume (m ³)	Duration (hr)	Peak (L/min)	Volume (m ³)	Duration (hr)	Peak (L/min)	
11/6/07	1.0	0.65							
11/9/07	1.5	4.4							
11/12/07	5.6	7.0	1.0	1.1	35				
11/13/07	2.5	1.8	0.60	0.55	48				
11/15/07	18	5.9	28	5.3	822	75	19	>327	0.45
11/26/07	1.3	0.25	0.95	0.35	113				
12/2/07	6.4	4.1	6.8	2.0	354	11	7.3	176	0.58
12/6/07	3.3	4.1							
12/7/07	4.6	10	0.46	1.1	9.0				
12/16/07	22	13	68	7.9	501	105	29	>327	0.97
12/23/07	3.8	1.1	6.2	1.3	238	9.7	9.0	148	0.83
12/26/07	8.6	6.6	10	4.4	108	34	17	212	1.0
12/28/07	10	4.7	19	4.9	501	53	19	>327	1.1
12/30/07	6.9	10	9.0	3.6	143	33	23	228	1.7
1/6/08	1.5	2.2	0.39	0.83	15				
1/10/08	2.3	3.4	1.0	0.78	50				
1/11/08	2.5	1.4	3.4	1.5	104	3.8	8.8	38	1.2
1/30/08	0.76	1.3	0.12	0.23	13				
2/6/08	2.0	0.13	5.7	0.43	1077	1.4	5.9	17	0.77
2/18/08 am	0.51	0.067	0.13	0.17	20				
2/18/08 pm	3.6	1.8	4.1	2.0	65	7.3	8.4	95	1.5
3/1/08	0.76	0.2	0.28	0.25	30				
3/4/08	12	8.8	27	5.3	391	68	18	>327	0.95
3/7/08	12	7.1	25	5.5	554	69	15	>327	1.1
3/8/08	3.0	6.2	2.4	2.5	65	18	20	51	0.35
3/16/08	7.1	7.2	9.2	3.3	148	22	12	228	1.4
3/19/08	10	3.7	22	3.7	534	52	9.7	>327	0.82
3/20/08	2.3	0.65	7.1	1.9	554	18	12	202	0.17
4/3/08	15	11	24	9.8	173	70	19	>327	2.6
4/6/08	7.1	9.3	11	5.8	335	27	18	182	1.6
4/11/08	2.0	0.22	4.7	0.43	770	0.10	1.8	1.5	1.4
4/20/08	43	12	129	7.9	1467	119	21	>327	0.98
4/21/08	25	20	83	9.5	991	150	39	>327	0.15
4/26/08	12	5.4	25	3.9	1282	44	15	>327	0.40
4/28/08	21	11	48	8.4	905	109	31	>327	1.2
5/8/08	63	15	167	16	2008	231	29	>327	0.52
5/10/08	5.8	4.5	14	5.5	215	43	26	309	0.37

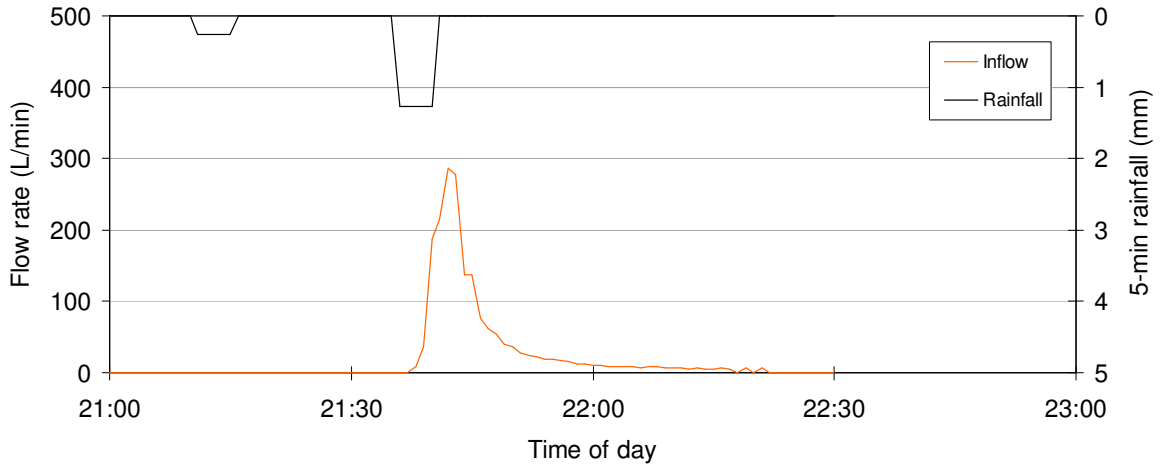


Figure A-1. Hydrograph and hyetograph for April 25, 2007.

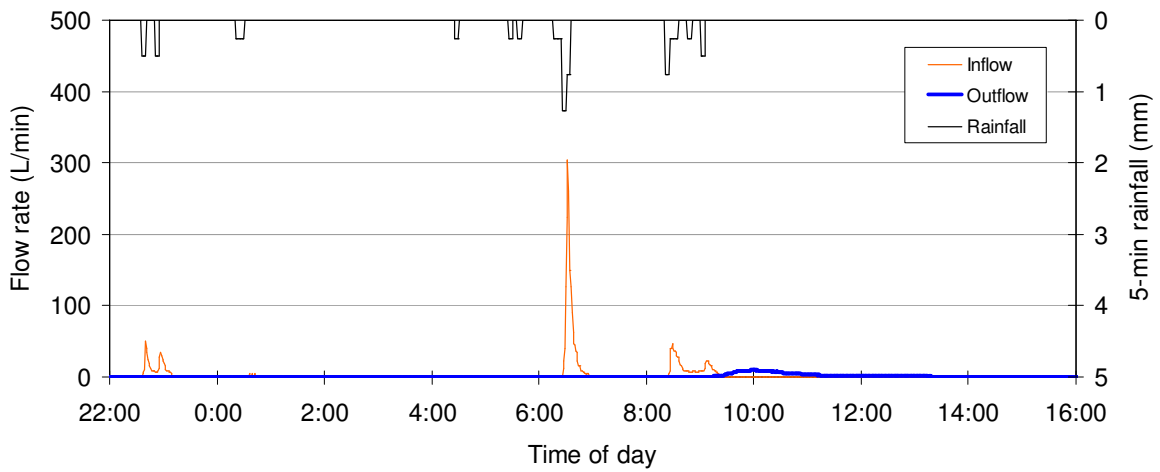


Figure A-2. Hydrographs and hyetograph for April 26, 2007.

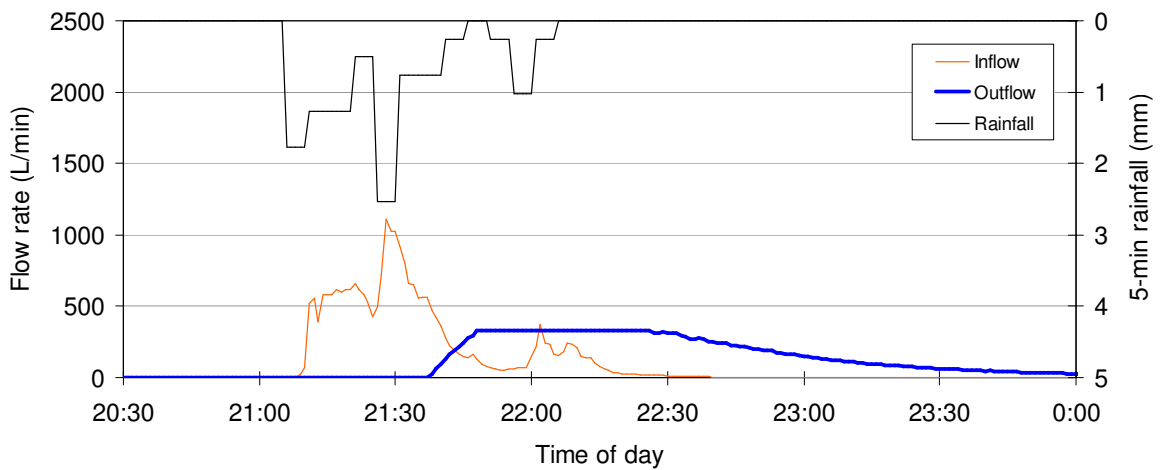


Figure A-3. Hydrographs and hyetograph for May 12, 2007.

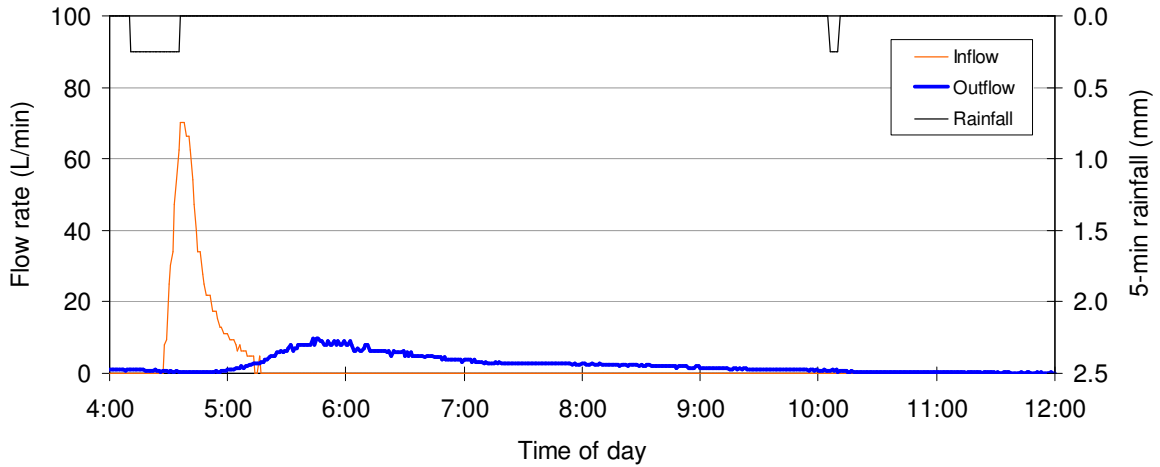


Figure A-4. Hydrographs and hyetograph for May 13, 2007.

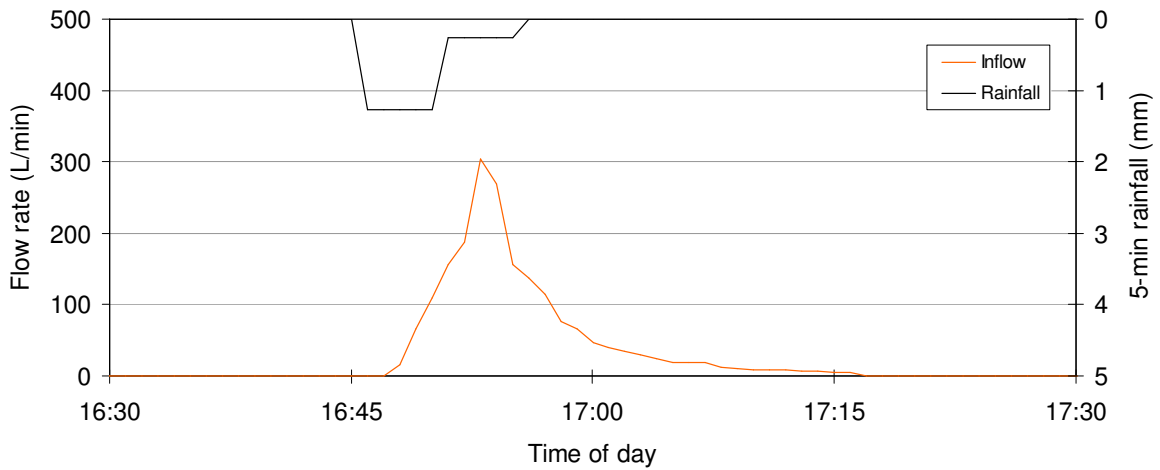


Figure A-5. Hydrograph and hyetograph for May 16, 2007.

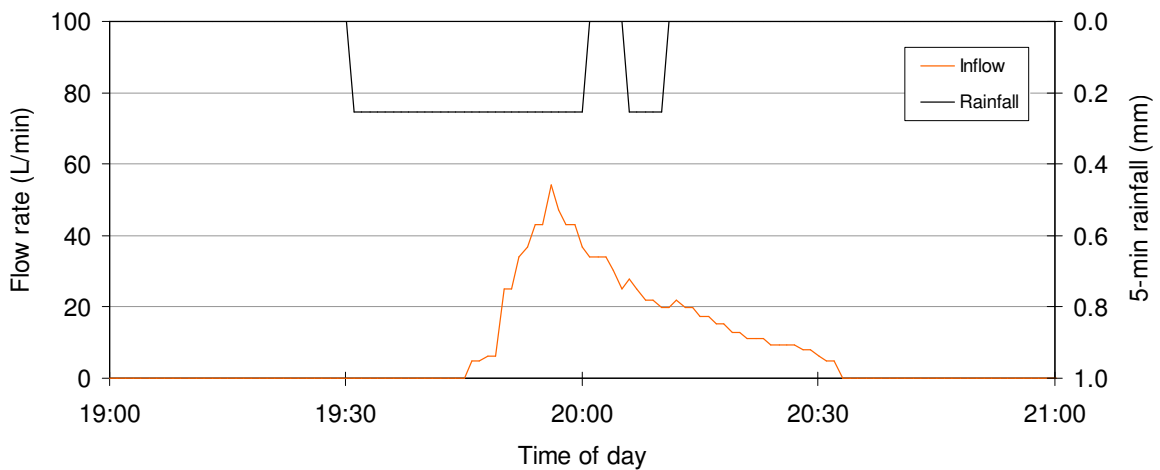


Figure A-6. Hydrograph and hyetograph for May 27, 2007.

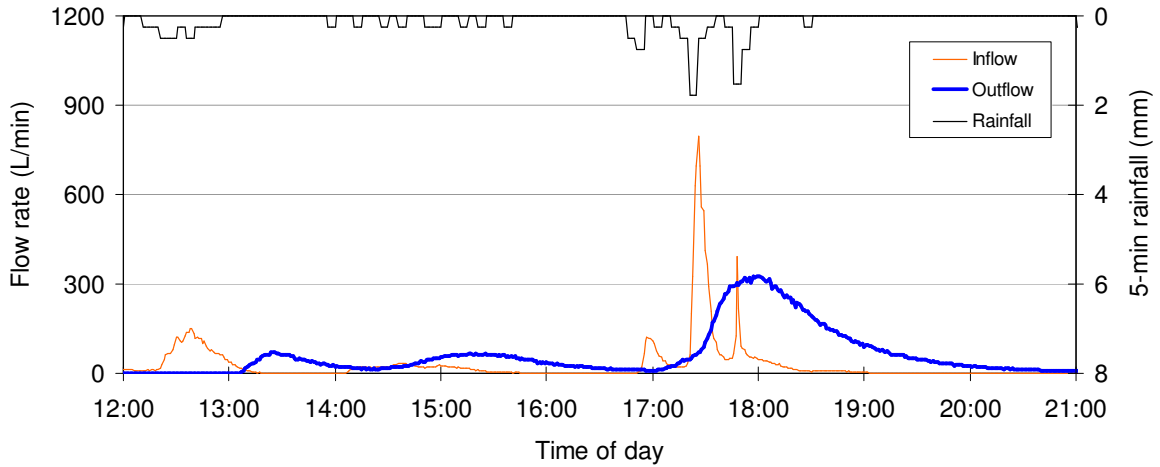


Figure A-7. Hydrographs and hyetograph for June 3, 2007.

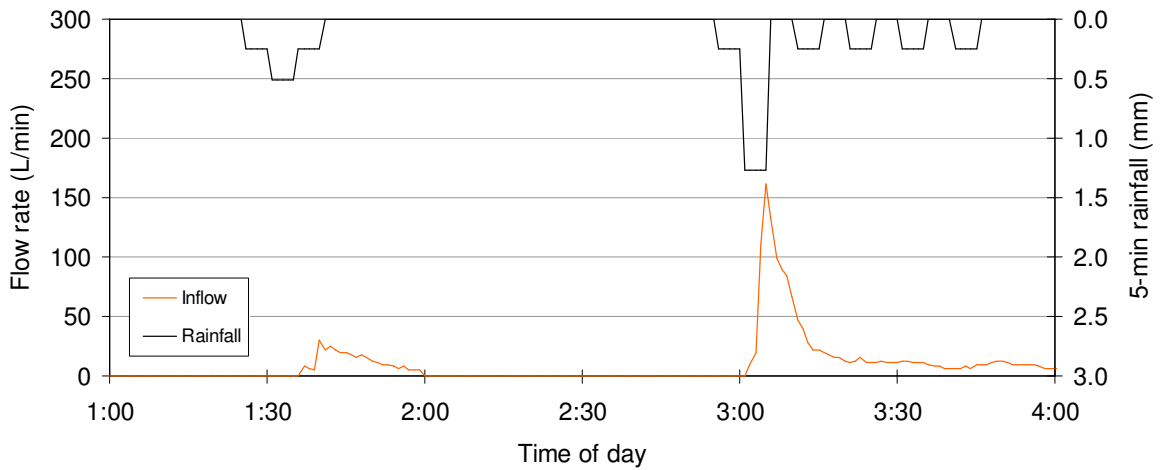


Figure A-8. Hydrograph and hyetograph for June 20, 2007.

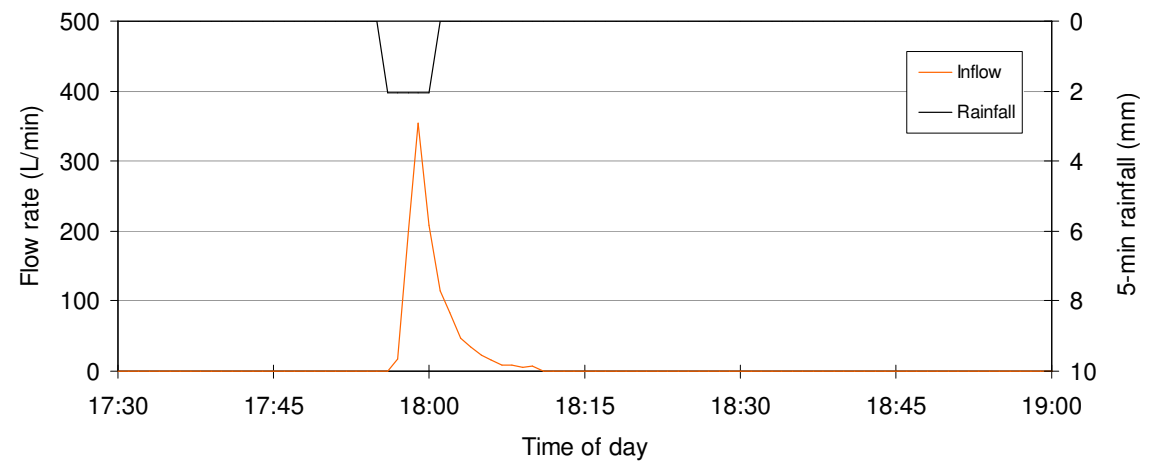


Figure A-9. Hydrograph and hyetograph for June 21, 2007.

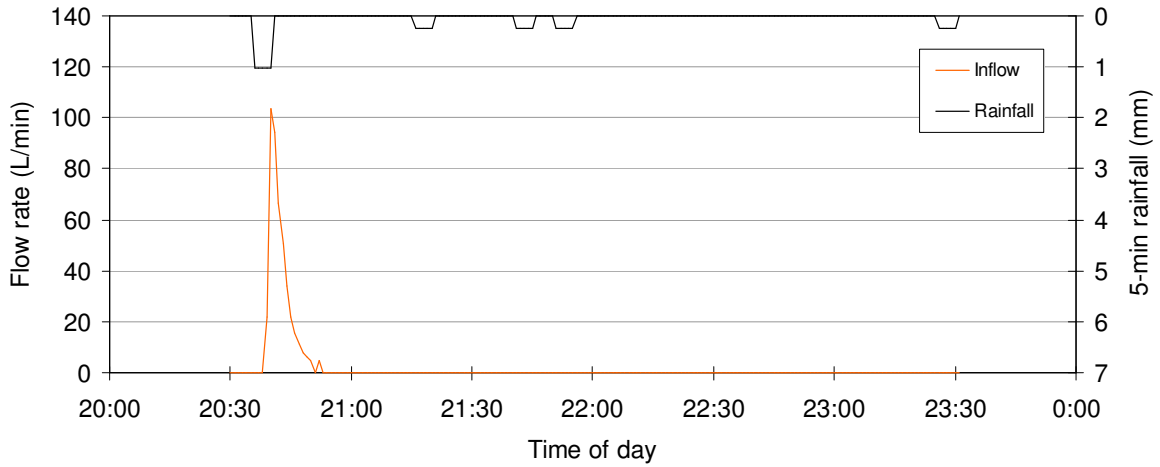


Figure A-10. Hydrograph and hyetograph for June 28, 2007.

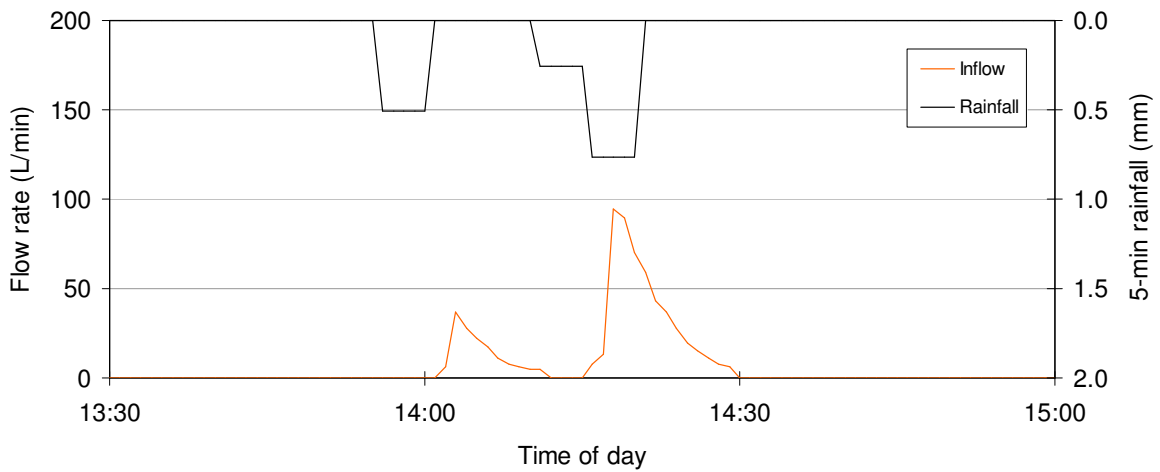


Figure A-11. Hydrograph and hyetograph for July 5, 2007.

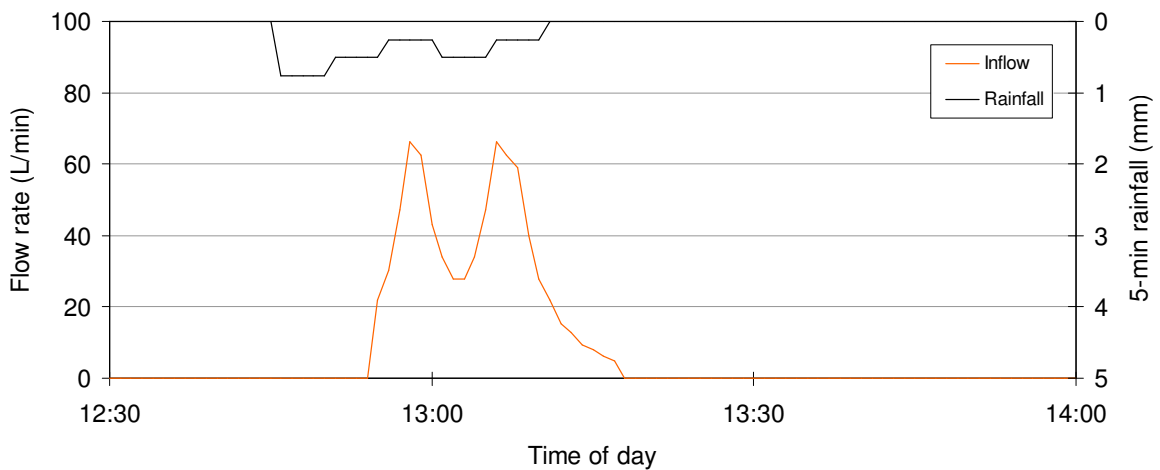


Figure A-12. Hydrograph and hyetograph for July 10, 2007.

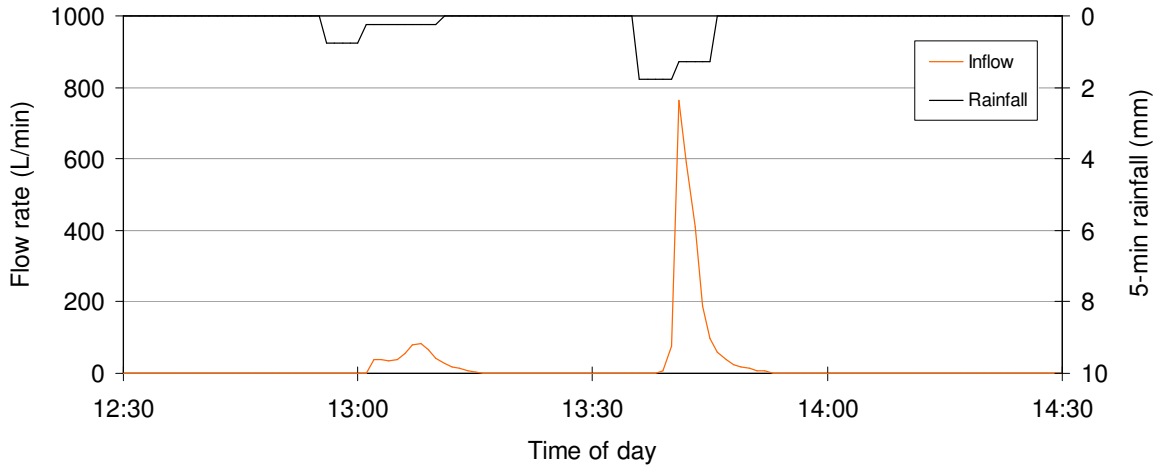


Figure A-13. Hydrograph and hyetograph for July 11, 2007.

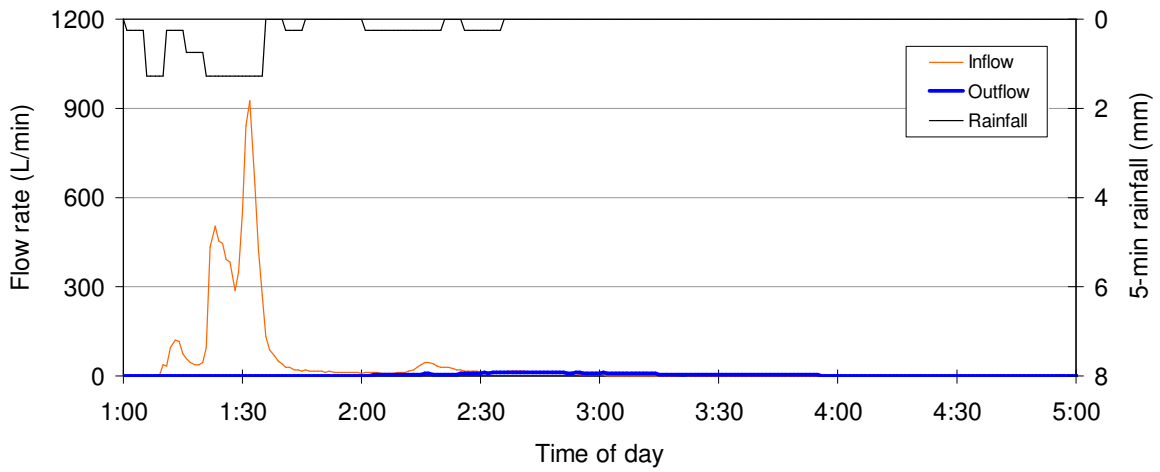


Figure A-14. Hydrographs and hyetograph for July 28, 2007 – AM.

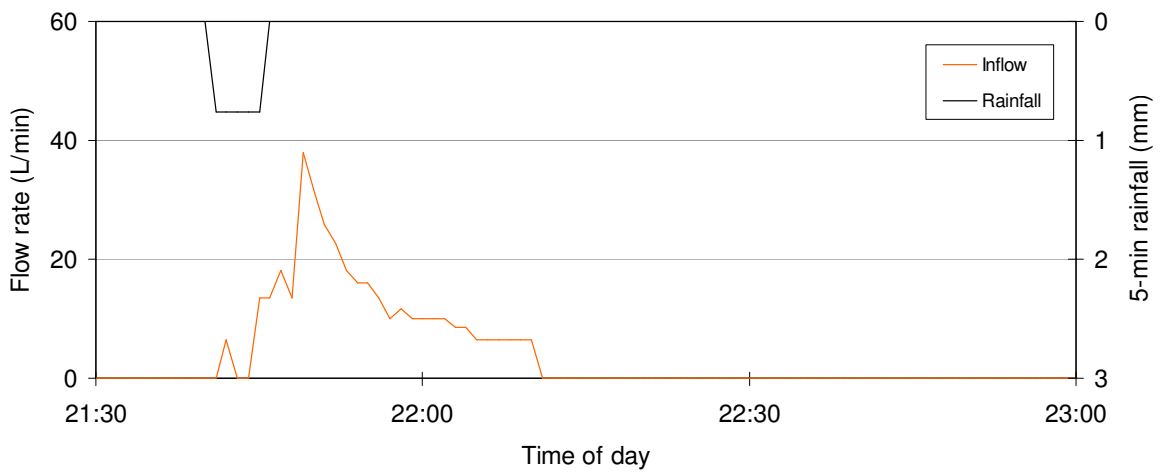


Figure A-15. Hydrograph and hyetograph for July 28, 2007 – PM.

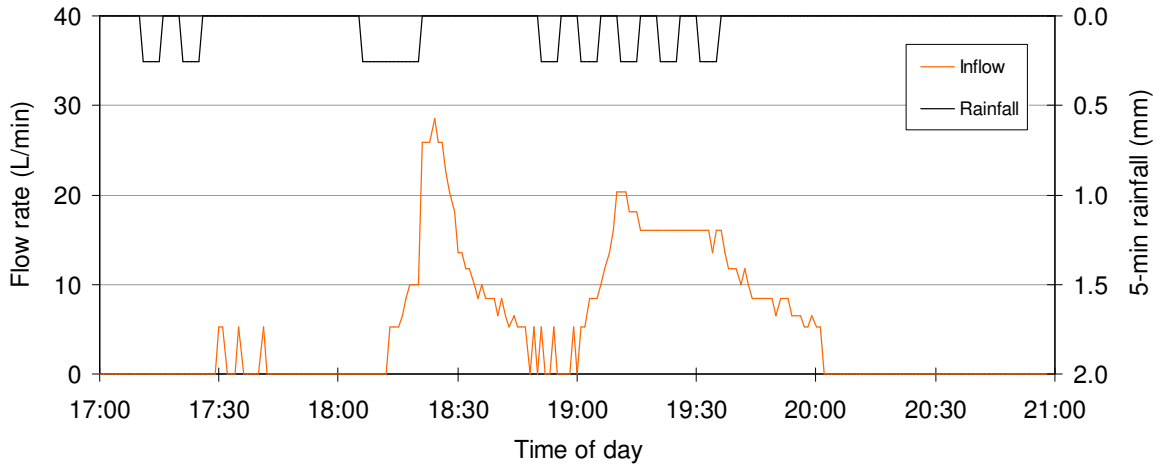


Figure A-16. Hydrograph and hyetograph for July 29, 2007.

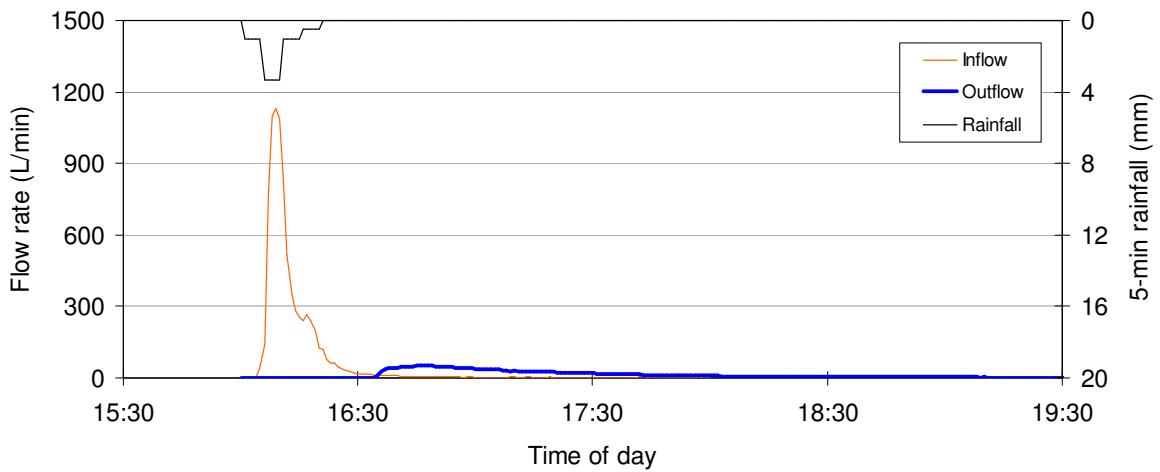


Figure A-17. Hydrographs and hyetograph for July 30, 2007.

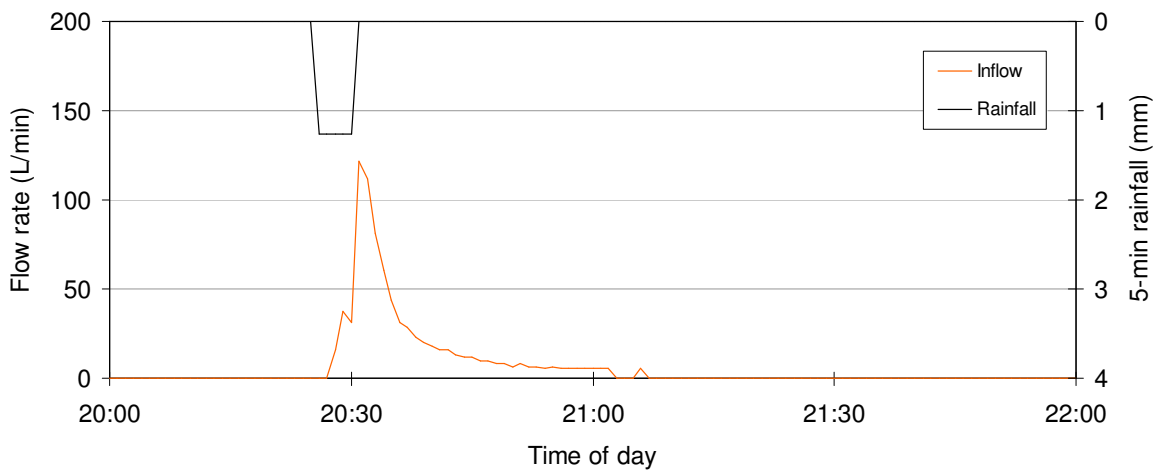


Figure A-18. Hydrograph and hyetograph for August 9, 2007.

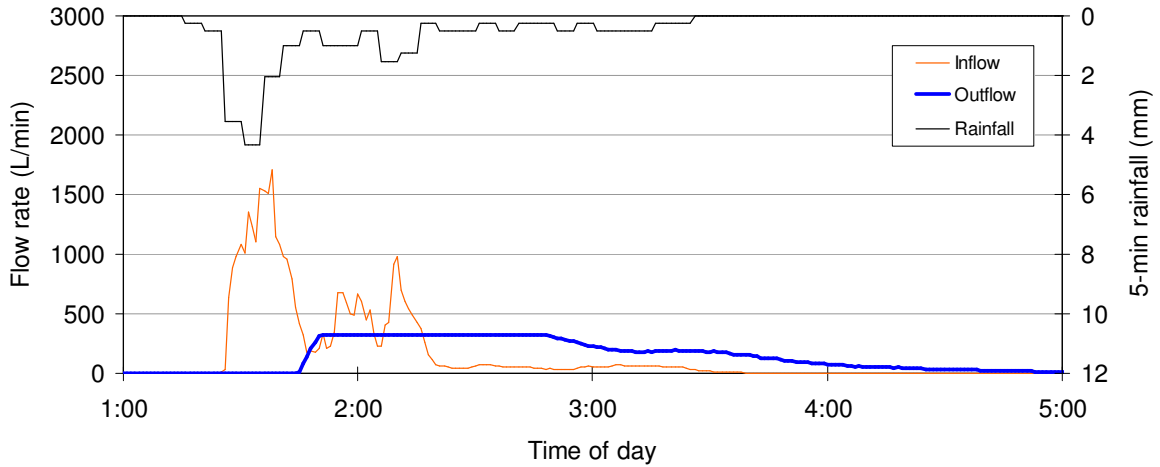


Figure A-19. Hydrographs and hyetograph for August 20, 2007 – AM.

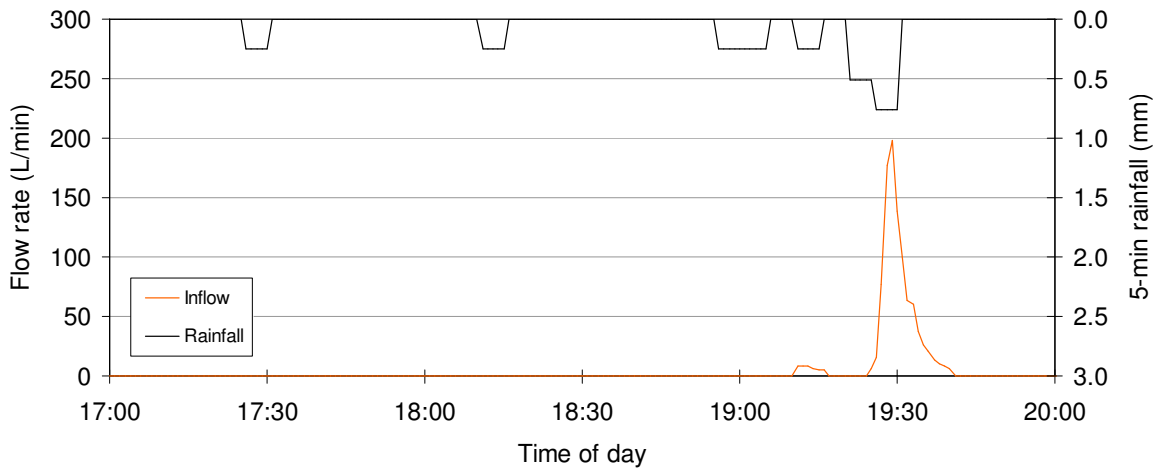


Figure A-20. Hydrograph and hyetograph for August 20, 2007 – PM.

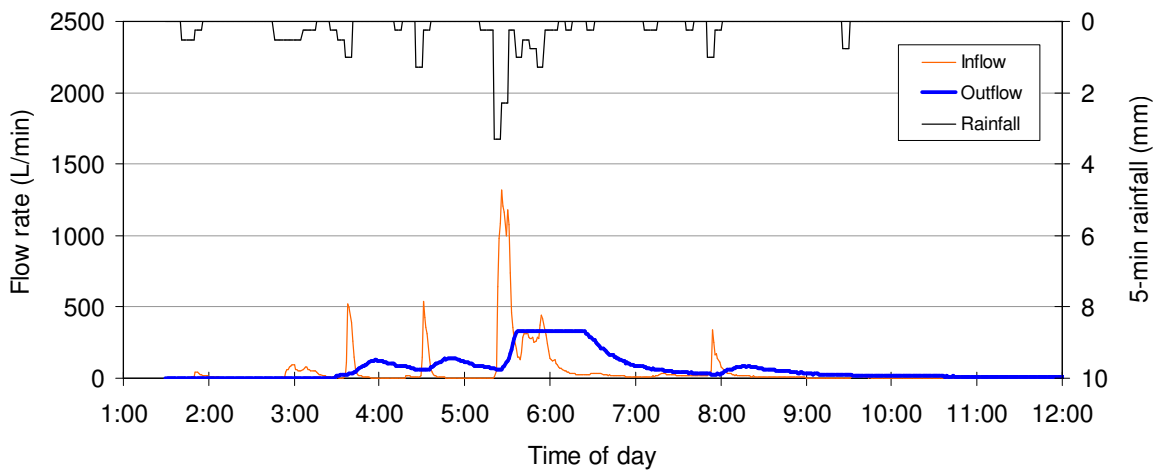


Figure A-21. Hydrographs and hyetograph for August 21, 2007.

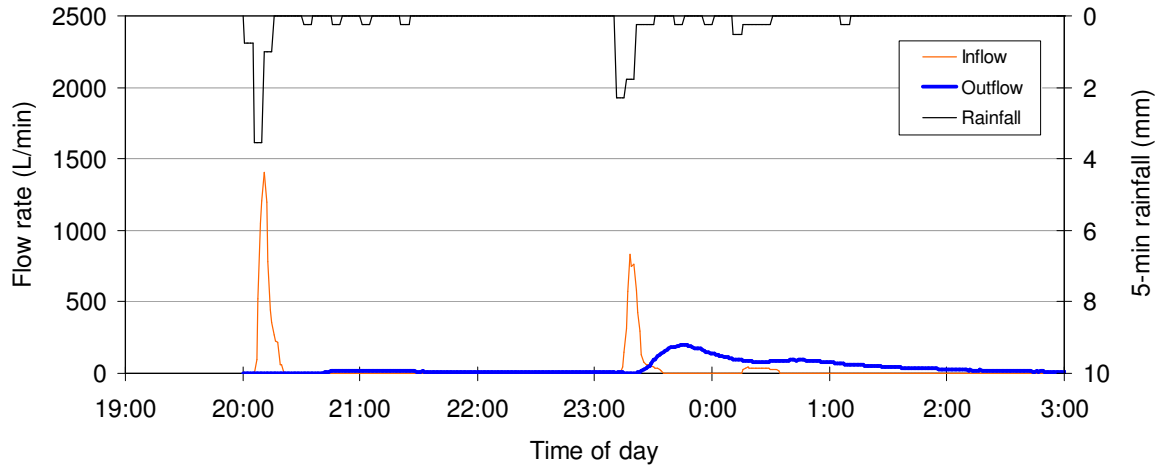


Figure A-22. Hydrographs and hyetograph for August 25, 2007.

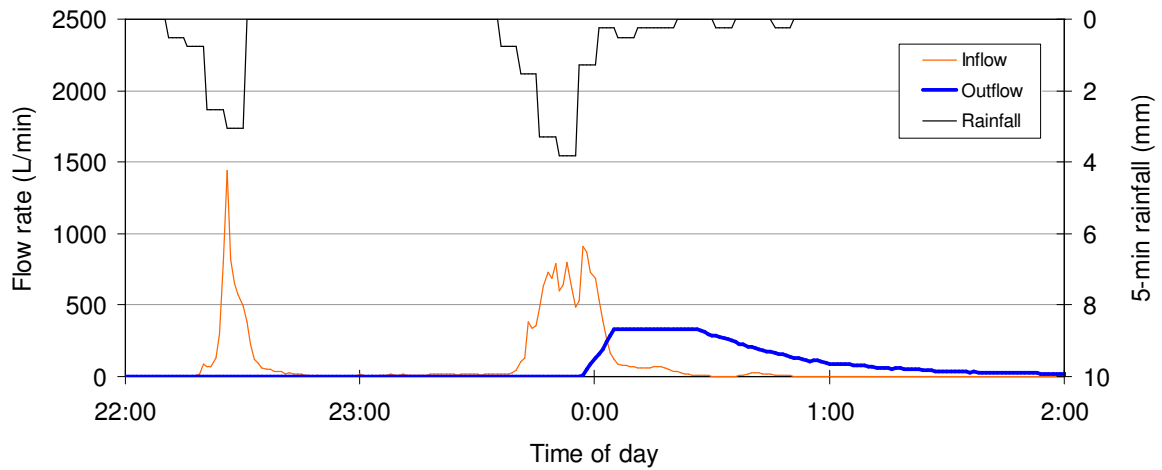


Figure A-23. Hydrographs and hyetograph for September 10, 2007.

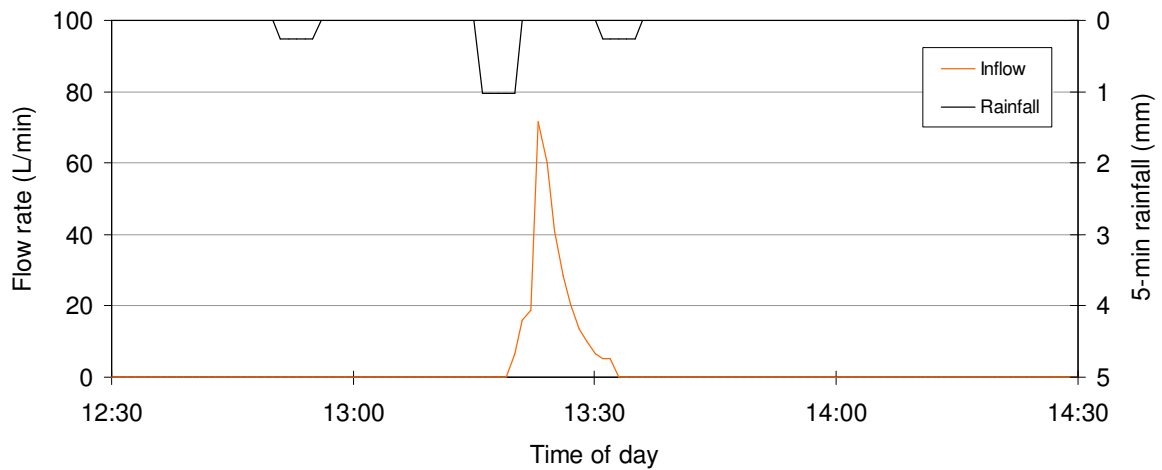


Figure A-24. Hydrograph and hyetograph for September 11, 2007.

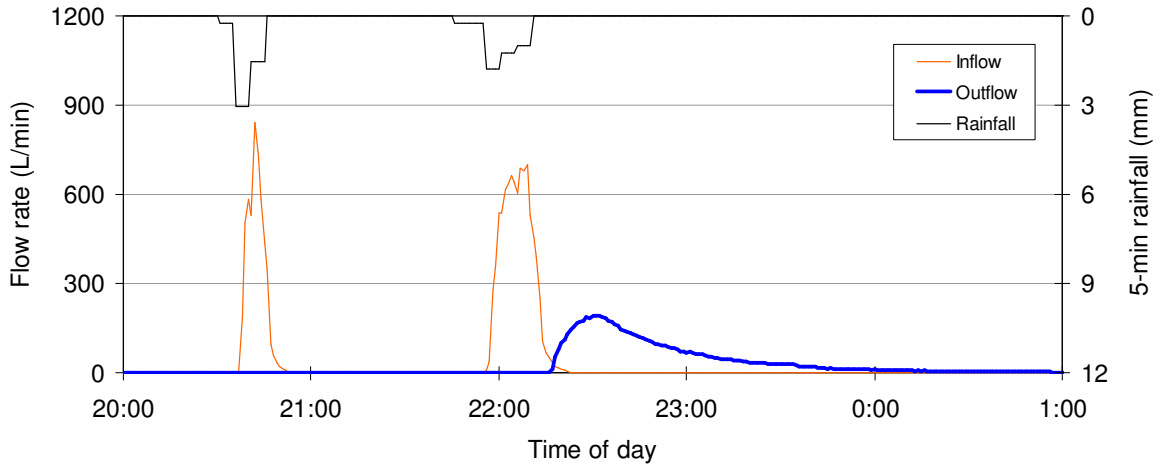


Figure A-25. Hydrographs and hyetograph for October 19, 2007.

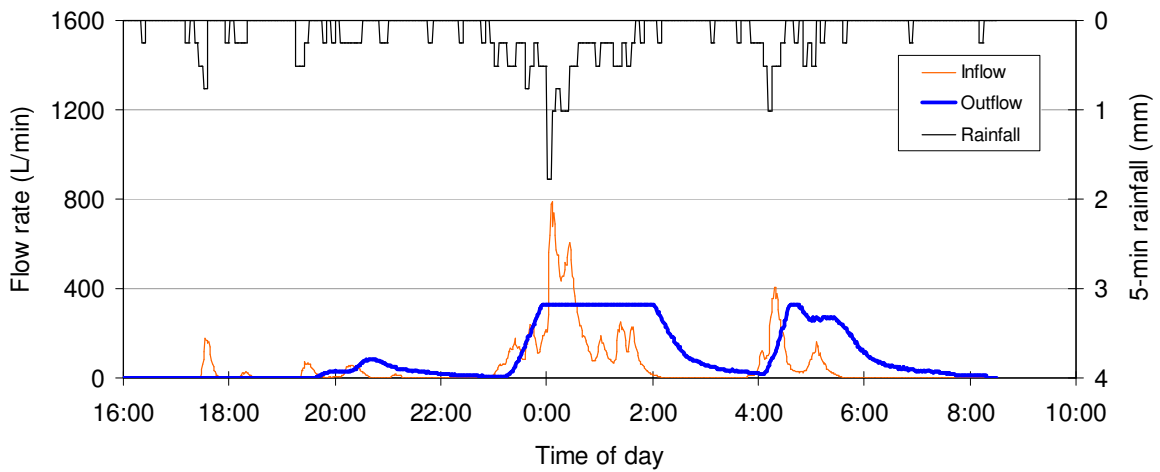


Figure A-26. Hydrographs and hyetograph for October 24, 2007.

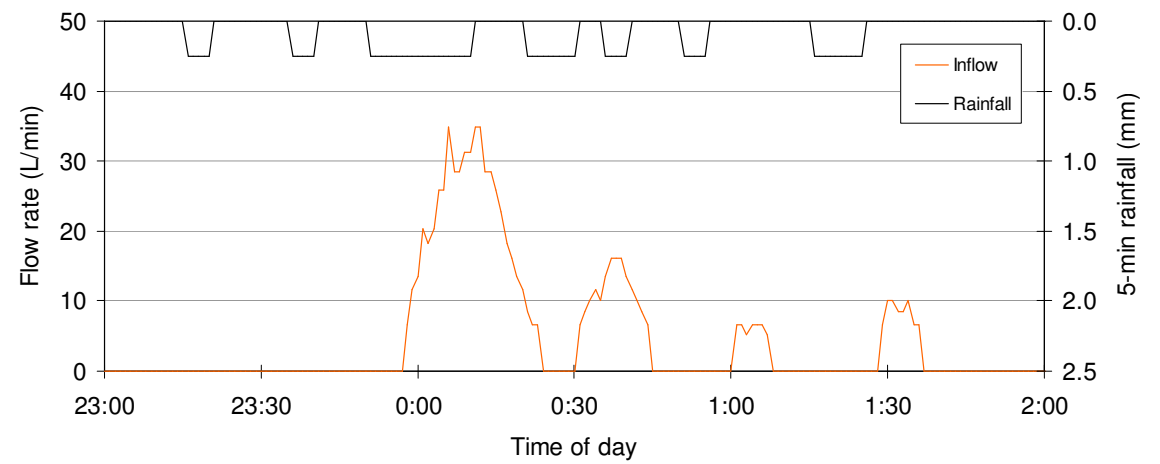


Figure A-27. Hydrograph and hyetograph for November 12, 2007.

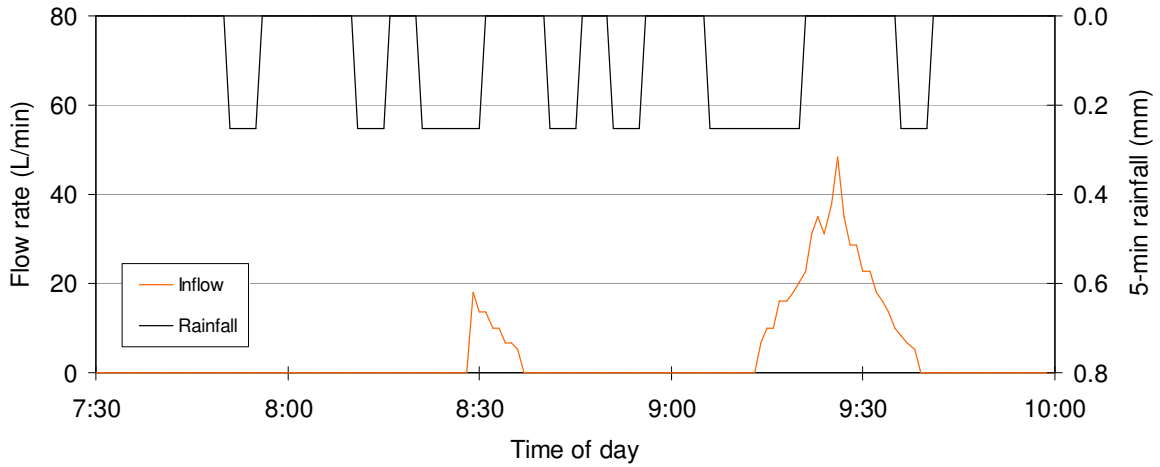


Figure A-28. Hydrograph and hyetograph for November 13, 2007.

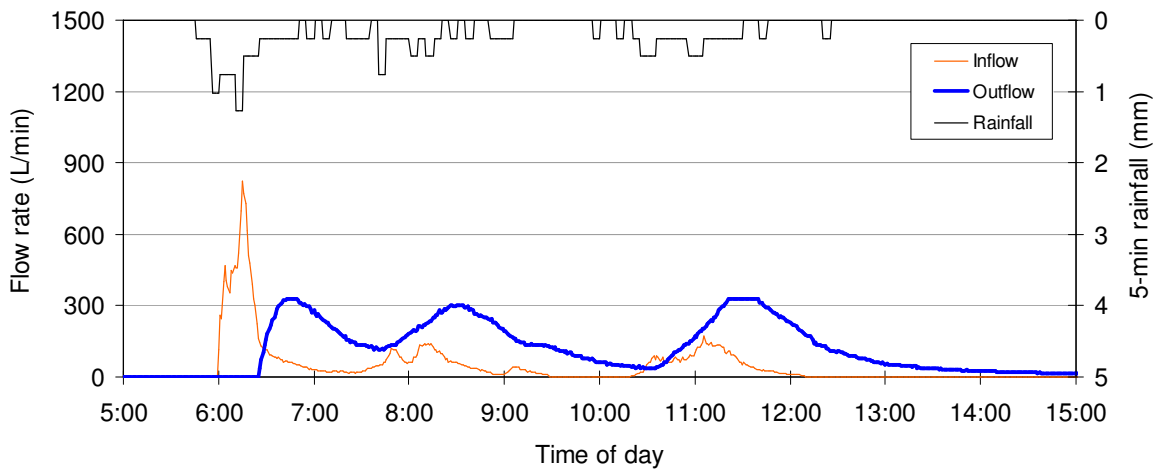


Figure A-29. Hydrographs and hyetograph for November 15, 2007.

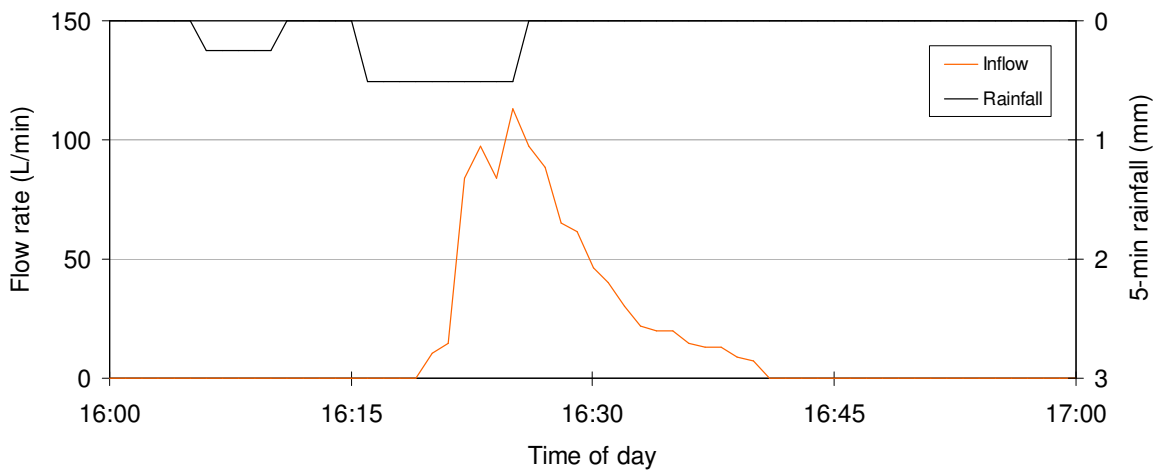


Figure A-30. Hydrograph and hyetograph for November 26, 2007.

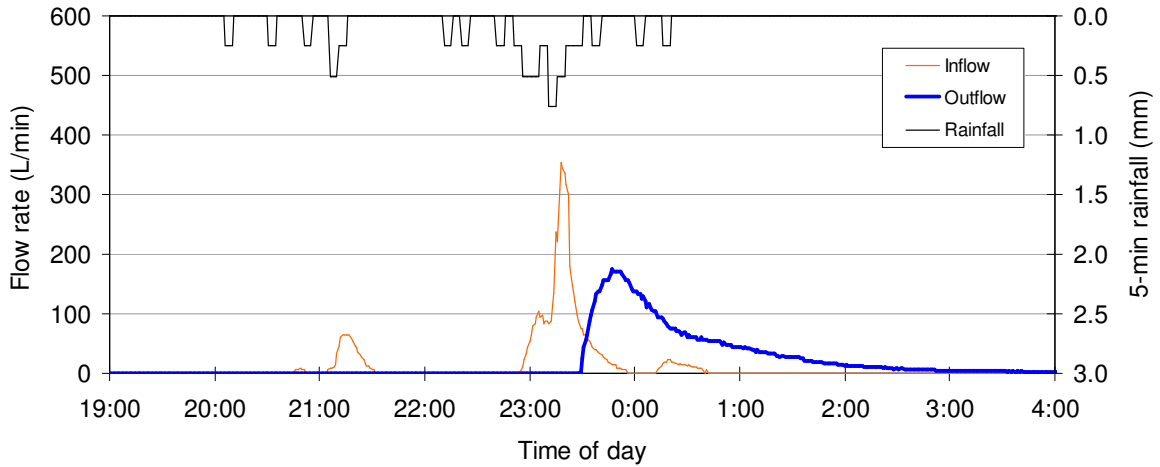


Figure A-31. Hydrographs and hyetograph for December 2, 2007.

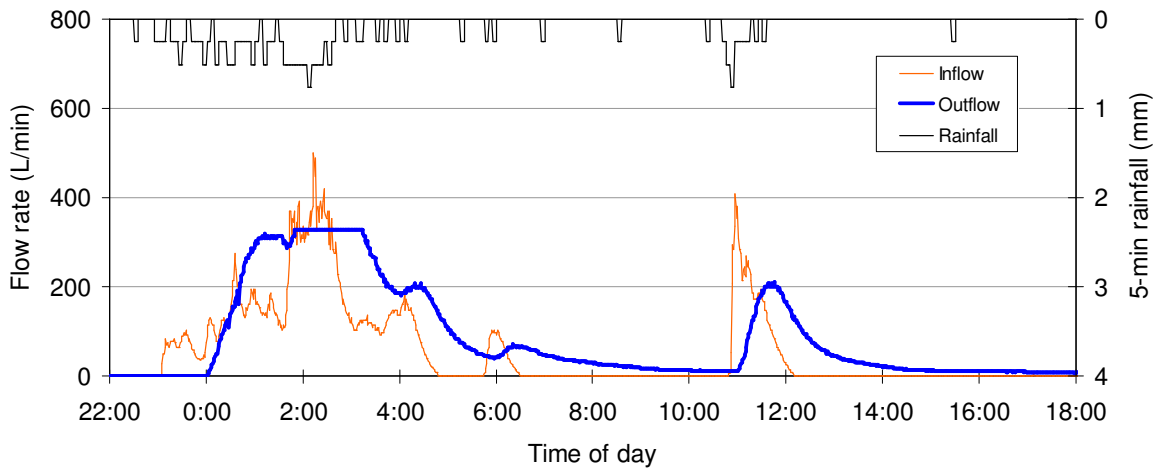


Figure A-32. Hydrographs and hyetograph for December 16, 2007.

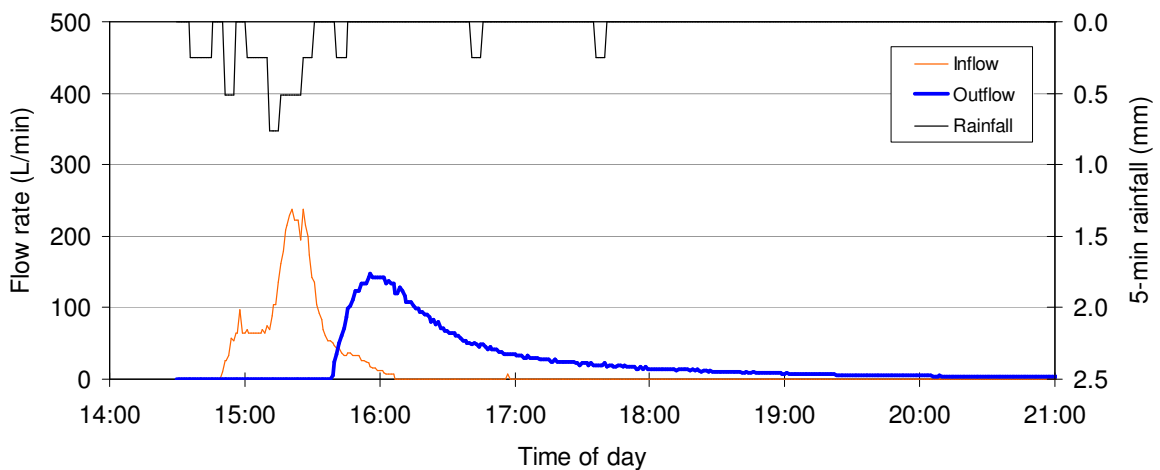


Figure A-33. Hydrographs and hyetograph for December 23, 2007.

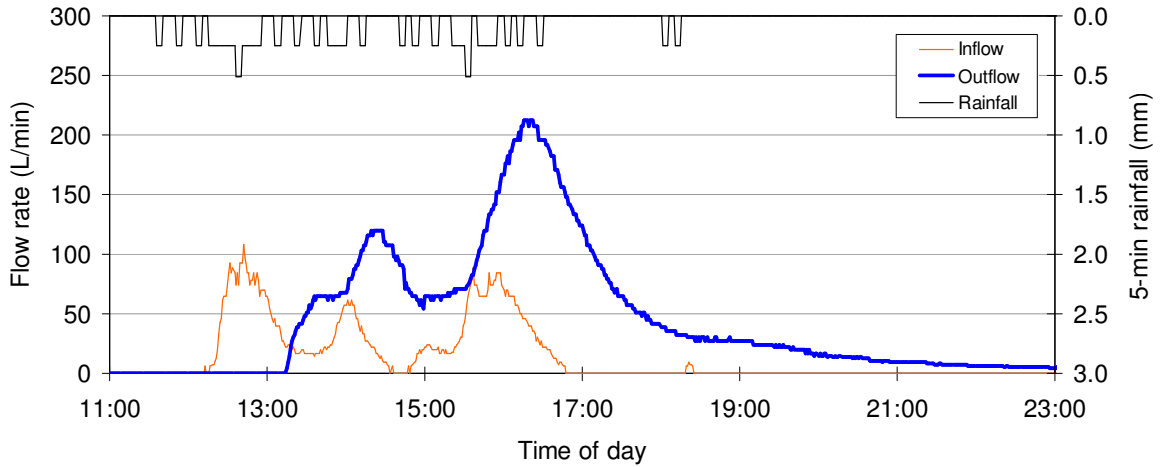


Figure A-34. Hydrographs and hyetograph for December 26, 2007.

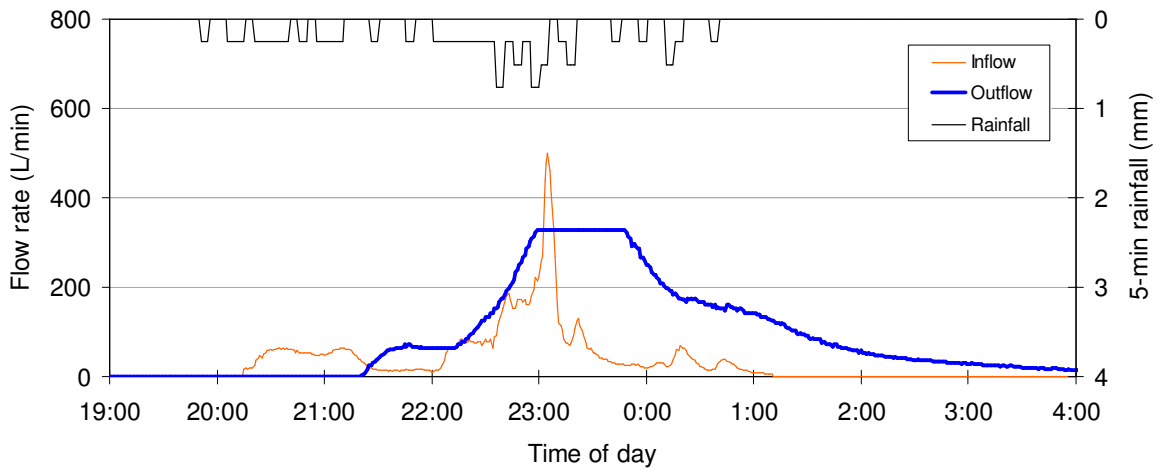


Figure A-35. Hydrographs and hyetograph for December 28, 2007.

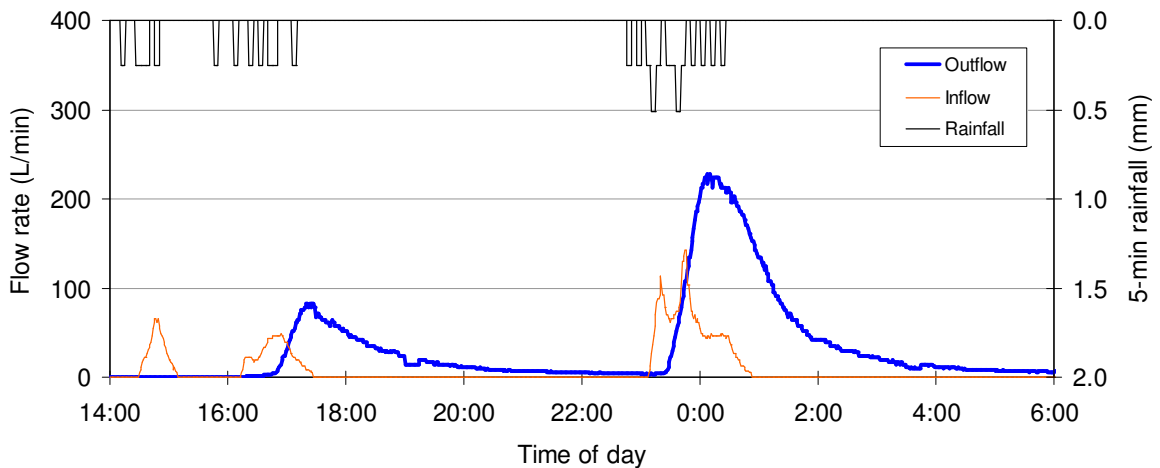


Figure A-36. Hydrographs and hyetograph for December 30, 2007.

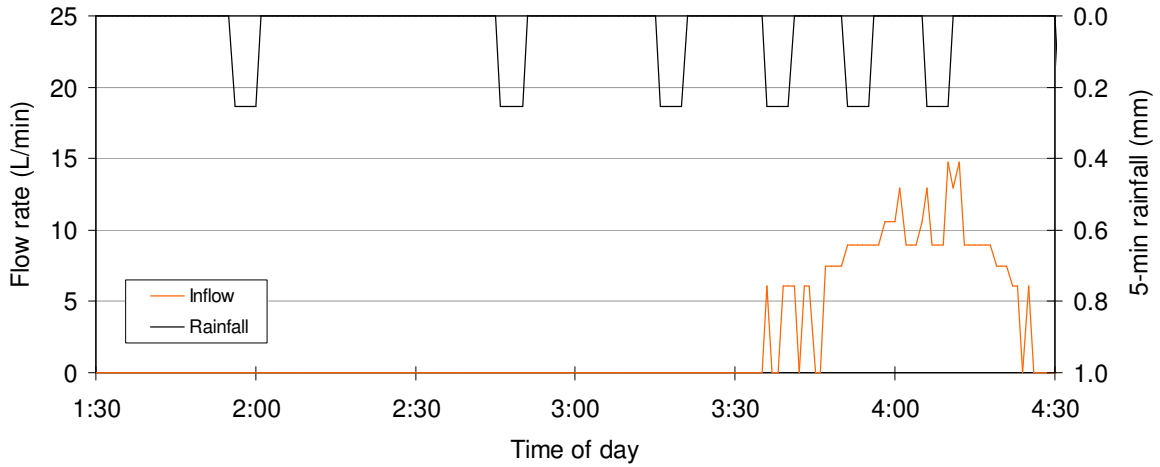


Figure A-37. Hydrograph and hyetograph for January 6, 2008.

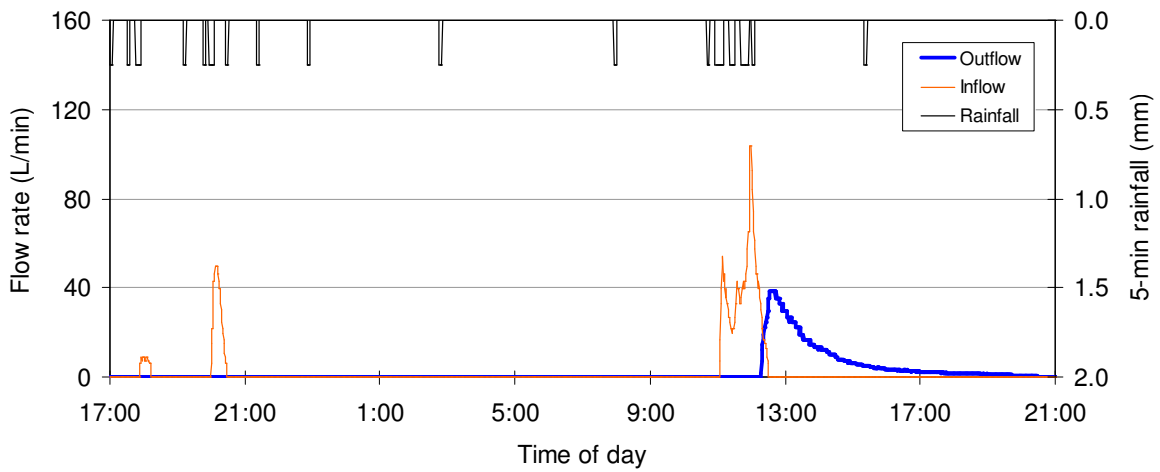


Figure A-38. Hydrographs and hyetograph for January 10 – 11, 2008.

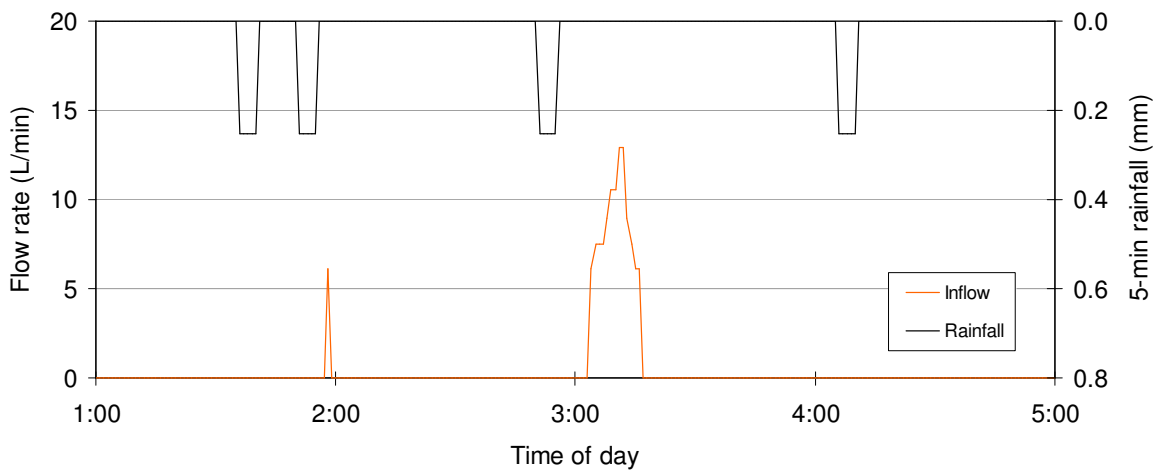


Figure A-39. Hydrograph and hyetograph for January 30, 2008.

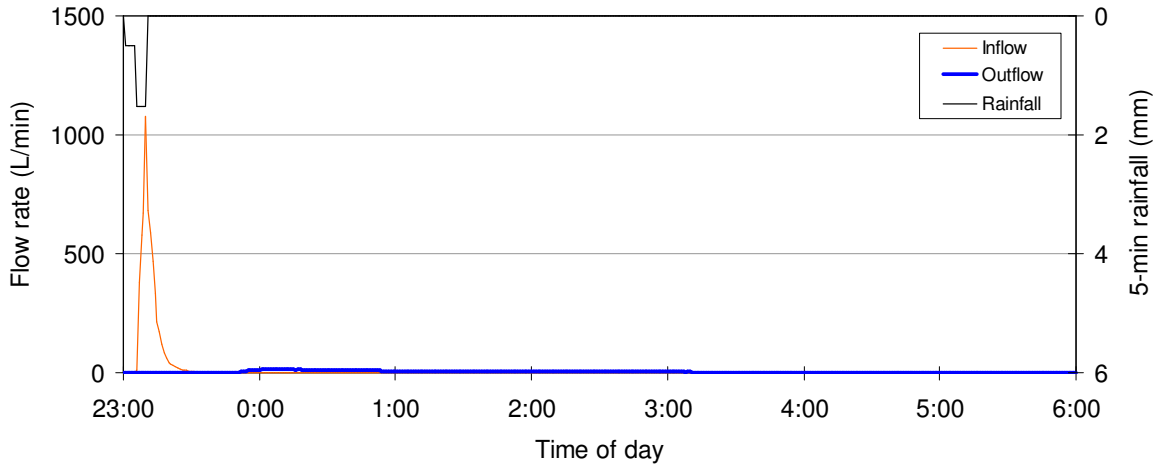


Figure A-40. Hydrographs and hyetograph for February 6, 2008.

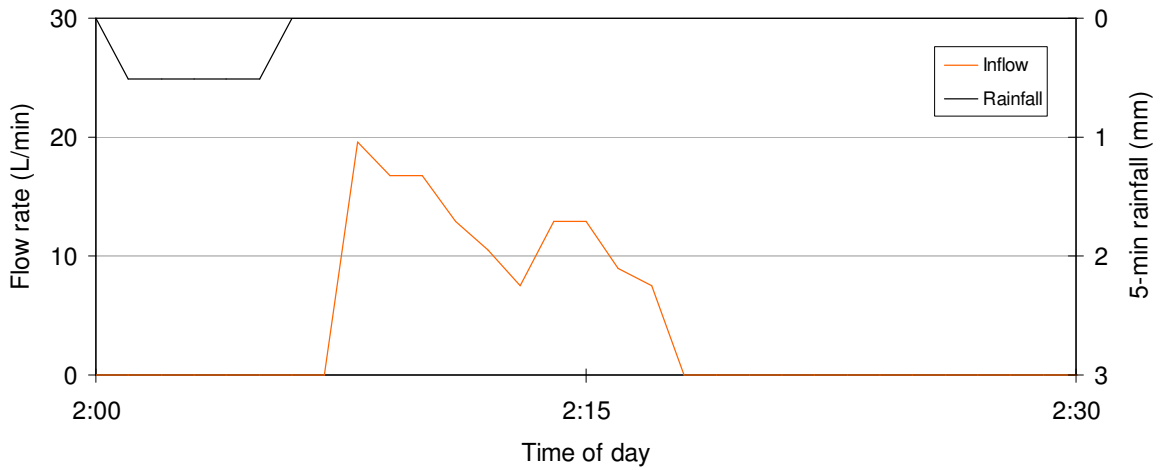


Figure A-41. Hydrograph and hyetograph for February 18, 2008 – AM.

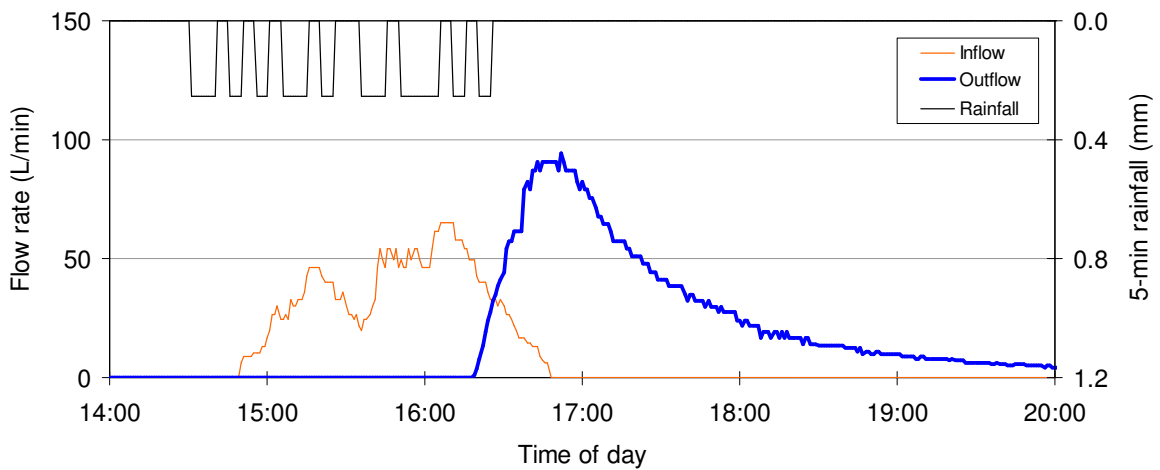


Figure A-42. Hydrographs and hyetograph for February 18, 2008 – PM.

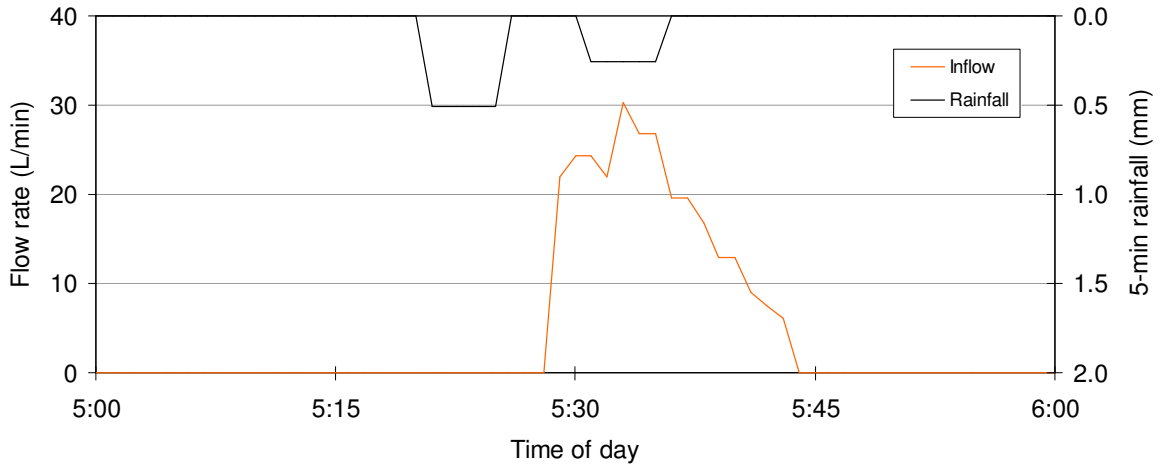


Figure A-43. Hydrograph and hyetograph for March 1, 2008.

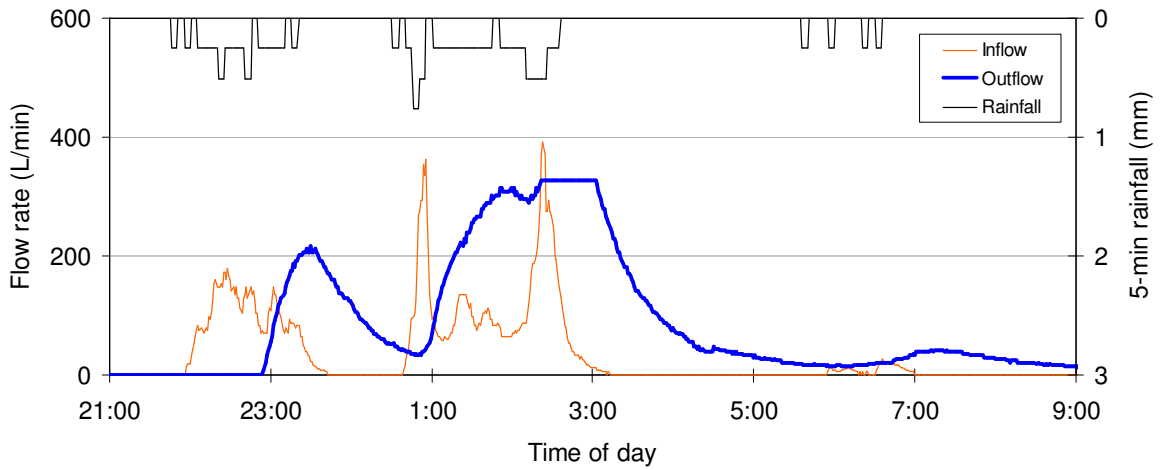


Figure A-44. Hydrographs and hyetograph for March 4, 2008.

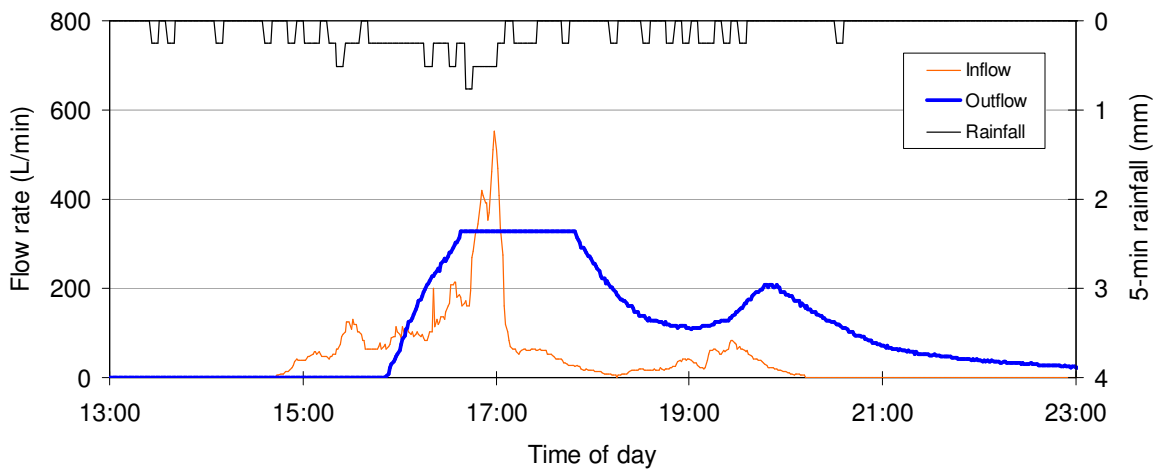


Figure A-45. Hydrographs and hyetograph for March 7, 2008.

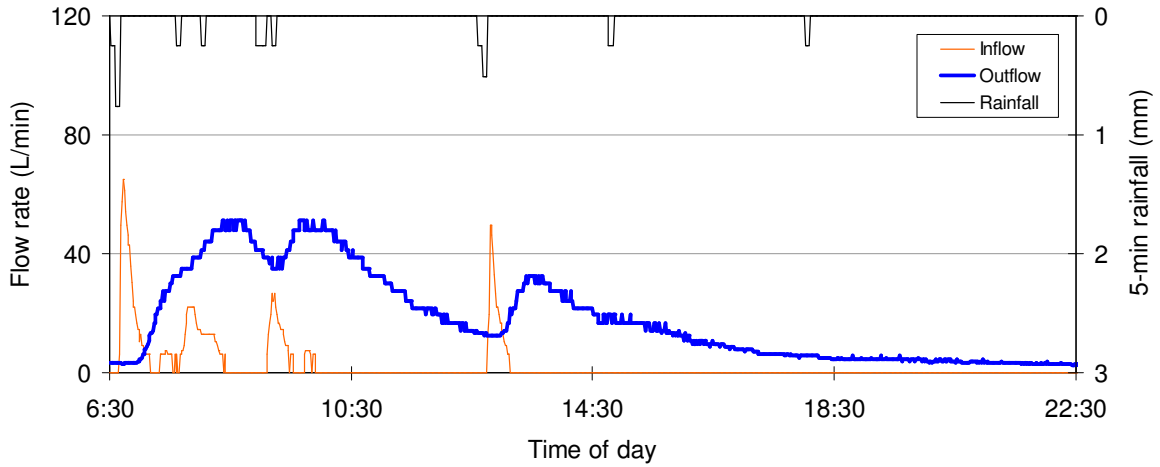


Figure A-46. Hydrographs and hyetograph for March 8, 2008.

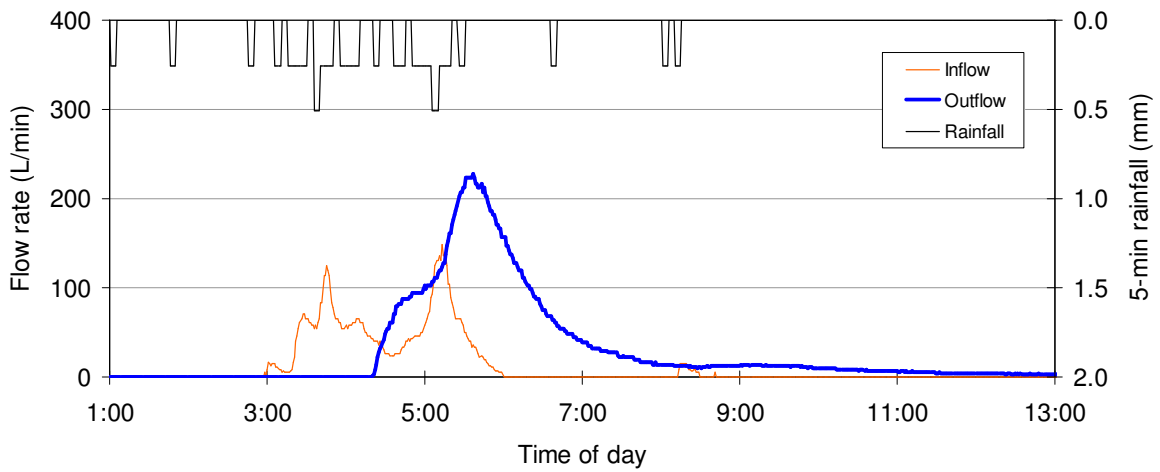


Figure A-47. Hydrographs and hyetograph for March 16, 2008.

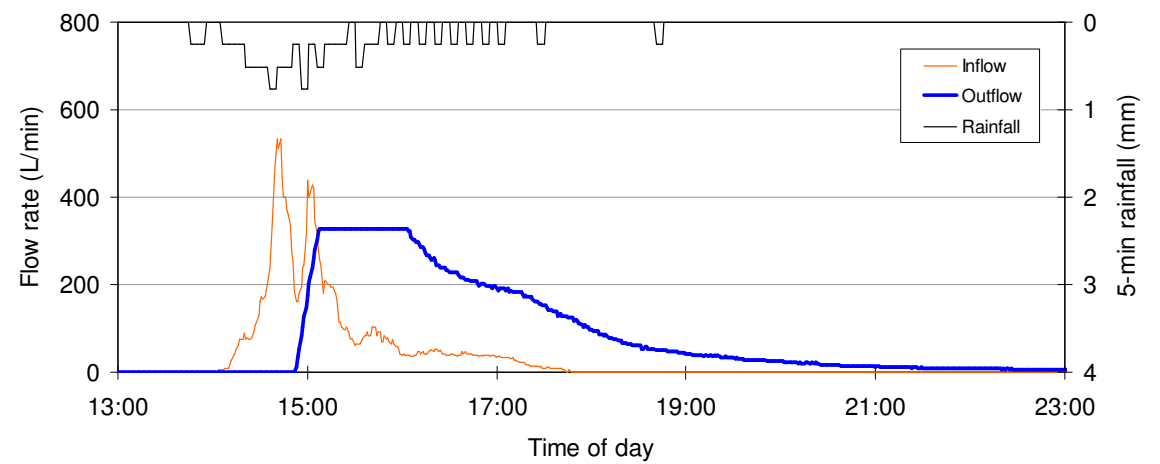


Figure A-48. Hydrographs and hyetograph for March 19, 2008.

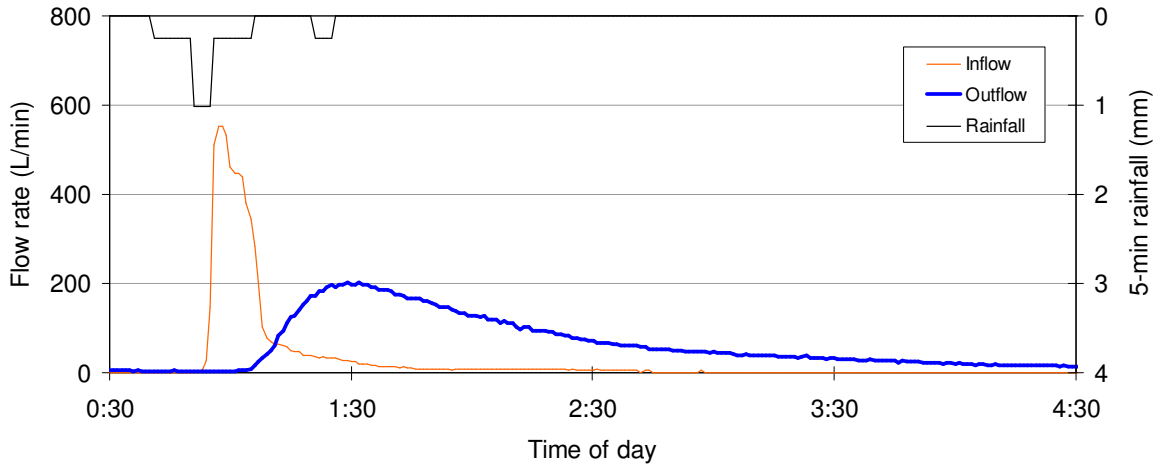


Figure A-49. Hydrographs and hyetograph for March 20, 2008.

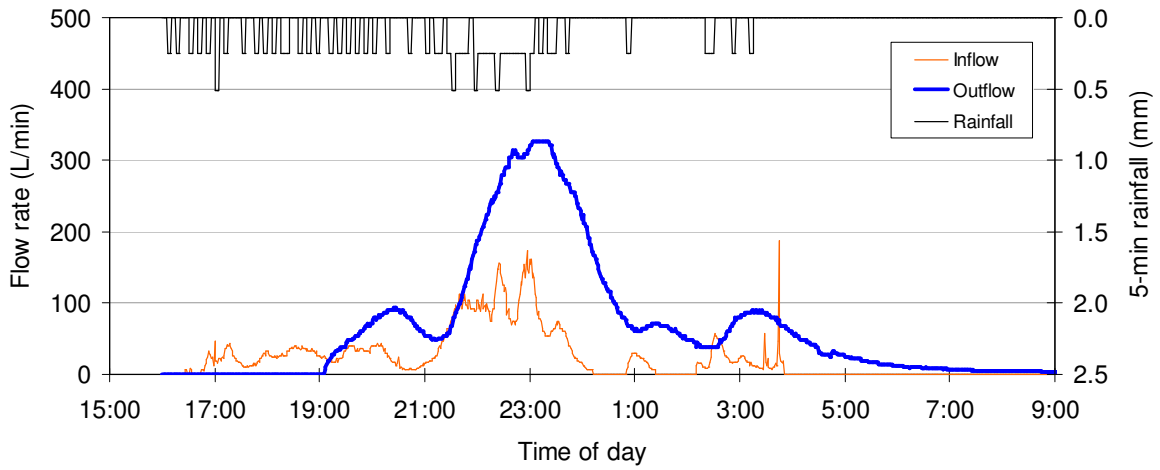


Figure A-50. Hydrographs and hyetograph for April 3, 2008.

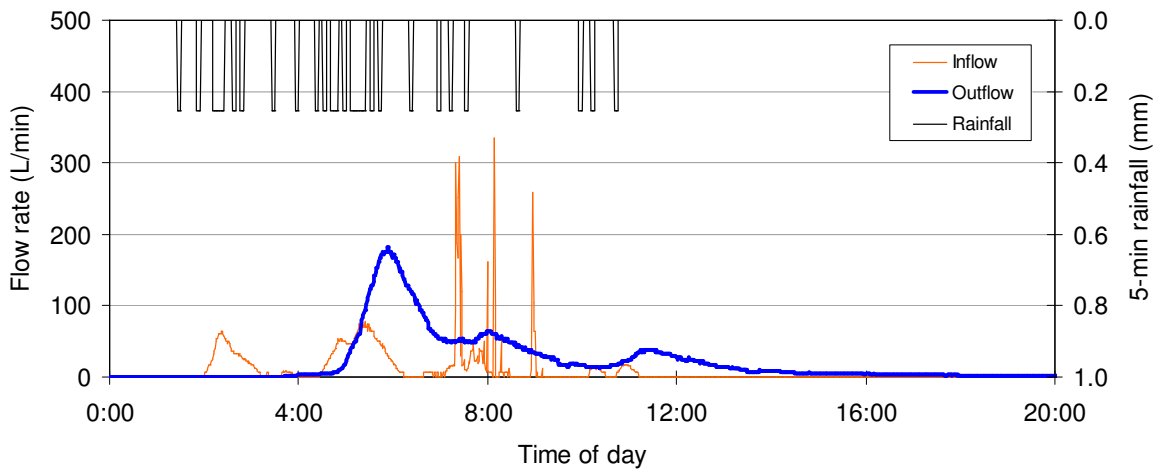


Figure A-51. Hydrographs and hyetograph for April 6, 2008.

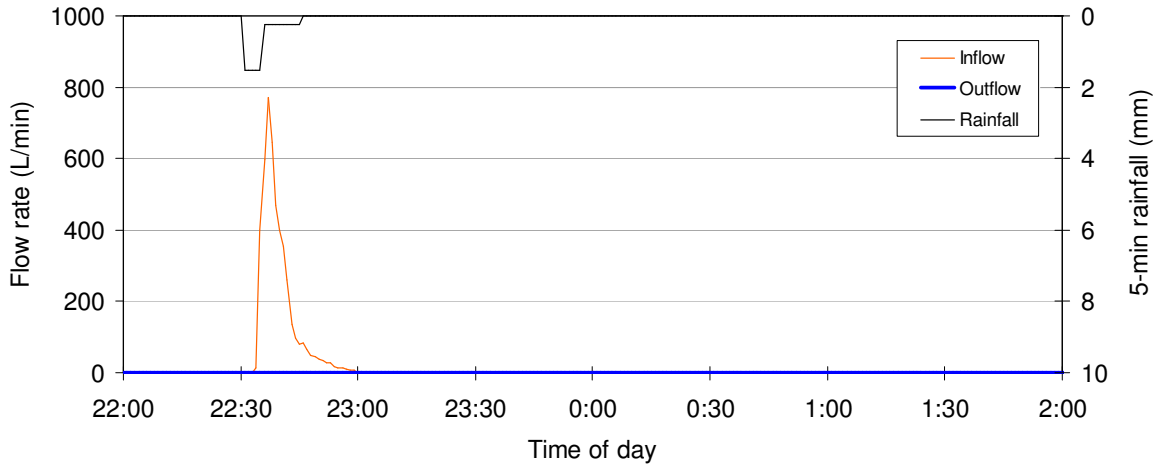


Figure A-52. Hydrograph and hyetograph for April 11, 2008.

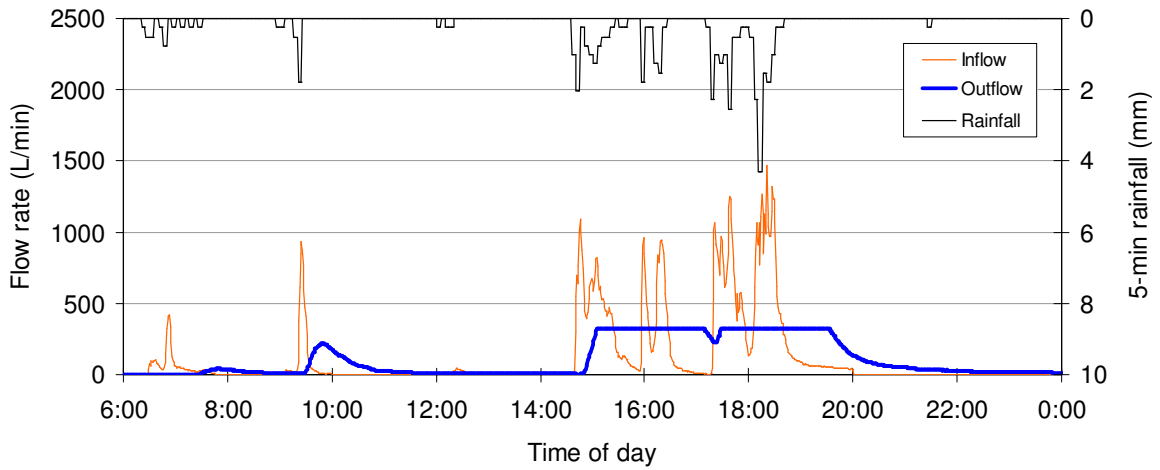


Figure A-53. Hydrographs and hyetograph for April 20, 2008.

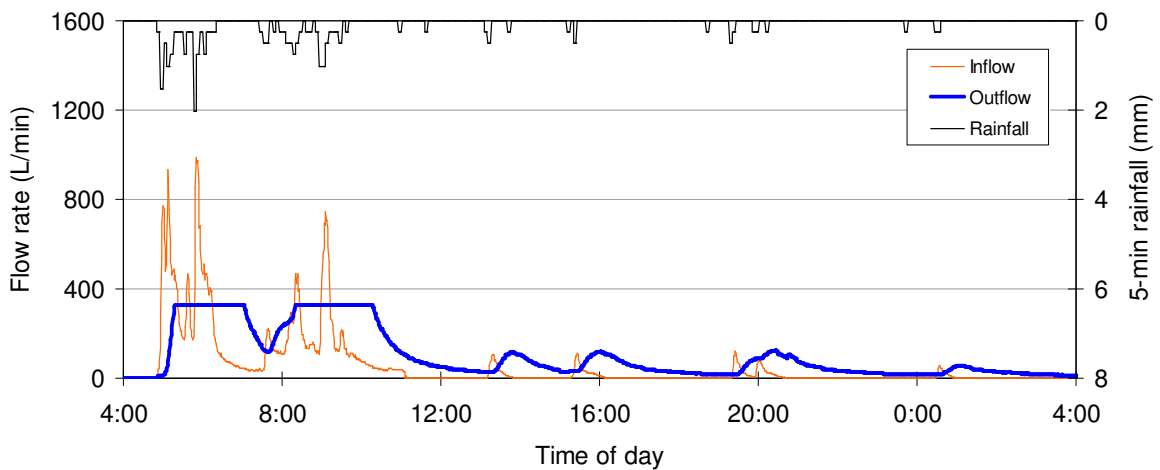


Figure A-54. Hydrographs and hyetograph for April 21, 2008.

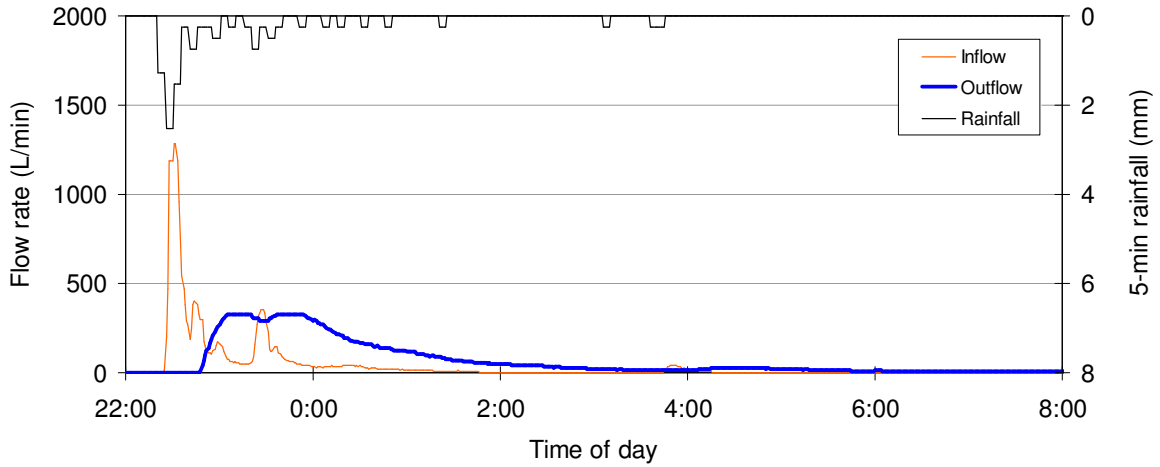


Figure A-55. Hydrographs and hyetograph for April 26, 2008.

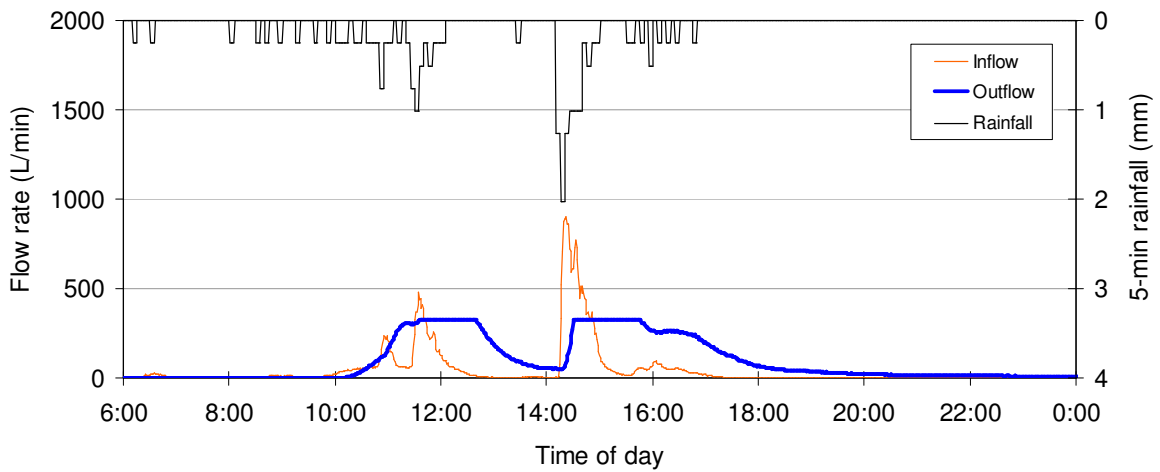


Figure A-56. Hydrographs and hyetograph for April 28, 2008.

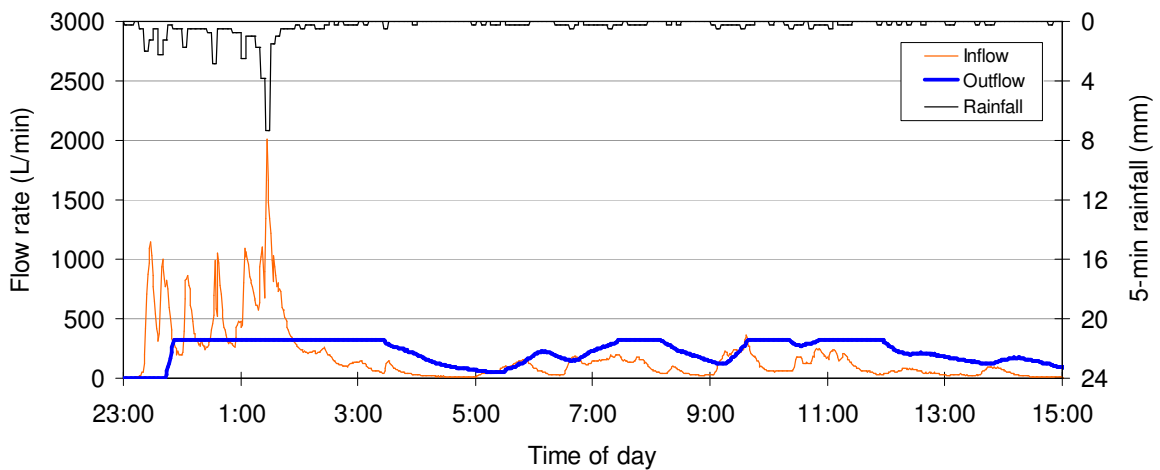


Figure A-57. Hydrographs and hyetograph for May 8, 2008.

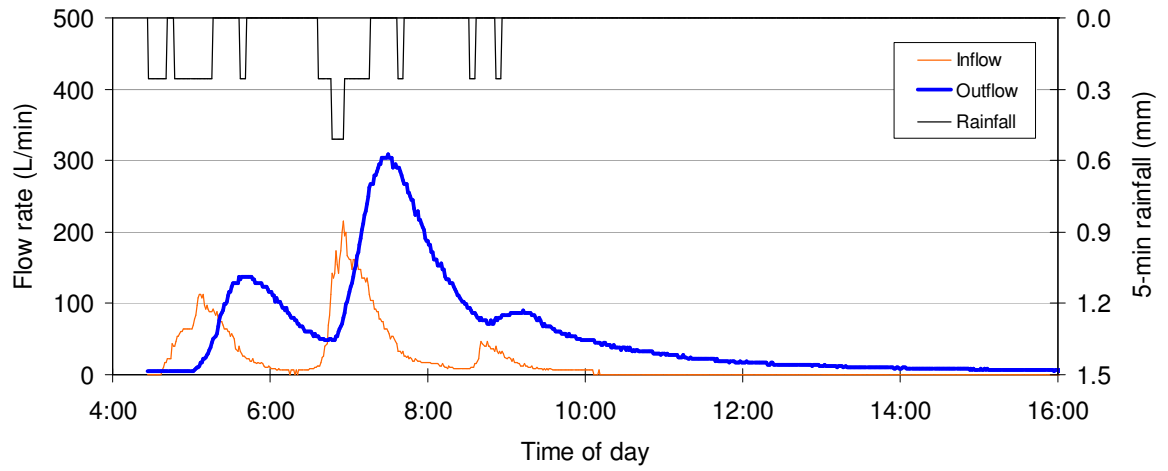


Figure A-58. Hydrographs and hyetograph for May 10, 2008.

Table A-2. Pollutant concentrations in each bottle for the July 28, 2007 (AM) event.

Pollutant	Concentration in each bottle (mg/L)			
	Inflow 1	Inflow 2	Inflow 3	Inflow 4
Chloride	99	22	51	42
Nitrate*	1.6	0.51	0.78	0.72
TKN*	3.1	1.0	1.3	1.2
TP*	0.39	0.058	0.084	0.071
Lead	0.041	0.012	0.0073	0.007
Zinc	0.79	0.18	0.11	0.11
BOD	41	11	11	8.3
TSS	226	44	16	14

Pollutant	Concentration in each bottle (mg/L)	
	Outflow 1	Blank
Chloride	93	0.035
Nitrate*	1.1	0
TKN*	2.1	0.16
TP*	0.26	0
Lead	0.0039	0.0007
Zinc	0.024	0.0027
BOD	0	0.40
TSS	28	14

* Nitrate and total Kjeldahl nitrogen (TKN) are expressed as N; TP is expressed as P.

Table A-3. Pollutant concentrations in each bottle for the Sep. 10, 2007 event (first burst).

Pollutant	Concentration in each bottle (mg/L)		
	Inflow 1	Inflow 2	Blank
Chloride	100	52	0.068
Nitrate*	3.9	1.0	<0.2
TKN*	11	1.9	0.03
TP*	0.57	0.12	0
Lead	0.045	0.0092	0.0006
Zinc	1.3	0.39	0.0054
BOD	32	0	0
TSS	n/a	25	1

* Nitrate and total Kjeldahl nitrogen (TKN) are expressed as N; TP is expressed as P.

Table A-4. Pollutant concentrations in each bottle for the Oct. 19, 2007 event.

Pollutant	Concentration in each bottle (mg/L)		
	Inflow 1	Inflow 2	Inflow 3
Chloride	22	22	6.4
Nitrate*	0.78	0.81	0.28
TKN*	9.5	6.2	1.9
TP*	0.23	0.19	0.064
Lead	0.029	0.020	0.0096
Zinc	1.1	0.60	0.35
BOD	35	22	8.6
TSS	180	92	44

Pollutant	Concentration in each bottle (mg/L)			
	Outflow 1	Outflow 2	Outflow 3	Blank
Chloride	63	91	81	0.22
Nitrate*	1.0	1.3	1.4	0.024
TKN*	4.5	4.6	4.6	0.073
TP*	0.31	0.22	0.21	0
Lead	0.0050	0.0040	0.0040	0.00060
Zinc	0.040	0.029	0.029	0.0048
BOD	11	7.5	16	2.2
TSS	56	36	36	0.70

* Nitrate and total Kjeldahl nitrogen (TKN) are expressed as N; TP is expressed as P.

Table A-5. Pollutant concentrations in each bottle for the Nov. 12, 2007 event.

Pollutant	Concentration in each bottle (mg/L)		
	Inflow 1	Inflow 2	Blank
Chloride	130	130	0.054
Nitrate*	1.2	0.83	0.024
TKN*	2.9	1.9	0.41
TP*	0.24	0.10	0
Lead	0.017	0.006	0.00040
Zinc	0.42	0.21	0.0031
BOD	12	0.90	0.1
TSS	77	24	0

* Nitrate and total Kjeldahl nitrogen (TKN) are expressed as N; TP is expressed as P.

Table A-6. Pollutant concentrations for the Nov. 13, 2007 event. Unused outflow bottles from the Nov. 12 event were installed in the inflow sampler for this event. As a result, the blank from Nov. 12 was considered to be applicable.

Pollutant	Concentration in each bottle (mg/L)
	Inflow 1
Chloride	
Nitrate*	0.67
TKN*	2.5
TP*	0.29
Lead	0.023
Zinc	0.54
BOD	11
TSS	87

* Nitrate and total Kjeldahl nitrogen (TKN) are expressed as N; TP is expressed as P.

Table A-7. Pollutant concentrations in each bottle for the Dec. 2, 2007 event.

Pollutant	Concentration in each bottle (mg/L)			
	Inflow 1	Inflow 2	Inflow 3	Inflow 4
Chloride	14	11	7.7	12
Nitrate*	0.44	0.39	0.33	0.23
TKN*	0.85	0.73	0.88	0.59
TP*	0.10	0.11	0.11	0.079
Lead	0.0084	0.011	0.0079	0.0052
Zinc	0.55	0.45	0.31	0.19
BOD	38	42	29	28
TSS	49	76	43	20

Pollutant	Concentration in each bottle (mg/L)			
	Outflow 1	Outflow 2	Outflow 3	Blank
Chloride	194	116	115	0
Nitrate*	0.50	0.47	0.50	0
TKN*	0.94	0.70	0.67	0
TP*	0.17	0.15	0.17	0.014
Lead	0.0027	0.0025	0.0023	0.00050
Zinc	0.030	0.023	0.021	0.0035
BOD	20	22	29	3.1
TSS	8.0	12	14	0

* Nitrate and total Kjeldahl nitrogen (TKN) are expressed as N; TP is expressed as P.

Table A-8. Pollutant concentrations in each bottle for the Dec. 23, 2007 event.

Pollutant	Concentration in each bottle (mg/L)			
	Inflow 1	Inflow 2	Inflow 3	Inflow 4
Chloride	149	113	62	84
Nitrate*	0.32	0.25	0.16	0.17
TKN*	1.4	1.0	0.77	0.84
TP*	0.14	0.094	0.11	0.068
Lead	0.038	0.032	0.023	0.011
Zinc	0.83	0.64	0.48	0.24
BOD				
TSS	384	208	176	52

Pollutant	Concentration in each bottle (mg/L)		
	Outflow 1	Outflow 2	Blank
Chloride	321	330	0.51
Nitrate*	0.32	0.27	0.0014
TKN*	1.1	0.83	0.27
TP*	0.16	0.16	0
Lead	0.0050	0.0037	0.0007
Zinc	0.051	0.038	0.0029
BOD	0	0	0.0
TSS	30	10	0

* Nitrate and total Kjeldahl nitrogen (TKN) are expressed as N; TP is expressed as P.

Table A-9. Pollutant concentrations in each bottle for the Jan. 10, 2008 event.

Pollutant	Concentration in each bottle (mg/L)			
	Inflow 1	Inflow 2	Inflow 3	Inflow 4
Chloride	93	93	97	91
Nitrate*	0.63	0	1.6	0.92
TKN*	2.0	3.2	3.6	2.5
TP*	0.12	0.22	0.47	0.28
Lead	0.026	0.16	0.076	0.036
Zinc	0.78	2.9	0.97	0.66
BOD				
TSS	208	895	432	244
Pollutant	Concentration in each bottle (mg/L)			
	Outflow 1	Outflow 2	Blank	
Chloride	212	192	0	
Nitrate*	0.83	0.83	0	
TKN*	1.2	1.1	0.33	
TP*	0.18	0.15	0	
Lead	0.0075	0.0054	0.0001	
Zinc	0.085	0.064	0.0021	
BOD				
TSS	39	23	0	

* Nitrate and total Kjeldahl nitrogen (TKN) are expressed as N; TP is expressed as P.

Table A-10. Pollutant concentrations in each bottle for the Feb. 18, 2008 (PM) event.

Pollutant	Concentration in each bottle (mg/L)			
	Inflow 1	Inflow 2	Inflow 3	Inflow 4
Chloride	464	384	311	288
Nitrate*	1.4	1.2	1.2	1.2
TKN*	2.4	1.9	2.0	1.3
TP*	0.19	0.15	0.14	0.11
Lead	0.079	0.060	0.046	0.041
Zinc	0.70	0.76	0.56	0.49
BOD	15	11	1.1	0
TSS	192	234	148	142

Pollutant	Concentration in each bottle (mg/L)			
	Outflow 1	Outflow 2	Outflow 3	Blank
Chloride	1118	482	484	0.25
Nitrate*	1.1	0.92	0	0
TKN*	1.4	1.2	1.1	0.10
TP*	0.31	0.17	0.16	0
Lead	0.0094	0.011	0.0086	0.0019
Zinc	0.091	0.078	0.068	0.012
BOD	0	0	0	0
TSS	50	48	46	2

* Nitrate and total Kjeldahl nitrogen (TKN) are expressed as N; TP is expressed as P.

Table A-11. Pollutant concentrations in each bottle for the April 3, 2008 event.

Pollutant	Concentration in each bottle (mg/L)			
	Inflow 1	Inflow 2	Inflow 3	Inflow 4
Chloride	79	55	46	57
Nitrate*	0.59	0.38	0.28	0.17
TKN*	1.7	1.3	1.2	0.77
TP*	0.13	0.090	0.072	0.047
Lead	0.012	0.0079	0.0068	0.0053
Zinc	0.57	0.37	0.32	0.21
BOD	17	17	7.2	7.2
TSS	62	66	48	38

Pollutant	Concentration in each bottle (mg/L)			
	Outflow 1	Outflow 2	Outflow 3	Blank
Chloride	267	240	169	0.19
Nitrate*	0.95	0.70	0.37	0
TKN*	2.1	1.5	1.2	0.17
TP*	0.28	0.25	0.21	0.005
Lead	0	0.0030	0.0022	0.0001
Zinc	0.0003	0.067	0.044	0.0044
BOD	9.0	8.4	8.4	1.3
TSS	19	7.0	0	0

* Nitrate and total Kjeldahl nitrogen (TKN) are expressed as N; TP is expressed as P.

Table A-12. Pollutant concentrations in each bottle for the April 26, 2008 event.

Pollutant	Concentration in each bottle (mg/L)			
	Inflow 1	Inflow 2	Inflow 3	Inflow 4
Chloride				
Nitrate*	0.87	0.77	0.64	0.31
TKN*	2.9	2.2	1.8	1.3
TP*	0.27	0.19	0.15	0.15
Lead	0.017	0.0057	0.0038	0.0023
Zinc	0.39	0.24	0.23	0.16
BOD	14	5.4	4.8	1.8
TSS	94	47	29	22
Pollutant	Concentration in each bottle (mg/L)			
	Outflow 1	Outflow 2	Outflow 3	Blank
Chloride				
Nitrate*	0.87	0.62	0.53	0
TKN*	1.6	1.2	1.4	0.029
TP*	0.30	0.24	0.26	0.031
Lead	0.0022	0.0017	0.0017	0
Zinc	0.049	0.040	0.039	0.0021
BOD	7.8	2.4	15	0
TSS	23	21	18	1.8

* Nitrate and total Kjeldahl nitrogen (TKN) are expressed as N; TP is expressed as P.

Table A-13. Inflow and outflow event mean concentrations (EMC) for each sampled event. Change in EMC is calculated as a percent of the inflow EMC. Negative values signify concentration reductions.

Date	Result	Chloride	Nitrate*	TKN*	TP*	Lead	Zinc	BOD	TSS
7/28/07 (AM)	In (mg/L)	43	0.79	1.5	0.14	0.019	0.32	18	84
	Out (mg/L)	93	1.1	2.1	0.26	0.0039	0.024	0	28
	% change	116	40	34	87	-79	-93	-100	-66
9/10/07 (1st burst)	In (mg/L)	79	2.6	6.9	0.37	0.029	0.91	18	LE
	Out (mg/L)	0	0	0	0	0	0	0	0
	% change	-100	-100	-100	-100	-100	-100	-100	n/a
10/19/07	In (mg/L)	15	0.57	5.5	0.15	0.019	0.66	21	102
	Out (mg/L)	76	1.2	4.5	0.26	0.0044	0.034	11	45
	% change	398	109	-18	74	-76	-95	-46	-56
11/12/07	In (mg/L)	130	0.94	2.2	0.14	0.0091	0.27	4.4	40
	Out (mg/L)	0	0	0	0	0	0	0	0
	% change	-100	-100	-100	-100	-100	-100	-100	-100
11/13/07	In (mg/L)	NM	0.67	2.5	0.29	0.023	0.54	11	87
	Out (mg/L)	0	0	0	0	0	0	0	0
	% change	n/a	-100	-100	-100	-100	-100	-100	-100
12/2/07	In (mg/L)	11	0.31	0.7	0.096	0.0073	0.31	31	39
	Out (mg/L)	157	0.49	0.8	0.16	0.0026	0.026	22	10
	% change	1380	58	10	72	-65	-92	-29	-74
12/23/07	In (mg/L)	88	0.20	0.91	0.099	0.024	0.50	NM	182
	Out (mg/L)	323	0.30	1.0	0.16	0.0046	0.047	NM	24
	% change	269	52	10	61	-81	-91	n/a	-87
1/10/08	In (mg/L)	92	0.81	2.6	0.27	0.054	1.0	NM	338
	Out (mg/L)	203	0.83	1.2	0.17	0.0066	0.076	NM	32
	% change	120	1.8	-55	-36	-88	-92	n/a	-91
2/18/08	In (mg/L)	326	1.3	1.6	0.13	0.049	0.56	3.3	160
	Out (mg/L)	762	0.70	1.2	0.23	0.0094	0.081	0	48
	% change	134	-44	-21	79	-81	-86	-100	-70
4/3/08	In (mg/L)	58	0.22	0.89	0.057	0.0060	0.26	8.4	42
	Out (mg/L)	184	0.45	1.3	0.22	0.0021	0.043	8.4	2.3
	% change	218	101	49	286	-65	-83	0.72	-94
4/26/08	In (mg/L)	NM	0.67	2.2	0.21	0.0099	0.29	8.4	61
	Out (mg/L)	NM	0.74	1.5	0.27	0.0020	0.045	8.0	22
	% change	n/a	11	-34	30	-80	-84	-5.6	-65

* Nitrate and total Kjeldahl nitrogen (TKN) are expressed as N; TP is expressed as P.

Table A-14. Inflow and outflow pollutant mass for each sampled event. Change in mass is calculated as a percent of the inflow mass. Negative values signify mass reductions.

Date	Result	Chloride	Nitrate*	TKN*	TP*	Lead	Zinc	BOD	TSS
7/28/07 (AM)	In (g)	405	7.4	14	1.3	0.17	3.0	168	784
	Out (g)	75	0.89	1.7	0.21	0.0031	0.019	0	22
	% change	-82	-88	-89	-84	-98	-99	-100	-97
9/10/07 (1st burst)	In (g)	526	18	46	2.5	0.19	6.1	118	LE
	Out (g)	0	0	0	0	0	0	0	0
	% change	-100	-100	-100	-100	-100	-100	-100	n/a
10/19/07	In (g)	213	8.0	77	2.1	0.26	9.2	288	1425
	Out (g)	588	9.2	35	2.0	0.034	0.26	86	346
	% change	176	16	-54	-3.6	-87	-97	-70	-76
11/12/07	In (g)	125	0.91	2.1	0.14	0.0088	0.27	4.3	39
	Out (g)	0	0	0	0	0	0	0	0
	% change	-100	-100	-100	-100	-100	-100	-100	-100
11/13/07	In (g)	NM	0.40	1.5	0.17	0.014	0.33	6.3	52
	Out (g)	0	0	0	0	0	0	0	0
	% change	n/a	-100	-100	-100	-100	-100	-100	-100
12/2/07	In (g)	73	2.1	5.1	0.65	0.050	2.1	214	267
	Out (g)	1752	5.5	9.1	1.8	0.029	0.29	248	115
	% change	2314	158	80	181	-43	-86	16	-57
12/23/07	In (g)	540	1.2	5.6	0.61	0.15	3.1	NM	1122
	Out (g)	3134	2.9	9.7	1.5	0.045	0.46	NM	231
	% change	480	139	73	154	-70	-85	n/a	-79
1/10/08	In (g)	410	3.6	12	1.2	0.24	4.4	NM	1503
	Out (g)	777	3.2	4.5	0.65	0.025	0.29	NM	122
	% change	89	-12.3	-62	-45	-89	-93	n/a	-92
2/18/08	In (g)	1348	5.2	6.5	0.53	0.20	2.3	14	664
	Out (g)	5579	5.2	9.1	1.7	0.069	0.59	0	353
	% change	314	-1.1	40	217	-66	-75	-100	-47
4/3/08	In (g)	1377	5.3	21	1.4	0.14	6.1	199	991
	Out (g)	12966	32	94	15	0.15	3.0	594	163
	% change	841	495	342	1043	3.2	-50	199	-84
4/26/08	In (g)	NM	17	56	5.4	0.25	7.3	213	1551
	Out (g)	NM	32	64	12	0.086	2.0	347	938
	% change	n/a	90	13	123	-66	-73	62	-39

* Nitrate and total Kjeldahl nitrogen (TKN) are expressed as N; TP is expressed as P.

Appendix B

MEDIA ANALYSIS DATA

Table B-1. Total metal and organic matter (OM) content of 2006 surface samples. Range of two replicates is shown. A single value is shown if a replicate was lost.

Sample	Pb (mg/kg)	Cu (mg/kg)	Zn (mg/kg)	OM (%)
1A	7.2 – 17	24 – 24	53 – 56	1.6 – 2.3
1B	39 – 40	38 – 45	174 – 188	6.6 – 7.2
1C	21 – 28	31 – 33	85 – 91	3.8 – 3.9
2A	69 – 69	55 – 55	277 – 297	16 – 18
2B	51 – 59	43 – 44	224 – 232	11 – 12
2C	67 – 72	47 – 51	264 – 268	13 – 13
3A	66	43 – 44	240	23 – 25
3B	60 – 66	43 – 45	249 – 250	23 – 27
3C	38 – 40	35 – 38	181 – 186	18 – 19
4A	33 – 36	27 – 28	136 – 140	20 – 22
4B	39 – 41	30 – 33	153 – 157	22 – 22
4C	29 – 30	26 – 27	119 – 121	20 – 21
7A	6.9 – 7.9	12 – 14	32 – 36	6.2 – 6.8
7B	28 – 30	28 – 29	116 – 119	33 – 33
7C	42 – 42	35 – 54	165 – 166	34 – 34
5A	25 – 26	28 – 30	117 – 118	31 – 33
5B	17 – 18	21 – 22	88 – 90	25 – 26
5C	13 – 21	19 – 19	65 – 69	18 – 19
6A	47	30 – 31	136	7.1 – 8.1
6B	47 – 55	46 – 48	259 – 259	17 – 19
6C	45	41 – 43	207	13 – 15

Table B-2. Organic matter (OM) content and media pH of 2006 core segments.

Segment	Depth (cm)	Media type	OM (%)	pH
1A	0 – 3	Organic	7.0 – 8.2	6.2
1B	3 – 6	BSM	1.8 – 1.8	5.9
1C	6 – 9	BSM	1.7 – 1.8	5.8
1D	9 – 12	BSM	0.6 – 0.8	5.6
1E	12 – 18	BSM	1.7 – 1.8	5.6
1F	18 – 27	BSM	1.3 – 1.4	5.5
1G	33 – 48	BSM	2.0 – 2.0	5.3
1H	48 – 78	BSM	2.4 – 2.6	5.1
1I	78 – 90	BSM	0.9 – 1.1	5.8
2A	0 – 3	Organic	12 – 13	5.7
2B	3 – 6	Organic	7.5 – 9.6	5.4
2C	6 – 9	Organic	42 – 43	5.1
2D	9 – 12	Organic	11 – 13	5.3
2E	12 – 18	BSM	1.7 – 2.7	5.3
2F	18 – 48	BSM	2.5 – 2.6	5.3
2G	48 – 78	BSM	2.2 – 2.5	5.1
2H	78 – 90	BSM	0.9 – 1.0	5.1
3A	0 – 2	Organic	30 – 33	5.7
3B	2 – 4	Organic	28 – 36	5.6
3C	4 – 7	BSM	2.7 – 2.8	5.4
3D	7 – 10	BSM	1.5 – 1.5	5.4
3F	16 – 48	BSM	1.6 – 2.0	5.2
3H	78 – 90	BSM	1.1 – 1.2	6.3
4A	0 – 3	Organic	24 – 26	5.6
4B	3 – 6	BSM	2.3 – 2.4	5.4
4C	6 – 9	BSM	1.6 – 2.3	5.4
4D	9 – 12	BSM	2.1 – 2.1	5.4
4G	48 – 63	BSM	1.9 – 2.0	5.1
7A	0 – 2.5	Organic	13 – 16	5.8
7B	2.5 – 5	Organic	15 – 17	5.9
7C	5 – 8	BSM	3.1 – 3.8	5.8
7E	11 – 17	BSM	2.3 – 2.8	5.5
7H	78 – 86	BSM	1.1 – 1.2	5.0
5A	0 – 2	Organic	21 – 35	n/a
5B	2 – 4	Organic	12 – 14	5.7
5C	4 – 7	BSM	2.0 – 2.0	5.6
5E	10 – 16	BSM	1.9 – 1.9	5.4
5H	78 – 90	BSM	1.3 – 1.8	5.1
6A	0 – 2.5	Organic	8.4 – 10	5.8
6B	2.5 – 5	Organic	8.1 – 9.0	5.6
6C	5 – 8	BSM	4.4 – 5.0	5.6
6F	17 – 48	BSM	2.0 – 2.1	5.2
6H	78 – 90	BSM	0.8 – 1.0	5.6
Orig BSM	n/a	BSM	1.9 – 2.1	5.2

Table B-3. Lead concentration depth profile for 2006 media cores. SE = sequential extraction. Range of two replicates is shown for each fraction and for total lead. A single value is shown if a replicate was lost.

Segment	Depth (cm)	Media type	F1 (mg/kg)	F2 (mg/kg)	F3 (mg/kg)	F4 (mg/kg)	F5 (mg/kg)	Total (mg/kg)	Method
1A	0 – 3	Organic	0.1 – 0.1	2.8 – 3.2	5.1 – 5.6	16 – 16	12 – 12	35 – 36	SE
1B	3 – 6	BSM	0.1 – 0.1	0.9 – 1.0	1.8 – 2.3	4.8 – 4.8	0.9 – 1.1	8.6 – 9.2	SE
1C	6 – 9	BSM	0.1 – 0.1	0.7 – 0.9	1.8 – 1.9	3.3 – 3.4	0.9 – 1.2	7.0 – 7.4	SE
1D	9 – 12	BSM	0.1 – 0.1	0.1 – 0.3	1.5 – 1.7	1.3 – 1.3	0.4 – 0.4	3.6 – 3.6	SE
1E	12 – 18	BSM						1.0 – 1.7	3050B
1F	18 – 27	BSM						1.0 – 1.1	3050B
1G	33 – 48	BSM						0.9 – 0.9	3050B
1H	48 – 78	BSM						0.8 – 2.4	3050B
1I	78 – 90	BSM						0.8 – 1.7	3050B
2A	0 – 3	Organic	0.1	4.0 – 4.2	6.9 – 7.9	37 – 41	11 – 12	60 – 65	SE
2B	3 – 6	Organic	0.1 – 0.1	2.5 – 2.6	4.5 – 5.1	18 – 19	3.5 – 3.8	29 – 30	SE
2C	6 – 9	Organic	0.1 – 0.1	1.4 – 1.5	2.1 – 2.6	5.2 – 6.0	4.2 – 5.0	14 – 14	SE
2D	9 – 12	Organic	0.1 – 0.1	2.4 – 2.6	3.1 – 3.5	7.5 – 9.1	1.1 – 1.1	14 – 16	SE
2E	12 – 18	BSM	0.1 – 0.1	0.7 – 0.9	2.1 – 2.1	2.2 – 2.6	0.6 – 0.8	5.9 – 6.3	SE
2F	18 – 48	BSM						2.5 – 2.8	3050B
2G	48 – 78	BSM						2.2 – 2.9	3050B
2H	78 – 90	BSM						1.3 – 1.8	3050B
3A	0 – 2	Organic	0.1 – 0.1	5.6 – 5.7	16 – 16	36 – 38	8.2 – 8.5	66 – 68	SE
3B	2 – 4	Organic	0.1	5.2 – 5.3	9.8 – 11	22 – 23	3.5 – 3.9	42 – 42	SE
3C	4 – 7	BSM	0.1 – 0.1	0.5 – 0.7	2.3 – 2.4	2.6 – 3.0	0.6 – 0.7	6.1 – 6.9	SE
3D	7 – 10	BSM	0.1 – 0.1	0.5 – 0.5	1.7 – 2.2	2.1 – 2.3	0.7 – 0.9	5.1 – 6.0	SE
3F	16 – 48	BSM						2.1 – 2.6	3050B
3H	78 – 90	BSM						1.7 – 2.1	3050B
4A	0 – 3	Organic	0.1	2.6 – 2.8	7.5 – 7.5	14	3.6	28 – 28	SE
4B	3 – 6	BSM	0.1 – 0.1	0.6 – 0.6	1.8 – 1.8	1.9 – 2.7	0.6 – 0.6	5.0 – 5.7	SE
4C	6 – 9	BSM	0.1 – 0.1	0.2 – 0.3	2.2 – 2.3	1.8 – 2.4	0.6 – 0.8	5.0 – 5.8	SE
4D	9 – 12	BSM	0.1 – 0.1	0.2 – 0.3	1.9 – 2.0	1.8 – 1.9	0.5 – 0.6	4.6 – 4.8	SE
4G	48 – 63	BSM						2.4 – 2.5	3050B
7A	0 – 2.5	Organic	0.1 – 0.1	1.9 – 2.7	3.1 – 3.6	6.6 – 8.1	0.8 – 1.2	12 – 16	SE
7B	2.5 – 5	Organic	0.1 – 0.1	1.4 – 1.5	2.7 – 2.8	4.4 – 4.6	0.8 – 1.1	9.7 – 9.8	SE
7C	5 – 8	BSM						2.9 – 3.5	3050B
7E	11 – 17	BSM						2.7 – 4.5	3050B
7H	78 – 86	BSM						1.7 – 2.2	3050B
5A	0 – 2	Organic	3.6 – 5.1	0.9 – 1.2	2.4 – 3.2	2.9 – 3.7	0.5 – 1.3	10 – 14	SE
5B	2 – 4	Organic	1.1 – 1.4	0.7 – 0.7	2.1 – 3.6	3.1 – 4.1	0.4 – 0.4	7.3 – 10	SE
5C	4 – 7	BSM						1.8 – 2.3	3050B
5E	10 – 16	BSM						2.2 – 2.2	3050B
5H	78 – 90	BSM	0.1 – 0.1	0.7 – 0.8	2.1 – 2.2	1.3 – 1.4	0.4 – 0.7	4.6 – 5.2	SE
6A	0 – 2.5	Organic	0.1	2.9 – 3.2	6.2 – 6.5	16 – 16	5.0 – 5.5	30 – 31	SE
6B	2.5 – 5	Organic	0.1 – 0.1	1.3 – 1.4	1.5 – 1.5	3.9 – 4.2	6.1 – 7.4	7.3 – 7.9	SE
6C	5 – 8	BSM						1.3 – 1.6	3050B
6F	17 – 48	BSM						2.0 – 2.2	3050B
6H	78 – 90	BSM						2.3 – 2.3	3050B
Orig BSM	n/a	BSM	0.1 – 0.1	0.4 – 0.4	2.0 – 2.1	2.7 – 3.2	0.8 – 1.0	6.3 – 6.7	SE
Orig BSM	n/a	BSM						2.6 – 2.7	3050B

Table B-4. Copper concentration depth profile for 2006 media cores. SE = sequential extraction. Range of two replicates is shown for each fraction and for total copper. A single value is shown if a replicate was lost.

Segment	Depth (cm)	Media type	F1 (mg/kg)	F2 (mg/kg)	F3 (mg/kg)	F4 (mg/kg)	F5 (mg/kg)	Total (mg/kg)	Method
1A	0 – 3	Organic	0.3 – 0.3	1.2 – 1.3	9.4 – 10	5.4 – 5.5	15 – 19	31 – 36	SE
1B	3 – 6	BSM	0.2 – 0.2	0.5 – 0.6	1.2 – 1.4	6.7 – 7.4	1.4 – 1.7	10 – 11	SE
1C	6 – 9	BSM	0.2 – 0.2	0.4 – 0.6	1.0 – 1.7	6.1 – 9.6	1.6 – 2.6	9.4 – 15	SE
1D	9 – 12	BSM	0.1 – 0.2	0.9 – 1.0	1.1 – 1.2	6.4 – 7.0	0.9 – 1.0	9.7 – 10	SE
1E	12 – 18	BSM						5.3 – 5.5	3050B
1F	18 – 27	BSM						2.5 – 6.3	3050B
1G	33 – 48	BSM						5.3 – 7.2	3050B
1H	48 – 78	BSM						6.5 – 7.4	3050B
1I	78 – 90	BSM						2.5 – 2.5	3050B
2A	0 – 3	Organic	0.3	1.1 – 1.1	23 – 27	7.1 – 8.0	13 – 14	45 – 51	SE
2B	3 – 6	Organic	0.1 – 0.1	0.6 – 0.6	5.4 – 6.3	6.9 – 8.2	5.7 – 7.1	19 – 22	SE
2C	6 – 9	Organic	0.3 – 0.3	0.6 – 0.7	21 – 23	13 – 14	13 – 14	49 – 50	SE
2D	9 – 12	Organic	0.3 – 0.4	0.8 – 0.8	8.3 – 9.2	5.7 – 6.7	2.6 – 2.7	19 – 19	SE
2E	12 – 18	BSM	0.1 – 0.1	0.4 – 0.5	0.3 – 0.5	5.7 – 6.6	2.0 – 2.6	8.5 – 10	SE
2F	18 – 48	BSM						9.3 – 11	3050B
2G	48 – 78	BSM						8.4 – 8.8	3050B
2H	78 – 90	BSM						2.5 – 2.5	3050B
3A	0 – 2	Organic	0.4 – 0.4	0.7 – 0.8	26 – 27	10 – 12	11 – 11	50 – 50	SE
3B	2 – 4	Organic	0.5	0.7 – 0.7	11 – 12	8.5 – 10	5.6 – 5.9	27 – 29	SE
3C	4 – 7	BSM	0.2 – 0.2	0.4 – 0.4	0.9 – 0.9	5.4 – 5.4	1.1 – 1.5	8.1 – 8.4	SE
3D	7 – 10	BSM	0.1 – 0.2	0.5 – 0.5	0.6 – 0.7	7.5 – 7.9	1.8 – 1.9	11 – 11	SE
3F	16 – 48	BSM						6.3 – 6.3	3050B
3H	78 – 90	BSM						5.1 – 6.1	3050B
4A	0 – 3	Organic	0.2	0.4 – 0.4	11 – 14	9.7	9.2	31 – 34	SE
4B	3 – 6	BSM	0.2 – 0.2	0.4 – 0.5	0.7 – 0.7	5.3 – 5.6	1.5 – 1.7	8.1 – 8.7	SE
4C	6 – 9	BSM	0.2 – 0.2	0.3 – 0.4	0.5 – 0.5	5.1 – 6.2	0.9 – 1.1	7.1 – 8.4	SE
4D	9 – 12	BSM	0.2 – 0.3	0.3 – 0.3	0.5 – 0.6	6.4 – 6.6	1.1 – 1.2	8.7 – 9.0	SE
4G	48 – 63	BSM						7.9 – 8.3	3050B
7A	0 – 2.5	Organic	0.3 – 0.6	0.4 – 0.4	9.0 – 11	5.0 – 5.6	2.1 – 3.5	19 – 19	SE
7B	2.5 – 5	Organic	0.3 – 0.3	0.4 – 0.5	6.0 – 7.0	4.0 – 4.7	2.0 – 2.3	13 – 15	SE
7C	5 – 8	BSM						6.3 – 7.6	3050B
7E	11 – 17	BSM						8.1 – 9.6	3050B
7H	78 – 86	BSM						2.5 – 2.5	3050B
5A	0 – 2	Organic	6.6 – 8.2	1.2 – 1.3	7.2 – 9.4	4.2 – 5.5	2.0 – 2.4	24 – 25	SE
5B	2 – 4	Organic	1.8 – 2.0	0.6 – 0.7	6.4 – 15	3.9 – 4.2	1.3 – 1.5	14 – 23	SE
5C	4 – 7	BSM						5.6 – 6.5	3050B
5E	10 – 16	BSM						5.8 – 7.5	3050B
5H	78 – 90	BSM	0.1 – 0.1	0.2 – 0.2	0.2 – 0.3	6.3 – 7.7	2.1 – 2.5	9.0 – 11	SE
6A	0 – 2.5	Organic	0.1	0.6 – 0.6	4.7 – 5.6	3.3 – 3.5	7.1 – 7.4	16 – 17	SE
6B	2.5 – 5	Organic	0.2 – 0.2	0.9 – 1.0	14 – 16	6.4 – 6.7	5.5 – 6.2	28 – 30	SE
6C	5 – 8	BSM						11 – 11	3050B
6F	17 – 48	BSM						5.8 – 6.2	3050B
6H	78 – 90	BSM						2.5 – 2.5	3050B
Orig BSM	n/a	BSM	0.1 – 0.1	0.1 – 0.2	0.1 – 0.3	8.1 – 9.5	2.9 – 3.1	11 – 13	SE
Orig BSM	n/a	BSM						10 – 13	3050B

Table B-5. Zinc concentration depth profile for 2006 media cores. SE = sequential extraction. Range of two replicates is shown for each fraction and for total zinc. A single value is shown if a replicate was lost.

Segment	Depth (cm)	Media type	F1 (mg/kg)	F2 (mg/kg)	F3 (mg/kg)	F4 (mg/kg)	F5 (mg/kg)	Total (mg/kg)	Method
1A	0 – 3	Organic	14 – 15	55 – 58	36 – 37	49 – 52	23 – 23	177 – 184	SE
1B	3 – 6	BSM	5.7 – 6.2	10 – 11	8.6 – 9.9	19 – 20	8.2 – 8.9	54 – 54	SE
1C	6 – 9	BSM	5.3 – 5.7	9.0 – 9.8	6.7 – 7.4	18 – 18	10 – 11	50 – 51	SE
1D	9 – 12	BSM	2.5 – 5.3	5.8 – 6.2	5.1 – 5.2	11 – 12	6.2 – 6.4	32 – 34	SE
1E	12 – 18	BSM						19 – 20	3050B
1F	18 – 27	BSM						15 – 17	3050B
1G	33 – 48	BSM						16 – 20	3050B
1H	48 – 78	BSM						14 – 14	3050B
1I	78 – 90	BSM						4.8 – 5.7	3050B
2A	0 – 3	Organic	26	61 – 67	52 – 58	72 – 78	27 – 29	239 – 255	SE
2B	3 – 6	Organic	16 – 17	22 – 24	22 – 25	34 – 39	21 – 23	115 – 129	SE
2C	6 – 9	Organic	12 – 13	20 – 24	26 – 26	38 – 40	39 – 41	136 – 142	SE
2D	9 – 12	Organic	7.4 – 7.8	9.9 – 10	9.7 – 9.9	25 – 26	9.0 – 9.3	62 – 63	SE
2E	12 – 18	BSM	2.5 – 2.5	5.2 – 5.5	2.5 – 2.5	17 – 19	6.9 – 7.0	34 – 37	SE
2F	18 – 48	BSM						17 – 18	3050B
2G	48 – 78	BSM						12 – 12	3050B
2H	78 – 90	BSM						4.0 – 4.8	3050B
3A	0 – 2	Organic	17 – 18	69 – 70	68 – 70	73 – 75	18 – 19	248 – 249	SE
3B	2 – 4	Organic	13	40 – 43	43 – 46	43 – 52	12 – 13	152 – 167	SE
3C	4 – 7	BSM	2.5 – 5.1	5.6 – 5.8	2.5 – 5.0	18 – 20	7.2 – 7.8	36 – 44	SE
3D	7 – 10	BSM	5.0 – 5.1	2.5 – 2.5	2.5 – 2.5	15 – 15	7.2 – 12	33 – 36	SE
3F	16 – 48	BSM						11 – 12	3050B
3H	78 – 90	BSM						4.8 – 4.9	3050B
4A	0 – 3	Organic	9.8	23 – 24	29 – 40	32	12	106 – 118	SE
4B	3 – 6	BSM	2.5 – 5.0	2.5 – 2.5	2.5 – 2.5	15 – 23	7.7 – 7.7	33 – 38	SE
4C	6 – 9	BSM	2.5 – 2.5	2.5 – 2.5	2.5 – 5.0	13 – 14	7.0 – 8.3	30 – 30	SE
4D	9 – 12	BSM	2.5 – 2.5	2.5 – 2.5	2.5 – 2.5	12 – 13	7.6 – 7.7	28 – 28	SE
4G	48 – 63	BSM						13 – 15	3050B
7A	0 – 2.5	Organic	2.5 – 2.5	14 – 16	15 – 17	22 – 24	6.2 – 7.0	59 – 66	SE
7B	2.5 – 5	Organic	2.5 – 2.5	8.0 – 9.2	10 – 13	17 – 20	5.6 – 6.4	43 – 51	SE
7C	5 – 8	BSM						16 – 16	3050B
7E	11 – 17	BSM						15 – 17	3050B
7H	78 – 86	BSM						4.7 – 5.5	3050B
5A	0 – 2	Organic	32 – 37	7.6 – 8.8	12 – 15	13 – 18	6.4 – 6.8	70 – 85	SE
5B	2 – 4	Organic	11 – 12	2.5 – 2.5	6.9 – 8.0	11 – 12	2.5 – 2.5	34 – 37	SE
5C	4 – 7	BSM						10 – 12	3050B
5E	10 – 16	BSM						11 – 13	3050B
5H	78 – 90	BSM	2.5 – 2.5	2.5 – 2.5	2.5 – 8.5	9.1 – 10	6.1 – 7.3	25 – 29	SE
6A	0 – 2.5	Organic	12	32 – 33	26 – 28	32 – 35	16 – 20	122 – 123	SE
6B	2.5 – 5	Organic	16 – 17	34 – 34	33 – 34	54 – 60	17 – 17	155 – 161	SE
6C	5 – 8	BSM						38 – 39	3050B
6F	17 – 48	BSM						10 – 12	3050B
6H	78 – 90	BSM						9.0 – 10	3050B
Orig BSM	n/a	BSM	2.5 – 2.5	2.5 – 5.4	2.5 – 2.5	13 – 14	7.4 – 7.8	29 – 31	SE
Orig BSM	n/a	BSM						16 – 20	3050B

Table B-6. Characteristics of August 2008 media samples for lead bioavailability analysis. Range of two replicates is shown for *in vitro* (IV)-extractable and total lead. Particles (last row) were collected in concrete inflow channel. One replicate of sample 1 top-B was lost during total metal extraction. Range of two replicates is shown for OM.

Media characteristics of bioavailability samples									
Sample	Depth (cm)	Media	IV-ext. Pb (mg/kg)	Total Pb (mg/kg)	IVBA (%)	RBA (%)	ABA (%)	pH	OM (%)
1 top-A	0 – 3	Organic	42 – 51	77 – 78	60	50	25	6.3	25 – 26
1 top-B	0 – 5	Organic	50 – 52	83	62	51	26	6.1	25 – 26
2 top	0 – 3.5	Organic	39 – 41	64 – 69	60	50	25	5.5	19 – 19
2 bottom	3.5 – 7	Organic	41 – 43	59 – 64	69	57	29	5.3	13 – 14
3 top-A	0 – 4	Organic	42 – 43	67 – 74	61	51	25	5.3	23 – 23
3 top-B	0 – 4.5	Organic	35 – 38	60 – 61	60	50	25	5.2	20 – 21
6 top	0 – 3.5	Organic	31 – 33	53 – 55	59	49	24	5.7	11 – 12
6 middle	3.5 – 9	Mixed	20 – 21	36 – 37	55	46	23	5.4	11 – 11
6 bottom	9 – 12	BSM	12 – 13	21 – 22	59	49	24	5.4	7.0 – 7.0
Particles	n/a	Particles	30 – 32	46 – 53	62	52	26	7.0	5.4 – 5.8

Appendix C

MATLAB SCRIPTS

```
% Rainfall processor script for MATLAB
% rain.m
% Run before dist.m.
%
% Written by Philip Jones 7/7-15/08
%
% This code steps through 5-minute rainfall data and builds a list of storms. The depth and
% duration of each storm is defined by all rain gauge tips that are bracketed in the input data
% by inter-event dry periods equal to or greater than a user-specified value. For instance, if
% the user specifies a six-hour inter-event dry period, two rain gauge tips occurring 5 hours and
% 55 minutes apart would be considered as part of the same storm. Two rain gauge tips occurring
% six hours apart would be considered as part of two separate storms.
%
% INPUT DATA lists time and depth of rainfall recorded in 5-minute intervals, non-zero values only
% Column 1: Julian day in each year
%         2: Cumulative Julian day, 2002-2006 (1/1/02 = 1)
%         3: Year
%         4: Hour + minute (hhmm) of a 5-minute interval with at least one rain gauge tip recorded
%         5: Rainfall depth (mm) in that five-minute interval
% OUTPUT DATA is saved in "storms" matrix and written to "results" file.
% Column 1 in storms matrix: Julian day in each year
%         2: Hour and minute
%         3: Year
%         4: Rain depth in mm
%         5: Duration in hours
%         6: Average intensity, mm/hr
%         7: Absolute start time (relative to 1/1/02) in units of days
%         8: Antecedent dry time, in units of days

clear all
DryPeriod = input('How many inter-event dry hours are used to define storms? ');
% Number of dry HOURS separating storms, used to
% define when storms begin and end.
load data.dat;
% Reads from a file named data.dat. Contains rainfall
```



```

len = size(data);
len = len(1,1);
n = 1;
pos = 1;
while n <= len,
    hhmm = data(n,4);
    AbsStartTime = data(n,2) + floor(hhmm/100)/24 + (hhmm - 100*floor(hhmm/100))/1440;

    storms(pos,1) = data(n,1);
    storms(pos,2) = data(n,4);
    storms(pos,3) = data(n,3);
    storms(pos,4) = data(n,5);
    storms(pos,7) = AbsStartTime;
    x = n + 1;

    if x <= len
        hhmm = data(x,4);
        AbsEndTime = data(x,2) + floor(hhmm/100)/24 + (hhmm - 100*floor(hhmm/100))/1440;
    end
    if (AbsEndTime - AbsStartTime >= DryPeriod/24) | x > len
        storms(pos,5) = 5/60;
        if storms(pos,4) < 0.3
            storms(pos,6) = 0;
        else
            storms(pos,6) = storms(pos,4)/storms(pos,5);
        end
        n = n + 1;
    else
        OldAbsEndTime = AbsEndTime;
        while (AbsEndTime - OldAbsEndTime < DryPeriod/24) & (x <= len),
            storms(pos,4) = storms(pos,4) + data(x,5);
            x = x + 1;
            OldAbsEndTime = AbsEndTime;
            if x <= len
                hhmm = data(x,4);
                AbsEndTime = data(x,2) + floor(hhmm/100)/24 + (hhmm - 100*floor(hhmm/100))/1440;
            end
        end
    end
end

```

```

% data from 12/1/02 - 11/30-06, inclusive.
% Number of lines in data.dat

% Position in list of storms that the code is building

% Numerical string indicating hours and minutes
% Start time = Julian day + hours/24 + minutes/1440
% Record Julian day
% Record hour and minute
% Record year
% Record first (possibly only) rain depth for event
% Record absolute start time, in units of days.
% Step to next line in input rain data; may or may not
% be part of the same storm.
% If the end of the input data hasn't been reached
% Numerical string indicating hours and minutes
% If time to next rain burst exceeds
% user-defined inter-event dry period
% 5-minute duration recorded for isolated bursts
% If rainfall is only a single 0.01" (0.245 mm) burst
% Assign an intensity of zero to isolated 0.01" bursts
% For isolated bursts > 0.01", calc I

% Increment to next line in input rainfall data
% If time to next rain < inter-event dry period
% Step through the data to find the end of the storm
% Add to rainfall total for this event
% Increment to next line in input data

% If the end of the input data hasn't been reached
% Numerical string indicating hours and minutes
% New value of potential end time of current event

```

```

    end
    storms(pos,5) = 24*(OldAbsEndTime-AbsStartTime);           % Record event duration in hours
    storms(pos,6) = storms(pos,4)/storms(pos,5);               % Record average intensity (in/hr)
    n = x;
end
if pos > 1
    storms(pos,8) = storms(pos,7) - (storms(pos-1,7) + storms(pos-1,5)/24);
                                                % Antecedent dry time in days is dry period between end
                                                % of last event and start of current event
else
    storms(pos,8) = 0;                                       % First event in list has undefined antecedent dry time
end
pos = pos + 1;                                             % Ready to record next storm event
end
save results storms -ASCII -TABS                          % Write storm list to file

```

```

% Cumulative infiltration model for MATLAB
% dist3.m
% Run rain.m first.
%
% Written by Philip Jones 7/15-17/08
%
% This model assumes that the cell has a uniform media infiltration rate (cm/hr). This rate
% does not change over the long term, with weather conditions, within a storm, or spatially
% across the surface. Assume uniform wetting across the width of the cell. At any time,
% water flows into the cell only far enough for the infiltration flow rate (downward through
% the media) to match the inflow rate. Ponding occurs if inflow rate exceeds the maximum
% infiltration flow rate through the entire cell surface. Storm hydrographs are represented
% as symmetrical triangles. Triangle base is storm duration and peak Q is calculated using
% total rainfall and storm duration.

% User input
InfiltrRate = input('Average steady-state media infiltration rate, cm/hr? ');
P = input('Type 1 to plot each storm. Otherwise, no plots will be made. ');
if isempty(P)
    P = 0;
elseif P ~= 1
    P = 0;
end
inc = input('Number of increments? '); % Flow rate increments between 0 and max infiltration Q.
                                        % These also divide the cell surface into "inc" successive
                                        % slices along the axis of the cell. Each is as wide as
                                        % the cell, with length equal to (cell length)/inc. The
                                        % script uses 4 years of storm data to calculate the
                                        % cumulative volume infiltrating through each slice.

% Define cell and watershed characteristics
DA = 0.62*4046.856; % Drainage area (m^2), converted from 0.62 acres
C = 0.9; % Runoff coefficient
TopArea = 14217; % Area at top of cell (cm^2), excluded from analysis
                % because inflow enters below it
BottomArea = 2383; % Area (cm^2) at bottom of cell, excluded from analysis
                % because the width becomes narrower
CSA = 247543 - TopArea - BottomArea; % Total cell surface area (cm^2), minus top & bottom areas
PondingDepth = 27; % (cm), based on height of riser above cell surface
PondingVol = PondingDepth * CSA / 1000; % Ponding volume (liters)
MIQ = CSA*InfiltrRate/1000; % Max infiltration flow rate (l/hr) through entire cell

```

```

% surface that does not cause ponding

% Initialize variables
LenStorms = max(size(storms)); % Get # storms from rain.m results - run rain.m first!
FlowRates = transpose([0:MIQ/inc:MIQ]); % List of flow rates (l/hr) with "delta Q" of MIQ/inc
areas = (FlowRates/1000)/(InfiltrRate/100); % Wetted areas (m^2) corresponding to each flow rate
distances = areas*0.4505; % Distances (m) along cell axis corresponding to wetted
% areas. Based on linear best fit of 6 measured pairs
% of area and distance, zero intercept (R^2 = 0.9997)

len = max(size(distances)); % Get number of distances (same as # of areas and Q's)
CumVol = zeros(len,1); % List of cumulative infiltrated vol (m^3) at each dist

% Main body of program
for n = 1:LenStorms, % Step through entire storms list generated by rain.m
    if storms(n,6) ~= 0 % Ignore isolated 0.245 mm bursts. Intensity of these
        % events was set to 0 by rain.m
        depth = storms(n,4); % Total rainfall (mm)
        dur = storms(n,5); % Total storm duration (hours)
        Qpeak = 1000*2*(depth/1000)*(DA/2)*C/dur; % Qpeak (l/hr) using triang. hydrograph
        if P == 1 % Plots hydrograph and flow rates, if requested by user
            clf % Clear figure
            subplot(1,3,1); % Hydrograph is one of three subplots on Figure 1
            hold on % Don't replace one plot with a subsequent plot
            axis([0, dur, 0, 1.1*max([Qpeak,MIQ])]); % Max y axis value is storm peak Q or max
            % infilt flow rate, whichever is larger
            plot([0, dur/2,dur],[0, Qpeak,0],'b:'); % Triangular hydrograph is dotted blue line
            plot([0,dur*0.1],[FlowRates,FlowRates],'g:'); % Q's (l/hr), 0 - max infilt Q, green lines
            xlabel('Duration (hr)');
            ylabel('Q (l/hr)');
            title(sprintf('%4.3g mm rain',storms(n,4))); % Title of plot is rainfall depth
        end
        slope = Qpeak / (dur/2); % Slope of rising limb
        ReachedPeak = 0; % Marker for whether hydrograph peak has been reached
        StormVol = zeros(len,1); % List of incremental infiltration vols (m^3), i.e. the
        % volumes that infiltrate into each slice of the cell
        for x = 2:len, % Step thru list of flow rates, from 0 to max infilt Q
            if Qpeak > FlowRates(x) % If storm peak exceeds any flow rate in the list
                avgQ = (FlowRates(x) + FlowRates(x-1))/2; % Avg Q between current and previous Q
                diffQ = MIQ/inc; % Difference between current and prev Q (always the same)
                RisingTime = avgQ/slope; % Time at which avg Q is reached on rising limb
                RectangleArea = (dur - 2*RisingTime)*diffQ; % Incremental vol (l) calculated as
            end
        end
    end
end

```

```

                                                                    % base (hr) X height (l/hr)
StormVol(x) = RectangleArea/1000;                                % Record increm. vol (m^3) @ current loc.
if P == 1                                                        % Plotting, if requested by user (red lines)
    subplot(1,3,1);                                             % Plot the rectangle for this volume calculation
    a = RisingTime;                                             % Rectangle's height X width = volume infiltrating into
    b = FlowRates(x-1);                                         % one slice of the cell surface, in this storm
    plot([a, a, dur-a, dur-a, a],[b, b+diffQ, b+diffQ, b, b],'r-');
end
end
if (ReachedPeak == 0) & (Qpeak < FlowRates(x))                % If storm peak Q is less than current Q
                                                                    % (peak Q is too low to reach back of cell)
    ReachedPeak = 1;                                           % This calc. only done once per storm
    RisingTime = FlowRates(x-1)/slope;                          % Time at which last exceeded Q was reached
    TriangleArea = (1/2)*(dur - 2*RisingTime)*(Qpeak - FlowRates(x-1)); % Vol @ triangle tip
    StormVol(x) = TriangleArea/1000;                            % Record increm. vol (m^3) @ current loc.
    if P == 1                                                  % Plot triangle if requested (red lines)
        a = RisingTime;
        b = FlowRates(x-1);
        plot([a, dur/2, dur-a, a],[b, Qpeak, b, b],'r-');
        disp(sprintf('No ponding. Flow didn''t reach back of cell.')); % Verbal summary
    end
end
end
if (Qpeak > MIQ)                                                % Storm peak Q exceeds cell's max infilt Q
    RisingTime = MIQ/slope;                                     % First time in storm at which this occurs
    ExcessVol = (1/2)*(dur - 2*RisingTime)*(Qpeak - MIQ);      % Top triangle is total excess volume
    if ExcessVol < PondingVol                                   % If cell can contain excess w/o overflowing
        StormPV = ExcessVol;                                   % then ponding vol = excess inflow volume
    else                                                        % If the excess vol exceeds ponding vol, use
        StormPV = PondingVol;                                  % max cell ponding vol; the rest overflows
    end
    IncrementalPV = (StormPV/(len - 1))/1000;                  % Ponding vol (m^3) infiltrates uniformly
                                                                    % thru all cell slices, so divide it evenly
    StormVol = StormVol(:) + IncrementalPV;                    % Add to all incremental vols for this storm
    StormVol(1) = 0;                                           % The first cell is always zero
    if P == 1                                                  % Plot the infiltrated ponding volume
        base = dur - 2*RisingTime;                             % Base of triangle or trapezoid
        if StormPV == ExcessVol                                % In this case, ponding vol is a triangle
            d = base/2;                                        % d is the x-value of the triangle peak
            height = Qpeak - MIQ;                              % Height of triangle
            disp(sprintf('Ponding, but no overflow. All inflow infiltrated through cell.'));
        end
    end
end

```

```

else
    d = (base - sqrt(base^2 - 4*StormPV/slope))/2; % Top of trapezoid = base - 2*d
    height = 2*StormPV/((base + base - 2*d)); % Trapezoid height
    disp(sprintf('Ponding with overflow.'));
end
a = RisingTime;
b = MIQ;
plot([a, a+d, a+base-d, a+base, a],[b, b+height, b+height, b, b],'b'); % Triang or trap
end
end
CumuVol = CumuVol + StormVol; % Add incremental volumes from this storm
% to cumulative incremental volumes

if P == 1
    subplot(1,3,2);
    plot(distances,StormVol,'b.');
```

% Plot this storm's increm vols vs distance

```

    title('Incremental volumes in this storm');
    xlabel('Flow distance (m)');
    ylabel('Volume (m^3)');
    subplot(1,3,3);
    plot(distances,CumuVol,'k.');
```

% Plot cumulative increm vols vs distance

```

    title('Cumulative incremental volumes');
    xlabel('Flow distance (m)');
    ylabel('Volume (m^3)');
    pause
end
end
end
dAreas = areas - transpose([0,transpose(areas([1:len-1]))]); % Get area (m^2) of each slice by
% subtracting area(x-1) from area(x)
dAreas = dAreas([2:len]); % Get rid of zero at beginning of list
CumuVol = CumuVol([2:len]);
distances = distances([2:len]);
DepthInfiltrated = CumuVol./dAreas; % Divide incremental vols by increm. areas to
% get total water depth (m) infiltrating thru
% each slice. Independent of # of increments

```

REFERENCES

- Adachi, K., Tainosho, Y. (2004). "Characterization of Heavy Metal Particles Embedded in Tire Dust." *Environ. Int.*, 30(8), 1009-1017.
- Adediran, S.A., Kramer, J.R. (1987). "Copper Adsorption on Clay, Iron-Manganese Oxide and Organic Fractions Along a Salinity Gradient." *Appl. Geochem.*, 2(2), 213-216.
- Ahnstrom, Z.S., Parker, D.R. (1999). "Development and Assessment of a Sequential Extraction Procedure for the Fractionation of Soil Cadmium." *Soil Sci. Soc. Am. J.*, 63(6), 1650-1658.
- Aist, Kent. Personal communication. 22 Mar. 2007.
- Alloway, B.J. (1995). "Soil Processes and the Behaviour of Metals." In *Heavy Metals in Soils*, ed. B.J. Alloway. Blackie Academic & Professional, New York.
- American Public Health Association (APHA), American Water Works Association, Water Environment Federation. (1995). *Standard Methods for the Examination of Water and Wastewater*. 19th ed. APHA, Washington, DC.
- Ayyub, B.M., McCuen, R.H. (2003). *Probability, Statistics, and Reliability for Engineers and Scientists*. Chapman & Hall/CRC, Washington, DC.
- Bäckström, M., Karlsson, S., Allard, B. (2004). "Metal Leachability and Anthropogenic Signal in Roadside Soils Estimated from Sequential Extraction and Stable Lead Isotopes." *Environ. Monit. Assess.*, 90(1-3), 135-160.
- Bohn, H.L., McNeal, B.L., O'Connor, G.A. (2001). *Soil Chemistry*. Wiley, New York.
- Bratieres, K., Fletcher, T.D., Deletic, A., Zinger, Y. (2008). "Nutrient and Sediment Removal by Stormwater Biofilters: A Large-Scale Design Optimisation Study." *Water Res.*, 42(14), 3930-3940.
- Chang Chien, S.W., Wang, M.C., Huang, C.C. (2006). "Reactions of Compost-Derived Humic Substances with Lead, Copper, Cadmium, and Zinc." *Chemosphere*, 64(8), 1353-1361.
- Cheng, M., Coffman, L.S., Clar, M.L. (2003). "Low-Impact Development Hydrologic Analysis." In *Wet-Weather Flow in the Urban Watershed*, ed. Richard Field and Daniel Sullivan. Lewis Publishers/CRC Press, Washington, DC.

- Code of Federal Regulations (CFR). (2007). "Toxicity Characteristic." 40 CFR § 261.24. Available at http://edocket.access.gpo.gov/cfr_2007/julqtr/pdf/40cfr261.24.pdf. Retrieved 23 July 2008.
- Code of Federal Regulations (CFR). (2008). "Secondary Maximum Contaminant Levels." 40 CFR § 143.3. Available at http://edocket.access.gpo.gov/cfr_2008/julqtr/pdf/40cfr143.3.pdf. Retrieved 10 Feb. 2009.
- Code of Maryland Regulations (COMAR). (2006). "Numerical Criteria for Toxic Substances in Surface Waters." 26.08.02.03-2. Available at <http://www.dsd.state.md.us/comar/26/26.08.02.03-2.htm>. Retrieved 7 Feb. 2009.
- Councell, T.B., Duckenfield, K.U., Landa, E.R., Callender, E. (2004). "Tire-Wear Particles as a Source of Zinc to the Environment." *Environ. Sci. Technol.*, 38(15), 4206-4214.
- Covelo, E.F., Andrade, M.L., Vega, F.A. (2004a). "Heavy Metal Adsorption by Humic Umbrisols: Selectivity Sequences and Competitive Sorption Kinetics." *J. Colloid Interface Sci.*, 280(1), 1-8.
- Covelo, E.F., Alvarez, N., Andrade, M.L., Vega, F.A., Marcet, P. (2004b). "Zn Adsorption by Different Fractions of Galician Soils." *J. Colloid Interface Sci.*, 280(2), 343-349.
- Davies, B.E. (1995). "Lead." In *Heavy Metals in Soils*, ed. B.J. Alloway. Blackie Academic & Professional, New York.
- Davis, A.P., Shokouhian, M., Sharma, M., Minami, C. (2001a). "Laboratory Study of Biological Retention for Urban Stormwater Management." *Water Environ. Res.*, 73(1), 5-14.
- Davis, A.P., Shokouhian, M., Ni, S. (2001b). "Loading Estimates of Lead, Copper, Cadmium, and Zinc in Urban Runoff from Specific Sources." *Chemosphere*, 44(5), 997-1009.
- Davis, A.P., Shokouhian, M., Sharma, H., Minami, C., Winogradoff, D. (2003). "Water Quality Improvement Through Bioretention: Lead, Copper, and Zinc Removal." *Water Environ. Res.*, 75(1), 73-82.
- Davis, A.P., McCuen, R.H. (2005). *Stormwater Management for Smart Growth*. Springer, New York.
- Davis, A.P. (2007). "Field Performance of Bioretention: Water Quality." *Environ. Eng. Sci.*, 24(8), 1048-1064.

- Davis, A.P. (2008). "Field Performance of Bioretention: Hydrology Impacts." *J. Hydrol. Eng.*, 13(2), 90-95.
- Dean, C.M., Sansalone, J.J., Cartledge, F.K., Pardue, J.H. (2005). "Influence of Hydrology on Rainfall-Runoff Metal Element Speciation." *J. Environ. Eng.*, 131(4), 632-642.
- Dechesne, M., Barraud, S., Bardin, J. (2005). "Experimental Assessment of Stormwater Infiltration Basin Evolution." *J. Environ. Eng.*, 131(7), 1090-1098.
- Dietz, M.E., Clausen, J.C. (2005). "A Field Evaluation of Rain Garden Flow and Pollutant Treatment." *Water, Air, and Soil Pollut.* 167(1-4), 123-138.
- Dietz, M.E., Clausen, J.C. (2006). "Saturation to Improve Pollutant Retention in a Rain Garden." *Environ. Sci. Technol.*, 40(4), 1335-1340.
- District of Columbia Water and Sewer Authority (DCWASA). (2004). "CSO Overflow Predictions for Average Year." Available at [http://www.dcwasa.com/education/css/CSO Overflow Predictions - Updated 8-2004.pdf](http://www.dcwasa.com/education/css/CSO%20Overflow%20Predictions%20-%20Updated%208-2004.pdf). Retrieved 7 April 2009.
- Drexler, J.W., Brattin, W.J. (2007). "An *In Vitro* Procedure for Estimation of Lead Relative Bioavailability: With Validation." *Hum. Ecol. Risk Assess.* 13(2), 383-401.
- Dunne, T. Leopold, L.B. (1998). *Water in Environmental Planning*. W.H. Freeman and Company, New York.
- Elliott, H.A., Liberati, M.R., Huang, C.P. (1986). "Competitive Adsorption of Heavy Metals by Soils." *J. Environ. Qual.*, 15(3), 214-219.
- Flint, K.R., Davis, A.P. (2007). "Pollutant Mass Flushing Characterization of Highway Stormwater Runoff from an Ultra-Urban Area." *J. Environ. Eng.*, 133(6), 616-626.
- Hatt, B.E., Fletcher, T.D., Deletic, A. (2008a). "Hydraulic and Pollutant Removal Performance of Fine Media Stormwater Filtration Systems." *Environ. Sci. Technol.*, 42(7), 2535-2541.
- Hatt, B.E., Fletcher, T.D., Deletic, A. (2008b). "Hydraulic and Pollutant Removal Performance of Stormwater Biofiltration Systems at the Field Scale." *J. Hydrol.*, 365(3-4), 310-321.
- Hendershot, W.H., Lalonde, H., Duquette, M. (1993). "Soil Reaction and Exchangeable Acidity." In *Soil Sampling and Methods of Analysis*, ed. Martin R. Carter for Canadian Society of Soil Science. Lewis Publishers, Ann Arbor.

- Holmgren, G.S.S., Meyer, M.W., Chaney, R.L., Daniels, R.B. (1993). "Cadmium, Lead, Zinc, Copper, and Nickel in Agricultural Soils of the United States of America." *J. Environ. Qual.*, 22(2), 335-348.
- Hsieh, C., Davis, A.P., Needelman, B.A. (2007). "Nitrogen Removal from Urban Stormwater Runoff Through Layered Bioretention Columns." *Water Environ. Res.*, 79(12), 2404-2411.
- Hua, J., An, P., Winter, J., Gallert, G. (2003). "Elimination of COD, Microorganisms and Pharmaceuticals from Sewage by Trickling Through Sandy Soil Below Leaking Sewers." *Water Res.*, 37(18), 4395-4404.
- Hunt, W.F., Jarrett, A.R., Smith, J.T., Sharkey, L.J. (2006). "Evaluating Bioretention Hydrology and Nutrient Removal at Three Field Sites in North Carolina." *J. Irrig. Drain. Eng.*, 132(6), 600-608.
- Hunt, W.F., Smith, J.T., Jadlocki, S.J., Hathaway, J.M., Eubanks, P.R. (2008). "Pollutant Removal and Peak Flow Mitigation by a Bioretention Cell in Urban Charlotte, N.C." *J. Environ. Eng.*, 134(5), 403-408.
- Jang, A., Seo, Y., Bishop, P.L. (2005). "The Removal of Heavy Metals in Urban Runoff by Sorption on Mulch." *Environ. Pollut.*, 133(1), 117-127.
- Jin, X., Bailey, G.W., Yu, Y.S., Lynch, A.T. (1996). "Kinetics of Single and Multiple Metal Ion Sorption Processes on Humic Substances." *Soil Sci.*, 161(8), 509-520.
- Jones, R., Burgess, M.S.E. (1984). "Zinc and Cadmium in Soils and Plants Near Electrical Transmission (Hydro) Towers." *Environ. Sci. Technol.*, 18(10), 731-734.
- Kaushal, S.S., Groffman, P.M., Likens, G.E., Belt, K.T., Stack, W.P., Kelly, V.R., Band, L.E., Fisher, G.T. (2005). "Increased Salinization of Fresh Water in the Northeastern United States." *Proc. Natl. Acad. Sci. USA*, 102 (38), 13517-13520.
- Kelley, M.E., Brauning, S.E., Schoof, R.A., Ruby, M.V. (2002). *Assessing Oral Bioavailability of Metals in Soil*. Battelle Press, Columbus.
- Kreeb, L.B., McCuen, R.H. (2003). *Hydrologic Efficiency and Design Sensitivity of Bioretention Facilities*. University of Maryland, College Park, MD.
- Li, H., Davis, A.P. (2008a). "Heavy Metal Capture and Accumulation in Bioretention Media." *Environ. Sci. Technol.*, 42(14), 5247-5253.
- Li, H., Davis, A.P. (2008b). "Urban Particle Capture in Bioretention Media. I: Laboratory and Field Studies." *J. Environ. Eng.*, 134(6), 409-418.

- Li, H., Davis, A.P. (2009). "Water Quality Improvement Through Reductions of Pollutant Loads Using Bioretention." *J. Environ. Eng.*, in press.
- Maryland Department of the Environment (MDE). (2000). *2000 Maryland Stormwater Design Manual Volumes I & II*. MDE, Baltimore, MD. Available at http://www.mde.state.md.us/programs/waterprograms/sedimentandstormwater/stormwater_design/index.asp. Retrieved 7 April 2009.
- Maryland Department of the Environment (MDE). (2008). "Cleanup Standards for Soil and Groundwater." Baltimore, MD. Available at [http://www.mde.state.md.us/assets/document/Working Cleanup Standards Doc 4-11-08\(1\).pdf](http://www.mde.state.md.us/assets/document/Working_Cleanup_Standards_Doc_4-11-08(1).pdf). Retrieved 23 July 2008.
- McCuen, R.H., Moglen, G.E. (1988). "Multicriterion Stormwater Management Methods." *J. Water Resour. Plan. Manage.*, 114(4), 414-431.
- Muthanna, T.M., Viklander, M., Gjesdahl, N., Thorolfsson, S.T. (2007). "Heavy Metal Removal in Cold Climate Bioretention." *Water, Air, and Soil Pollut.*, 183(1-4), 391-402.
- Navarro, M.C., Pérez-Sirvent, C., Martínez-Sánchez, M.J., Vidal, J., Marimón, J. (2006). "Lead, Cadmium and Arsenic Bioavailability in the Abandoned Mine Site of Cabezo Rajao (Murcia, SE Spain)." *Chemosphere*, 63(3), 484-489.
- Nightingale, H.I. (1975). "Lead, Zinc, and Copper in Soils of Urban Storm-Runoff Retention Basins." *J. Amer. Water Works Assoc.*, 67(8), 443-446.
- Nightingale, H.I. (1987). "Accumulation of As, Ni, Cu, and Pb in Retention and Recharge Basins Soils from Urban Runoff." *Water Res. Bull.*, 23(4), 663-671.
- Nörrstrom, A.C., Jacks, G. (1998). "Concentration and Fractionation of Heavy Metals in Roadside Soils Receiving De-Icing Salts." *Sci. Tot. Environ.*, 218(2-3), 161-174.
- Novotny, V., ed. (1995). *Nonpoint Pollution and Urban Stormwater Management*. Technomic, Lancaster, PA.
- Oomen, A.G., Hack, A., Minekus, M., Zeijdner, E., Cornelis, C., Schoeters, G., Verstraete, W., van de Wiele, T., Wragg, J., Rompelberg, C.J.M., Sips, A.J.A.M., van Wijnen, J.H. (2002). "Comparison of Five In Vitro Digestion Models to Study the Bioaccessibility of Soil Contaminants." *Environ. Sci. Technol.*, 36(15), 3326-3334.
- Ott, R.L., Longnecker, M. (2001). *An Introduction to Statistical Methods and Data Analysis*. Duxbury, Pacific Grove, CA.

- Petersen, E.J., Jennings, A.A., Ma, J. (2006). "Screening Level Risk Assessment of Heavy Metal Contamination in Cleveland Area Commons." *J. Environ. Eng.*, 132(3), 392-404.
- Petrović, M., Kaštelan-Macan, M., Horvat, A.J.M. (1999). "Interactive Sorption of Metal Ions and Humic Acids Onto Mineral Particles." *Water, Air, and Soil Pollut.*, 111(1-4), 41-56.
- Prestes, E.C., dos Anjos, V.E, Sodr , F.F., Grassi, M.T. (2006). "Copper, Lead, and Cadmium Loads and Behavior in Urban Stormwater Runoff in Curitiba, Brazil." *J. Braz. Chem. Soc.*, 17(1), 53-60.
- Prince George's County Department of Environmental Resources (PGDER), Programs and Planning Division. (2002). *Prince George's County Bioretention Manual*. Largo, MD. Available at <http://www.princegeorgescountymd.gov/Government/AgencyIndex/DER/ESG/Bioretention/bioretention.asp>. Retrieved 12 June 2008.
- Prince George's County Department of Environmental Resources (PGDER). (2004). *Part V – Special Prov.* Bid No. DER-2004-0024.
- Ray, A.B., Selvakumar, A., Tafuri, A.N. (2006). "Removal of Selected Pollutants from Aqueous Media by Hardwood Mulch." *J. Haz. Mat.*, 136(2), 213-218.
- Ruby, M.V., Schoof, R., Brattin, W., Goldade, M., Post, G., Harnois, M., Mosby, D.E., Casteel, S.W., Berti, W., Carpenter, M., Edwards, D., Cragin, D., Chappell, W. (1999). "Advances in Evaluating the Oral Bioavailability of Inorganics in Soil for Use in Human Health Risk Assessment." *Environ. Sci. Technol.*, 33(21), 3697-3705.
- Sansalone, J.J., Buchberger, S.G. (1997). "Partitioning and First Flush of Metals in Urban Roadway Storm Water." *J. Environ. Eng.*, 123(2), 134-143.
- Sansalone, J.J., Hird, J. (2003). "Treatment of Stormwater Runoff from Urban Pavement and Roadways." In *Wet-Weather Flow in the Urban Watershed*, ed. Richard Field and Daniel Sullivan. Lewis Publishers/CRC Press, Washington, DC.
- Smolders, E., Degryse, F. (2002). "Fate and Effect of Zinc from Tire Debris in Soil." *Environ. Sci. Technol.*, 36(17), 3706-3710.
- Sposito, G. (2008). *The Chemistry of Soils*. Oxford University Press, New York.
- Stagge, J.H. (2006). *Field Evaluation of Hydrologic and Water Quality Benefits of Grass Swales for Managing Highway Runoff*. Master's Thesis. University of Maryland, College Park.

- Strecker, E.W., Quigley, M.M., Urbonas, B.R., Jones, J.E, Clary, J.K. (2001). "Determining Urban Storm Water BMP Effectiveness." *J. Water Resour. Plan. Manage.*, 127 (3), 144-149.
- Sun, X., Davis, A.P. (2007). "Heavy Metal Fates in Laboratory Bioretention Systems." *Chemosphere*, 66(9), 1601-1609.
- Turer, D., Maynard, J.B., Sansalone, J.J. (2001). "Heavy Metal Contamination in Soils of Urban Highways: Comparison Between Runoff and Soil Concentrations at Cincinnati, Ohio." *Water, Air, and Soil Pollut.*, 132(3-4), 293-314.
- United States Environmental Protection Agency (EPA), Office of Solid Waste and Emergency Response. (1992). "Method 1311. Toxicity Characteristic Leaching Procedure." Washington, DC. Available at <http://www.epa.gov/epawaste/hazard/testmethods/sw846/pdfs/1311.pdf>. Retrieved 23 July 2008.
- United States Environmental Protection Agency (EPA), Office of Solid Waste and Emergency Response. (1996). "Method 3050B. Acid Digestion of Sediments, Sludges, and Soils." Washington, DC. Available at <http://www.epa.gov/epawaste/hazard/testmethods/sw846/pdfs/3050b.pdf>. Retrieved 8 Sep. 2006.
- United States Environmental Protection Agency (EPA), Office of Solid Waste and Emergency Response. (2007). "Estimation of Relative Bioavailability of Lead in Soil and Soil-Like Materials Using *In Vivo* and *In Vitro* Methods." OSWER 9285.7-77. Washington, DC. Available at http://epa.gov/superfund/health/contaminants/bioavailability/lead_tsd.pdf. Retrieved 20 Mar. 2008.
- United States Environmental Protection Agency (EPA), Office of Solid Waste and Emergency Response. (2008a). "Standard Operating Procedure for an *In Vitro* Bioaccessibility Assay for Lead in Soil." EPA 9200.1-86. Washington, DC. Available at http://epa.gov/superfund/health/contaminants/bioavailability/pdfs/pb_ivba_sop_final.pdf. Retrieved 1 Nov. 2008.
- United States Environmental Protection Agency (EPA), Office of Water. (1986). "Quality Criteria for Water." EPA 440-5-86-001. Washington, DC. Available at <http://www.epa.gov/waterscience/criteria/goldbook.pdf>. Retrieved 14 Feb. 2009.
- United States Environmental Protection Agency (EPA), Office of Water. (2003). "National Primary Drinking Water Standards." EPA 816-F-03-016. Washington, DC. Available at <http://www.epa.gov/safewater/consumer/pdf/mcl.pdf>. Retrieved 10 Feb. 2009.
- United States Environmental Protection Agency (EPA), Region III. (2008b). "Risk-Based Concentration Table." Philadelphia, PA. Available at <http://www.epa.gov/reg3hwmd/risk/human>. Retrieved 23 July 2008.

Vega, F.A., Covelo, E.F., Chao, I., Andrade, M.L. (2007). "Role of Different Soil Fractions in Copper Sorption by Soils." *Comm. Soil Sci. Plant Anal.*, 38(19-20), 2887-2905.

Walsh, C.J., Roy, A.H., Feminella, J.W., Cottingham, P.D., Groffman, P.M., Morgan, R.P. (2005). "The Urban Stream Syndrome: Current Knowledge and the Search for a Cure." *J. N. Am. Benthol. Soc.*, 24(3), 706-723.

Weinstein, Neil. Personal communication. 1 Aug. 2008.

Young, G.K., Stein, S., Cole, P., Kammer, T., Graziano, F., Bank, F. (1996). "Evaluation and Management of Highway Runoff Water Quality." FHWA-PD-96-032. U.S. Department of Transportation, Washington, DC.